University of New Caledonia

Institute of Exact and Applied Sciences

University of Parma

Department of Chemistry, Life Sciences and Environmental Sustainability

- Philosophy Degree in Earth Sciences, Mineralogy –

ALTERATION OF ASBESTIFORM MINERALS UNDER SUB-TROPICAL CLIMATE: MINERALOGICAL MONITORING AND GEOCHEMISTRY.
THE EXAMPLE OF NEW CALEDONIA.

Author
Jasmine Rita Petrieglieri

Supervisor
Dr. Peggy Gunkel-Grillon
Co-Supervisor
Dr. Emma Salvioli-Mariani

December 15th, 2017

University of New Caledonia

Institute of Exact and Applied Sciences

University of Parma

Department of Chemistry, Life Sciences and Environmental Sustainability

- Philosophy Degree in Earth Sciences, Mineralogy –

ALTERATION OF ASBESTIFORM MINERALS UNDER SUB-TROPICAL CLIMATE: MINERALOGICAL MONITORING AND GEOCHEMISTRY.
THE EXAMPLE OF NEW CALEDONIA.

Jasmine Rita Petriglieri

PhD Committee

Prof. Jean-Luc Grosseau-Poussard, *Referee*, Université de la Rochelle, France

Prof. Alessandro F. Gualtieri, *Referee*, Università di Modena e Reggio Emilia, Italy

Prof. Hamid Amir, *Inspector*, Université de la Nouvelle Calédonie, NC

Prof. Bice Fubini, *Inspector*, Università di Torino, Italy

Dr. Alessandro Cavallo, *Inspector*, Università degli Studi di Milano-Bicocca, Italy

Dr. Peggy Gunkel-Grillon, *Supervisor*, Université de la Nouvelle Calédonie, NC

Dr. Emma Salvioli-Mariani, *Co-Supervisor*, Università di Parma, Italy

December 15th, 2017

List of contents

Introduction

"Asbestos" is generally defined as a commercial and regulatory term applied to a group of six minerals that has grown with a specific crystal habit and exhibits unique physical-chemical and technological proprieties such as flexibility, large surface area and heat resistance (Williams et al. 2013). The six minerals are the serpentine mineral chrysotile, also known as "white asbestos", and the amphibole minerals amosite (fibrous-asbestiform variety of grunerite, also known as "brown asbestos"), crocidolite (fibrous-asbestiform variety of riebeckite, commercially known as "blue asbestos"), as well as anthophyllite, tremolite and actinolite asbestos (IARC 2012, EU 2003). The start of the modern asbestos industrial age is dated at the second half of 19th century, with the exploitation of the chrysotile deposits in Northern Italy and in Canada. Ross *et al.* (2008) estimated that more than 95% of commercially developed asbestos ore deposits were chrysotile asbestos. Actually, many of these deposits are natural, non-occupational or non-anthropogenic, while others result from widespread use of asbestos-containing products (Gunter et al. 2007a, b).

Nowadays, the controversial debate between the various scientific and regulatory disciplines on the definition of the term *asbestos* is still open (Alleman and Mossman 1997). Actually, there is no conclusive and shared definition of *fibre*, *asbestos*, and other related terms in published literature. To the mineralogical community, for example, the term *fibre* is a textural term meaning that the material looks and, more importantly, behaves as a fibre; thus, it can curve and bend under force (Gunter et al. 2007a). The term *fibrous* refers to a (mineral) phase whose crystalline habit consists of fibres whether the phase contains separable fibres or not. On the other hand, the term *asbestiform* refers to a type of morphology where a mineral has longitudinal (lengthwise) parting, and thus it can be split into individual fibres (Gunter et al. 2007a).

The inadequate and incomplete definition of asbestos has resulted, as noted by the International Agency for Research on Cancer (IARC) Working Group, in «taxonomic confusion of lack of standardized operating definitions for fibres» (Kane et al. 1996; IARC 2012). In the regulatory community, the definition used by the Occupational Safety and Health Administration (OSHA), National Institute for Occupational Safety and Health (NIOSH) and World Health Organisation (WHO) for a regulated form of asbestos is limited to those structures which have certain size and shape characteristics: particles have to be longer than 5 μm and with a defined length-to-width aspect ratio of 3:1, under optical microscopy. IARC (2012) recommended that, apart from the different scientific views, the critical dimensions of the fibres of the regulated fibre standards to be used in toxicology and occupational regulations are based, with few exceptions, on the WHO (1997) fibre definition: aspect ratio ≥ 3:1, length ≥ 5 μm, diameter ≤ 3 μm using a phase-contrast optical microscope. The definition of the *aspect-ratio*, the relationship of the fibre length

to its diameter, generally helps analysts in the quantification of breathable fibres from the point of view of regulation and health. It should be noted that the aspect-ratio criteria were never meant to define a fibre, but they were developed only as counting criteria used to determine the amount of hazardous fibres in an industrial material, where it was known that the source of the material is generally a commercial asbestos product. The regulatory definition given by NIOSH has recently been integrated and published in a Bulletin entitled *"Asbestos Fibers And Other Elongate Mineral Particles: State Of The Science And Roadmap For Research"* (NIOSH 2011; Williams et al. 2013). In that contribution it is clear that all particles, including minerals in a non-asbestiform habit (e.g. acicular or prismatic fragments) may be counted as fibres when their length is >5 μm and aspect ratio is ≥ 3:1 under optical microscopy. NIOSH actually classified the term fibres by replacing it with the term *elongated mineral particles*, a term intended to include both asbestiform and non-asbestiform mineral habits that meet the specified dimensional criteria, according to the established protocol (NIOSH 2011). Moreover, there is a growing consensus that the regulatory definition of *"asbestos"* should be expanded to include other fibrous-asbestiform minerals with asbestiform habit that have been shown to cause diseases (e.g. fluoro-edenite asbestos, erionite) or which are potentially toxic to human (e.g. balangeroite).

Inhalation is the most important route of exposure of mineral fibres, that becomes causes of concern also in the case of exposition to natural deposits of asbestos (IARC 2012). Naturally occurring asbestos (NOA) is present in the natural environment – rocks and soils – as a result of geological processes. Weathering and human activity may disturb NOA-bearing rocks or soils and release mineral fibres into the air, which constitutes a potential greater risk to human exposure by inhalation. It should be noted that NOA refers to asbestos that has not been extracted and refined for commercial purposes, but rather to asbestos that has been exposed unintentionally by excavation, road grading, or mining. The disturbed NOA fibres are at risk of being dispersed into the air and off-site, especially if they are contained in soils of easily aerosolizable particle sizes, tracked out on construction vehicles, or located in dry, windy areas (Wagner 2015). NOA are characterized by a heterogeneous composition, consisting of intermixed fibres morphologies and mineral phases. Because of this complexity the analytical investigation of NOA requires a multidisciplinary analytical approach. In the natural environment, asbestiform amphiboles occur in relatively low quantities throughout the earth's crust, compared to serpentine chrysotile (Virta 2002). However, amphibole exposure is much greater than chrysotile one. This is due mainly to the fact that amphiboles are much more widespread than chrysotile (Gunter et al. 2007a).

The results of all the epidemiological cohort, *in vitro* and *in vivo* studies demonstrate that exposure via inhalation of asbestos minerals causes lung diseases, in particular asbestosis, lung cancer or carcinoma, and mesothelioma (Mossman et al. 1983; Kane et al. 1996; Boffetta 1998; Hodgson and Darnton 2000; Ross et al. 2008; Brown et al. 2012).

Asbestosis is a non-malignant diffuse interstitial fibrosis on the lung tissue. High asbestos exposure leads to scarring of the lung, causing it to become stiff, resulting in a restriction in pulmonary function and a reduction in the lung's ability to exchange CO_2 for oxygen. It is a typical lung disease developed after continuous exposure in the working environment with a latency period of about 10-20 years. *Lung cancer* includes squamous carcinoma, small or oat-cell carcinoma, and adeno-carcinoma. It is a typical lung disease provoked by a contaminated working environment with a latency period of about 15-20 years. *Malignant mesothelioma* (MM) is the cancer of the pleura, pericardium and peritoneal membranes which surround the lung, heart and abdominal cavities, respectively. Mesothelioma may developed as a consequence of exposure in both working and living environments with a latency period of about 20-40 years. In addition, the presence of benign plaques consisting of collagen deposits, sometimes calcified, in parietal pleura, may indicate the future development of asbestos diseases.

The fibrogenicity and carcinogenicity of asbestos fibres are now known to be related primarily to four factors: 1) a length greater than about 8 μm, as below this size the fibre can be easily removed by lung macrophages; 2) a fibre diameter less than about 3 μm, allowing the fibre to be inhaled into the gas-exchanging part of the lung; 3) fibre insolubility in the acidic lung milieu (pH = 4-4.5) developed during intracellular phagocytosis; 4) a sufficient dose to the target organ (Seaton et al. 2010). Thus, the pathogenic potential of asbestos depends also upon its biopersistence in the human body. *Biopersistence* is defined as the ability of a fibre (or a particle in general) to be *biodurable*, to persist in the lung, larynx, pleural and peritoneal linings to physico-chemical processes such as dissolution, leaching, breaking, splitting, and to survive physiological clearance (Oberdörster 2000; Bernstein et al. 2005; Utembe et al. 2015). Both *in vitro* techniques to determine fibre biodurability at different pHs and *in vivo* tests to determine the overall biopersistence in the lungs have been developed (Oberdörster 2000). At present, the global scientific community agrees that there is no evidence of a threshold level of exposure to asbestos fibres below which there is no risk of mesothelioma (Collegium Ramazzini 2011).

It has been largely demonstrated that different fibrous minerals have different toxicity (Fubini and Otero Arean 1999; Fubini and Fenoglio 2007). An analytical strategy to discriminate and characterize, with certainty, the different varieties of the asbestiform fibres is therefore a prerequisite. One of the main goal of this work is to test and compare the more traditional mineralogical and petrological methods, generally involved in the study of fibres minerals, in order to improve the diagnostic strategy required for the establishment of an effective environmental monitoring system.

Under humid tropical to sub-tropical conditions, weathering processes and supergene mineralizations are one of the main responsible for fibres release of asbestos minerals. Under these climate conditions, natural deposits of asbestos shall be subjected to a

further process of alteration. The New Caledonia proved to be a good example for the investigation of impact of supergene alteration on the genesis and release of fibres into the environment. The New Caledonia is one of the largest world producers of nickel ore which is formed by the alteration of ultramafic rocks. Almost all outcrops of geological units and open mines contain serpentine and amphibole, also as asbestos varieties (Lahondère 2007; DIMENC-SGNC 2010). The presence of fibrous minerals in mining exploitation and storage sites requires attention due to health problems and for the safety of operators. In the geological context of New Caledonia, mining companies must therefore deal with the problem of natural occurrence of asbestos.

On the basis of this starting point, the Thesis has been organized in 5 Chapters.

In the Chapter I, a picture of New Caledonia geographical and geological settings was depicted. In the last decades, an increasing awareness of asbestos health hazard due to environmental exposure was recorded. Mining activity, focused on nickel extraction from lateritic ore deposits, must deal with the natural occurrence of asbestos and fibrous minerals. In order to decrease the risk due to asbestos exposition, mining companies developed a monitoring prevention plan based on a visual *in situ* classification. Moreover, a brief description of New Caledonian legislation was realised. The regulation of New Caledonia is the only one in the world to classify the serpentine antigorite as asbestos.

Chapter II illustrates a brief digression on mineralogy of main serpentine and amphibole minerals involved in this study. In addition, a general description of performances of analytical methods involved has been made. Polarized light microscopy (PLM), X-ray powder diffraction (XRPD), scanning (SEM) and transmission electron microscopy (TEM) and micro-Raman spectroscopy were used in the investigation of the samples. Furthermore, a particular attention was dedicated to techniques which considered the possibility to employ a benchtop or a portable equipment, as XRPD and Raman spectroscopy. Studied samples, selected at different degree of alteration, include serpentines such as chrysotile, and fibrous antigorite, as well as tremolite-amphibole. Sampling was realized by the geological sector of mining companies using the mining nomenclature.

The Chapter III is dedicated to the mineralogical study of Caledonian mineral fibres. The analytical performances, advantages and limits, of the analytical techniques were compared. In addition, performances of a portable Raman equipment, to be used in field, were evaluated against other laboratory methods. A handheld Raman device was tested in laboratory to check its reliability. Moreover, all analytical methods were tested even in presence of strongly fibrous, altered samples to verify the impact of alteration on the goodness of the analytical data recorded. Finally, data obtained with analytical techniques have been compared with the identification realized on field, by mining geologists, employing visual morphological criteria.

In Chapter IV a preliminary geochemical investigation has been approached. A detailed study of chemical composition of mineral fibres at increasing degree of alteration was carried out. Analysis of major and trace elements were realized with ICP-OES and ICP-MS spectrometry, in order to evaluate the chemical signature of samples subjected to supergene alteration. Moreover, two batch-leaching experiments, aimed to simulate the weathering processes under a controlled environment, have been launched. The experiments will allow to evaluate the capability of the fibrous minerals to release or capture (absorption) heavy metals, mainly Ni, Co, Cr and Fe. The first experiment aimed to reproduce experimentally the rainwater action on antigorite, chrysotile and tremolite samples apparently not altered (minimum degree of alteration). During the second experiment a chelating chemical agent was used to force extraction. The objective was to observe the behaviour of samples under extreme conditions of extraction. Finally, the role of leaching processes in the physical-mechanical dissociation of rock fragments into fibres was evaluated.

Chapter V focused on the investigation of real environmental risk in mining context. Several tests were performed on ore deposit soils, to evaluate the presence (or not) of fibrous, potentially breathable, fibres in contaminated soils. Moreover, a portable Raman equipment was tested *in situ*, directly on the mining front, under normal environmental conditions (sun, strong wind, high temperature, etc.).

Résumé

Sous climat humide tropical ou subtropical, les processus d'altération supergène sont les principaux responsables de la formation et de la libération des fibres d'amiante dans l'environnement. Plus du tiers de la Nouvelle Calédonie est recouvert d'unités ultrabasiques altérées, riches en minerai de Ni. L'exploitation minière du Ni doit composer avec la présence d'affleurements d'amiante et de minéraux fibreux de type serpentine et amphibole. Dans ce contexte, les sociétés minières doivent prévenir les risques sanitaires liés à l'exposition environnementale aux fibres minérales. Actuellement, il n'existe pas de technique analytique capable de caractériser instantanément une fibre d'amiante *in situ*, en fournissant des informations sur la distribution de taille, la morphologie, la composition chimique et le degré d'altération associés. Cependant, la connaissance de tous ces paramètres est nécessaire pour évaluer le risque sanitaire associé à l'exposition. L'utilisation des dispositifs portable tels quels la spectrométrie Raman et la Microscopie Optique à Lumière Polarisée (MOLP) représente la stratégie la plus efficace pour améliorer l'acquisition et l'interprétation des données, y compris pour les échantillons fortement fibreux et altérés. De plus, des analyses géochimiques préliminaires ont révélé que l'effet mécanique de la circulation des fluides entre les fibres et lamelles, associé à la lixiviation chimique des éléments à l'interface

roche/eau, favorisent la dissociation des fibres et leur libération dans l'environnement. Un focus a été réalisé sur l'antigorite fibreuse, reconnue comme amiante uniquement dans la réglementation calédonienne.

Riassunto

In condizioni climatiche umide tropicali e sub-tropicali, i processi di alterazione supergenica sono tra i maggiori responsabili nella formazione e liberazione di fibre asbestiformi nell'ambiente. La Nuova Caledonia è ricoperta da più di un terzo della sua superficie da unità ultrabasiche alterate, ricche in minerali di Nichel. L'estrazione mineraria a cielo aperto deve perciò conformarsi con la presenza di minerali di amianto e minerali fibrosi del gruppo del serpentino e dell'anfibolo. In questo contesto, è compito delle compagnie minerarie prevenire il rischio sanitario legato all'esposizione ambientale. Ad oggi, non esiste una tecnica analitica capace di caratterizzare istantaneamente una fibra di asbesto *in situ*, fornendo informazioni sulla distribuzione dimensionale, sulla morfologia, sulla composizione chimica e sul grado di alterazione associato. Tuttavia, la conoscenza di questi parametri è indispensabile nella stima reale del rischio associato all'esposizione. L'introduzione di una strategia analitica semplice e immediata, basata sull'utilizzo di strumentazioni portatili quali la spettroscopia Raman e la Microscopia Ottica a Contrasto di Fase (MOLP-CF), si è dimostrata decisiva nella discriminazione e caratterizzazione delle diverse fasi, anche per quei campioni fibrosi più fortemente alterati. Analisi geochimiche preliminari hanno inoltre dimostrato come l'effetto meccanico della circolazione dei fluidi tra le fibre e lamelle, associato alla lisciviazione chimica degli elementi all'interfaccia roccia/acqua, favorisca la dissociazione delle fibre e la loro liberazione nell'ambiente. Una particolare attenzione è stata dedicata allo studio dell'antigorite fibrosa, classificata come amianto unicamente a titolo preliminare dalla legislazione caledoniana.

ASBESTOS HEALTH HAZARDS

IN NEW CALEDONIA:

A REVIEW.

I.1. An escalating awareness in asbestos health concerns

Natural occurrence of fibrous minerals in New Caledonia has been admitted for more than 20 years (INSERM U88 1997). Until recently, asbestos hazard and potential exposure of workers were differently managed according to professions - private earthworks, civil engineering, quarries, mines - and to geological exposure of employees (Trotet 2012). At national level the growing awareness of the risks linked to asbestos fits into a large-scale surveillance program, launched by the government of France, and focused on the evaluation of health hazard on the French continent. Haute Corse and New Caledonia result to be the largest French areas containing asbestos in ophiolite outcrops (ANSES 2010). For all these reasons, at the end of 2005, the government of New Caledonia decided to launch an expertise in order to better evaluate potential professional exposure. The combined work of major institutions and local authorities of New Caledonia (DASS-NC, Province, etc.) in cooperation with research organizations (BRGM, CNRT, UNC, Institute Pasteur, IRD) allows to improve knowledges about this complex subject. The creation of a detailed geological map of the natural occurrences of asbestos and fibrous minerals became a prerequisite. Thus, since 2007, a great work of survey of the different amphibole and serpentine (fibrous) varieties on the outcrops, usually connected to Ni-laterite deposits, was carried out (DIMENC-SGNC 2010; Lahondère 2007; Lahondère and Maurizot 2009). As a result, many outcrops of geological units in open mines contain serpentine and amphibole, also as asbestos. While tremolite-amphibole is mainly present in central and northern New Caledonia terranes, serpentine chrysotile and fibrous-lamellar antigorite occur in peridotites (Lahondère 2012). The huge variety of asbestiform minerals and their distribution over a large part of the island make environmental asbestos a major public health issue for New Caledonia.

I.1.1. ASBESTOS HEALTH RISK RELATED TO ENVIRONMENTAL EXPOSURE

Depending on the source of fibre emissions, three kinds of exposition are possible:
> *Industrial or (para-)professional* asbestos exposition includes all contacts with fibres emitted during factory-made processing: mining extraction operations, manufacturing of materials, production of thermal isolations, carriage of raw and/or final products. At present, the health risk value admitted by French regulation for professional exposition is over the threshold of 10 fibres per air litre (decree No. 2015/789). In urban context, *domestic exposition* results from the presence in air of fibres coming from the alteration and degeneration of various industrial materials commonly used by buildings industry. Conversely, into the *environment*, exposure is directly related to the presence of geological outcrops containing asbestos and/or fibrous minerals. Also in this case, people may be directly impacted in their everyday life.

Risks connected with exposure to domestic and environmental emissions of fibres are still not thoroughly investigated (ANSES 2010). It should be noted that airborne asbestos may be released from naturally occurring asbestos deposits and, absent appropriate engineering controls, may pose a potential health hazard if these rocks are crushed or exposed to natural weathering and erosion or to human activities that create dust (Lee et al. 2008). Natural contexts can be thus considered as unconfined sites of study with a great intrinsic diversity, not only related to the environmental source but also to the potential activities that can cause the suspension of pathogenic fibres. The core of the issue is whether the risk parameters associated with exposures to commercial asbestos can or should not be applied to all potential sources of passive exposition. Lee *et al.* (2008) emphasize how difficult it is to reliably correlate the presence of mineral outcrops belonging to the asbestos family and the impact on health. On the contrary, this ambiguity does not exist during occupational exposures because of direct manipulation of fibres (e.g. industrial materials) or operation producing suspension of fibres (e.g. mining). Authors insisted on the fact that the risk assessment methodology and the analytical technology needed to support inferences on passive exposition are available, but have not yet been organized and implemented as necessary to resolve the controversy of environmental (or domestic) exposition to asbestos (Lee et al. 2008). Furthermore, Berman and Crump (2003) highlight that none of the terms used in professional framework to define an asbestos can be actually reflected the associated risk for health. In regulations, in fact, asbestos definitions are based exclusively on morphological and dimensional criteria, and they do not take sufficient account of physical-chemical properties of fibres that control reactions in human body. In environmental contexts, exposure is due to a large diversity of fibrous minerals whose impact on the health of exposed people is much greater than the regulated asbestos minerals (Gazzano et al. 2005; Groppo et al. 2005; Turci et al. 2005). This results in a greater variability of the chemical compositions and physical properties of the fibres emitted and therefore a different reactivity of the organism for each case (Fubini and Otero Arean 1999; Fubini and Fenoglio 2007). Furthermore, to be more accurate, the term asbestos refers only to six fibrous minerals initially exploited by industry and currently classified as dangerous by most of institutions or organisations for occupational safety and health (e.g. IARC, NIOSH, WHO, SIA).

It is worth noting that, in nature, minerals belonging to asbestos families can appear (fortunately!) in a cohesive, indurated, not-fibre-emitting form (Lahondère 2012). In that precise moment, the identification of these mineral phases in geological sites is therefore not significant in terms of health risk assessment.

In order to identify the effects of environmental asbestos related to domestic exposure of New Caledonian populations, several epidemiological studies were conducted on mining sites and municipalities more impacted by mesothelioma and pleural cancer cases

Figure I.1. Typical examples of Melanesian house in New Caledonia, where the wooden structure is covered (internally and externally) by walls of raw earth and tremolite-Pö whitewash. Strong alteration and leaching are visible on the parts exposed to weather (Quénel and Cochet 2001).

(Goldberg et al. 1991, 1995, Luce et al. 1994, 2000, 2004, Baumann et al. 2007, 2011; Houchot 2008). The highest rate of mesothelioma diagnosis was limited to Melanesian group, both male and female, predominantly in rural areas. Here, the most significant air concentrations of asbestos fibres were identified near the houses, on tracks, during whitewash mixture preparation, and inside houses during housework activities. Luce *et al.,* (2004) report some concentration values of tremolite fibres up to 39 fibres/litre (24h exposure time) in indoor domestic context. Outdoor, near the houses, these concentrations were lower but could reach 12 fibres/litre (24h exposure time). The use of Pö, a traditional white-coloured wall covering purely composed of asbestiform tremolite-type amphibole, was at the origin of asbestos diseases (Fig. I.1; Quénel and Cochet 2001; Luce et al. 2004). In addition, further statistical data correlated to epidemiological studies display how the presence of fibrous serpentine in tracks and soils represents one of the main significantly factors connected to mesothelioma (Baumann et al. 2007, 2011; Lahondère 2007). The lack of comprehensive scientific data on toxicology of non-regulated fibrous minerals helps to understand difficulties in assessing the potential risk due to environmental exposition.

In addition, recent studies have demonstrated how asbestos exposure has a negative impact not only on physical health, but also in psychological and community components of populations. Members of a community exposed to asbestos develop a subjective perception of themselves as impotent and alone in face of the illness and death (e.g. Eternit Factory, Casale Monferrato, Torino, Italy; Granieri 2015).

I.1.2.   THE ASBESTOS REGULATION IN NEW CALEDONIA

On 25 August 2010, the Government of New Caledonia legislated and promulgated his first regulation on asbestos materials. Modifying previously labour code, the decree No.

2010/82 (*Déliberation N°82 du 25 Aout 2010*) requires the establishment of a risk card for workers and a number of constraints for employers, especially in terms of identification of asbestos and quantification of fibres emitted.

In contrast to European and worldwide legislations, New Caledonia decree classifies serpentine antigorite as asbestos, but it fails to mention the amphiboles amosite, actinolite, anthophyllite and crocidolite (Table I.1). This directive is the first in the world to introduce a new fibrous mineral in regulations. Moreover, it is important to remember that no one code makes difference between antigorite and fibrous-asbestiform antigorite. In addition, no standard samples - provided for example by UICC Cancer Global Control - exist for measurement of airborne antigorite fibres concentration, which lead to some difficulties in asbestos risk prevention and management.

Moreover, legislative text of New Caledonia does not indicate any analytical method for the identification and quantification of fibres emitted. Any decision in this respect remains related to French regulation. Within the context of French legislation, in April 2012, a decree *ad hoc* was promulgated to state NF X43 269 as the reference standard on sampling and complete characterisation of the six-regulated asbestos fibres. This reference describes the analytical techniques and related procedures provided for air quality investigation in workplaces containing asbestos (e.g. diaphragm filter sampling, fibre counting). Transmission and scanning electron microscopies, coupled to energy-dispersive X-ray spectroscopy (TEM-EDS and SEM-EDS), associated with phase light microscopy (PLM) are the three methods clearly indicated by the norm to identify and quantify asbestos fibres in materials (ACMs). Normally involved in standardized recognition and counting of asbestos fibres in ACMs specimens, PLM has the only disadvantage to not determine the chemical nature of the observed fibres. Moreover, the observation of fine sub-micrometric asbestos-particles is possible only by means of electron microscopy devices. Due to its high performances, TEM microscopy allows to acquire at the same time an image giving the size (the size distribution) and the

		SERPENTINE		AMPHIBOLE				
		Antigorite	Chrysotile	Amosite	Actinolite	Anthophyllite	Crocidolite	Tremolite
	2003/18/CE		✓	✓	✓	✓	✓	✓
	Délibération 82 du 25 Août 2010	✓	✓					✓
	NF X43 269		✓	✓	✓	✓	✓	✓
	D.Lgs. n257 del 25/07/2006		✓	✓	✓	✓	✓	✓
	AHERA-TSCA Title II		✓	✓	✓	✓	✓	✓

Table I.1. Definition of asbestos minerals by major regulations around the world. New Caledonia is the only country to classify serpentine antigorite as asbestos.

morphology of the characterized particles, their crystallographic structures (SAED - electron diffraction mode) and finally their chemical compositions (EDX detector). It is, therefore, the most complete methodology in asbestos characterisation. For this reason, since 2012, TEM results as the reference technique for the standardized counting of asbestos particles. Unfortunately, this technique presents some non-negligible disadvantages, one of which is the impossibility to became a routinely technique.

Finally, the New Caledonian decree No. 2010/82 does not report any indication about environmental exposure issue. Actually, an exhaustive regulatory framework dedicated to environmental exposure, made up of specific regulatory requirements, codes of practice and regulatory guidance, is still lacking. With respect to air measurement in outdoor work conditions, for example, most sampling parameters (e.g. type of filter, type of device, flow rate, volume and duration of sampling) are not universally and equally applied by laboratories. In common practise, operators adapt from time to time any parameter to different natural environment situations (meteorological conditions, expected variation in concentrations, distance from the source of emission), referring to French decree NF X43 050 specifically designed to ACMs (January 1996, NF X43 050: *Air quality. Determination of the asbestos fibre concentration by transmission electron microscopy. Indirect method.*). For these reasons, specific studies must be carried out by specialized laboratories in order to introduce more appropriate diagnostic methods and protocols.

As a consequence of the entry into force of the new regulation, asbestos issue became a problem of public domain in New Caledonia. A good surveillance program, which should involve some measures of management, has become imperative. By definition ANSES (2010), a complete monitoring prevention plan in environmental exposition context concerns:

a) the realization of mapping at the regional and/or municipal level;
b) the dissemination of requirements related to ongoing work on soils containing asbestos;
c) an information campaign of potential and real risks meant for populations and institutions (governments, municipalities, building societies, etc.);
d) an assessment of the real exposure risk for populations living in proximity of natural outcrops; and finally
e) a medical surveillance strategy.

At present, only few countries, such as USA and Italy (Emilia Romagna plan prevention), present a regulated procedure defining management protocols. Conversely, other countries delegate to specialized institutions and/or laboratories the improvement of existing procedures. The French government has commissioned BRGM (Bureau de Recherches Géologiques et Minières) geologists for this purpose. In this respect, in

recent years several fine maps from 1/10000 to 1/25000 were realized by experts geologists in France, Upper Corsica and New Caledonia (ANSES 2010; DIMENC-SGNC 2010).

Good regulations should be a model for using science as a tool in the management of risk related to exposure of mineral fibre dusts. The first benefit of a correct decision-making strategy is the development of the professional-mining activities in safety. To provide useful measurements for management, the only strategy possible is monitoring risk areas, involving correct identification of asbestos fibres, mapping, epidemiology inquiries, studies of density population in hazardous areas, analysis of air quality. As well an exhaustive toxicology investigation of all asbestiform fibres is therefore necessary.

I.2. Geographical and geological breakdown of asbestos

The New Caledonia is located in the southwest Pacific Ocean, 1500 km east from Australia, 2000 km north from New Zealand and cover a land area of 18575 km^2. Covered by ultrabasic units for more than a third of its surface, it is one of the largest world producers of nickel ores (Fig. I.2).

I.2.1. GEOLOGICAL SETTING OF NEW CALEDONIA

Placed along the Circum-Pacific Belt, in a complex set of marginal basins and continental or volcanic ridges, New Caledonia is composed of several islands that are parts of the Norfolk and Loyalty Ridges. The main island *Grande Terre*, together with Belep Islands (to north) and Isle of Pines (to south), lies at the Norfolk Ridges, which is composed by a mosaic of volcanic, sedimentary and metamorphic terranes. Conversely, the Loyalty Islands, running more or less continuously parallel to the Norfolk Ridge, represent the emerged part of the sinuous submarine Loyalty Ridge. Generally considered to be an Eocene island arc, their geology is actually still poorly known, due to the lack of basement outcrops and a thick carbonate cover (Cluzel et al. 2001).
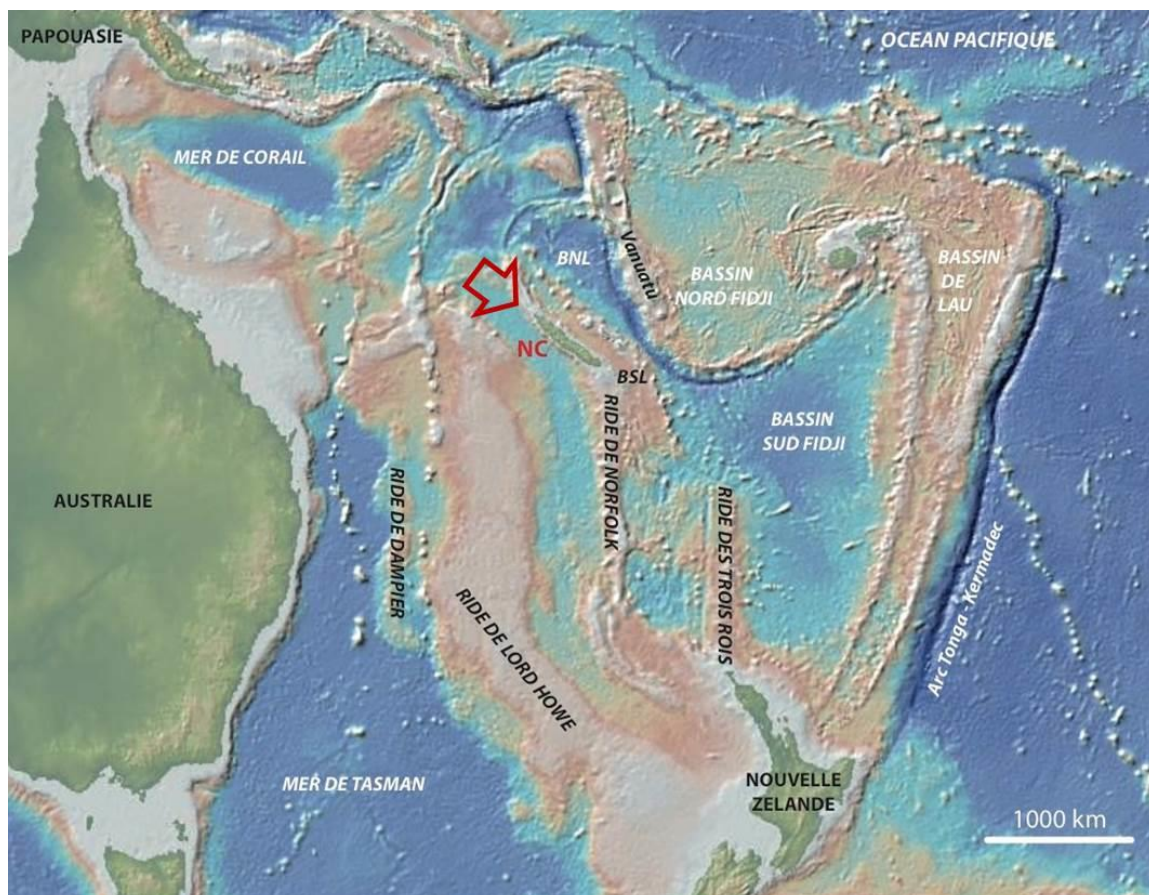

Figure I.2. Geological setting of the archipelago of New Caledonia (GeomapApp® software, after Ulrich 2010). NC: New Caledonia; BSL: South-Loyalty Basin; BNL: North-Loyalty Basin.

The geological evolution of New Caledonia may be divided into three major events, starting from the Early Permian period. The Gondwana phase, the oldest one, occurring during the Permian-Early Cretaceous, is related to the evolution of the south-east Gondwana active margin, and the Mesozoic marginal basin opening and subsequently closure. The Koh terrane, Teremba terrane, Boghen terrane and the central chain unit, constitute the current relics of this first geological phase (Fig. I.3). During the Late Cretaceous-Eocene, a rifting event produced the isolation of slices of the older Gondwanaland margin, and its subsequent extension into the Cenozoic convergence. The Diahot and Pouebo terranes are the witnesses of the convergent activity. The collision between the Loyalty island arc with the Norfolk continental ridge stopped the subduction and led to the Late Eocene obduction (ultrabasic unit, Collot et al. 1987; Aitchison et al. 1995; Cluzel et al. 2001). Finally, during the post-Eocene, New Caledonia definitely emerged. This episode mainly correspond to the development of regolith that, associated to minor tectonic events, led to the present morphology and development of supergene nickel ores (Cluzel et al. 2012). Chevillotte *et al.,* (2006) date the nickel ores formation of New Caledonia during the Neogene, by tropical weathering of the large allochthon nappe of ultramafic peridotites (Fig. I.4).
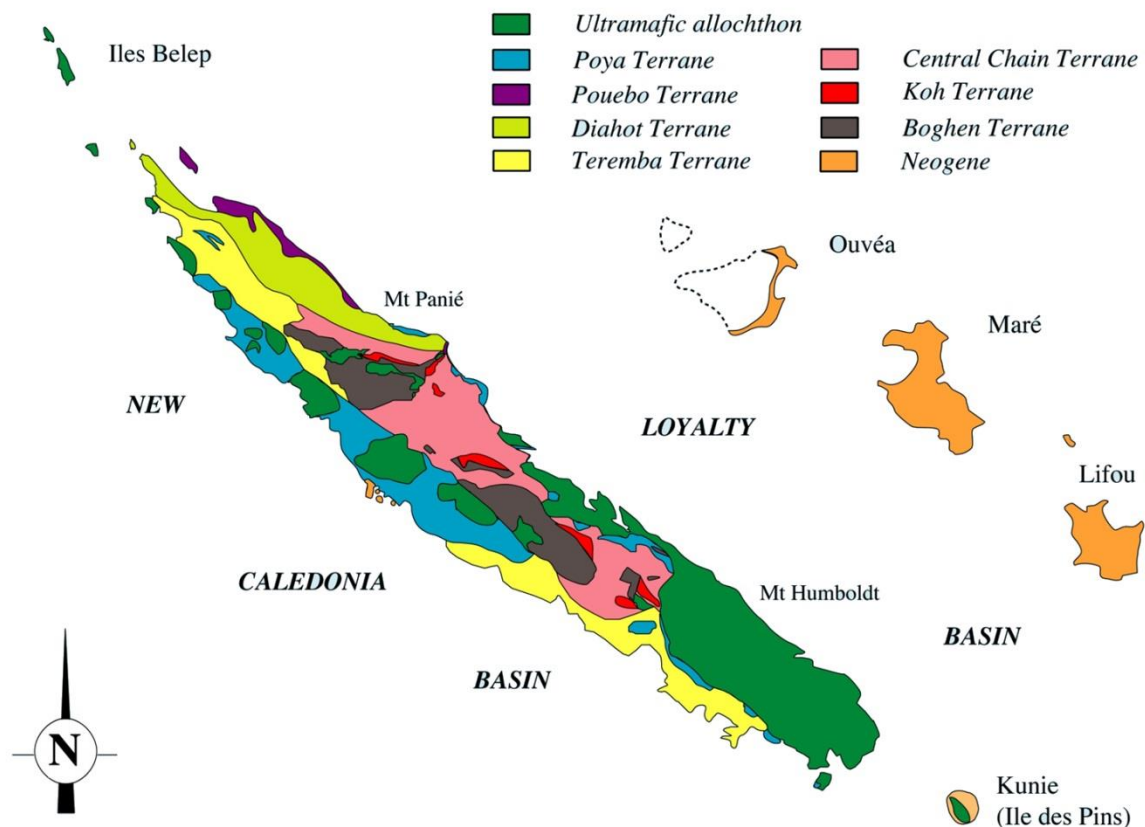

Figure I.3. Geological map of New Caledonia (modified after Cluzel et al. 2001).
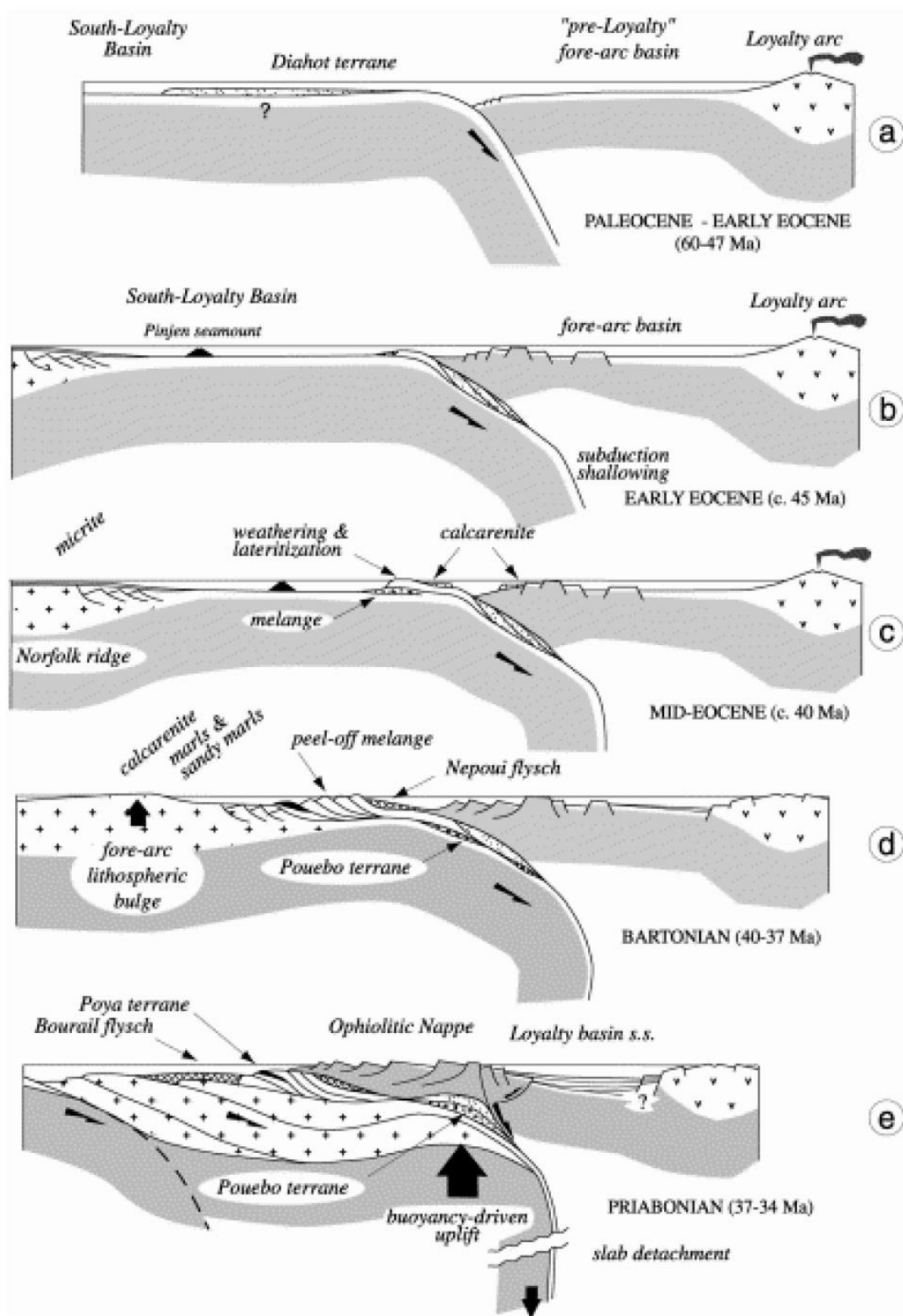
Figure I.4. Synthetic view of the evolution of the Eocene accretion/subduction complex of New Caledonia (not to scale; modified after Cluzel et al. 2001).
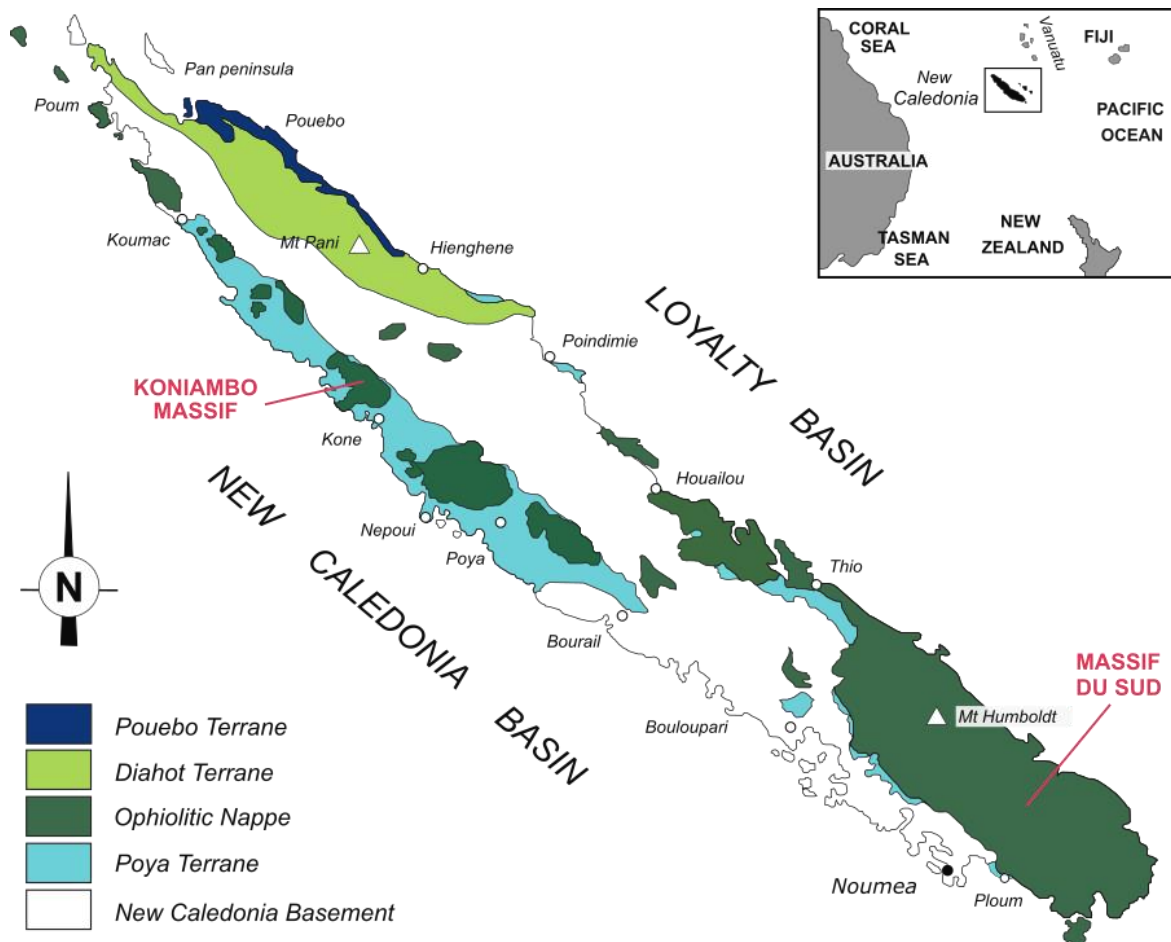
Figure I.5. Geological sketch map of the ultramafic allochthon of New Caledonia (modified after Cluzel et al. 2001).

The origin of the New Caledonia ophiolite, one of the largest and best-exposed continuous peridotite complex in the world, is still debated. The peridotite nappe overlies the "proto New Caledonian continent", resulting from the complex geological stories of the Mesozoic margin, after the Cenozoic convergence. The ultramafic peridotite complex, 300 km long, 50 km wide and 2 km thick, is certainly the most prominent terrane of New Caledonia (Ulrich et al. 2010). It is composed of a main massif – *Grand Massif du Sud* – located in the southernmost part of the island, and several tectonic klippes isolated by the erosion along the west coast (e.g. Koniambo Massif; Fig. I.5). This unit is dominantly formed of partially to totally hydrated upper mantle rocks, harzburgite-dunite and rare spinel- and plagioclase- lherzolite, with minor ultramafic (pyroxenite, wehrlite) and mafic cumulates (layered gabbros; Prinzhofer 1981). The allochthonous unit is largely fractured and crosscut by basalts, dolerites, micro-diorites and various felsic dykes at all levels. Locally, amphibole lenses, about 200 m length and 10-50 m wide, appear at the base of serpentinite, above Poya basalt (Cluzel et al. 2012). As a consequence of cooling and low temperature hydration of the oceanic mantle lithosphere, the degree of serpentinization may range from 20 to 60 volume%.

In addition, a more extensive serpentinization occurs also at the basal layer of the Peridotite Nappe, the *tectonic serpentinite sole*, consisting of a porphyroclastic mylonite (20-200 m thick) which likely formed during obduction (Avias 1967; Orloff and Gonord 1968; Rawling and Lister 1999; Cluzel et al. 2012; Lagabrielle et al. 2013).

I.2.2. OCCURRENCE OF ASBESTIFORM MINERALS IN THE GEOLOGICAL UNITS OF NEW CALEDONIA

As mentioned above, since 2007 a great work of survey of asbestiform minerals was carried out on the field, mapping in detail the type of occurrences, the alteration status and potential dispersion of mineral fibres naturally occurring at the outcrops (BRGM-LEPI-INSERM-Lahondère 2007). Mapping operation constantly evolves, adding more information from year to year. As clearly shown in figure I.6 almost all outcrops of geological units in open mines contain serpentine and amphibole, also as fibrous varieties (Lahondère 2007; DIMENC-SGNC 2010). According to the current understanding, the Boghen terrane in the central unit, the ultrabasic complex related to mining context, and the northern metamorphic complex of the Grande Terre Island, are the three geological units most impacted by the presence of asbestiform mineral fibres (Lahondère 2007, 2012).

In the central chain unit, the presence of dykes of serpentinites occurs mainly at the Boghen and Ouango-Netchaot massifs. The metasedimentary Boghen unit is composed of several more or less extensive isolated massifs made up of serpentinites. Here, asbestiform tremolite-amphibole in association with secondary chrysotile is largely observed (e.g. Houaïlou; Cluzel and Pelletier 1994). In addition, a small amount of potentially asbestiform fibres of serpentine, subjected to a high degree of alteration, was detected close to Ouégoa (Lahondère 2007).

In ultrabasic units, instead, the more or less serpentinized peridotite assemblages show the widespread presence of serpentine minerals combined with minor amount of tremolite-amphibole. Generally, serpentinized peridotites, occurring in the serpentinite sole, at the base of lateritic profile, are cut by large fault planes with prismatic-lamellar crystals from centimetres to decimetres. These planes appear fresh and lamellae are parallel and welded together. Conversely, at the top of lateritic profile, close to pedolitic horizons, these blades become more altered, fragmented and associated with fibres that seem to be originated from the extreme cleavage (fraying) of these same lath-shaped crystals. They are largely interpreted as crystallizations of antigorite. Several veins, from millimetre to centimetre, of chrysotile may also occur (Lahondère 2007, 2012; Ulrich 2010; Quesnel 2015; Quesnel et al. 2016).
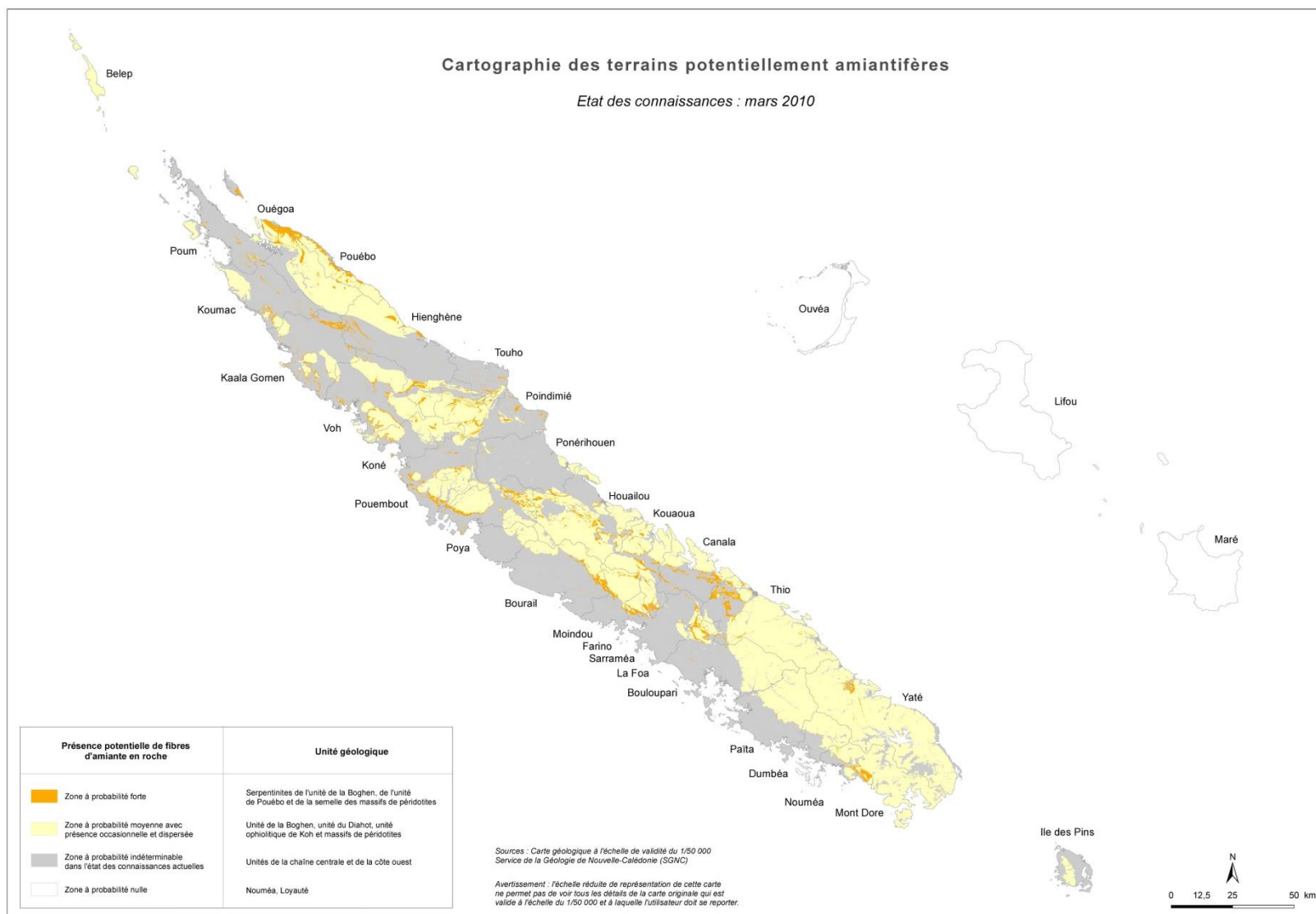
Figure I.6. Geological map of natural occurrence of asbestiform minerals in New Caledonia terrains (DIMENC-SGNC, BRGM 2010).

Finally, the northest metamorphic complex consists of a set of gneiss and mica schists corresponding to a complex assemblage of sediment, basalt and ultrabasic rocks; it is also characterized by the presence of glaucophanites and eclogites. Several veins of secondary chrysotile can be observed. Soapstone (or steatite) blocks also occurs. Occurrences of minerals of the tremolite-actinolite series are frequently reported in literature. Conversely, the presence of fibrous-asbestiform varieties of this family has been underestimated (Cluzel et al. 1995; Carson et al. 2000; Marmo et al. 2002).

In order to evaluate the real risk related to exposition to mineral fibres, this descriptive phase of investigation has to be supplemented with an accurate metrology study to the determination and quantification of fibres on rocks, on solid materials (soils, renders) and on air (air measurements).

I.3. The ultrabasic units, source of Nickel ores

New Caledonia's mining industry depends upon the nickel contained in weathered peridotites. Ni-laterite deposits are characterized by an absolute enrichment of concentration of nickel in the saprolite zone, which consist of serpentine, neo-formed goethite, smectitic clays and garnierite. Much of the nickel is re-precipitated within the saprolite by substituting Ni for Mg in secondary hydrous silicates (which can contain up to 5 wt.% Ni) and in neo-formed silicate, the garnierite, which can grade over 20 wt.% Ni (Pelletier 1996; Butt and Cluzel 2013).

I.3.1. Ni-LATERITE ORE DEPOSITS

I.3.1.1. General processes and classification

Nickel laterite ores are the product of intensive deep weathering of ultramafic rocks, under humid tropical to sub-tropical conditions. They account for nearly 60% of the world's nickel production, and they still remain the major source of Ni in the foreseeable future. Nickel grade is generally over 1 wt.% and is hosted in a variety of secondary oxides, hydrous Mg-silicates and smectites (Butt and Cluzel 2013).

Lateritisation involves the breakdown of primary mafic minerals and release of their chemical components into groundwater, leaching of mobile components, residual concentration of immobile or insoluble components, and formation of new minerals which are stable in the weathering environment (Table I.2). All these processes combined together produce a vertical succession of horizons of differing chemistry and mineralogy: the laterite profile. The structure of laterite profile is governed by the differential mobility of the elements in the weathering zone. The detailed structure of a regolith (i.e. the weathered rock) may varies greatly, and in any one place it is the result of the dynamic interplay of climatic and geological factors such as topography, drainage, tectonics, structures and parent rock lithologies. The capture of nickel by neo-formed minerals produced by the alteration of primary minerals under the new environmental conditions leads to nickel enrichment to ore grade (Elias 2002).

A typical weathering profile shows, by definition, some or all of the following horizons, from the protolith to the surface: bedrock, saprock, saprolite, plasmic zone, mottled zone or ferruginous earthy saprolite, lateritic residuum (ferruginous and/or aluminous duricrust or cuirasse) and soil (Fig. I.7; Eggleton 2001). Here saprolite may comprise over 80% of the total thickness of the profile. Only the horizons containing some significant concentrations of nickel are commercially defined as Ni-laterites.

GENERAL PROCESSES	… IN ULTRAMAFIC ROCKS
1. Leaching of mobile constituents: alkalis, alkaline earths	Breakdown of olivine, pyroxene, serpentine and leaching of Mg, Ni, Mn, Co
2. Formation of stable secondary minerals: Fe and Al oxides, clays	Goethite formation, smectite formation, absorption of Ni from solution
3. Partial leaching of less mobile components: silica, alumina, Ti	Leaching of silica in rainforest and moist savanna climates
4. Mobilisation and partial re-precipitation of redox-controlled constituents: Fe, Mn	Precipitation of Mn oxides and absorption of Ni and Co from solution
5. Retention and residual concentration of resistant minerals: zircon, chromite, quartz	Residual chromite concentration

Table I.2. Main processes of chemical weathering and their effects in ultramafic rocks (Elias 2002).

Depending on the dominant Ni-host mineralogy, Ni-laterite deposits are classified into three main ore types: oxide or limonitic deposit, hydrous Mg-silicate deposit, and smectitic or clay mineral deposit. Most of nickel lateritic profiles have two ore types, an oxidant component and either an hydrous silicate component or a clay component (Brand et al. 1998; Berger et al. 2011). Because of distinct industrial processes of extraction required for the different mineral hosts, the largest mines tend to exploit only one type of mineralisation.

Dominated by Fe oxy-hydroxides such as goethite, αFeOOH, *oxide or limonitic deposits* occur in the middle to upper zones of the weathering profile. Here, nickel is hosted mainly in goethite, by the substitution for Fe and/or by absorption processes. The overlying upper plasmic zone and vesicular-nodular duricrust are leached, and rarely contain more than 0.03 wt.% Ni. Downwards, the transition from saprolite containing Ni-rich ferruginous oxide ore to lower saprolite and saprock is marked by a sharp increase in MgO content, from less than 2 wt.% to more than 20 wt.% (Mg-discontinuity) and an increasing abundance of silicates, such as secondary serpentine, some other hydrous silicates, smectites and residual primary minerals (Fig. I.7). Many oxide deposits contain abundant secondary silica, such as chalcedony and quartz. Silicification is a common weathering product of ultramafic rocks, especially in dunites and serpentinized dunites, in which the low Al content prevents the formation of clay minerals (Butt and Cluzel 2013).

Hydrous Mg silicate deposits are the highest-grade deposits (locally 2 wt.% to more than 5 wt.% Ni) and, historically, represent the majority of Ni-lateritic ores. They form in the lower part of the weathering profile, in the saprolitic zone, usually in the form of bright green-coloured assemblages, commonly referred to as "garnierite". Composed by Ni-rich Mg-talc and serpentine-like minerals, garnierite is not a single mineral but a mixture of poorly-ordered talc (willemseite), smectite (simelite-kerolite series) and serpentines
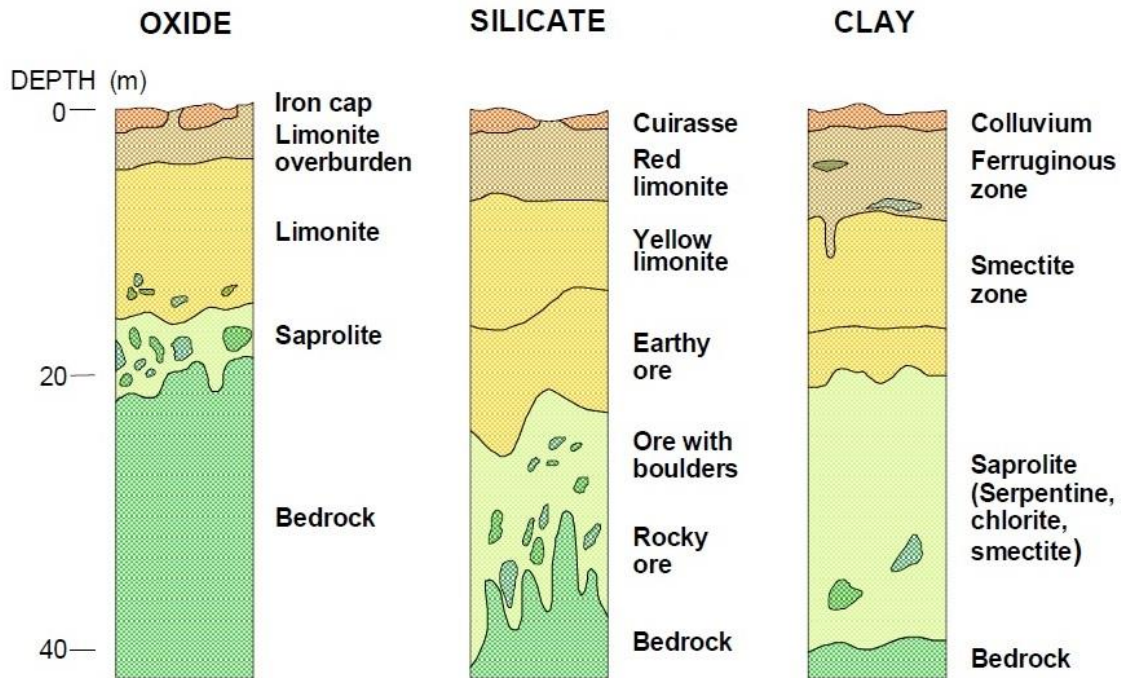
Figure I.7. Lateritic profiles developed on serpentinized ultramafic rocks showing the main Ni-laterite ores (modified after Elias 2002).

(pecoraite-lizardite series); these minerals have a composition that varies from magnesian to nickeliferous end-members (Fig. I.7; Brindley and Hang 1973). These deposits are typical of the *accretionary terranes* of the Circum-Pacific Belt, the Caribbean and Balkans, on serpentinized dunite-harzburgite peridotites (ophiolites). The tectonic activity of these environments, especially the effects of uplift, results in a regolith with greater drainage that promotes the formation of hydrous Mg-silicate deposits, but high erosion rates may limit their thickness and degree of preservation. The nature and abundance of hydrous Mg-silicates developed in free-draining environments is also strictly related to serpentinization degree of peridotite bedrock (Golightly 1979; Pelletier 1996). In fact, in rocks not serpentinized, oxide-rich deposits with rare hydrous silicates are more common. In weakly to moderately serpentinized rocks, the silicate zone is thicker and consists predominantly of neo-formed garnierite as veins, fracture-filling and coatings, and Fe-Mg smectites formed from olivine. However, Ni is also hosted by altered primary lizardite, where it is exchanged for Mg in octahedral sites (Manceau and Calas 1985). In highly serpentinized rocks, Ni-rich altered lizardite is the main ore minerals.

Clay mineral deposits generally take place in *cratonic terranes* from serpentinized peridotitic bedrock. They consist of Ni-bearing swelling clays, where Ni-rich saponite and smectite (nontronite, Fe-montmorillonite, etc.) occur in the middle to upper saprolitic and pedolitic horizons and form the main ore minerals (Fig. I.7). Although the presence of thick Ni-bearing clays in regolith has long been known, Ni-laterite deposits constituted by

clay minerals have only recently been recognized and exploited as ore deposit (Elias et al. 1981; Monti and Fazakerley 1996; Elias 2002; Kadır et al. 2015).

I.3.1.2. Ni deposits of New Caledonia

Historically, most of the Ni production from lateritic ores came from the rich deposits of New Caledonia, which have been mined since 1875. Dates back to the early 20th century, the establishment of the Thio mine is the most ancient nickel exploitation site of the island and the first in the world. Its own Ni-extraction mining activity is currently in operation.

Ni-laterite deposits of New Caledonia were formed during the Miocene-Pliocene by lateritic weathering of obducted harzburgite-dunite peridotite nappe, in which both residual and absolute economic nickel concentration have resulted from supergene enrichment (Troly et al. 1979; Chevillotte et al. 2006). Ni-laterites formation starts with the emplacement and serpentinization of the ultramafic protolith, followed by exposure to a humid sub-tropical climate and the development of a deep intensely weathered regolith. During this phase, Ni is concentrated in goethite and/or smectite and, because of the loss of Mg and Si, enrichment is largely residual. Subsequently, these deposits were subjected to further tectonic and/or climatic changes. Where uplift was considerable, loss of materials by leaching, and/or erosion, increased. This process is offset, economically at least, by the continuous weathering and enrichment of Ni in neo-formed hydrous Mg-silicates in the surviving regolith. Consequently, the current nickel deposits are the remnants of the large regolith that initially wrapped the whole island and was removed during the recent episodes of positive epeirogenesis and the variation of sea level (Chardon and Chevillotte 2006; Chevillotte et al. 2006). These geological events have led to a complex weathering profile. From not-weathered peridotite to the top of the regolith the various horizons are: bedrock, saprock (rocky ore and earthy ore), saprolite, soft yellow limonite (a clay soil rich in Fe-oxide), red limonite (a clay soil containing small grains of Fe-oxide) and finally cuirasse (Fig. I.8, Cluzel and Vigier 2008; Sevin 2014).

As clearly shown in figure I.8, spheroidal-type weathering is very common in New Caledonia, where saprolite consists of millimeter- to decimeter-scale blocks, and the intensity of weathering increases from core to edge. Partly weathered primary lizardite, in which Mg has been exchanged by Ni, is a significant host mineral in many deposits (Golightly 1979; Pelletier 1996). In addition, Ni is hosted by a wide variety of neo-formed silicate minerals, some of which can be very rich in Ni (3-40 wt.% Ni). Many of the neo-formed silicate minerals occur as boxworks and veins, in place with secondary silica, following shears, joints and grain boundaries and precipitated as coatings on the
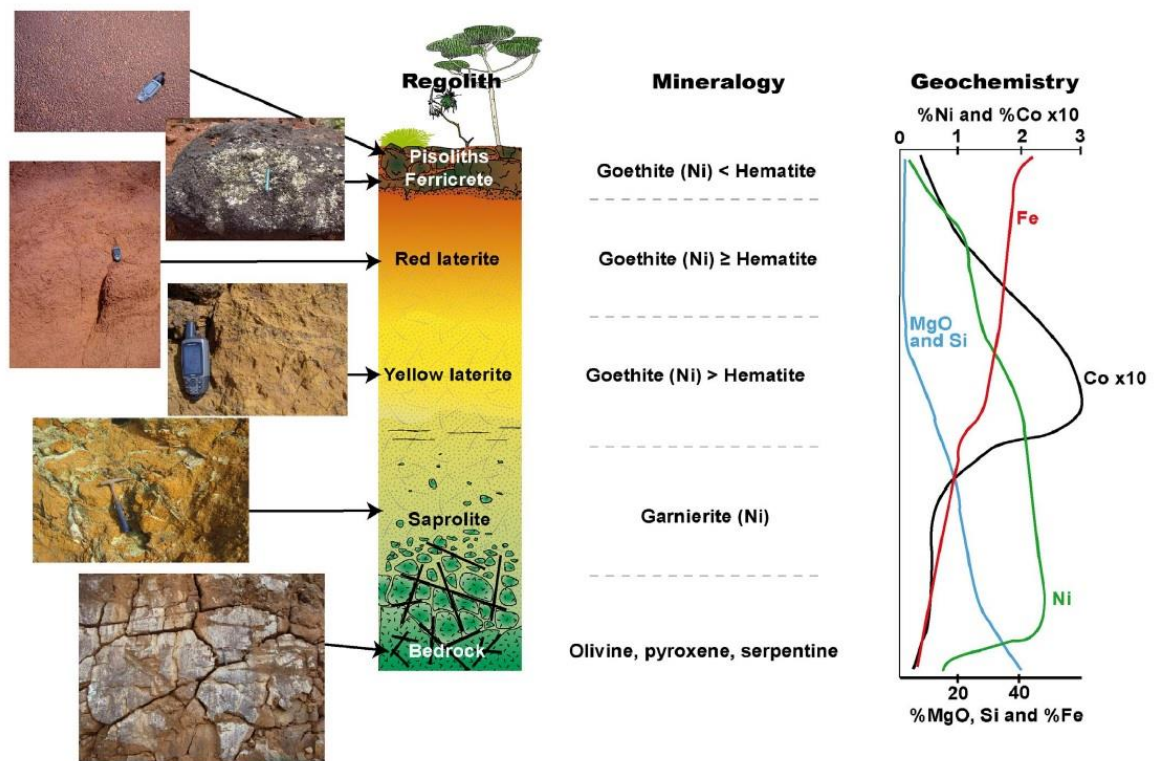
Figure I.8. Schematic lateritic weathering profile of New Caledonia regolith, including selected field photographs, geochemistry and mineralogical information (Sevin 2014).

saprolite blocks (Table I.3). In other hand, the decrease of Ni content from the bottom to the top of the lateritic profile seems to be related to the increase of goethite crystallinity (Dublet et al. 2015). Owing to the high relief and the high erosion rate, the thickness of regolith in New Caledonia rarely reaches 40 m; silicate ores are 10-15 m thick. Where preserved, the upper parts of the profile are similar to those of oxide deposits, showing a cuirasse (Freyssinet et al. 2005; Wells et al. 2009; Golightly 2010; Butt and Cluzel 2013). For the features described above, these Ni-laterite profiles are typically classified as both oxide-ore and/or hydrous Mg-Ni-silicate deposits. Mining company at Goro (south of New Caledonia), for example, plans to exploit both mineralisation types.

Mine geologists generally called *"garnierites"* any green, Ni-rich, mineral phase and *"dewellite"* any whitish material with only a few wt.% Ni (Cluzel and Vigier 2008). The nickeliferous serpentine end-member is often called nepouite (Pelletier 1996). Many other minerals are present in the nickel ores of New Caledonia; most of them are silicates (montmorillonite, sepiolite, saponite, amesite, chlorite, and phlogopite) and oxides with a typical green colour and containing variable amounts of Ni, from a few tens up to 40 wt.% (Tab. I.3, Cluzel and Vigier 2008; Butt and Cluzel 2013). Serpentine minerals are commonly found in saprolitic zone currently mined in New Caledonia, also as asbestos varieties, owing to their ability to withstand better the oxidation processes (Lahondère 2012; Trotet 2012).

OXIDE ORE

Goethite	Oxide	$\alpha\text{-}(Fe^{3+})O(OH)$	2% Ni, 0.2% Co
Asbolane	Oxide	$(Ni^{2+},Co^{3+})_xMn_4{+}(O,OH)_4\cdot nH_2O$	16% Ni, >4% Co
Lithiophorite	Oxide	$(Al,Li)Mn_4{+}O_2(OH)_2$	1% Ni, ~7% Co

HYDROUS Mg-SILICATE ORE

Ni lizardite - népouite	Serpentine	$(Mg,Ni)_3Si_2O_5(OH)_4$	6–33% Ni
7Å garnierite	Serpentine	Variable, poorly defined	15% Ni
Nimite	Chlorite	$(Ni_5Al)(Si_3Al)O_{10}(OH)_8$	17% Ni
14Å garnierite	Chlorite	Variable, poorly defined	3% Ni
Falcondoite	Sepiolite	$(Ni,Mg)_4Si_6O_{15}(OH)_2\cdot6H_2O$	24% Ni
Kerolite-willemseite	Talc	$(Ni,Mg)_3Si_4O_{10}(OH)_2$	16–27% Ni
10Å garnierite	Talc	Variable, poorly defined	20% Ni

CLAY SILICATE ORE

Nontronite	Smectite	$Na_{0.3}Fe_2{}^{3+}(Si,Al)_4O_{10}(OH)_2\cdot nH_2O$	~4% Ni
Saponite	Smectite	$(Ca/2,Na)_{0.3}(Mg,Fe^{2+})_3(Si,Al)_4O_{10}(OH_2)\cdot4H_2O$	~3% Ni

Table I.3. Primary ore minerals present in Ni-laterite deposits (Ni and Co in wt.%; Butt and Cluzel 2013).

I.3.2. ASBESTOS OCCURRENCES IN THE ULTRABASIC UNITS

The presence of stress fields seems to be important for the formation of asbestos (Gunter et al. 2007a). More generally, the ophiolites favour the formation of fibrous minerals, especially Mg-rich ones, not only by the composition of parental rocks, pressure and temperature conditions, but also by the presence of stress fields. Asbestos forms within ultrabasic rocks along shear, fault, and dilation zones, and at contacts with intruded dikes and sills (Ross and Nolan 2003; Gunter et al. 2007a). These are area of weakness within which magmatic fluids can be easily introduces.

Two types of asbestos fibres are frequent at the outcrop: *cross-fibres*, that grow filling joints in rocks, and *slip-fibres*, that form along the face of a fault plane. Cross-fibres occur within cracks formed when the rock undergoes dilation due to tectonic stress, a process in which parallel cracks and fissures form open spaces in the rock. The process of folding in layered rocks can also produce openings or dilation cavities between adjacent layers. Asbestos crystallizes from a fluid phase, the fibres nucleating on a wall of the crack or cavity and growing toward the opposite wall; thus the term cross-fibres (Fig. II.9a). Slip-fibres form within the fault and shear zones, the fibres crystallizing or recrystallizing from solutions that move within the two rock faces that compose the shear or slip plane (II.9b).

In ultrabasic complex, prograde reaction results in antigorite in massive serpentinite, with or without magnetite, but at lower temperature a mixture of chrysotile and lizardite
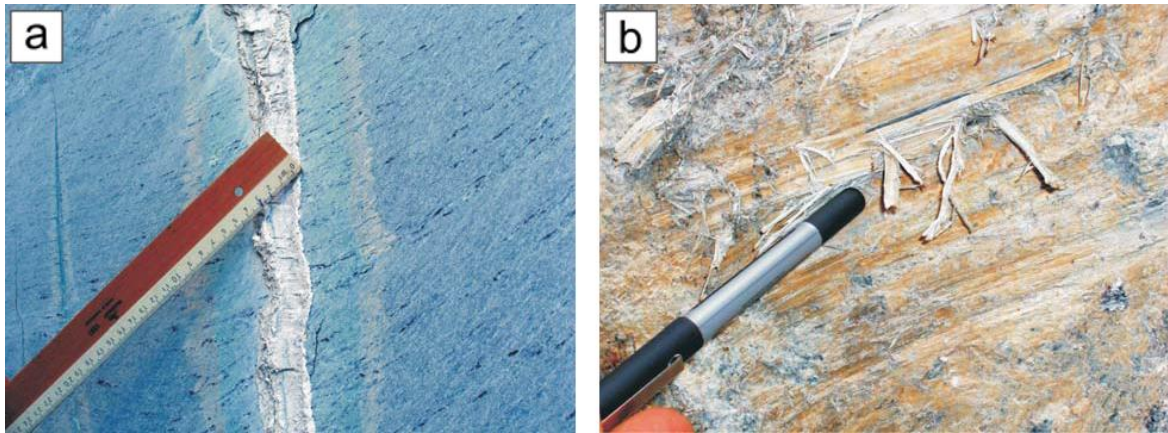
Figure II.9. Chrysotile asbestos veins: (a) cross-fibre vein with hydrothermal selvage; (b) slip-fibre vein (Cavallo and Rimoldi 2013).

may occur. In a typical chrysotile-asbestos deposit, e.g. at Cassiar mine in British Columbia, the variety of serpentine occurring with increasing temperature follow the sequence: pseudomorphous retrograde lizardite → lizardite + chrysotile → chrysotile + antigorite → antigorite. Actually, the sequence of events which leads to the formation of chrysotile veins is not known with certainty, although various possibilities have been discussed. For instance, fibres may form at the same time as the matrix serpentine rock from the same parental material, or they crystallize later. In the latter case, they may replace existing material, perhaps starting at a fissure and growing inwards, or they may grow in pre-existing fissures from solutions which permeate the rock. Equally, asbestiform amphiboles form as alteration products of pyroxenes at low temperature, as in the notorious case of vermiculite mine in Libby, Montana. The geological conditions that leads to the formation of amphibole asbestos and asbestiform amphiboles (i.e. some type of regional stress environment) would also form the other types of fibrous minerals (Gunter et al. 2007a, 2007b).

Natural occurrence of fibrous minerals in peridotites of the northern and southern part of the Grande Terre is well known (Lahondère 2007, 2012). Despite of the large number of geological studies existing on ophiolite of New Caledonia, a comprehensive understanding of mechanisms responsible for serpentinization is still lacking (Orloff and Gonord 1968; Trescases 1975; Barnes et al. 1978; Ulrich et al. 2011; Evans et al. 2013; Frost et al. 2013; Mothersole et al. 2017). Orloff and Gonord (1968) firstly experienced the huge variety of serpentinized outcrops interesting the peridotitic assemblages of New Caledonia. A gradual decrease of serpentinization degree from the bottom (totally serpentinized) towards the top of regolith profiles (no evidence of serpentinization) is observed. Moreover, probably due to different thermodynamic conditions in according to geodynamic context, several generations of serpentine minerals may occur in the ultrabasic units, from the *serpentinite sole*, at the bottom, until *serpentines fractures linked*, toward the top (Lahondère 2007; Audet 2008).

According to Ulrich (2010), *the serpentinite sole*, at the bottom of the ophiolite, is dominated by lizardite (up to 90%), secondary chrysotile, which occurrence consists of millimeter crack-seals veins, and antigorite, which only crystallized in veins. If the formation of the lizardite can be easily related to abyssal history of the ophiolite for the lherzolite and to its supra-subduction history for the harzburgite, the origin of the antigorite veins is more questionable. Ulrich *et al.,* (2010, 2011) relate this contrasted serpentinization to an upward hydration of the Peridotite nappe by metasomatic fluids released from the downgoing slab during the Eocene convergence. The occurrence of antigorite within the sole is interpreted as related to hotter fluid circulation (T >400 °C) when the HP-LT Diahot units were rising up beneath the ophiolite. As further discussed, this result accounts for the creation of a major rheological discontinuity forming the entire basal sole of the ultramafic sheet. Study on oxygen isotopes indicates that chrysotile was formed later, likely during obduction, by the circulation of meteoric fluids through micro-fractures (Ulrich et al. 2010), with higher water/rock ratios (Evans et al. 2013; Frost et al. 2013; Mothersole et al. 2017). In the upper part of ultrabasic units, serpentinites generally outcrop along tectonic structural discontinuities as fractures, faults and shear zones (Leguere 1976; Lahondère 2012), as also asbestiform habits (e.g. fibrous antigorite; Lahondère 2007).

In mining context, all four main varieties of the serpentine group, associated to minor tremolite, were observed. While polygonal serpentine and chrysotile occur in highly serpentinized zones, mostly at the base of ophiolite, antigorite is usually closely related to the main faulting pattern (Quesnel et al. 2016). Lizardite is the most common serpentine which overprints olivine and, in minor extent, pyroxene minerals of the parental peridotite. Moreover, chrysotile and fibrous antigorite serpentine appear intimately associated to tremolite-actinolite amphiboles, which increase the potential health risk due to exposition.
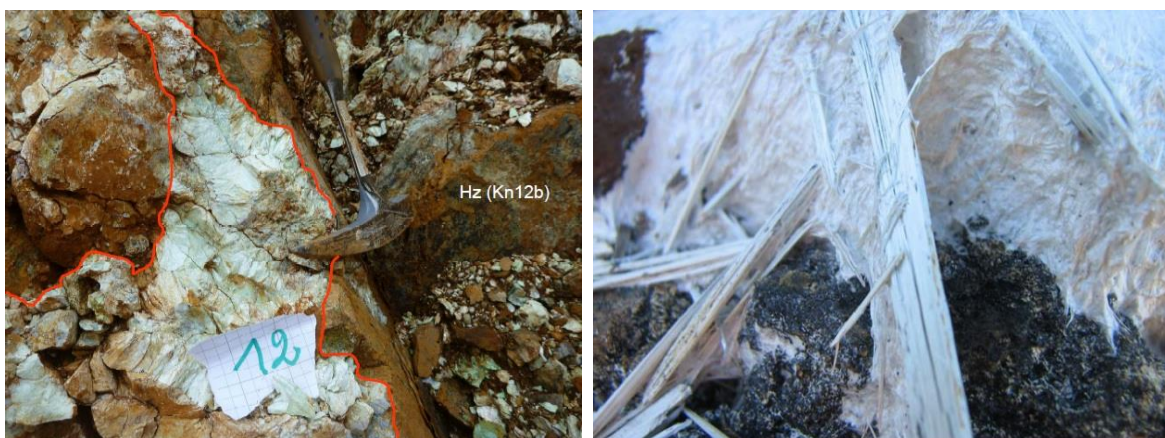

Figure I.10. Massive to fibrous tremolite-type amphibole in (a) fractures and (b) veins, Koniambo Massif, NC (from (a) Mission XTRATA Amiante 2012, Petriglieri 2014*; (b) Lahondère 2007).*
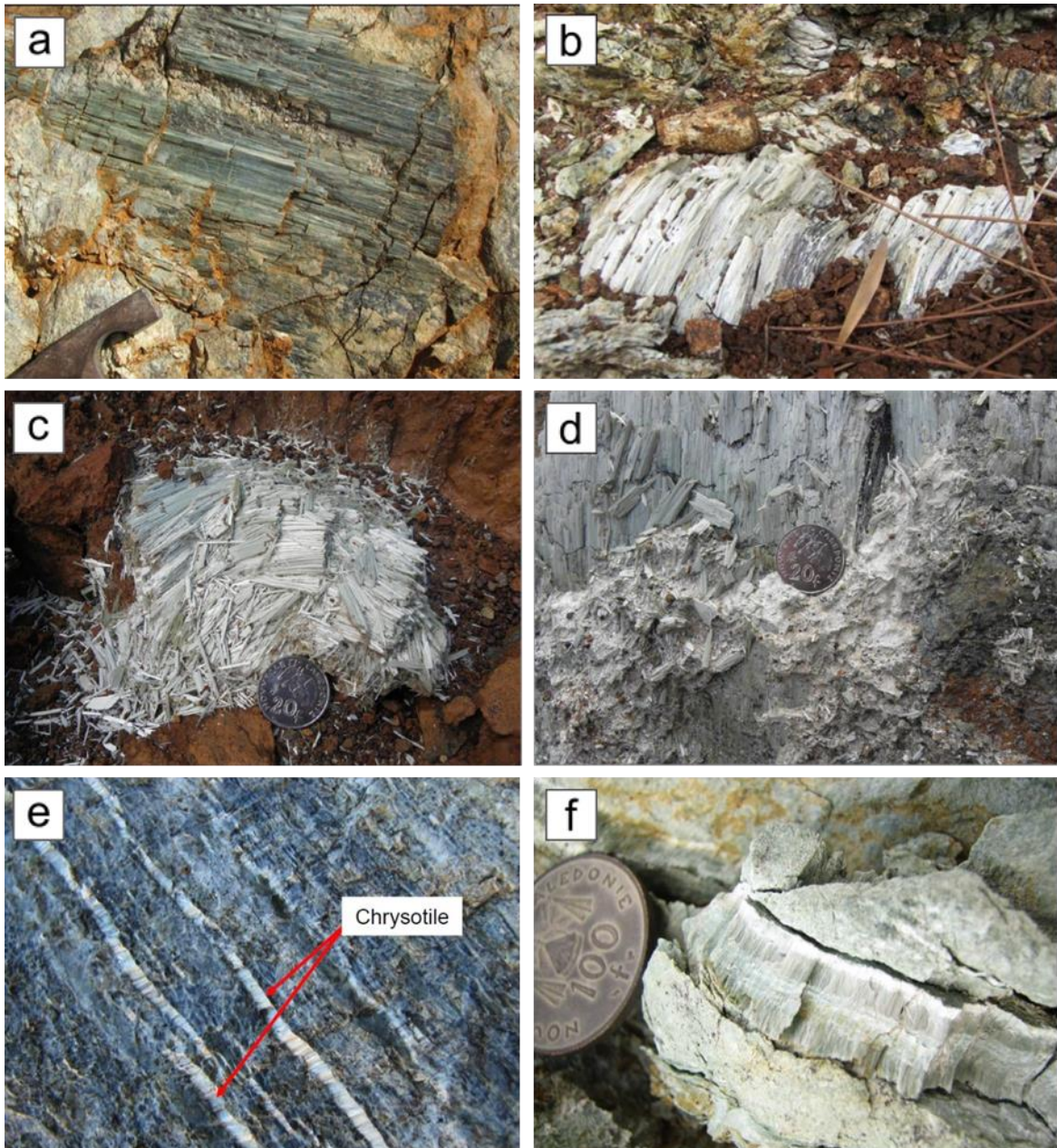
Figure I.11. Natural occurrence of more or less altered fibrous-lamellar antigorite (a-d) and chrysotile in veinlets (e-f) (modified after Lahondère 2007, 2012).

At the macroscopic scale, tremolite is present in the form of veins, from less than 1 mm to several centimetres, or associated with sliding planes crosscutting peridotites (Fig. I.10, e.g. Koniambo Massif). Serpentinized peridotites show a large network of fault planes and veins, containing lamellar crystals of antigorite (Fig. I.11a), centimetres to decimetres in length, and more or less continuous veinlets of chrysotile (Fig. I.11e,f). In the less altered areas, generally at the base of saprolite horizon, the antigorite blades are parallel and welded to one another. Moving upwards in the regolite profile, the blades are subjected to intense deformation and cleavage until the formation of fibres. The antigorite assumes a fibrous-lamellar habit with endings in chrysotile (Fig. I.11b,c). In

highly altered horizons, due to strong mechanical separation and cleavage, antigorite has a completely transformed morphological appearance and is associated to asbestiform fibrous products (Fig. I.11d). Therefore, antigorite, non-fibrous when fresh, gradually cleaves with weathering giving fibrous-like particles, which are not strictly asbestos fibres according to law definition, but their asbestiform nature may have potential effect on health.

Based on a large mapping of the Koniambo massif, Quesnel (2015) provides several guidelines for the identification of the main serpentine minerals at the sampling scale.

Dark lizardite is widespread in the serpentinite sole, and occurs as diffuse grain-scale network in the peridotite and as veinlets from 1 mm to 5 cm wide (Fig. I.12a). It can also occur on the margins of faults and shear zones involving antigorite, chrysotile or polygonal serpentine (Fig. I.12b). Lizardite rarely forms macroscopic fibres. Antigorite, green to dark-green coloured, occurs mainly with a fibrous-lamellar habit, often displaying splintery ends (Fig. I.11a-d). Single fibres or aggregates of fibres can also occur. Polygonal serpentine, instead, has been very little described in New Caledonia geological units (Ulrich 2010). Despite this lack of information, recent evidences confirm its non-negligible presence at the outcrop. Within fault zones, antigorite and polygonal serpentine are both able to form macroscopic slicken-fibres with a clear staircase geometry (Fig. I.13c). In order to distinguish these two varieties, the main argument is textural. Antigorite has a platy-fibrous appearance with fibres often several centimetres long. In contrast, polygonal serpentine is massive, matte, and develops only short slicken-fibres (Fig. I.13a,b; Quesnel 2015; Quesnel et al. 2016). Moreover, polygonal serpentine is pale-green whereas antigorite is generally darker. However, in the
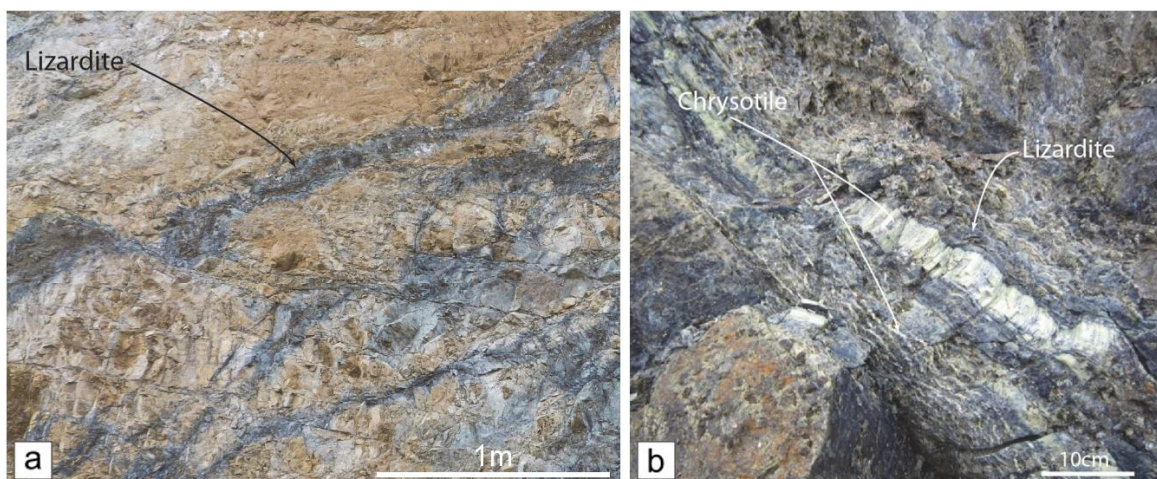

Figure I.12. Natural occurrence of lizardite in serpentine assemblage of Koniambo massif. Lizardite occurs as a) diffuse grain-scale network of veinlets from 1 mm to 5 cm wide; and b) on the margins of faults and shear zones involving chrysotile serpentine (Quesnel 2015; Quesnel et al. 2016).
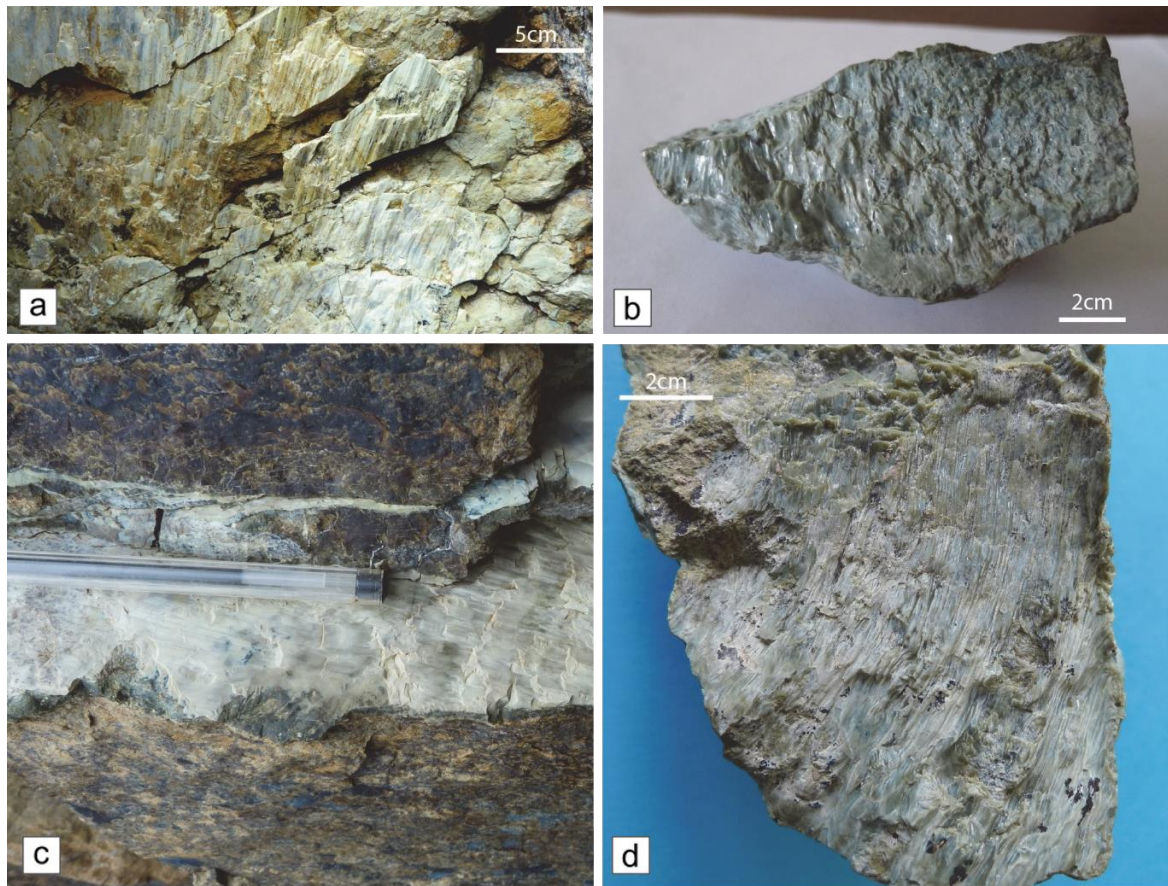
Figure I.13. Massive, matte pale-green crystallization of polygonal serpentine, Koniambo massif (Quesnel 2015; Quesnel et al. 2016).

lateritic horizons, weathering modifies the colours and polygonal serpentine tends to become olive-green. Some fault planes show mixed morphological properties, with a clear platy-fibrous nature but a pale-green colour and a matte aspect. Antigorite and polygonal serpentine are also involved in shear zones. There, antigorite forms distinct lamellae whereas polygonal serpentine is more massive despite the development of a pronounced cleavage (Quesnel et al. 2016). Finally, chrysotile, with its typical asbestiform habit, occurs as very thin whitish veins (Fig. I.11e-f). Dense networks of subparallel veinlets are locally observed, characterized by a zebra-like appearance (Fig. I.11e).

I.3.3. ALTERATION STATUS OF FIBRES

As a result of weathering processes in humid sub-tropical conditions, mineral fibres of New Caledonia occur with different morphologies, coupled with different degrees of alteration. In this context, the term *alteration* refers to a physico-mechanical modification in the appearance and/or shape of amphibole and serpentine minerals. In fact, increasing the degree of alteration, massive assemblages gradually cleave into

Figure I.14. Fibrous-lamellar antigorite showing several degrees of alteration at the outcrop, Koniambo massif, New Caledonia. (from Mission XTRATA Amiante 2012, Petriglieri 2014).

lamina or needle-like acicular crystals. This progressively loss of cohesion leads to the disappearance of the original structure, and conversely to the appearance of individual asbestiform fibres (Fig. I.11a,d). At present, there are no evidences concerning a chemical variation of these fibres (e.g. leaching processes, absorption…). Therefore, minerals which have been subjected to supergene alteration may vary from prismatic-platy through acicular-lamellar to asbestiform. Moreover, both serpentine and amphiboles may occur in association with mineral fibres of the same species and, as often occurs, with different species to form both bundles of fibres and/or aggregates of randomly oriented fibres. As reported in figure I.14 fibres displaying different degrees of alteration may exist simultaneously at the same outcrop. Unfortunately, a really understanding of this phenomenon is still lacking.

I.3.4. THE PLAN PREVENTION OF MINING COMPANIES

In the geological context of New Caledonia, in which weathering processes and supergene mineralization are one of the main responsible for fibre genesis of asbestos minerals, mining companies must therefore deal with the problem of natural occurrence

of asbestos. In order to decrease the risk due to the asbestos exposition, a monitoring prevention plan has been implemented. This program involves two major phases, a first step of survey of fibrous minerals on the field (mapping) and then an analytical characterisation of the fibres in laboratory. With the aim of a better evaluation and description of all types of asbestos occurrences, mining geologists have introduced a classification based on colour, morphology and release of these fibres. An example of this nomenclature for serpentine antigorite is shown in Table I.4. All these parameters depict an increasing alteration status, from *#1* to *#4*, correlated with rising risk resulting in a greater capacity in the dispersion of fibres. Fresh serpentine and/or amphibole minerals (degree of alteration *#1*) display a cohesive texture with poorly or no cleavage. With the gradual increase of alteration degree, several individual fibres appear (*#3*), until the disappearance of the original structure and the loss of cohesive minerals. A mineralogical transformation process (formation of talc, silicification, etc.) can eventually occur. Second step, related to laboratory activities for identification and quantification of mineral fibres refers to French regulation NF X43 050. The latter establishes TEM, SEM and PLM as standard analytical techniques in investigation of asbestos. This two-stage approach has several non-negligible restrictions.

ALTERATION DEGREE	VISUAL FEATURES	ANTIGORITE
Alteration **#1**	Antigorite with poorly or no cleavage in thin laminas.	
Alteration **#2**	Antigorite as bundles of laminas or needles.	
Alteration **#3**	Appearance of individual fibres.	
Alteration **#4**	Disappearance of the original structure, loss of cohesion and strong transformation of the mineralogy (talc).	

Table I.4. Typical example of nomenclature of naturally occurring asbestos minerals adopted by mining geologists (by courtesy of Glencore-XTRATA mining company).

Subjectivity in the discrimination of morphological criteria and potential misinterpretation are the main sources of error in the preliminary step of identification on the field. Because of the wide range of natural shapes, morphologies, and alteration status presenting by mineral fibres impacted by weathering, it seems very difficult to distinct with certainty the types of fibres. Furthermore, this operation requires a great deal of experience and, not insignificant, an excellent mineralogical background. Nevertheless, a significant margin of error is expected. With respect to laboratory investigations, electron microscopy techniques generally consist of laboratory devices, not including portable apparatus. Anyway, several benchtop SEM and TEM instruments are commercially available. Unfortunately, due to their compact system, they are not yet sufficiently performing in the characterisation of asbestos materials. Moreover, electron microscopies are not suitable to be quickly routinely techniques of investigation. In fact, they need skilled microscope operators, several time for sample preparation and data acquisition, and they have high analytical costs. Lastly, they permit to analyses very little specimens, too little compared to the outcrop volume. On the other hand, PLM is an optical routinely technique widely used across the world for the analysis of fibres concentrations of bulk building materials (ACMs). Curiously, it is not generally used with naturally samples.

Chapter II.

MINERALOGY OF ASBESTOS:

SAMPLING AND METHODS.

II.1. Mineralogical background

A brief mineralogical description of the major fibrous minerals involved in this study is here reported. Essentially, asbestiform minerals of serpentine and amphibole are both silicates sharing a fibrous-asbestiform crystal habit but holding very different structural units at a molecular scale (Gualtieri 2017). Despite the significant differences in structural arrangements and chemical compositions, mineral fibres show a very similar morphological and mechanical behaviour at both macro- and microscale, making their discrimination arduous. Only a thorough understanding of their complex nature will provide the correct identification of these minerals and the potential health risk associated to them.

II.1.1. SERPENTINE

The serpentine group is composed by hydrous minerals (about 13 wt.% H_2O) formed during the relative low-temperature (below 500 °C) hydration of peridotites and pyroxenites, by the alteration of Mg-rich olivine and orthopyroxene (Wicks and O'Hanley 1988; O'Hanley 1996). Serpentine generally form under a wide range of temperatures (from about 200 to 600 °C), including Earth surface conditions and hot hydrothermal temperatures. They play an essential role in numerous geological settings and control the rheology of the lithosphere where aqueous fluids interact with ultramafic rocks (Evans et al. 2013; Hirth and Guillot 2013).

Basically, Mg-rich serpentine minerals are type 1:1 trioctahedral phyllosilicates, with an approximate formula $Mg_3Si_2O_5(OH)_4$. A brucite-like Mg-rich trioctahedral sheet (O) is closely linked on one side to a single tetrahedral silicate sheet (T), consisting of a pseudo-hexagonal network of linked SiO_4 with approximate parameters a 5.3 Å, b 9.2 Å (Fig. II.1a,b). The basic TO structural unit is a polar layer; the distance between the TO structural units is approximately 7.3 Å (Fig. II.1c; Wicks and Whittaker 1975; Evans et al. 2013). As shown in figure II.1c, two crystallographic independent hydrogen atoms are present in the crystal structure. One of them, H_4, is located in the centre of the pseudo-hexagonal ring and it does not form any hydrogen bond. The other one, H_3, links adjacent layers through hydrogen bonds. Therefore, hydroxyls are present in all serpentine minerals in two different positions: at the centre of the six-fold ring of SiO_4 tetrahedra in the T layer (inner OH groups) and in the interlayer space linked to the O layer (outer OH groups; Auzende et al. 2004).

Mg-rich serpentine minerals show a dimensional misfit between tetrahedral-octahedral layers of around 3-5% (Bailey 1988b). This interlayer stress is compensated by a wide structural complexity of these mineral species, where the mismatch compensation normally occurs by chemistry changes or through a structural modification of the layers.
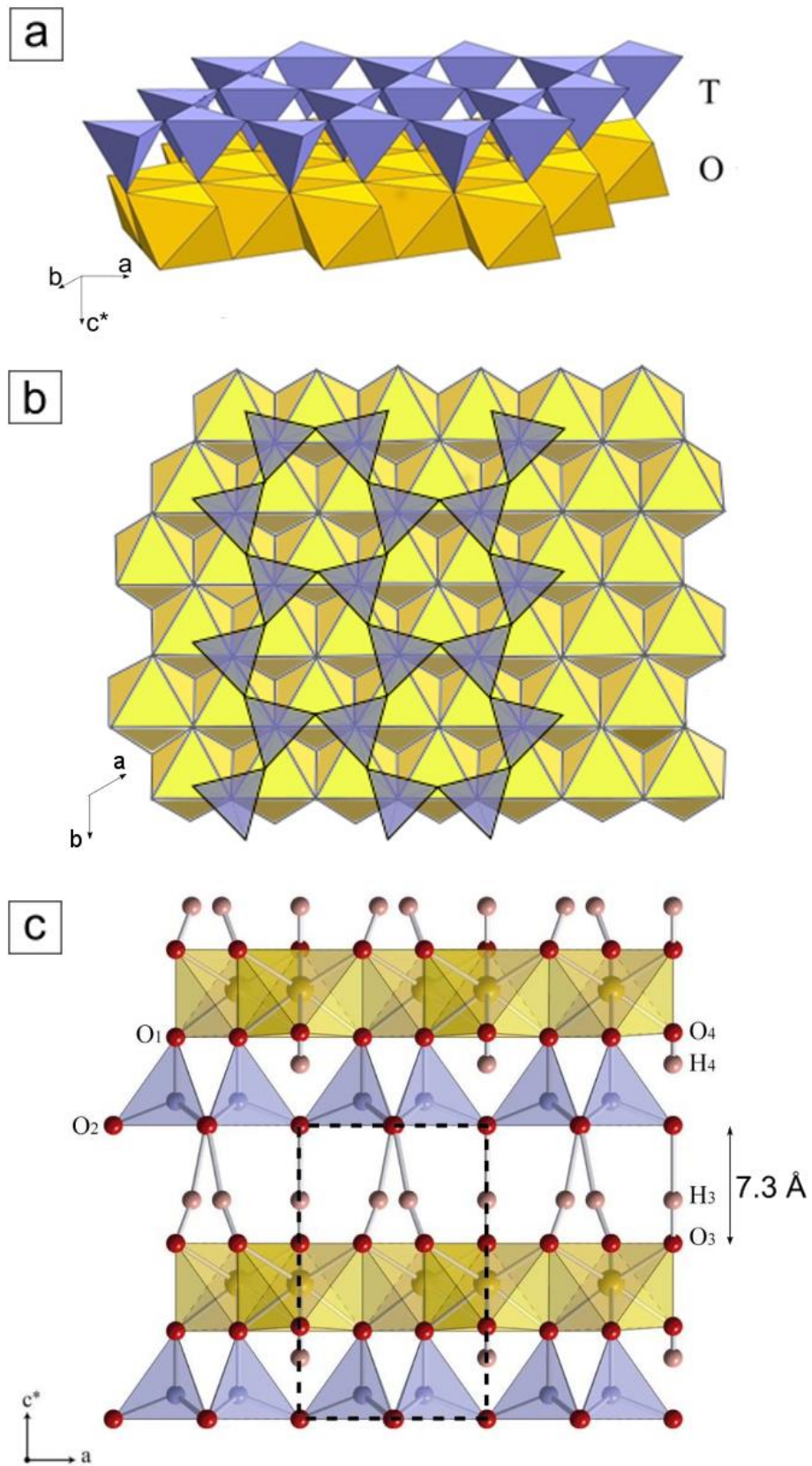
Figure II.1. Crystal structure configuration of 1:1 Mg-rich serpentine. The ideal layer unit with Si-centred tetrahedral (T) sheets joined to Mg-centred octahedral (O) sheets in units with a 1:1 ratio and a distance of 7.3 Å along the c axis (a & c modified after Auzende 2003).

	Lizardite		Antigorite	(Clino)Chrysotile
				$Mg_3[Si_2O_5](OH)_4$
	Trigonal-Hexagonal		Monoclinic	Monoclinic
α	1.538-1.554		1.558-1.567	1.532-1.549
β	1.546-1.560		1.565	1.546-1.560
γ	1.546-1.560		1.562-1.574	1.545-1.556
δ	0.006-0.008		0.004-0.007	0.013-0.017
$2V_\alpha$	-		37-61° OAP ⊥(010)	42°
Orientation	-		α∼‖z, γ = y	-
Dispersion	-		r > v	-
Density(meas.)	2.55(3)		2.65	2.53(1)
Density(calc.)	2.57		2.61	2.61
Hardness	2.5		2.5 - 3.5	2.5
Cleavage	{0001} perfect		{001} perfect; observed on {100} and {010}	fibrous ‖a-axis
Twinning	-		occasional	-
Colour	Green, light yellow to white; colourless to pale green in thin section		Green, blue-green, white; colourless to pale green in thin section	White, grey, pale green; colourless to pale green in thin section
Unit cell				
Space group	P31m	P6₃cm	Pm	Cc
	a = 5.325(5)Å	a = 5.318(4)Å	a ∼ 33-51 Å	a ∼ 5.34 Å
	c = 7.259(7) Å	c = 14.54(1) Å	b ∼ 9.25 Å	b ∼ 9.24 Å
	Z = 2 *	Z = [4] *	c ∼ 7.26 Å	c ∼ 14.69 Å
			β ∼ 91.3° ; Z = 2	β 93.6° **

for natural lizardite-1T (P31m) and lizardite-2H_1 (P6₃cm) (Mellini and Zanazzi 1987)

**for two-layer synthetic clinochrysotile (Falini et al. 2004)*

Table II.1. Main mineralogical optical and structural parameters of serpentines (after Deer et al. 1992).

In fact, good compensation results in a nearly constant layer curvature, with the larger octahedral sheet on the convex side. However, such curvature weakens the H-bonding between the layers. H-bonding tries to maintain flat layers, but this competes with the requirement of misfit compensation. As a result, the layers are locally either curved or flat (Evans et al. 2013).

The microstructure classification of the four main varieties – lizardite, antigorite, chrysotile and polygonal serpentine – is based on the change of curvature of the tetrahedral-octahedral layer structure (Whittaker and Zussman 1956; Bailey 1988b; Wicks and O'Hanley 1988). Lizardite has a flat crystal structure, where the planar sheet has an ideal layer topology. Antigorite shows a corrugated-wavy layer characterized by a modulated structure. Chrysotile with the cylindrical-spiral wrapping of the 1:1 layers exhibits a fibrous structure (Whittaker and Zussman 1956; Cressey et al. 1994; Pollastri et al. 2016), and polygonal serpentine shows an alternation of flat and curved sectors and

displays an intermediate structure between chrysotile and lizardite varieties (Mitchell and Putnis 1988; Burzo 2009). In addition to the more familiar species, some microstructures have been recognized only recently with the transmission electron microscope (TEM). Polyhedral serpentine, for example, occurs as facetted, onion-like nanospherules (Baronnet et al. 2007). It forms from altered pyroxene in Al- and Fe^{3+} - bearing media at 300 °C and P_{H2O} = 0.7 kbar (Evans et al. 2013).

The four varieties of serpentine are not polymorphs *stricto sensu*. Chrysotile preserves the general formula $Mg_3Si_2O_5(OH)_4$ even if it has a small deviation from the ideal composition for the presence of very small amount of Al or Fe. Antigorite has a small depletion of $Mg(OH)_2$ because of the inversions in curvature. In lizardite, different cations are required to stabilize the structure and its formula should be written as $(Mg_{3x}M_x)$ $[Si_{2x}M_xO_5(OH)_4]$, where Al, Fe, Cr, are in M, and x is usually around 0.1 (Burzo 2009). More in general, although serpentine shows only minor substitutions for Mg and Si, it may have a significant enrichment in cations, as Al, Fe and Ni (e.g. nepouite, amesite). Because of the many different ways in which the layers 1:1 may be stacked and to the wide occurrence of disorder, defects and dislocations, different polytypes are possible (e.g. Lizardite 1T; Bailey 1988a).

Generally, lizardite and chrysotile are more stable at lower temperature and pressure conditions, whereas antigorite is considered to be the high-temperature phase of serpentine. In the MgO-SiO_2-H_2O system, lizardite is more stable than chrysotile at 200 and 300 °C and 0.7 kbar. Laboratory syntheses suggest that chrysotile might be more stable than lizardite above 400 °C. According to Evans (2007) chrysotile growth is favoured in fluid-filled voids; thus it is certainly more common in recrystallized or tectonized serpentine. Antigorite grows from lizardite and chrysotile with increasing metamorphic grade at temperature above 320 °C. The transition from lizardite to antigorite + brucite would occur with a steep negative *dP/dT* slope at approximately 300 °C. This makes chrysotile metastable at any temperature (Evans et al. 1976, 2013; Wunder and Schreyer 1997; Evans 2004). Moreover, other laboratory experiments have shown that antigorite breaks down at 640 °C and 2GPa in the pure system and at about 700 °C under Al saturation. Furthermore, in natural system with Al, Cr, Fe^{2+}, and Fe^{3+}, inversions in order of serpentine stability with respect to the simple system may be possible. Essentially, antigorite breaks down at 600-700 °C, following the reaction antigorite → forsterite + talc + H_2O at P <2 GPa, and antigorite → forsterite + enstatite + H_2O at higher pressure (Evans et al. 2013).

Because of their coiled habit, chrysotile and polygonal serpentine are generally considered as the prevailing fibrous forms of the serpentine group. Actually, recent studies show the presence of a fibrous shape of antigorite variety (Groppo and Compagnoni 2007a, 2007b; Lahondère 2007; Keeling et al. 2008, 2010; Fitz Gerald et al. 2010; Fitzgerald and Harty 2014).

II.1.1.1. Chrysotile

Although chrysotile is the least abundant serpentine in nature, it is the main constituent of commercial asbestos (95%). In general chrysotile occurs in veins of silky fibres, most commonly in mildly prograde metamorphosed serpentinite as slip-fibres along shear zones, and less frequently as mass fibres (Wicks and O'Hanley 1988). Moreover, it may be a minor component in retrograde lizardite serpentinites (Cressey 1979) and in prograde antigorite serpentinites (Mellini et al. 1987).

Chrysotile occurs mainly as filling of fractures that crosscut serpentinites. The repeated opening of fractures causes the different orientations of the fibres: perpendicular, inclined or parallel to the walls of the fracture. Fibres, generally less than 1 cm length, can reach as much as 15 cm (Deer et al. 1992).

At the microscale, chrysotile consists of multiwall nanotubes or nanoscrolls; a non-deformed chrysotile fibre has an outer diameter <100 nm and an inner diameter ≥4 nm, and it may reach several centimetres in length (Fig. II.2a; Yada 1967, 1971). The fibrous nature of chrysotile is due to cylindrical (Fig. II.2b) or spiral (Fig. II.2c) curved layers usually around the *a*-axis (clino- and ortochrysotile). In the rare parachrysotile, which more frequently occurs in synthetic samples, the curvature axis is *b*.

Clinochrysotile (chrysotile-$2M_{c1}$) is the most abundant variety and occurs alone or mixed with less amounts of orthochrysotile (chrysotile-$2O_{c1}$), or rarely with minor amount of parachrysotile. The three types of chrysotile have the same structural motif and composition, but the stacking mode of the subsequent layers differs.

A single cylinder or spiral arrangement is usually called *fibril* (Yada 1967, 1971). Since the
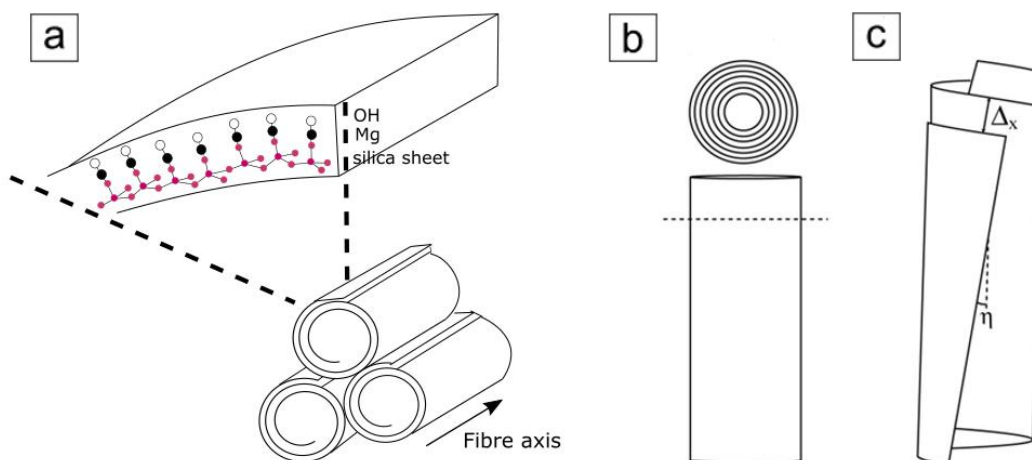

Figure II.2. Crystal structure of chrysotile. Rolling of the TO layers in serpentine (a) to form a tubular cylindrical (b) or spyral (c) structure which may form single chrysotile fibrils.

layers cannot withstand bending too tightly, the rolls, having inner channels of about 5-8 nm in diameter (Cressey et al. 1994), may be empty or filled with silica or an Fe-rich amorphous phase (Bloise et al. 2009a, 2012). Moreover, the cross section of the cylinders can be circular, spiral, elliptical or deformed (Yada 1971).

Several cylindrical polytypes exist for chrysotile. More frequently observed in synthetic (nano)chrysotile samples, two peculiar microstructures occurs, in particular conical and cone-in-cone shapes (Yada and Iishi 1977; Smolikov et al. 2013), and tubular and tube-in-tube type (Falini et al. 2004; Roveri et al. 2006). Conical serpentine nanofibres were recognized in natural samples, in isotropic veins of serpentinite along the Santa Ynez Fault, in the Blue Canyon, at north of Santa Barbara, California (Andreani et al. 2004). The presence of impurities in chemical composition in chrysotile fibres, even in trace amount, is at the origin of the variability of shapes observed: hollow cylinder, non-hollowed cylinder, tube-in-tube, spiralized (helical), conically wrapped and cone-in-cone fibres (Yada and Iishi 1977; Roveri et al. 2006; Bloise et al. 2009a, 2009b, 2010).

It is generally accepted that fundamental fibrils present various diameters, presumably depending on the growth conditions of samples in each locality. Natural chrysotile fibres mostly have outer and inner diameters of respectively 22-27 nm and 7-10 nm (Whittaker 1957; Cressey and Whittaker 1993; Baronnet and Belluso 2002; Vigliaturo 2015). In several cases, the outer diameter can be as small as 5 nm and the inner diameter can be as large of 50 nm (Wagner 2015). In any case, the diameter invariably does not exceed 100 nm. Evidently, the thinnest fibrils consist of a single sheet.
Basically the diameter of chrysotile fibre tends to increase with the increase in the fibre length, and the long fibres tend to be more curvilinear (Sporn 2014). Depending on the formation mechanism, the length of chrysotile fibres in rocks is extremely variable, from several millimetres to a few micrometres (Bloise et al. 2014).

As mentioned above, chrysotile shows just a least deviation from the ideal composition of serpentine, containing very little Al or Fe. Substitution may occur in both tetrahedral and octahedral sheets (Ballirano et al. 2017). Al^{3+} can replace both Si^{4+} and Mg^{2+} in the T and O sheets, respectively, with an average content <0.9 wt.% Al_2O_3 (Wicks and Plant 1979). Fe^{2+} and Fe^{3+} can also replace Mg^{2+} in the O sheet while replacement of Si^{4+} in the T sheet is minor and infrequent. FeO may be present in natural chrysotile up to 6 wt.% (Wicks and Plant 1979). Both Fe^{2+} and Fe^{3+} can replace Mg in the octahedral sheet and Fe^{3+} may eventually replace Si^{4+} although this position may preferentially host Al^{3+}. Recent studies suggest the presence of both Fe^{3+} and Fe^{2+} exclusively in six-fold coordination (Pollastri et al. 2015). In chrysotile, trace metals such as Cr, Mn, Co, Ni and Cu represent almost exclusively isomorphous substitutes for Mg. Trace-metal substitution in chrysotile is usually more restricted than in other serpentine lizardite and antigorite minerals (Wicks and O'Hanley 1988; Bloise et al. 2009b, 2010). Moreover, their

concentrations are highly variable among the different samples, due to the different geochemical processes involved in their formation (Bloise et al. 2016).

Similar asbestiform fibres were observed for pecoraite, the Ni analogue of clinochrysotile (Faust et al. 1969, 1973; Brindley and Maksimovic 1974; Golightly and Arancibia 1979; Song et al. 1995). It is worth noting that in the past, the name pecoraite was attributed to all minerals with fibrous 7 Å morphologies in which Ni is the dominant octahedral cation. Since Ni^{2+} is only slightly smaller than Mg^{2+}, comparable lateral misfit between the tetrahedral and octahedral sheets occurs for Ni-rich compositions as for Mg-rich chrysotile. Thus, the misfit leads to curling of the 1:1 layers into tubular-shaped forms.

II.1.1.2. Polygonal Serpentine

Initially referred to as *Povlen chrysotile* (Krstanovic and Pavlovic 1964; Middleton and Whittaker 1976), polygonal serpentine term was proposed in 1976 by Cressey and Zussman because of its structure, which consist of a polygonal-tubular structure where polygonal sectors arrange lizardite-like flat layers and chrysotile. Firstly observed by Zussman *et al.*, in 1957, in the following years this serpentine phase has been the subject of several interesting studies (e.g Cressey 1979; Mellini 1986; Chisholm 1991, 1992; Baronnet et al. 1994; Cressey et al. 1994, 2010, Baronnet and Devouard 1996, 2005; Dodony 1997; Mugnaioli et al. 2007). In polygonal serpentine the elongation of the fibres is according to *a*-axis, and transverse sections show that flat lath-like layers are stacked to form polygonal sectors. Typically, either 15 or 30 sectors, which may or may not surround a core of cylindrical chrysotile, are observed (Fig. II.3; Cressey and Zussman 1976; Middleton and Whittaker 1976; Chisholm 1991, 1992; Baronnet et al. 1994). Furthermore, the core may also be composed of planar layers, antigorite and partially curved layers, and bundles of fibres. The angular discontinuity between neighbouring sectors is structurally controlled and it is another way of overcoming the problem of mismatching components. Polygonal serpentine may be viewed as a less metastable microstructure compared to chrysotile (Mitchell and Putnis 1988). Devouard *et al.*, (1997) suggests that the origin of polygonalization is probably controlled by temperature and/or growth (kinetics) parameters. Contrary to the assertion of Wicks and O'Hanley (1988), the polygonal serpentine is now considered as a variety of serpentine because it has its own configuration with respect to those of chrysotile, lizardite, and antigorite.

Surprisingly, polygonal serpentine is not rare in nature. On the contrary, it is widespread in serpentinites, where it may constitute a remarkable percentage (Wagner 2015; Belluso et al. 2017). In general, chrysotile and asbestiform polygonal serpentine occur commonly mixed in the same bundles (e.g. Mellini 1986). As natural occurrence of asbestos, polygonal serpentine is abundant, for example, in serpentinites of the Italian Wester Alps
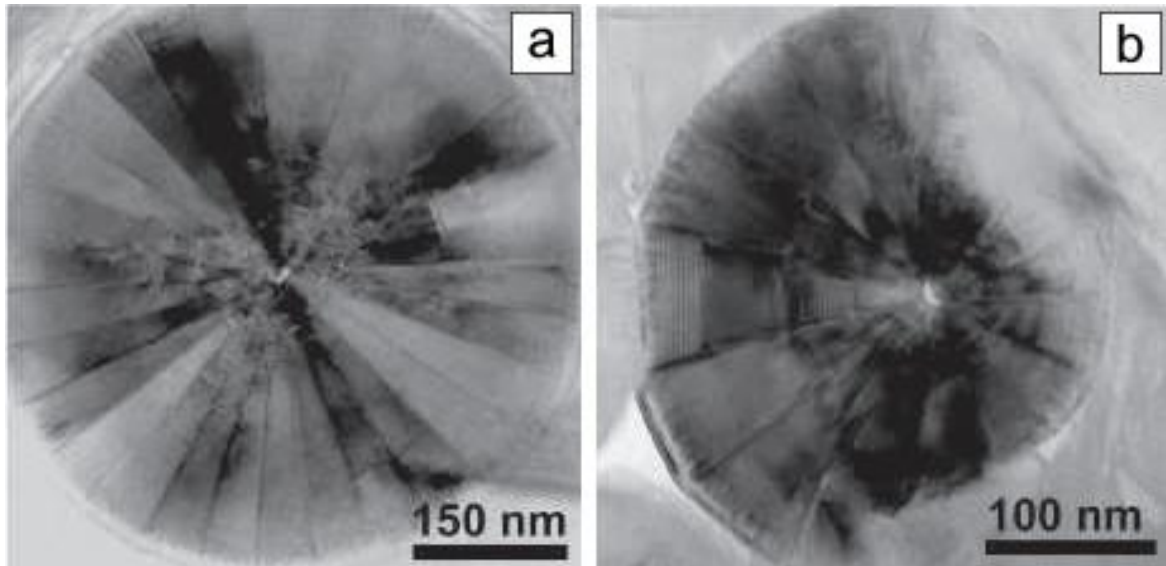
Figure II.3. TEM images of (a) PS-30 with regular habit; and (b) PS-15 with unequal growth in different sectors, from specimens cut perpendicular to the vein lineation (modified after Mugnaioli et al. 2007).

(Mellini 1986) and southwestern Italy (Bloise et al. 2014), and along the coast in northern California (USA) where it is associated with various minerals belonging to the serpentine mineral groups (Wagner 2015). Recently Quesnel *et al.*, (2016) reports the presence of polygonal serpentine in New Caledonia ultrabasic peridotite Nappe, at the Koniambo massif.

II.1.1.3. Antigorite

Antigorite, the high-temperature phase of serpentine, commonly occurs in partially recrystallized and metamorphosed serpentinites. There, it generally forms interlocking, elongated, blade-shaped crystals that overprint earlier-formed serpentinites. Antigorite is common in prograde regional and contact metamorphic serpentine (Mellini et al. 1987; Wicks and O'Hanley 1988). Stable to 720 °C and 2 GPa, antigorite may carry large amounts of water into the upper mantle during subduction of hydrated ultrabasic rocks (Ulmer and Trommsdorff 1995).

Antigorite displays curved, wavy layers. The octahedral sheet is continuous and wavy, whereas the tetrahedral sheet undergoes periodic reversals along the *a*-axis so that it connects to the adjacent octahedral sheets forming concave half-waves (Fig. II.4; Capitani and Mellini 2004). The reversals allow serpentine layers to be bound through strong, mainly covalent Si-O bonds. This explains the lack of easy cleavage and the enhanced hardness and seismic velocities of antigorite compared to those of lizardite and chrysotile.

The antigorite structure is an as-growth modulated structure, and the wavelength along the *a*-axis can be indicative of the composition and P-T conditions of the metamorphic rocks containing the mineral (Mellini et al. 1987). Compared to other serpentine phases, it has a slightly but significant lower Mg/Si ratio since some octahedron are omitted at layer inversions; there is also a small deficiency in hydroxyl groups.

The structure of antigorite (*Pm* space group) has *b* and spacing of (001) cell parameters similar to those of lizardite and chrysotile (*b* = 9,25 Å e c = 7,25 Å; Table II.1.; Deer et al. 1992; Capitani and Mellini 2004), whereas the *a* cell parameters ranges mostly between 33 and 51 Å. The large extension of A, which represents the wavelength of modulation, is explained by the curvature of serpentine layers around *y* and by their inversion to form
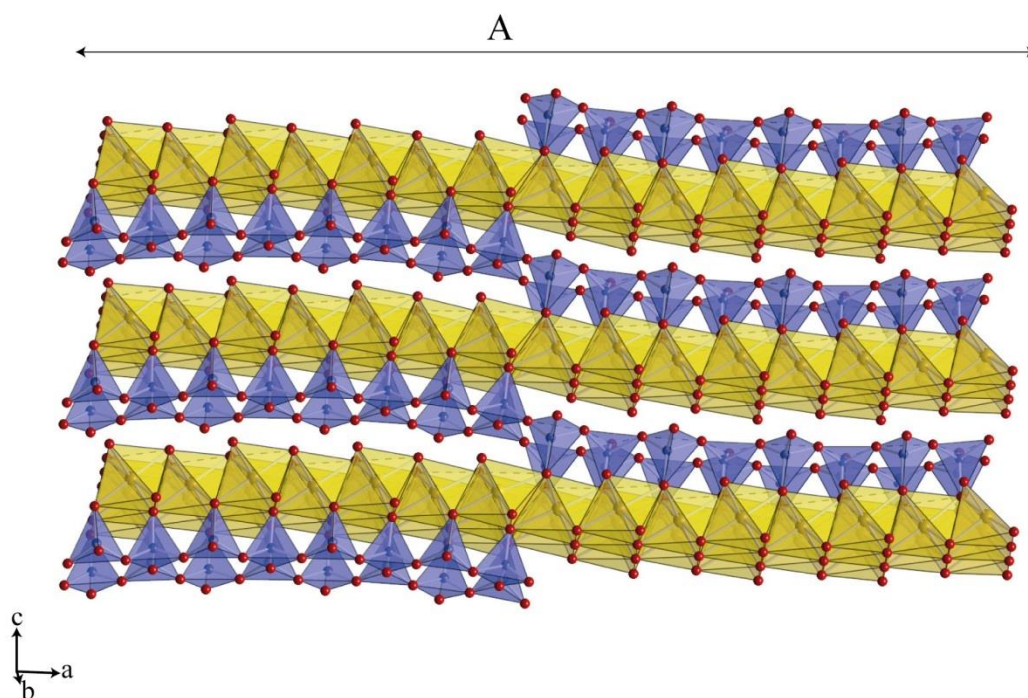

Figure II.4. Typical wavy structure of antigorite along its b-axis. A represents the wavelength of modulation (Auzende 2003).

the corrugated sheet structure with periodicity *a* (Fig. II.4). When different discrete numbers of tetrahedra (*m* value) and/or octahedra occur in the wavelength of the structure, A may assumes different values and different antigorites form. Values of A can also vary within a single antigorite crystal. The *m* value is not coincident with the A periodicity.

Historically, the complex modulated structure of antigorite was first envisaged by Onsager (in Robinson and Shaw 1952), after X-ray diffraction experiments of Aruja (1945). Onsager proposed for the first time a corrugated-sheet structure for antigorite, describing the unit cell and symmetry of a sample with *m* = 17. Antigorite shows a 1:1

layer structure with inversion every 43.3 Å in the *a* direction. Here, bending of the layers produces an undulating plate and not a chrysotile-like cylindrical habit. Instead of the normal hexagonal arrangement of the basal oxygens of tetrahedron, it was suggested that they form rectangles and octagons at the inversion line. The distance between successive inversions was estimated 5.2 Å. Later, additional studies confirmed the Onsager *alternating wave model* as microstructure of antigorite. The main feature is a wave-like corrugation of the octahedral layer with tetrahedral layers attached at the convex side, flipping at each inversion point to the other side of the octahedral layer. HRTEM and electron diffraction data revealed variable modulations. In addition to the basic 43.3 Å periodicity (m = 17), other A values indicating integer values of m were observed (Zussman et al. 1957; Bates 1959; Chapman and Zussman 1959; Kunze 1961).
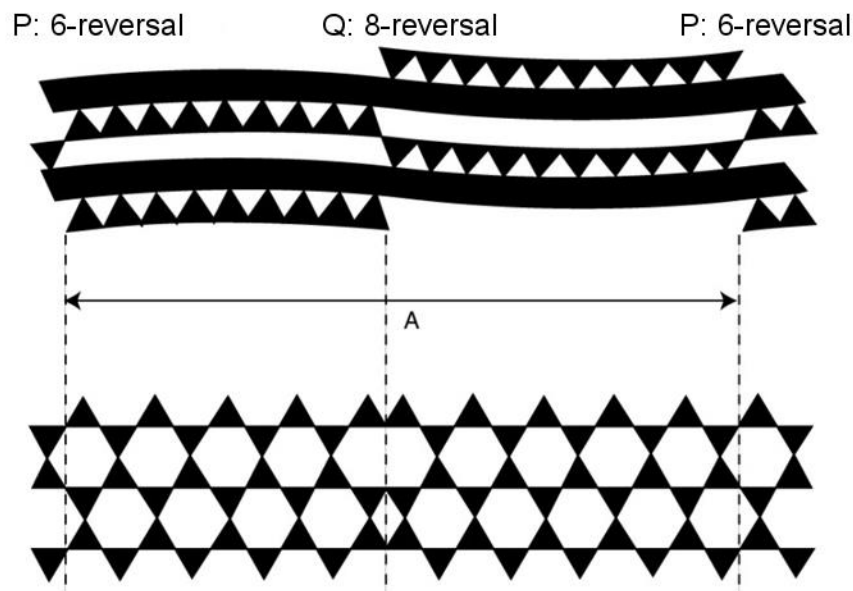

Figure II.5. Model of projection along [010] (up) and [001] (down) of the antigorite m=19 structure. P reversal at 6 tetrahedra; Q reversal at 4 or 8 tetrahedra.

The structural modulation of antigorite may be described also as a polysomatic series. Basically, polysomes are structures that can be created by combining two or more structurally and stoichiometrically distinct types of slab modules (Veblen 1991). Thus, polysomatic series are groups of structures that are made up of different ratios of the same types of slabs (e.g. A, AA, AB, AAB etc.). Therefore, antigorite can be represented as a polysomatic series based on three types of slabs: 1) a lizardite slab; 2) a slab with six-membered rings where the direction of the apical oxygens is reversed; 3) a similar slab with eight- and four-membered rings (Fig. II.5). The number of lizardite slabs in each unit cell can be varied, producing a polysomatic series of discrete antigorite structure having different *a* parameters of the unit-cell and different variations in composition (Uehara and Shirozu 1985; Capitani and Mellini 2004, 2005, 2006, 2007).

Finally, in recent years Capitani and Mellini (2004, 2005, 2006, 2007) describe the modulated crystal structure of predominant antigorite polysomes, $m = 17$ and $m = 16$, confirming precedent models of Onsager & Uehara. The two polysomes differ in the number of [010] tetrahedral strips (17 vs. 16) and [010] octahedral strips (16 vs. 15) along the [100] modulation wave. Although they differ in space group symmetries and in cell contents, they reveal a very similar behaviour in interaction between different slabs, which matches the lizardite bonding geometry. The most abundant antigorite polysome in nature ($m = 17$) supports the monoclinic symmetry (Fig. II.6).

Regular and continuous octahedral sheets (M1 to M16) were pseudo-sinusoidal developed along a-direction, with flexure lines every eight octahedra (between M8 and M9 and between M16 and M1). Continuous tetrahedral sheets (T1 to T17) link the concave side of the octahedral sheet, inverting polarity every nine and eight tetrahedral (between T9 and T10 and between T17 and T1). This sheet has six-membered rings, like in the basic 1:1 lizardite structure, and regular reversals, which are characterized by two possible configurations. The six-reversals occur between T17 and T1 and consist of six-membered tetrahedral rings, but with two tetrahedra pointing in one direction (+) and four in the opposite direction (-). The eight reversals, between T9 and T10, consist of eight-membered tetrahedral rings (four pointing + and four -) and alternate along [010] with four membered tetrahedral rings (two pointing + and two -). Therefore, $m = 17$ antigorite polysome displays two, crystallographycally independent and physically different, half-waves defining asymmetric pseudo-sinusoidal modulation (Capitani and Mellini 2004). At the planes of inversion of the sinusoidal tetrahedral-octahedral layers, the Mg and OH content is reduced relative to Si. Therefore, the water and Mg content of antigorite increases, and the silicon content decreases with increasing wavelength A.
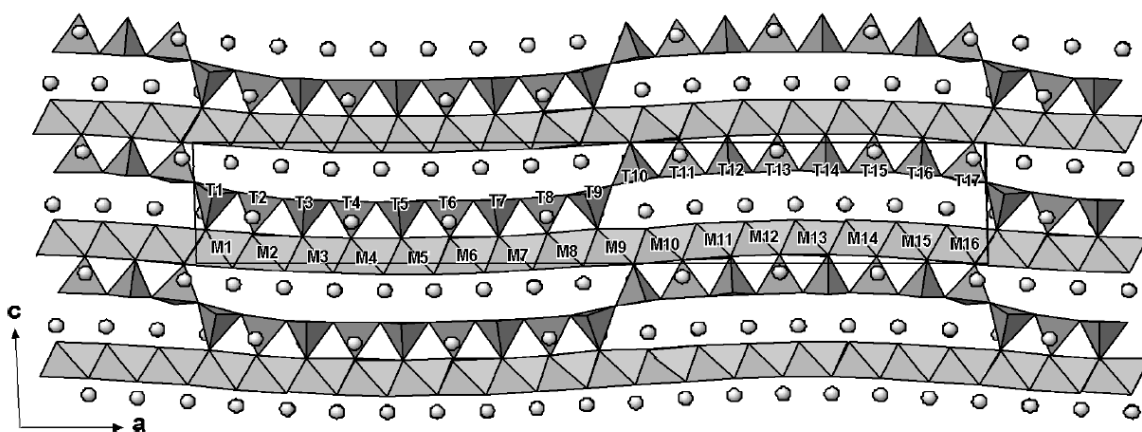

Figure II.6. [010] projection of the modulated crystal structure of the m = 17 antigorite polysome. A long half-wave (T1 to T9) alternates with a short half-wave (T10 to T17). The tetrahedral wave is linked to the concave side of a continuous, corrugated octahedral sheet (M sites). Circles represent hydrogen atoms. The [001] transverse modulation is evident as wave-shaped 1:1 layer (Capitani and Mellini 2004).

Assuming a pure MgO-SiO_2-H_2O composition, the water content of antigorite with m from 13 to 41 is in the range 12.09-12.72 wt.%. According to Mellini *et al.*, (1987), typical composition of antigorite are in the limited m range of 13-24, which would correspond to a water content of 12.09-12.52 wt.%.

Despite scientist community is generally in agreement with the existence and availability of both fibrous (potentially asbestiform) and massive antigorite, many authors still ignore its dual nature (Glenn et al. 2008). In the past, the name *picrolite* was used to describe antigorite samples generally defined as fibrous (Jones 1890; Chapman and Zussman 1959). Back in 1890, Robert H. Jones in his book "*Asbestos, Its Properties, Occurrence & Uses: With Some Account of the Mines of Italy and Canada*" refers to a large quantity of fibrous samples of serpentine antigorite discovered in Canadian mines as «*PICROLITE, "BASTARD ASBESTOS"*» (Fig. II.7). Recent remarks have focused again the public attention on potentially asbestiform nature of this not-yet-regulated fibrous mineral.


PICROLITE, "BASTARD ASBESTOS."

Figure II.7. Example of so-called picrolite asbestos of Canadian mines (Jones 1890).

II.1.2. AMPHIBOLES

Members of the amphibole group are common in a wide range of P-T environments in both igneous and metamorphic rocks. Among igneous rocks, they are found in all the major groups ranging from ultrabasic to acid alkaline types; the amphiboles are typical constituents of the intermediate members of the calc-alkaline serie. In addition, amphiboles crystallizes in a large variety of regionally metamorphosed rocks, from greenschist to lower granulite facies. They are less common in contact metamorphism; however, they are not rare in contact-metamorphosed limestones, dolomite and other Ca-rich sedimentary rocks (Deer et al. 1992).

Amphiboles are double-chain (ino)silicates with a Si(Al):O ratio of 4:1. Owing to the mono-dimensional character of their structural units (chains), and to the presence of strong bonds, amphibole structure looks normally elongated along the crystallographic *c*-axis. Therefore, fibrous-asbestiform shapes are very common (Table II.2).

The general chemical formula of the amphiboles can be written as

$$A\ B_2\ C_5\ T_8\ O_{22}\ W_2$$
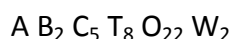
where A = Na, K, □, Ca, Li;

B = Na, Li, Ca, Mn^{2+}, Fe^{2+}, Mg;

C = Mg, Fe^{2+}, Mn^{2+}, Al, Fe^{3+}, Mn^{3+}, Ti^{4+}, Li;

T = Si, Al, Ti^{4+};

W = (OH), F, Cl, O^{2-}.

Minor elements such as Zn, Ni^{2+}, Co^{2+}, V^{3+}, Sc, Cr^{3+} and Zr are also observed in C site. As a consequence of the great chemical complexity of this group of minerals, there are many problems connected with the acquisition of chemical data, and calculation of the chemical formula (Hawthorne and Oberti 2007a). Hawthorne and Oberti (2007) stressed that the availability of detailed chemical data is a crucial point. The occurrence of multiple valence cations (Fe, Mn) in the same site and of light elements (H, Li) makes extremely difficult the determination of a reliable crystal-chemical formula (Ballirano et al. 2017). In the case of fibrous amphiboles the small dimensions of samples amplifies this effort by preventing the use of conventional analytical procedures.

In general, four large groups of amphibole are recognized, according to the prevalent cations in the B (or M4) site: calcic amphibole, alkali amphibole, sodic-calcic amphibole, and Fe-Mg-Mn amphibole (Hawthorne and Oberti 2007b).

The amphibole structure consists of two principal elements, a double chain of tetrahedra and a strip of edge-sharing octahedra, both of which extend in the *c*-direction (Fig. II.8a). There are two topologically distinct types of tetrahedra in the double chain that are designated T1 and T2, and three distinct types of octahedra that are designated M1, M2 and M3. The M4 site is at the junction of the strip of octahedra and the chain of tetrahedra, and the A site at the centre of a large cavity is below the hexagonal ring of tetrahedra (Fig. II.8a).

Mineralogical name	Commercial / Popular name	Regulated (2003/18/CE)	Chemical formula	Space group
Actinolite	Actinolite	✓	$\square Ca_2Fe^{2+}{}_5\ [Si_8O_{22}](OH)_2$	*C2/m*
Grunerite	Amosite	✓	$\square Fe^{2+}{}_2Fe^{2+}{}_5\ [Si_8O_{22}](OH)_2$	*C2/m*
Anthophyllite	Anthophyllite	✓	$\square Mg_2Mg_5\ [Si_8O_{22}](OH)_2$	*Pnma*
Riebeckite	Crocidolite	✓	$Na_2(Fe^{2+}{}_3Fe^{3+}{}_2)\ [Si_8O_{22}](OH)_2$	*C2/m*
Tremolite	Tremolite	✓	$\square Ca_2Mg_5\ [Si_8O_{22}](OH)_2$	*C2/m*
Fluoro-edenite	Fluoro-edenite		$NaCa_2Mg_5\ [Si_7AlO_{22}]F_2$	*C2/m*
Winchite	Winchite		$\square CaNa(Mg_4Al)\ [Si_8O_{22}](OH)_2$	*C2/m*

Table II.2. Regulated and not-regulated fibrous amphiboles of environmental interest.
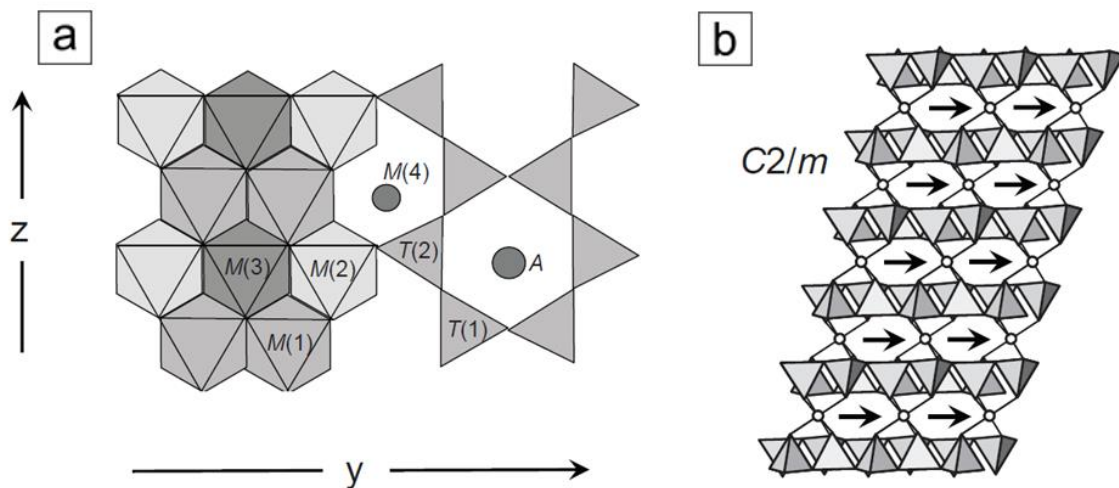
Figure II.8. Schematic representation of amphibole structure showing a) the chain of tetrahedra, the strip of octahedra, the M4 site and the A site; b) the stacking of layers projected down the a-axis for the C2/m structure type (Hawthorne and Oberti 2007a).

The basic feature of the structures of all amphiboles is the presence of $(Si,Al)_4$ tetrahedra linked to form chains which have the composition $(Si,Al)_4O_{11}$. These chains repeat along their length at intervals of approximately 5.3 Å and this defines the *c* parameter of the unit cell. Finally, they are separated and bonded together laterally by strips of M cations (Mg, Fe, etc.) and by the presence of additional hydroxyl ions.

The double chain of tetrahedra contains the two sites T1 and T2 that regularly alternate along the single chain; the chain is fixed to an adjacent one with a bridging oxygen between the two T1 tetrahedra. The M1, M2 and M3 sites are conventionally grouped together and they host the so-called C cations. They are octahedrally coordinated but in the case of M1 and M3 the coordination comprises two and four anions, respectively, which may be (OH), F, Cl and O^{2-}, according to chemistry. The C cations identify a strip of edge-sharing octahedra that is linked to the double chain of tetrahedra along the *a* and *b* axes. On the other hand the M4, hosting B cations, is located at the rim of the octahedra strip and is bonded to eight oxygen atoms in a square antiprism coordination. Finally, A site occurs within a cavity located between the back-to-back double-chain of tetrahedra. The size of the cations at M1, M2, M3 and M4 defines the way in which they are surrounded by oxygens of the $(Si, Al)O_4$ chains, and this in turn determines the positions of a pair of chains relative to one other. In most cases the stacking of chains is able to produce a monoclinic cell, as for example in tremolite (Fig. II.8b; Table II.2). The presence of similar sites, but not identical, in the amphibole structure (i.e. M1, M2, M3 octahedral; T1, T2 tetrahedra) provides a chance for the ordering of cations among them. In tetrahedra, Al strongly prefers T1 and in octahedral Al and Fe^{3+} prefer M2. The preference of Fe^{2+} between sites M1, M2, M3, M4 varies from one amphibole subgroup to another. The replacement Mg-Fe is a simple substitution which involves no charge

imbalance but it is critical to optical and physical properties of amphiboles and to their paragenesis (Hawthorne and Oberti 2007a).

In amphiboles, different ordered stacking sequences of tetrahedra-octahedral sheets along the *a*-direction are associated with different space-group symmetries. As a general rule, amphiboles of environmental interest crystallize in the monoclinic system, space group *C*2/*m* (Table II.2). The apical O atoms of the tetrahedra provide the anions for the coordination of the octahedra, and hence there is a stagger of ± c/3 between adjacent sheets of tetrahedra. For monoclinic amphiboles, this stagger is always in the same direction (Fig. II.8b).

A more detailed discussion of the Ca-amphibole tremolite will follow, with a particular attention to its fibrous variety, naturally occurring in New Caledonia units.

$Ca_2(Mg,Fe^{2+})_5[Si_8O_{22}](OH,F)_2$	
Monoclinic	
α	1.599-1.688
β	1.610-1697
γ	1.620-1.705
δ	0.027-0.017
$2V_\alpha$	86-62°
Orientation	γ:z 28-10°, $\beta = y$, OAP (010)
Dispersion	r < *v*, weak
Density	2.99-3.48
Hardness	5-6
Cleavage	{110} good; {100} parting; (110)(1-10) ~ 56°
Twinning	{100} simple, lamellar, common; {001} lamellar,rare
Colour	Tremolite: colourless or grey
	Actinolite: pale to dark green
	Fe-actinolite: dark-green to black
	→ in thin section colourless, pale green, deep green
Pleochroism	Tremolite: non-pleochroic
	Actinolite and Fe-actinolite: strength of pleochroism related to iron content, with α pale yellow, yellowish-green; β pale yellow-green, green; γ pale green, deep greenish-blue
Unit cell	a~ 9.85 Å, b~ 18.1 Å, c~ 5.3 Å, β ~ 105°
	Z = 2; space group *C*2/*m*

Table II.3. Mineralogical optical and structural parameters for tremolite–Fe-actinolite amphibole series (after Deer et al. 1992).

II.1.2.1. Fibrous tremolite

Tremolite is a metamorphic mineral which occurs in both contact and regionally metamorphosed rocks. It is one of the most constituents in low-grade regionally metamorphosed ultrabasic rocks such as tremolite-talc and tremolite-carbonate-antigorite schists. Unfortunately, it occurs largely in rocks that are currently subjected to excavation for various construction projects. In addition, tremolite fibres are usually present as accessory minerals in many talc deposits, where tremolite may be associated with asbestiform winchite and richterite (Van Gosen et al. 2004).

In the Mg-Fe series of Ca-amphiboles, the names tremolite, actinolite and Fe-actinolite (Table II.3) are used with Mg/(Mg + Fe) = 1.0-0.9, 0.9-0.5, 0.5-0.0, respectively. In tremolite M1, M2, M3 and M4 consist of Ca, while the A site is vacant. Actually, natural
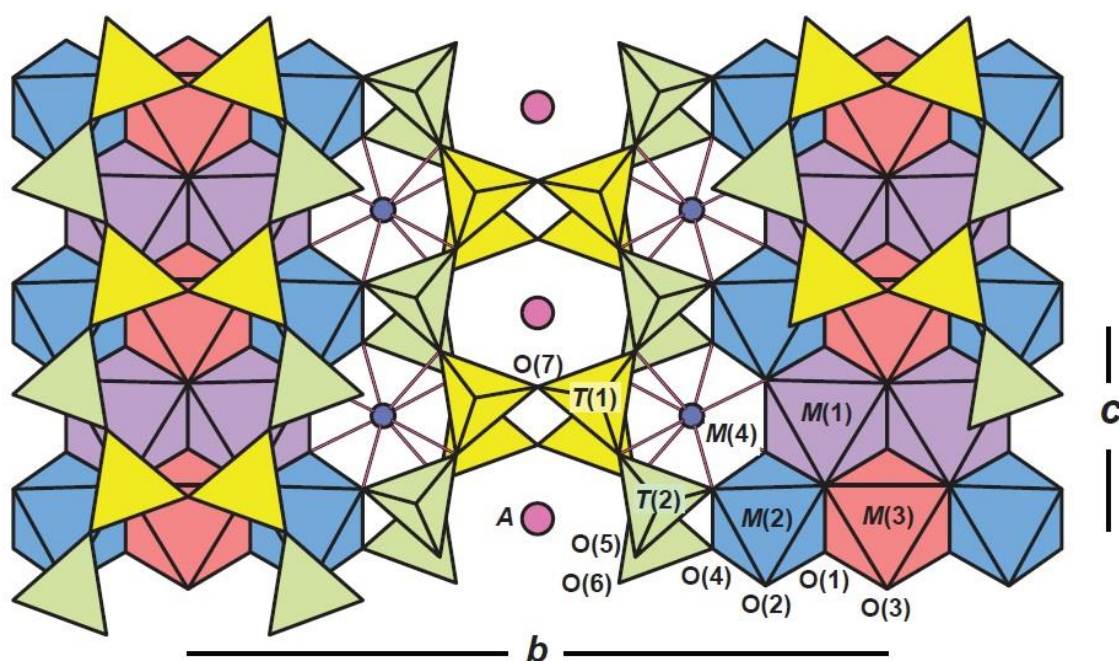
Figure II.9. Monoclinic C2/m tremolite structure projected onto (100). Polyhedra: T(1) = yellow, T(2) = pale green, M(1) = mauve, M(2) = blue, M(3) = red; sites: M(4) = blue circle, A = fuchsia circle (Hawthorne and Oberti 2007a).

samples show little variations in chemical composition compared to the ideal chemical formula. Higher contents of Fe generally occur in the more aluminous amphiboles. Replacement of Ca by Na accompanied by Al for Mg and/or Na in A site tends to be relatively rare in natural tremolite-actinolite.

Tremolite structure, space group *C2/m*, is schematically represented in figure II.9. Here, two distinct T1 and T2 sites are occupied by Si(Al), which are tetrahedrally coordinated and link to form one distinct type of double-chain of tetrahedra. Following the general

structural arrangement, the T1 and T2 tetrahedra alternate along the length of the double chain, and the T1 tetrahedra bridge across the double chain. On the other hand, three distinct octahedrally coordinated M sites are generally occupied by Ca cations, with 1, 1 and 2/*m* point symmetries, respectively. Within the strip of octahedra, extensive sharing of edges occurs between the M1, M2 and M3 octahedra. The double chain of tetrahedra binds to the strip of octahedra in the *b*-direction with T2-M2 linkage through common O4 oxygen atoms, and in the *a*-direction with T1 and T2 linkage through common O1 and O2 oxygen atoms. The M4 site is at the periphery of the strip of octahedra, has point symmetry 2, and is occupied by Ca cations. Finally, the A site, generally vacant in pure tremolite samples, occurs at the centre of a large cavity between the back-to-back double-chains of the structure (Fig. II.9).

Concerning crystal habits of tremolite natural samples, they may vary from prismatic through acicular to asbestiform. Furthermore, there is also to very hard compact microcrystalline variety nephrite, one of the two forms of precious jade.

II.1.3. CRYSTAL HABITS OF ASBESTOS AND NON-ASBESTIFORM MINERALS

The terms *asbestos* or *asbestiform minerals*, according to regulations of the world, refer only to those silicate minerals that occur in poly-filamentous bundles and that are composed of very long fibres with a relatively small diameter, most of them showing a high degree of flexibility (Ross et al. 2008; IARC 2012; Belluso et al. 2017). Actually, no conclusive and shared definition of *fibre*, *asbestos* and other related terms exists. The issue of asbestos definition is very important and requires clarification. Most of definitions reported in the past (e.g. U.S. Department of Labor 1975; IARC 1977) did not give specifications about fibre and fibrous designations, only referring to «six fibrous silicates classified as asbestos: the fibrous serpentine called chrysotile and the fibrous amphiboles actinolite, amosite, anthophyllite, crocidolite and tremolite» (U.S. Department of Labor 1975). NIOSH-OSHA (1980) firstly linked the concept of morphological "fibrosity" at the microscopic scale to these hazardous materials, involving a first generic definition of *aspect-ratio* (length-to-width >3:1; NIOSH-OSHA 1980; Lentzen et al. 1982; NIOSH 1990). In contrast to most of the asbestos definitions, Ross *et al.,* (1984) established arbitrarily an aspect-ratio of 20:1, but they did not restrain both length and width (or diameter) of the particles with fibrous-asbestiform habit. More recently, asbestos designations integrate several information about their properties (e.g. flexibility) and morphological features (e.g. long, thin; Veblen and Wylie 1993; Case et al. 2011). Nowadays, according to IARC (2012) there is still a lack of consistency in fibre classification and in asbestos categorisation. It should be noted that all dimensional criteria involved in regulatory surveys and carcinogenic studies (e.g. WHO criteria: length ≥5 µm, diameter ≤3 µm, length/diameter ratio ≥3:1) does not concern asbestos definition *strictu sensu*, but they are related to the determination of airborne fibres.

Sometimes they have been erroneously used also to indicate asbestos fibres. It is important to remember that for the WHO (1997) and others criteria concerning health issues, the dimensional standards for asbestos are based on the breathability of the specific particles (fibres). That is, the particle/fibre should be inhalable but also be able to penetrate down to the alveolar space. Nevertheless, fibres shorter than 5 μm, diffused abundantly in air and consequently breathable, can involve a health risk as well (Lemen 2004; Suzuki et al. 2005; Boulanger et al. 2014). Finally, on the basis of epidemiological data (ANSES 2014), *in vitro* (Gazzano et al. 2005; Groppo et al. 2005; Turci et al. 2005; Cardile et al. 2007; Pugnaloni et al. 2010) and *in vivo* (Wozniak et al. 1988, 1993) studies several asbestiform minerals, such as fibrous antigorite or balangeroite, have been classified as hypothetically toxic. Actually, no relevant chronic studies with these mineral fibres could be identified. Further investigations are therefore necessary (ANSES 2014).

However, crystal habit and morphology represent some of the main parameters involved in the evaluation of potential risk in health asbestos concerns. From a textural point of view, poly-filamentous bundles of hazardous fibres are characterized by fibres which easily separated from one another showing splaying ends (IARC 2012). The individual fibres, called fibrils, have tendency to grow along the fibre axis in parallel orientation to the bundle length (Ross et al. 2008). Actually, in the real cases a large number of intermediate situations occur. Are we really able to distinguish with absolute certainty an aggregate of cleavage fragments from a bundle of platy lath-shaped crystals of fibrous-lamellar antigorite? In this context, a universal terminology of different crystal shapes and morphology occurring for asbestiform and non-asbestiform minerals is necessary. According to last EMU School, held in Modena (Italy) in June 2017, entitles "*Mineral fibres: crystal chemistry, chemical-physical properties, biological interaction and toxicity*", the scientific community points the attention to the need to adopt a common vocabulary.
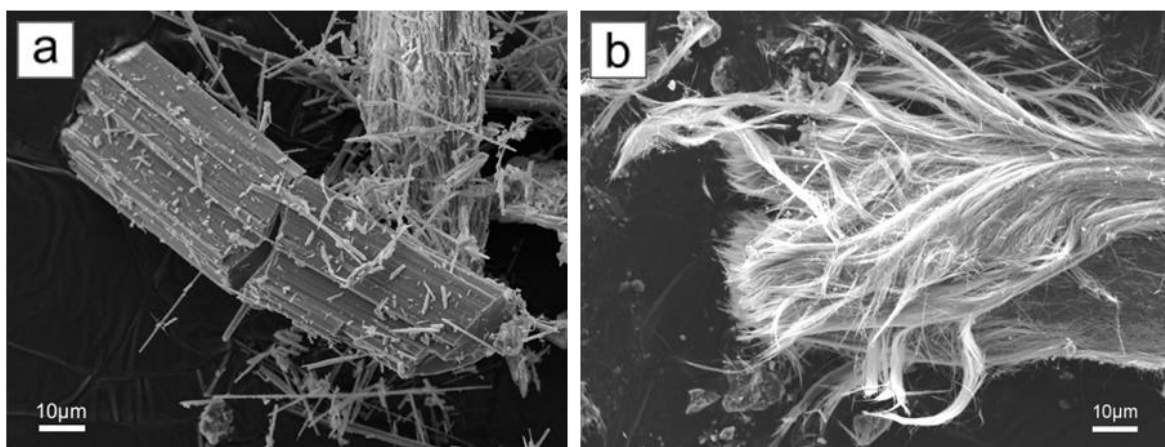

Figure II.10. a) Cleavage fragment of prismatic tremolite; b) Chrysotile fibre and bundles of fibres (SEM images).

An asbestos fibre is a bundle which can be subdivided into smaller bundles, and then into fibrils, where fibril is the thinnest component of fibre bundles, a single crystal. ISO 22262-2:2014 defined a fibril as «a single fibre of asbestos which cannot be further separated longitudinally into smaller components without losing its fibrous proprieties or appearance». Notice that fibres generally present frayed ends (Figure II.10b). Some of the other characteristics of asbestiform fibres are not only the length and thinness, with a high length-to-width ratio, but they are also flexible, with great tensile strength and in bundles with frayed or splayed ends. On the contrary, inflexible minerals characterized by crystals that grow in two or three dimensions and that cleave into fragments, rather than separate longitudinally into fibrils, are classified as mineral with a non-asbestiform habit. From the morphological point of view, they are identified as *cleavage fragments*. It is worth noting that these minerals may have the same chemical composition of the asbestos varieties (Fig. II.10a; IARC 2012). Their fragility encourages their rupture in small crystals that can aggregate, be irregular of form parallel beams. Cleavage fragments are portions of minerals that have broken primarily along crystallographic planes, though some fragments may form along non-crystallographic planes of weakness called "parting planes" (Belluso et al. 2017). Contrary to fibrous minerals they do not exhibit frayed or splayed ends, and they cannot be easily subdivided until they are isolated as fibrils (Fig. II.10).

In practise, cleavage fragments formed from non-asbestos minerals are not true mineralogical fibres (NIOSH 2011). Nevertheless, if they fit the regulated dimensional criteria, they can be counted as asbestos. To avoid confusion still existing in the exactly meaning of the term *fibre*, NIOSH (2011) indicates the use of the term *elongated mineral particles* (EMP) to all small particles with a minimum aspect ratio 3:1, comprising both asbestiform and non-asbestiform habits. Thus, the term EMP includes acicular, needle-like, columnar and prismatic habits in addition to cleavage fragments, as well as all fibres not-yet-regulated as asbestos (Fig. II.11).

From a mineralogical point of view, except for chrysotile which crystallizes with a typical tubular morphology, the shape of the other asbestos and asbestiform minerals is extremely variable. As reported in figure II.11 serpentine and amphibole minerals may display both lamellar and fibrous-asbestiform features. Considering single-crystal shapes, these minerals generally appear as elongated particles in the forms of: 1) bladed, lath-shaped crystals with idiomorphic ends, 2) lamellar, slat-shaped crystals with regular or partly ragged ends, 3) needle-like or acicular crystals, 4) prismatic crystals, and 5) tubular crystals with hollow (or not) bodies. All these elongated morphologies differ primarily in their length/width ratio. In the arrangement of these crystal morphologies, differences between parallel intergrowths of minerals and aggregates, in which individual particles platy parallel intergrowth of slat-shaped crystals and/or tubular fibrils and fibrous aggregates of columnar, tubular and lath-shaped crystals, are observed. In addition, several cases of intermediate fibrous-lamellar morphologies may occur (Fig. II.12).
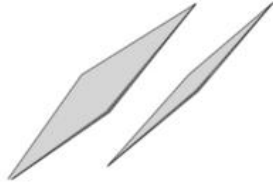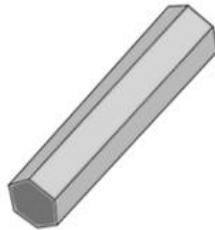
SINGLE-CRYSTAL SHAPES
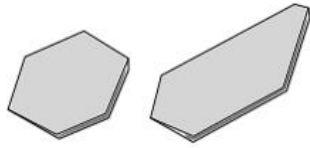
Bladed (fragment)
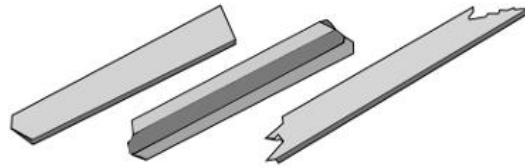
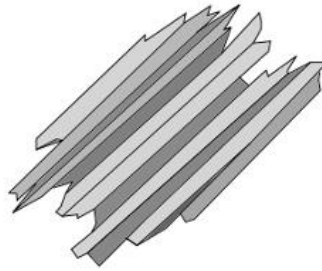Lamellar (fragment)

Needle-like

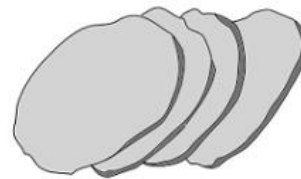Acicular

Prismatic

Tubular (fibril)

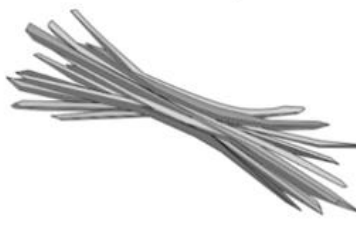## CRYSTAL- AGGREGATE PATTERNS OR ARRANGEMENTS

Columnar

Lamellar

Platy

Book-shaped

Fibrous

Fibrous (asbestiform)

Figure II.11. Principal crystal habits of natural asbestiform and non-asbestiform minerals.
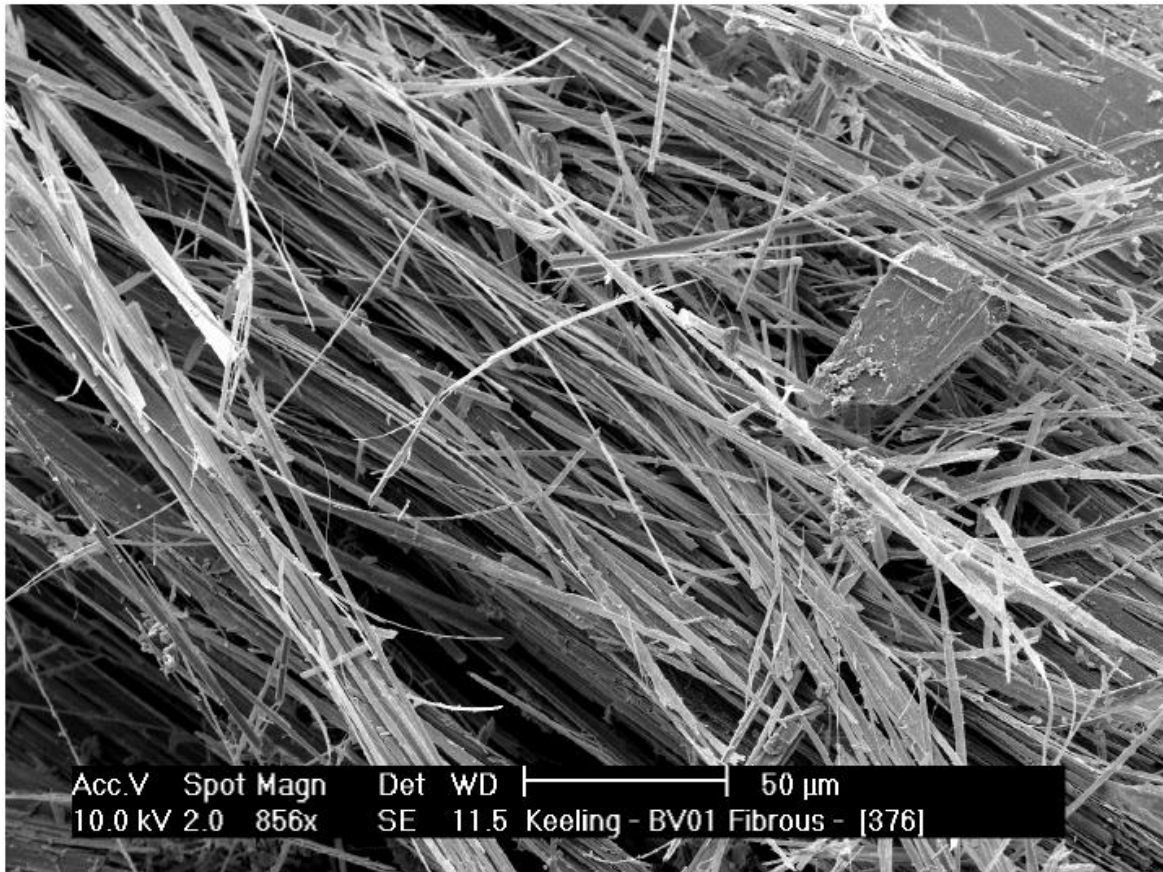
Figure II.12. Fibrous-lamellar crystals of antigorite from Rowland Flat area, Barossa Valley, South Australia. Fibrous aggregates, consisting of both lamellar-bladed and tubular crystals, present the typical splaying ends (Keeling et al. 2006).

Chrysotile is generally depicted as tubular particles or fibres which tend to form parallel intergrowth and aggregates of fibres. Actually natural chrysotile fibres consist of aggregates of bundles of long, very thin, flexible fibrils that resemble scrolls or cylinders (Fig. II.13a). Chrysotile forms irregular, curvilinear curly aggregates of fibril bundles with splayed ends. The sizes of each individual fibril, showing a diameter <0.1 µm and a length between 0.2 and 200 µm or even more, depend on the mode and kinetics of crystal growth. As mentioned above, other kinds of habits are involved, less frequently and generally associated to synthetic fibres: tube-in-tube, cone-in-cone, helical and spiral-like.

Closest to chrysotile habit, polygonal serpentine crystals appear as tubular fibrils elongated along *x*, stockier than chrysotile, forming bundles parallel to their *x* fibre axis. Their length is variable. Their fibrils can be longer than several micrometres but generally shorter than those of chrysotile (Baronnet and Belluso 2002; Belluso et al. 2017). The diameter is usually more than 0.1 µm (Papp 1990) but it may be 0.05-0.4 µm wide, with irregular, thin canals. Generally it presents irregular fibre terminations (Baronnet and Belluso 2002; Andreani et al. 2004).
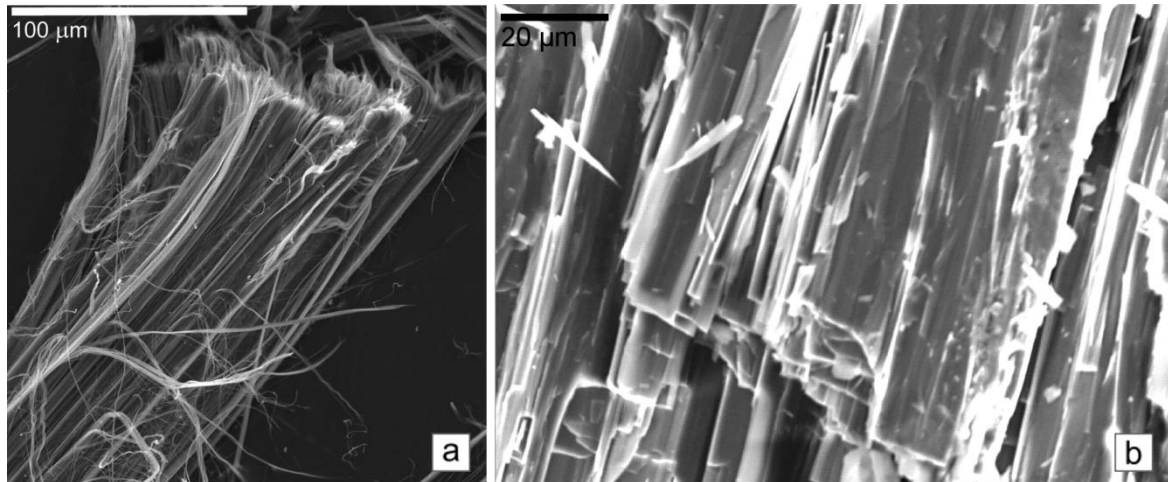
Figure II.13. Chrysotile (a) and antigorite (b) characteristic habit from Van Gosen (2007) *and* Rinaudo et al. (2003)*, respectively.*

Antigorite, due to its characteristic corrugated layer-lattice, gives rise to different habits, from bladed-columnar (Fig. II.13b) to asbestiform-fibrous crystals (Fig. II.12; Keeling et al. 2006, 2008). The electron microscope images show platy particles as well as lamellar intergrowths and aggregates. Furthermore, lath-shaped crystals with irregular or even ragged ends can be observed. When the dimensions of the elongated laths fit the dimensional criteria applied to regulated-asbestos, antigorite elongated particles generally appear flexible and longitudinally separated into thinner fibres, or more frequently into thinner fibrous-lamellae. In this case, antigorite fibres and fibro-lamellae shall be classified and counted as asbestos. Fibrous-lamellae, lath-shaped and elongated particles vary in length from several micrometres to some hundreds of millimetres, with smallest diameters of 0.08 µm, usually <1 µm, a large aspect ratio exceeding 100:1 (length and thickness, respectively; Cardile et al. 2007; Keeling et al. 2008, 2010; Fitz Gerald et al. 2010; Bloise et al. 2014). Moreover, their flexibility varies from stiff to moderate, with numerous fibres having a diameters <1 µm (Keeling et al. 2008). Antigorite fibres, aggregated in bundles, are parallel to each other and more or less randomly rotated around [010].

Amphiboles may occur in association with mineral fibres of the same species or, as often occurs, with different species to form both bundles of tightly packaged fibres and aggregates of randomly oriented fibres. The fibre axes are parallel or sub-parallel to the length of the bundle. Commonly, the most abundant intergrowths of asbestiform amphiboles consists of oriented tremolite fibres associated to talc, or anthophyllite fibres with talc (Stemple and Brindley 1960; Virta 1985). In this kind of associations, amphibole fibres are usually crystallographically rotated with respect to each other (Gunter et al. 2007a,b). The natural crystals of tremolite generally exhibit a columnar habit from prismatic to acicular or asbestiform (Fig. II.14). When the dimensions fit the regulated criteria, these elongated crystals are classified as asbestos.
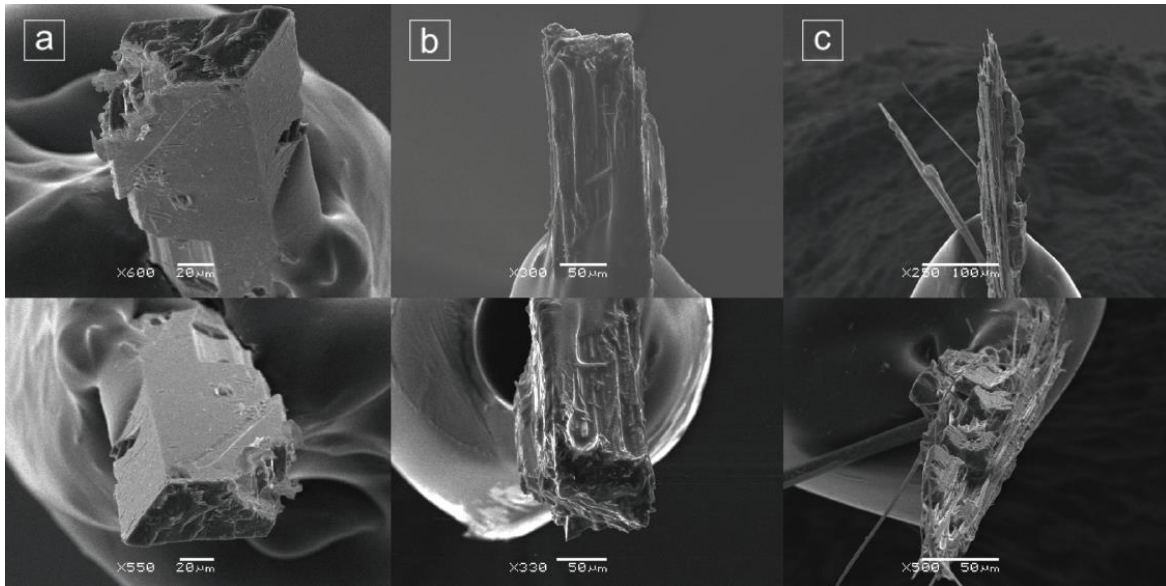
Figure II.14. Different amphibole morphologies from the Libby vermiculite deposit: a) blocky-prismatic, b)intermediate morphology, and c) acicular, fibrous-asbestiform (Sanchez and Gunter 2006; Gunter et al. 2007a).

Tremolite typically shows a long, thin and quite rigid prismatic habit, elongated according to [001] fibre axis and generally flattened along the (100) plane. Tremolite may occur as long, straight, parallel sided and lath-shaped aggregates, fairly flexible or as brittle, single fibrils as well as bundles of fibres. Fibrils have a diameter in the range 0.5-0.15 µm. The fibre length is normally more than 8 µm and generally is in the range 60-100 µm, although it can reach some ten of millimetres (Bloise et al. 2014). The width is normally <0.5 µm, but it varies from 0.1 µm to 0.3 µm (Langer et al. 1974; Davis et al. 1991; Vignaroli et al. 2014). Fibres show parallel sides, regular terminations and straight shapes.

II.2. General discussion on analytical methods

In recent years, a great work of investigation of mineral fibres has been carried out with the aim of better understand the mechanisms responsible for the carcinogenicity of asbestos. Almost all analytical techniques currently in use in the different lines of research have been tested. The entire scientific community is in agreement that analysis of asbestos is a complex task which involves different approaches depending on the characteristic of the sample (bulk, filter, rock) and, more important, on the purpose of assessment (Nichols et al. 2002; Cavariani et al. 2010).

The rising awareness in risk due to asbestos environmental exposition leads to a new interest in the *in situ* characterisation of regulated and not-yet-regulated mineral fibres. The principal methods, listed in the distinct norms and used by commercial-asbestos laboratories to identify asbestos, have therefore to be applied to natural samples. It should be remembered that physical and chemical properties of naturally occurring asbestos, in geological samples, are likely to be more complex and variable than asbestos encountered in manufactured products. In addition, some laboratories that routinely perform analysis of manufactured materials or air monitoring samples may not be familiar with the analysis of geological materials. The identification of the asbestiform minerals in a geologic sample is relatively straightforward. Moreover, the surface of mineral fibres may behave quite differently from the bulk. This diversity plays a potentially crucial role in modulating the chemical and biological reactivity of fibrous minerals. On the contrary, quantification of the amount of asbestiform minerals in a geological sample is more difficult. Consequently, it is important that geologists work closely with the laboratory to clearly define the analytical goals for the project.

In the past, misinterpretation in identification of asbestiform minerals led to a commercial use of minerals analogous to the six-regulated asbestos. This is the case, for example, of a small quarry of white asbestos near Rowland Flat, at north-east of Adelaide, in the South of Australia. Originally described as a mine of amphiboles (Ward 1937), subsequently the white asbestos was classify as chrysotile (Hiern 1976). Only in recent years, during a routine assessment of factors affecting rehabilitation of the abandoned mine site, mineralogical studies identified the white asbestos as fibrous antigorite (Keeling et al. 2006, 2008; Fitz Gerald et al. 2010). Misinterpretations are even more likely due to the great variability in morphologies and chemical composition of these groups of minerals. Additionally, the closely intergrowth, also at the sub-millimeter scale, of different asbestiform (and not) mineral phases complicates the identification process. A typical example is the geological occurrence of chrysotile and tremolite asbestos, associated to subordinated aggregates of fibrous antigorite, in metamorphosed ultrabasic rocks of the Ankara and Eskisehir areas, in north-western Turkey (Dogan and Emri 2000).

Detailed structural and chemical characterisation of asbestos minerals is very difficult to tackle for the small dimensions of crystals, the instability under different analytical probes and the extremely variable chemical composition, even for neighbouring fibres. Unless the fibrous habit, the serpentine minerals are seldom distinguishable from one another either in hand specimen and in thin section. All these disadvantages may be overcome by combining several techniques (e.g. X-ray Powder Diffraction to micro-Raman or IR spectroscopy), aimed at exploring the structure and chemical composition both at bulk and surface levels. It is well-known that unequivocal identification of asbestiform minerals requires sophisticated single-crystal X-ray diffraction or transmission electron microscopy techniques (Cavariani et al. 2010; Ballirano et al. 2017). Conversely, it is important to note that all analytical instruments can provide a useful contribution in the study of fibrous and asbestiform minerals. The introduction of a particular methodological protocol depends exclusively by the questions we have to answer, that is to say, the required observation scale. It should be remembered that most of the analytical techniques involved in the study of mineral fibres are conducted on a small quantity of sample, generally on few micrograms of material, which have to be selected in a representative way. During the phases of sample collection and preparation, all portions which appear macro- and microscopically different must be examined.

A short description of the main performances (advantages and/or disadvantages) of analytical instruments involved in this study is here reported.

II.2.1. MICROSCOPIES

The largest use of microscopic methods in the investigation of asbestos is a direct consequence of importance of morphology and size distribution in the evaluation of the asbestiform nature. In a research setting, all microscopic instruments may be used. Nevertheless, only by comparing analytical performances of different microscopes, the analyst can select the most appropriate analytical procedure (Table II.4). Optical techniques are usually applied both to the description of thin sections, for purpose of petrographic description and classification of rock samples, and to grain mounts, for identification of individual mineral grains using oil immersion methods. The main advantages of Polarized Light Microscopy (PLM) are to confirm the presence/absence of asbestos fibres in bulk materials and to determine their morphology (asbestiform vs. non-asbestiform). Electron microscopy techniques, instead, are of special importance into the investigation of smaller fibrous minerals and their admixture, because the smallest particles (fibres and fragments) cannot usually be solved by optical microscopy. Generally, Scanning Electron Microscopy (SEM) provides useful information on the texture of fibrous minerals, and on the distribution of minerals in them; whereas the higher resolution of Transmission Electron Microscopy (TEM) allows a more detailed

Information	PLM	SEM	TEM
	Morphology and mineral identification of fibres	Morphology and chemical composition of fibres	Morphology, chemical composition and crystal structure of fibres
Resolving power	0.2 µm	5 nm	0.2 nm
Normal working magnification	500x	2000x	10000x
Real analytical resolution	0.2 - 0.3 µm	50 - 100 nm	1 - 2 nm
Determination of asbestos mineral phases	PLM-DS	EDS	SAED & EDS

Table II.4. Comparison of performances of major microscopic techniques (modified after Cavariani et al. 2010).

characterisation of mineral structure, in term of evaluation of fibre dimensions. Actually the evaluation and quantification of the fibre size is obtained by SEM. TEM is involved when fibres are so thin and small that they cannot be solved by SEM (Cavariani et al. 2010). Furthermore, to determine the width of fibres, a specific sample-preparation procedure, involving ion-thinning preparation of fibres sectioned perpendicularly to the fibre axis, is required.

Energy Dispersive X-Ray Spectroscopy (EDS) is by far the most used routine method for chemical analysis related to asbestos work. EDS systems are commonly mounted on both SEMs and TEMs. Thus it is possible to obtain an EDS spectrum and a semi-quantitative chemical composition of micron-sized areas in the SEM and of submicron-sized areas in the TEM. However, EDS data are not as precise or accurate as Wavelength Dispersive Spectrometry (WDS). For these reasons, SEM and TEM are commonly used to identify asbestos in air monitoring samples collected from occupational settings; TEM is also used to identify asbestos in water samples. Selection of right electron optical imaging techniques (associated to chemical analysis) and preparation methods depend on the material itself and on the kind of information required.

Microscopic methods involved in this study are described below in order of increasing magnification.

II.2.1.1. Polarized Light Microscopy

Currently in use in investigation of ACMs, Polarized Light Microscopy (PLM) was the first widely used instrument in the asbestos regulatory field. As preliminary investigation device, PLM has been demonstrated an essential tool in the characterisation of mineral association of rock samples and remains the most familiar analytical technique to

geologists. As mentioned above, PLM may be applied both on thin petrographic section, for the identification of mineral assemblages and in the evaluation of their textures, and to elongated particles for identification of individual mineral particle using a dispersion staining method. Despite its considerable limits in detection of smaller fibres (<0.8 μm; Cavariani et al. 2010), this traditional method allows to make a first reliable identification, determining asbestiform from non-asbestiform habits.

Examination of petrographic thin sections (30 μm thick slices of rock glued to glass slides and polished) allows to obtain information on rock-type, mineralogy, texture, alteration, and metamorphic grade – all of which may be useful in the investigation of naturally occurring asbestos. However, identification of asbestos minerals in thin section is difficult. In fact, individual fibres are generally much thinner than the thickness of the thin section, so numerous fibres may overlap in a vein and other minerals may be under asbestos fibres. Additionally, due to thickness and 2-dimensional nature of the thin section, it is difficult to distinguish the crystal habit among asbestiform, fibrous, acicular and lamellar shapes. Using optical microscope observation only, some asbestiform minerals, such as fibrous antigorite and chrysotile, may be confused, especially when they display similar optical properties: fibrous-lamellar crystals, for both antigorite and chrysotile, may appear thin, pale-green to white and more or less flexibles (e.g. Keeling et al. 2006, 2008).

From a petrographic point of view, serpentine minerals occur with a wide variety of textures and optical appearances. Although they are sometimes recognisable, they often can be correctly interpreted only by the use of other complementary techniques, such as micro-Raman spectroscopy and TEM. Pseudomorphic *mesh* and *hourglass* textures, forming after transformation of olivine, amphibole, talc and chlorite, consist mainly of lizardite and secondary chrysotile; whereas pseudomorphic *bastite*, formed after pyroxene and amphiboles alteration, generally is composed by a mix of lizardite and chrysotile (Wicks and Whittaker 1977). Some of the components of those textures consist of lizardite platelets stacked perpendicular to the apparent fibre axis. Non-pseudomorphous textures, formed either from the same primarily minerals of from pseudomorphic serpentine textures, are instead composed mainly of *interpenetrating* and/or *interlocking* blades of antigorite. In addition, textures formed in serpentine veins occur. Antigorite and chrysotile asbestos can be easily recognized in veins. On the other hand, isotropic veinlets of chrysotile and lizardite are optically indistinguishable (Wicks and Whittaker 1977; O'Hanley 1996). The above classification of textures into pseudomorphic, non-pseudomorphic, and vein-types is in some respects an idealisation. In real cases this distinction appears more gradual (Wicks and Whittaker 1977). Actually, serpentine minerals occur most closely associated at the micro- and sub-micrometric scale than expected. It is not so curious to observe some micrometric veins of chrysotile among antigorite blades in a typical example of interpenetrating antigorite texture (Petriglieri et al. 2015). Contrary to serpentine minerals, Ca-amphiboles of tremolite-

actinolite series, observed in thin sections, display more distinctive features. They are easily recognised by their common lack of colour or very pale green, by higher birefringence and optical axial angle and by the presence of cleavage. Moreover, they usually display as acicular, needle-like to fibrous crystals with a medium relief. They also show a medium-high interference colour, which decreases with increasing of Fe^{2+} content. Furthermore, the distinction between tremolite-asbestos from acicular-actinolite crystals is not easy.

In this context, the distinction of various asbestiform minerals by means of thin section observation is difficult. Consequently, natural elongated particles are preferred for the identification of asbestos minerals. In this last case, it is possible to view particle boundaries and the splayed ends of fibres that are necessary to distinguish cleavage fragments from fibres.

PLM associated to Dispersion Staining method of observation (PLM/DS), and equipped with a phase contrast mask, is one of the main routinely technique used by specialized laboratories (e.g. Arpae - Agenzia regionale per la prevenzione, l'ambiente e l'energia dell'Emilia Romagna, Italy) for the analysis of fibre concentrations of bulk building materials. Each fibre type, sampled by selecting a few representative fibres or bundles, is placed on a microscope slide using the appropriate Refractive Index oil (e.g. RI 1.550 for Chrysotile, RI 1.605 for Tremolite; Health and Safety Executive 2006). Positive identification of asbestos requires the determination of several optical properties, such as morphology, colour and pleochroism, index of refraction, birefringence, extinction characteristics and sign of elongation, in the correct observation mode, as reported in table II.5. It is general opinion that the fine-grained nature of most serpentine specimens makes impossible to realize a complete optical description of serpentine minerals. Due to the similarity between the refractive indexes of lizardite, antigorite and chrysotile minerals, the distinction of these phases cannot be reliably with PLM but could be by PLM/DS. However, a specific work aimed to find the RI liquids that match as much as

Property	Observation mode
Morphology	All modes
Colour and pleochroism (if present)	Polariser only
Birifrangence (anisotropic behavior)	Crossed polars
Extinction characteristics	Crossed polars
Sign of elongation	Crossed polars with first order red compensator
RI assessment	Normally using a dispersion staining, or phase contrast, objective with polariser only

Table II.5. Identification requirements of a single asbestos fibre by means of PLM (Health and Safety Executive 2006).

possible the refractive index value of lizardite and antigorite varieties is still lacking. Conversely, the amphiboles minerals are generally considered more simply to identify by PLM/DS for their peculiar optical properties. Therefore, cummingtonite and winchite amphibole minerals may be confused with tremolite. It should be noted that the refractive indices and densities of members of the tremolite-actinolite series increase more or less linearly with increasing Fe content, which lead to a little, but not negligible, variation in optical proprieties. Although Fe-content remains the major source of variation, Mn-, Al- and F- content changes may also occur.

The dispersion staining technique uses high-dispersion oils, which gives peculiar bright colours to crystalline grains, indicative of the refractive index of the grain (Table II.8). Using colour charts developed for this purpose, the analyst is able to obtain an indirect measurement of the refractive index of the particle, observed when the fibre is aligned in a particular optical orientation. PLM/DS analysis is relatively low cost and widely available. It offers great sensitivity even at very low concentrations and the chance to generally differentiate the non-asbestiform and asbestiform habits. It is worth noting that not many other analytical methods offer all of these features. Conversely, the main limitation of the PLM/DS method is the size of the fibres. Although modern optical microscopes can resolve fibres with diameters less than 1 µm using special illumination techniques, the practical resolution limit with PLM/DS method is somewhat greater than 1 µm. In the case of soil samples, because of the small fibre sizes, PLM/DS may not adequately point out the presence of asbestos. If small fibres are a concern, other methods such as electron microscopies should be considered.

According to UK Health and Safety Executive (2006), a minimum of five high-dispersion liquids having Refractive Index (RI) values 1.550, 1.605, 1.640, 1.670 and 1.700 is commonly used to identify the six-regulated asbestos minerals. Other RI liquids may be required to achieve RI match between fibre and liquid. As reported in table II.6, Italian regulation (D.M. 06/09/94) states the use of minimum four high-dispersion liquids, slightly different in RI values (RI 1.550, 1.580, 1.670, 1.700). Both UK and Italian regulations report that the most difficulties occur in distinction between tremolite and actinolite (as members of a solid solution series), or between tremolite and anthophyllite amphiboles, having similar birefringence and RI values.

A preliminary identification based on the stereo microscopy evaluation is commonly used to select the most appropriate RI mounting liquid. As reported in table II.7 fibres can be classified tentatively on the basis of morphology and certain physical proprieties. Each fibre type so recognised is sampled by selecting a few fibres or fibre bundles. Fibres should be dry and relatively free from other particulate matter. Representative fibres or

Refractive Index Liquids

Asbestos	1.550				1.580				1.670				1.700			
	Dark Field		Phase Contrast		Dark Field		Phase Contrast		Dark Field		Phase Contrast		Dark Field		Phase Contrast	
	//	⊥	//	⊥	//	⊥	//	⊥	//	⊥	//	⊥	//	⊥	//	⊥
Amosite	(WHITE)		dark coloured, pale halo		(WHITE)		dark grey to black (small size)		yellow / orange	blue / purple	blue grey, orange halo	pale-blue, orange halo	indico-blue	celeste	celeste, mustard-yellow halo	white, purple-yellow halo
Anthophyllite	-	-	-	-	yellow	orange / yellow	dark-grey to black (small size) pale-whitish halo		blue	pale-blue	-	-	-	-	-	-
Crocidolite	(WHITE)		dark coloured to black (small size) pale-whitish halo		(WHITE)		dark grey to black (small size)		yellow / orange	yellow	blue-grey	violet-blue	purple / pink	pink to purplish-red	blue, orange halo	violet-blue, orange halo
Chrysotile	purple	blu	dark-celeste, orange halo	pale-celeste, orange halo	pale-blue	pale-blue	(WHITE) dark halo		(WHITE) celeste reflection		dark-brownish		(WHITE) celeste reflection		(WHITE)	
Tremolite	-	-	-	-	yellow	orange / yellow	dark-grey to black (small size) pale-whitish halo		blue	pale-blue	-	-	-	-	-	-

Table II.6. Staining colours for six-regulated asbestos minerals identification, by Italian regulation - D.M. 06/09/94. All observations have to be made with polar parallel (//) and perpendicular (⊥) to fibre direction.

PHYSICAL PROPERTY/APPEARANCE

Colour	Colourless/white	Colourless/white to grey brown			Greenish-grey deep blue	
Texture	Soft with bundles of sinuous fibres	Soft or harsh, may appear as easily visible parallel fibres bundles			Soft or harsh with parallel fibre bundles	
Appearance	Flexible fibres which cling to tweezers	Straight fibres easy to handle			Straight fibres easy to handle	
Lustre	Silky	Vitreous	Vitreous	Vitreous	Vitreous	Metallic (dark and highly reflective
Tensile strength	High	High	Medium	Low	Low	High
Tenacity	Flexible	Flexible	Flexible	Flexible	Flexible	Flexible
Elasticity	Inelastic	Elastic	Elastic	Elastic	Elastic	Elastic
Tentative asbestos type	Chrysotile	Amosite	Anthophyllite	Tremolite	Actinolite	Crocidolite
RI liquid for test	1.550	1.670	1.605	1.605	1.640	1.700

Table II.7. Use of physical properties and appearance under the stereo microscope to determine choice of RI liquid for PLM identification of asbestos fibres (Health and Safety Executive 2006).

fibre bundles are placed on a clean microscope slide into a drop of RI liquid, and a clean cover slip is lowered gently onto the slide. The RI of the liquid selected should be closed to one of the two observable fibre RIs for positive identification. With careful application of this method, a single fibre may be found in a few milligrams of dispersed material. In theory, for a fibre about 100 µm long and about 2 µm diameter, a detection limit in the order of 1 ppm by mass is expected (Health and Safety Executive 2006). Selection of large particles or fibre bundles may cause tilting of the cover slip and should be avoided. Moreover, it is important that all procedures be designed to avoid cross-contamination. Using white light illumination, when fibres are observed in matching RI liquids, a characteristic colour effect occurs (Table II.8). To better observe small bright particles, a black background may be involved. This observation method is general called Dark Field observation (Health and Safety Executive 2006). Different colours will be observed with the dispersion staining objective when the fibre is oriented parallel or perpendicular to the polariser, arising from the different RIs of asbestos fibres. Recording of the predominant colours is used to characterise the fibre RIs. Examples of the dispersion staining colours obtained with the UK-HSE references are listed and illustrated in table II.8, while table II.6 reports dispersion staining colours state by Italian regulation (D.M. 06/09/94).

Chrysotile
RI liquid = 1.550

Amosite
RI liquid = 1.670

Anthophyllite
RI liquid = 1.605

Tremolite
RI liquid = 1.605

Actinolite
RI liquid = 1.640

Crocidolite
RI liquid = 1.700

Phase Contrast

Dark field
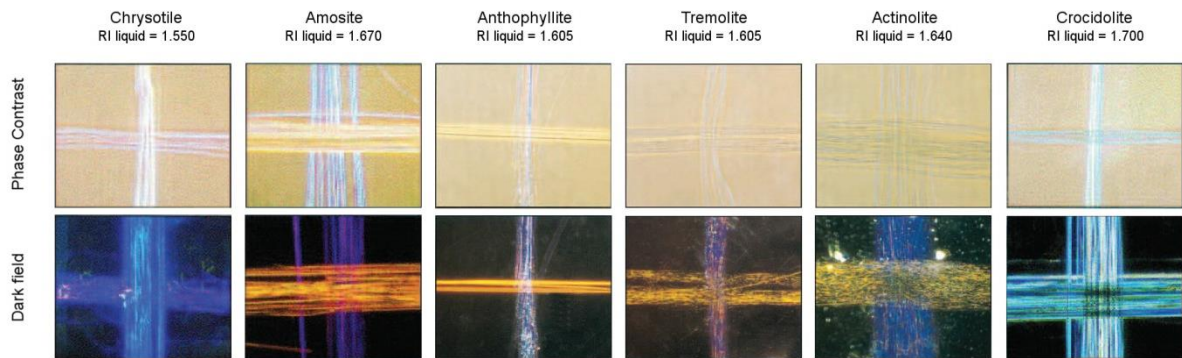
		Chrysotile	Amosite	Anthophyllite	Tremolite	Actinolite	Crocidolite
RI liquid Property		**1.550**	**1.670**	**1.605**	**1.605**	**1.640**	**1.700**
Morphology	Fibrous	Fibrous	Fibrous	Fibrous	Fibrous	Fibrous	Fibrous
Pleochroism	Fibre //	None	None	None	None	Green	Blue
	Fibre ⊥	None	None	None	None	Grey	Grey
Birefringence		Low	Moderate	Moderate	Moderate	Moderate	Low / anomalous
Extinction		Complete, or undulate with curved fibres; parallel	Complete; parallel	Complete; parallel	Complete; parallel or small angles	Complete; parallel or small angles	Complete; parallel
Sign of elongation		Usually positive (length slow)	Positive (length slow)	Positive (length slow)	Positive (length slow)	Positive (length slow)	Usually negative (length fast)
Dispersion staining Objective colours	Fibre //	Purple	Yellow	Yellow-orange	Yellow	Yellow-brown	Blue
	Fibre ⊥	Blue	Purple-red	Blue-red	Blue	Blue-purple	Blue
Phase Contrast	Fibre //						
	Fibre colour	Pale-blue	Grey	Dark-grey	Dark-grey	Dark-grey	Blue
	Halo colour	Orange	Yellow	Orange	Yellow	Yellow	Red-brown
Objective colours	Fibre⊥						
	Fibre colour	Pale-blue	Blue	Blue	Blue	Blue	Blue
	Halo colour	Orange	Orange	Orange-yellow	Orange	Orange	Red-brown
Refractive Index Ranges	ηα	1.537-1.554	1.670-1.675	1.596-1.654	1.599-1.620	1.619-1.658	1.680-1.692
	ηγ	1.545-1.557	1.683-1.694	1.625-1.667	1.622-1.641	1.641-1.677	1.683-1.700

Table II.8. Optical properties used to identify asbestos by PLM/DS. Fibre parallel (//) or fibre perpendicular (⊥) describes orientation with respect to polariser. Slight compositional variations will give rise to differences in the dispersion staining colours observed (modified after Health and Safety Executive 2006).

PLM/DS analysis were performed with the kind contribution of Dott. Orietta Sala, at the accredited laboratory of Arpae, at Reggio Emilia, in Italy. The following refractive indices were used for the identification of the asbestos fibres: RI 1.550 for chrysotile, RI 1.580 and 1.605 for tremolite, and the intermediate RI 1.5680 for not-chrysotile serpentine. Two microscope equipment (Leica DIALUX 20 EB and Leica DM4 B) have been used for the qualitative observations of samples.

II.2.1.2 Scanning Electron Microscopy

Scanning Electron Microscopy (SEM) is one of the techniques most commonly used in the study of mineral fibres. It allows obtaining high-magnification imaging, in which the complete characterisation of shape, size and aspect-ratio can be determined (Fig. II.15). SEM is often involved in the estimation of percentage of asbestos fibres (usually as area or particle percent), by visual or point counting methods. Qualitative or semi-quantitative chemical analysis is routinely performed on asbestos by means of an EDS system.
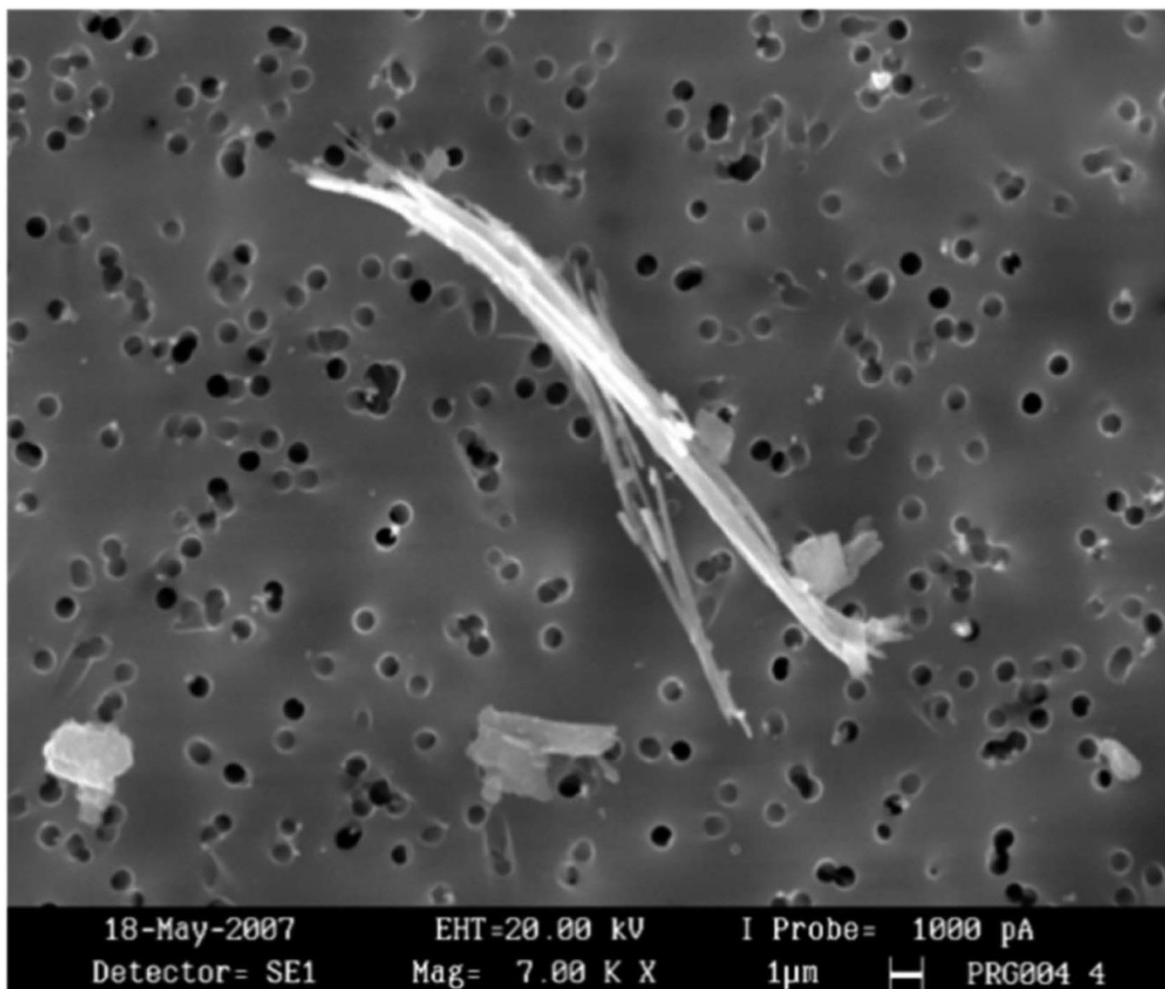
Figure II.15. Aggregates of chrysotile fibres observed by SEM (Cattaneo et al. 2012).

Compared to optical microscopy, SEM has an increased depth in field, which allows extending the particle resolution down to approximately 0.1 μm - at one order of magnitude smaller than PLM. Sub-millimetre sized fibres and cleavage fragments should be so investigated. Moreover, working on different accelerating voltages allows to better discriminate the general morphology (higher voltage, 10-15 kV), and also to focus on the study of the surface features (lower voltage, 5 kV). Although some modern SEMs are capable of resolving surface features at the angstrom scale, there is still much difficulty in obtaining adequate images of unit fibrils (about 30 nm). It should be remember that, because of their silicate chemistry and their consequent low electrical conductivity, asbestos samples have to be coated with a thin layer of carbon or metal coat (generally gold). Well-covered surfaces with good conductivity are an indispensable prerequisite for SEM analysis. Furthermore, a smooth and polished surface is recommended to obtain a reliably semi-quantitative analysis by EDS. For this reason, chemical analysis performed on thin sections results more reliable. Anyway, particles with irregular surfaces can be analysed, taking great care in the interpretation of data collected. Microanalysis by EDS is rapid but semi-quantitative. It is not sufficient for distinguishing different minerals with close chemical compositions (e.g. lizardite and antigorite). Moreover, the accuracy of the EDS data can be enhanced by using standards.

Secondary electron imaging (SEI) and semi-quantitative EDS microanalysis were carried out on both natural samples and thin sections with different scanning electron microscopes (SEM):

a) JEOL JSM-IT 300 LV/LA with Low Vacuum Mode equipped with an Oxford-X-Max EDS, available at ISEA Laboratory, University of New Caledonia. SEM images were collected with the valuable contribution of Monika Le Mestre, referent of SEM analysis for Axe-III of ISEA laboratory;

b) JEOL 6400 equipped with an Oxford-INCA EDS, at Department of Chemistry, Life Sciences and Environmental Sustainability, University of Parma;

c) LEICA 430i equipped with an ISIS EDS microanalysis and ZEISS EVO 40 equipped with Oxford-INCA EDS, available at the accredited Laboratory of Arpae - Agenzia regionale per la prevenzione, l'ambiente e l'energia dell'Emilia Romagna, Reggio Emilia, Italy.

SEI images were acquired at various magnifications and accelerating voltages, commonly 5-25 kV depending on the instrument used. EDS semi-quantitative analyses at University of Parma were performed under the following operating conditions: 15 kV and 1.2 nA, electron beam about 1 μm in diameter and 100 s counting time; errors are ±2-5 % for major components and ±5-10 % for minor components. Pure elements, simple oxides or simple silicate minerals are used as standards.
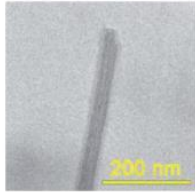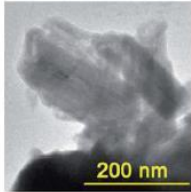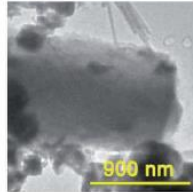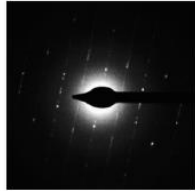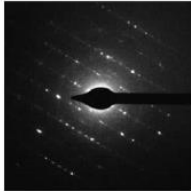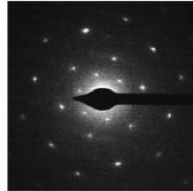
II.2.1.3 Transmission Electron Microscopy

Transmission Electron Microscopy (TEM) is the most complete method in the characterisation of mineral fibres. It combines many of the functions of standard mineralogical instruments such as, the petrographic microscope for optical and textural studies, X-ray diffractometer for structural data, electron microprobe analyser for determining chemical composition (Fig. II.16). This set of data makes the TEM a useful instrument for studying small particles. Additionally, each of these investigations may be made on a very fine scale. High Resolution TEM offers the unique ability to observe minerals, or any solid material, directly, in the real space, at the atomic scale. Whereas conventional methods provide information about the average macroscopic structural and chemical properties of a mineral specimen, HRTEM allows describing microstructural and micro-chemical properties. Furthermore, diffraction patterns (Selective Area Electron Diffraction - SAED) and chemical analysis (EDS, Electron Energy Loss Spectroscopy - EELS) can be taken from areas of a few micrometres up to a few nanometres across (and less than 1 nm on dedicated Scanning Transmission Electron Microscope - STEM instruments).

TEM instruments are complex and expensive. Due to their own complexity, an extensive operator training is required to obtain and analyse TEM data. TEM's high performances make it perfectly suitable for research. Unfortunately, the impossibility to be used as a routine analysis let its employment hard.

TEM is the only instrument capable of imaging the individual hollow-cored of chrysotile fibres. The absence of the core in TEM images, perpendicular to the fibre axis, represents the first tool to distinguish antigorite fibres from chrysotile in serpentine group minerals. Conversely, it is not so easy to distinguish polygonal serpentine from chrysotile, due to the small core, sometimes filled, and scarcely visible of serpentine polygonal phase (Belluso et al. 2017). Historically, TEM played a determining role in the comprehension of crystal structure of serpentine minerals (Yada 1967, 1971; Middleton and Whittaker 1976; Chisholm 1992; Cressey and Whittaker 1993; Cressey et al. 1994, 2008, 2010; Baronnet and Devouard 1996; Dodony 1997; Dódony et al. 2002; Capitani and Mellini 2005, 2006, 2007; Mugnaioli et al. 2007; Wagner 2015). In addition, TEM has proved to be crucial in investigation of defects, dislocations and structural disorder in antigorite crystals (Spinnler 1985; Mellini et al. 1987). In the study of polysomatism of antigorite, TEM analysis allows to understand that disorder varies systematically with metamorphic grade. While low-temperature antigorite (~400-460 °C) tends to be highly disordered, displaying a complex range of defects, high-temperature antigorite (up to 550 °C) is generally much better ordered (Mellini et al. 1987).

HRTEM observations have proved to be crucial for the study of disaggregation of asbestos amphiboles in fibres. HRTEM demonstrates that amphiboles cleave mainly along grain boundaries, and perhaps secondarily along planar defects (Veblen 1980).

Serpentine fiber type	Chrysotile	Polygonal serpentine	Lizardite lath
TEM/morphology			
Typical TEM image			
Fiber width[a] (nm)	42 ± 16	167 ± 71	505 ± 559
Central canal	Sharp, uniform	Thin, irregular	None
Fiber termination	Rounded/uniform	Angular/irregular	Square
Fiber side edges	Parallel	Parallel	Irregular
SAED			
Typical SAED			
Even-row spots	Weak	Strong	Strong
Odd-row spots	None	Weak	Strong
Odd-row streaks	Strong	Weak	None
Row spacing[a] (nm^{-1})	1.9 ± 0.2	1.9 ± 0.2	1.8 ± 0
% clino-	16	19	—
% ortho-	10	16	—
% Disordered or inclined fiber	74	66	—
STEM/EDS Mg/Si[a]	0.97 ± 0.26	0.96 ± 0.21	1.02 ± 0.03
Fe/Si[a]	0.08 ± 0.08	0.22 ± 0.31	0.18 ± 0.07
Al/Si[a]	0.00 ± 0.01	0.00 ± 0.01	0.04 ± 0.06

[a] Mean ± std. dev.

Figure II.16. TEM/SAED/EDS investigation of several serpentine minerals (modified after Wagner 2015).

Dorling and Zussman (1987), who examined about 50 samples of massive, prismatic, acicular and asbestiform tremolite and actinolite, assumed that chain width defects are more abundant in asbestiform amphibole than in massive amphibole.

Micrographs and TEM analysis included in this manuscript were carried out on natural samples with different transmission electron microscopes (TEM):

a) JEOL ARM 200F STEM, at Department of Materials Chemistry, National Institute of Chemistry, Ljubljana, Slovenia. The study was conducted By Dr. Ruggero Vigliaturo using a probe Cs corrected STEM, model ARM 200F mounting a high-brightness Cold Field Emission Gun (CFEG) operating at 80 kV. The microscope was equipped with an EDS system (Centurio 100 mm2, JEOL). Analyses were conducted in TEM mode together with SAED and EDS analysis to identify chrysotile fibres (>20 fibres for each sample performed). In addition to common TEM identification (Imaging, SAED and EDS) of asbestos fibres, Bright Field (BF) and Medium Angle Annular Dark Field (MAADF) STEM coupled with EDS mapping

have been applied. All the samples were tested for stability under the electron beam and the observations were made accordingly;

b) JEOL JEM 2010 equipped with an Oxford-INCA 100 EDS, available at the CIGS Laboratory, University of Modena and Reggio Emilia. The microscope operating at 100 kV, was equipped with double tilt holder. This set of measure was conducted with the kind contribution of Dott. Nicola Bursi Gandolfi;

c) JEOL JEM 1400 Plus equipped with an Oxford-X-Max EDS, at ISEA Laboratory, University of New Caledonia. The microscope operating at 120 kV, was equipped with double tilt holder. This set of measure was conducted by Dr. Michael Meyer and interpreted by Dr. Ruggero Vigliaturo.

The natural particle size of fibrous minerals permits preparation of the samples from suspension to obtain the specimen transmission. In addition, because of the poor flexibility of amphibole fibres, especially for tremolite-actinolite minerals, a gentle grinding procedure is required to reduce the fibres length. On the contrary, the grinding of chrysotile fibres in a mortar forms a matted aggregate which can be powdered with great difficulty. Generally, a few milligrams of sample are gentle grinding in ethanol (or sometimes in water) in an agate mortar. After suspending the powder in ethanol (or water), the suspension is subjected to ultrasound treatment in order to minimize fibre aggregation. Finally, one or several drops of the suspension were deposed on a carbon-supported Cu or Cr TEM grid.

II.2.2. X-Ray POWDER DIFFRACTION

Although X-Ray Powder Diffraction (XRPD) has been implemented in several countries (e.g. Italy) as one of the standard methods for determining asbestos content in bulk materials (e.g. D.M. 06/09/94), XRD methods have not been largely used for asbestos characterization. The very small quantity of samples commonly available for measurements of ACMs is the main reason for the low utilisation of this technique. However, with sample sizes of 100 mg and more, XRD can be a valuable method not only to identify the main minerals present but also to estimate mineral abundance. It is worth noting that only a sophisticated Rietveld approach allows obtaining reliable results for quantification. Furthermore, XRPD does not provide information about the morphology of materials. By definition, XRPD easily detects minerals present at 1 wt.% or lower. Actually, it is less sensitive with serpentine minerals (Nichols et al. 2002; Ballirano et al. 2017).

As a general rule, XRPD allows to easily distinguish a serpentine group mineral from an amphibole group mineral. However, a correct determination of which serpentine or amphibole mineral are presents results more difficult, or even not possible. Diffraction

Figure II.17. Example of benchtop XRPD instrument equipped with dome-type zero-background sample holder (Bruker-AXS D8 Advance, available at SCVSA Department, University of Parma).

patterns of minerals with closely related structures appear very similar, presenting slightly shift in peaks position, often smaller compare to the instrumental error. Using commercially available X-ray diffractometers (Fig. II.17), generally analysts may determine just the presence or absence of a serpentine mineral, which could be either lizardite (non-asbestiform) or chrysotile (asbestos). Additionally, at the beginning of the year 2000, after a critical examination of the reference XRPD patterns of serpentine minerals in Powder Diffraction File PDF-database, Wicks (2000) noted that many of the references in common use are inaccurate, misidentified, or of poor quality, making accurate identifications by this method difficult. At present, a complete database of different structures of serpentine minerals is still lacking.

However, XRPD method considered the possibility to employ a benchtop XRPD instrument. The opportunity to carry easily the instrument directly in the site of interest is a great advantage in mining context, where workers need to be given full and adequate information without delay. In this context, the association of XRPD with another complementary technique may provide a useful instrument in the determination and evaluation of the presence (or not) of the asbestos fibres.

X-Ray Powdered Diffraction patterns in this manuscript were collected using two different instruments:

a) Bruker-AXS D8 Advance diffractometer equipped with an Si(Li) solid state detector, at Department of Chemistry, Life Sciences and Environmental Sustainability, University of Parma. Intensity measures were run at 40 kV and 30 mA, using CuKα radiation (λ = 1.54178 Å) over a 2θ range from 4 to 80 °2θ in steps of 0.018°, with a counting time of 1s per step. In order to avoid any

contamination risk due to manipulation of hazardous materials, a dome-type zero-background sample holder was used (Fig. II.17);

b) X-Ray wide angle diffractometer INEL CPS 120, at ISEA Laboratory, University of New Caledonia. Operating conditions were 30 kV and 30 mA. The transmitted X-ray beam is produced from a filtered Co source $K_{\alpha 1}$ (λ = 0.178897 nm). The intensity of the diffracted beam is recorded with a curved position-sensitive detector, INEL CPS-120, between 0° and 120° (2θ) at a step size of 0.03° (Fig. II.18). Resolution width varies slightly from ∼0.10° to ∼0.15° in 2θ (from small angles to large angles). X-Ray diffraction patterns are acquired at all angles simultaneously. Using in reflection mode, the powder was simply put on horizontal sample carrier.
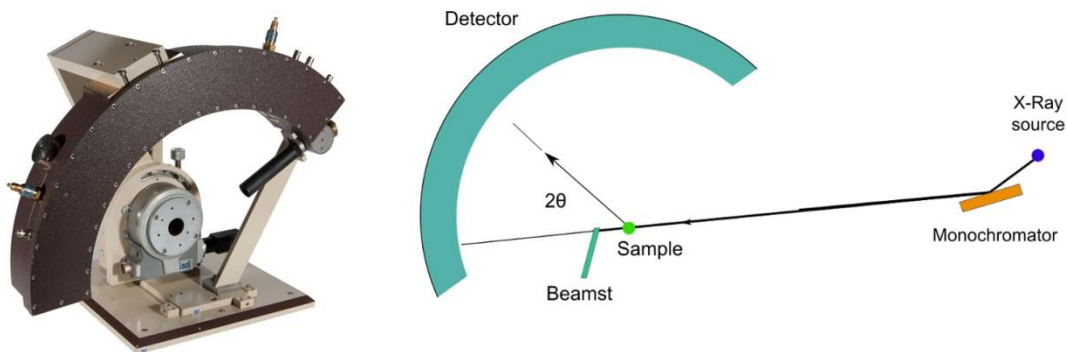
Figure II.18. X-Ray wide angle diffractometer INEL CPS 120 configuration (ISEA Laboratory, University of New Caledonia).

Random powder samples (about 0.1 to 1 g depending on the type of mounting method used) were prepared by gentle hand-grinding in an agate mortar, and then positioned into an appropriate sample holder. In order to correct the diffraction patterns for instrumental shift in 2θ position, a fixed quantity of SiO_2 (0,01 g, corresponding to 1 wt.% of sample holder capacity) was added as internal standard. All data interpretations were performed with the Match! Software.

II.2.3. RAMAN SPECTROSCOPY

II.2.3.1 micro-Raman Spectroscopy

Micro-Raman spectroscopy is a powerful tool for mineral characterization, providing information about structure and chemical composition. A Raman spectrum is a distinct molecular fingerprint of a particular material. About predominant geological applications,

Raman spectroscopy is of great importance in the study of phases of the same or very similar chemical composition (e.g. polymorphism, members of a solid solution series), and in the evaluation of phase transformations at high pressure/temperature conditions.

Compared to the other analytical techniques previously discussed, such as XRPD, SEM-EDS and TEM-EDS, micro-Raman spectroscopy has numerous advantages: it is a simple, rapid and non-destructive technique, which does not require any sample preparation. A good Raman spectrum can be obtained just by placing the specimen in the path of the spectrometer laser beam. Petrographic polished thin sections may therefore be studied, allowing the identification of the mineralogical association immediately, with a rapid acquisition of few minutes, pointing directly on minerals embedded in their textural context. Recently, micro-Raman spectroscopy was successfully tested in the characterisation of serpentine and amphiboles both on rock specimens (rock fragments and thin sections; Lemaire et al. 1999; Groppo et al. 2006; Ulrich 2010; Petriglieri et al. 2015; Quesnel 2015; Quesnel et al. 2016), and on ACMs (Bard et al. 2004; Rinaudo et al. 2005; Petry et al. 2006). Raman spectra have proved to be very sensitive to variations in chemical composition, allowing the discrimination of the different phases (Bard et al. 1997, 2004; Lemaire et al. 1999; Rinaudo et al. 2003, 2004; Auzende et al. 2004; Ulrich 2010; Petriglieri et al. 2015). Moreover, due to its high resolution power, it can be successfully used not only on massive specimens, but also in the investigation of fibre bundles and/or single micrometre-sized fibres (fibre of 1-2 μm in diameter; Bard et al. 2004; Rinaudo et al. 2005).

Raman spectra of serpentine minerals in the low wavenumber spectral range (150-1100 cm^{-1}), corresponding to the inner vibrational modes of the lattice and to Si–O_4 vibrations, appear quite comparable (Table II.9). In addition, the attribution is very complex because a small variation in the chemical composition or the presence of doping elements in the lattice may cause a change in the vibrational wavenumbers and can modify the relative intensities. Moreover, polytypism and polysomatism (i.e. in antigorite) can lead to a splitting of some of the main peaks. On the other hand, the vibrations of the OH
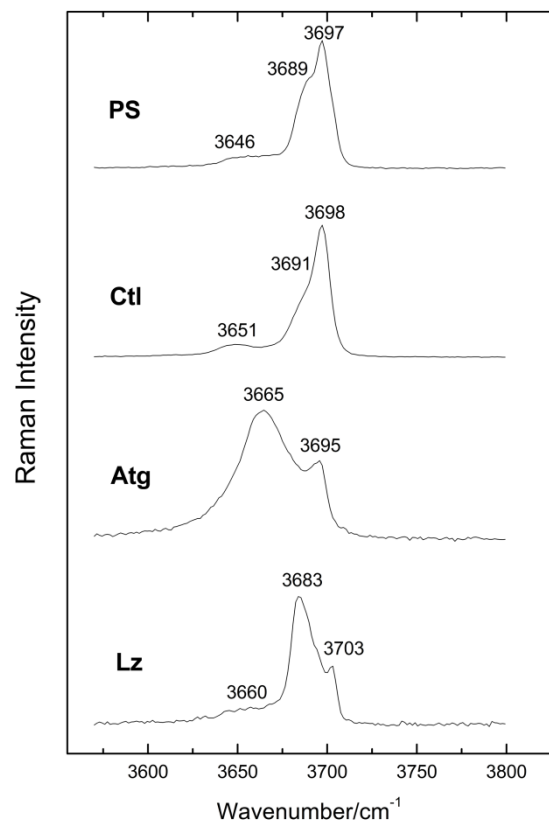
Figure II.19. Raman spectra obtained at 473.1 nm in the high-wavenumber region of polygonal serpentine, chrysotile, antigorite, and lizardite (Petriglieri et al. 2015).

Lizardite			Antigorite			Chrysotile			Polygonal serpentine		Attribution
Petriglieri et al. (2015)	Groppo et al. (2006)	Auzende et al. (2004)	Petriglieri et al. (2015)	Groppo et al. (2006)	Auzende et al. (2004)	Petriglieri et al. (2015)	Groppo et al. (2006)	Auzende et al. (2004)	Petriglieri et al. (2015)	Auzende et al. (2004)	
230 s	233	241	229 vs	230	235	232 vs	231	235		236	Vibrations O-H-O *
349 w	350	351	-	-	-	345 w	345	346		647	δ SiO$_4$
386 vs	388	393	377 vs	375	377	388 vs	389	391		391	Symmetric v_5 SiO$_4$ **
532 m	510	527	-	520	528	-	-	-		-	Deformation SiO$_4$-AlO$_4$ ***
621 m	630	-	631 m	635	-	622 w	620	-		-	Translation OH-Mg-OH *
689 s	690	695	687 s	683	685	691 vs	692	694		696	v_s Si-O$_b$-Si
-	-	-	1045 m	1044	-	-	-	-		-	v_{as} Si-O$_b$-Si ***
-	1096 ?	-	-	-	-	-	1105	-		-	v_{as} Si-O$_{nb}$
3660 w	3654	-			3641	3651 w		3649	3646 w	3646	v_s outer OH ****
3683 vs	3688		3665 vs		3666	3691 sh		3691	3689 sh	3689	v_s outer OH ****
3703 vs	3704		3695 vs		3693	3698 vs		3699	3697 vs	3697	v_s inner OH ****

vs very strong, s strong, m medium, w weak, vw very weak, sh shoulder. The band wavenumber is reported in cm^{-1}.

*(Rinaudo et al. 2003); **(Kloprogge et al. 1999); ***(Lazarev 1972); ****(Auzende et al. 2004).

Table II.9. Assignment of peaks in the Raman spectra at low-wavenumber and high-wavenumber regions of the main serpentine minerals obtained by Petriglieri et al., (2015)*, Groppo et al., (2006) and* Auzende et al., (2004)*.*

groups of water molecules (3550-3850 cm^{-1} high-wavenumber range) play a decisive role in the discrimination of these phases. OH group is a powerful probe to investigate the local geometry at the atomic scale, being very sensitive to variations in the geometry of the layers. Even cell size, symmetry, and octahedral site occupancy (cation substitutions) influence the number and position of the OH stretching bands (Balan et al. 2002; Auzende et al. 2004). For this reason, minerals of serpentine group show a characteristic doublet (Fig. II.19, Table II.9), indicating the kind of local arrangement of the structure. The precise attribution of the Raman peaks in the high-wavenumbers part of the spectra, in terms of vibrations of the different OH groups occurring in the serpentine minerals, was obtained by Auzende *et al.*, (2004), during investigation of the behaviour of serpentines at increasing pressures. The vibrations of the outer hydroxyl groups are assigned to the strongly pressure-dependent modes, while the inner ones are allocated to those less pressure sensitive (Auzende et al. 2004). The new assignment of the OH stretching bands allows a better attribution of the various OH bands to the different serpentine minerals, with a unique correspondence. This evident variability in the position and shape of the peaks has allowed a good discrimination of the four phases (Lemaire et al. 1999; Auzende et al. 2004; Ulrich 2010; Petriglieri et al. 2015).

Raman spectra of amphibole asbestos are generally sufficiently different to allow discrimination, as reported in table II.10 (Rinaudo et al. 2004). The members of the series tremolite-actinolite are an exception (Wang et al. 1988). Actually, an interesting preliminary study of Bersani *et al.*, (2014) proposes two simples and independent
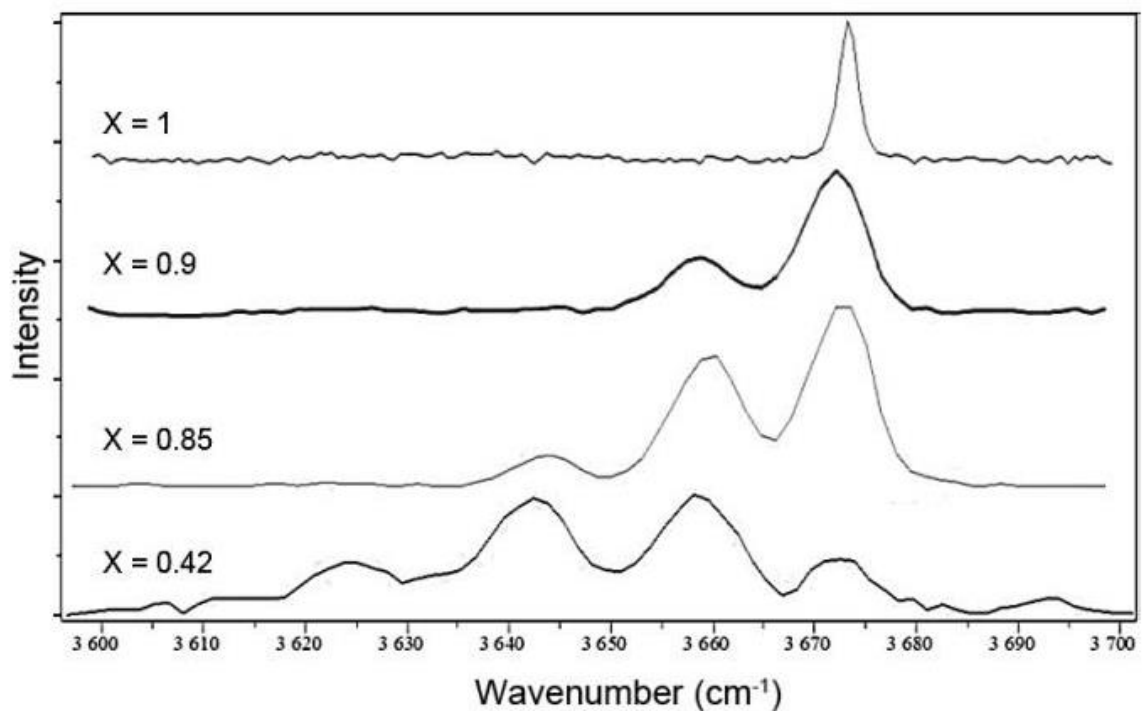
Figure II.20. Raman spectra at high wavenumbers of minerals of tremolite-actinolite series with different X ratios (Bersani et al. 2014).

Anthophyllite		Tremolite				Amosite			Crocidolite		
Rinaudo et al. (2005)	Bard et al. (1997)	Rinaudo et al. (2005)	Lewis et al. (1996)	Bard et al. (1997)	Blaha and Rosasco (1978)	Rinaudo et al. (2005)	Lewis et al. (1996)	Bard et al. (1997)	Rinaudo et al. (2005)	Lewis et al. (1996)	Bard et al. (1997)
						1093 vw		1093 vw			
									1082 s	1082 s	2085 s
		1062 m		1061 m	1061 m						
1044 s	1042 s		1044 w								
		1031 m		1028 m	1.30 m				1030 w	1034 vw	1032 m
						1020 s	1016 m	1020s			
							996 w, sh			986 w, sh	
						968 m	966 w	968 m	967 vs	971 m	969 vs
		950 w			947 w						
928 w		932 m		928 w	931 m						
						904 vw	906 w	903 vw			
									889 m	888 vw	891 s
									771 w	776 vw	772 m
		751 w			751 w						
		740 w			741 m				733 w	736 vw	737 m
699 w											
674 vs	671 vs	676 vs	677 s	672 vs	676 vs						
					670 sh						
						659 vs	657 s	658 vs	664 s	667 w	664 s
									577 s	581 m	577 vs
							556 w, sh	555 vw			
539 m									537 m	542 s	539 vs
		531 w			531 m	528 m	527 m	528 m			
		516 w			516 w						
503 vw						507 w	506 w, sh	506 w	506 w	506 w, sh	509 w
							462 w		470 w	472 w	469 m
433 m	430 m	438 w	428 m		439 m	423 w	422 w	421 m	428 m	432 w	
410 m	410 w	418 m		414 w	418 m						
		396 s		393 m	398 s	400 w	397 w	401 m			
387 m	384 m		383 m							387 w, sh	
		373 m			376 m				374 s		374 vs
364 w	362 m	-	-	369 m	-	368 w	367 w	364 m	360 sh	364 m	-
		355 vw			355 m						
342 vw		348 vw		349 vw	348 m	348 m	347 m	349 m			
	336 vw	335 vw	338 m		335m				331 m	331 m	332 m
										324 m	
304 m	304 m	306 w			307 w	307 w	312 w	309 w			
		290 w	299 m		295 w				300 m	300 m	297 s
						289 vw	282 w	287 w			
265 m	260		261 m		268 m				272 m	272 w	271
										206 w, sh	
254 w		254 m	248 w	251 w	254 m	252 w	252 w		246 m	253 m	249 s
		234 s		232 w	235 s						
222 vw		225 s		222 w	226 s						
					216 s	216 m	212 m		211 m	214 vw, sh	
					196 w				195 s		
188 m		180 s			182 s	182 vs					
		162 s			164 s	155 s			162 vs		

Table II.10. Comparison of the Raman spectra of asbestos amphiboles anthophyllite, tremolite, amosite and crocidolite, obtained by several authors using different excitation wavelengths: 632.8 nm (Rinaudo et al. 2004); 785 nm (Lewis et al. 1996); 632.8 nm (Bard et al. 1997); 514 nm (Blaha and Rosasco 1978). m: medium; s: strong; sh: shoulder; v: very; w: weak.

methods to evaluate the composition of nephritic minerals from their Raman spectrum. The first method is based on the position of Raman peak observed at 675 cm^{-1}, associated to symmetrical stretching of Si-O (A_g mode). A linear correlation between the peak position and the increasing Mg content is observed. Substituting Mg^{2+} with the heavier Fe^{2+}, a downshift from 675 cm^{-1} in pure tremolite to 667 cm^{-1} in Fe-rich actinolite ($X=Mg/(Mg+Fe^{2+})=0.5$, at the border with ferro-actinolite) occurs. On the other hand, the second method depends on the ratio of the OH stretching band areas. In the high-wavenumber region (3600-3700 cm^{-1}) a number of OH stretching bands (from 1 to 4) is present. The number and relative intensity of these bands depend on the $Mg/(Mg+Fe^{2+})$ value (X value). This is due to the fact that in nephrites the OH group vibrations are influenced by the three metal sites where Fe^{2+} or Mg^{2+} could be present. When only Mg is present (as in pure tremolite), only one peak (at 3675 cm^{-1}) is observed. As the amount of iron increases, the other peaks, related to different combinations of Fe^{2+} and Mg^{2+} in the sites close to OH, arise at lower wavenumber (Fig. II.20). From a simple statistical model based on the population of the three sites, the following relation useful to estimate the X value from the Raman spectrum was proposed: $X=(A12)/(1/3+A12)$, where A12 is the ratio between the areas of OH Raman bands at about 3675 and 3660 cm^{-1}, often the most visible ones. This second method is nearly insensitive to the spectrometer calibration (Bersani et al. 2014).

The micro-Raman technique has also confirmed that asbestos and non-asbestiform minerals might occur in the same samples, intimately associated at the microscale, even in the same micro-textural sites (Groppo et al. 2006; Petriglieri et al. 2015). The
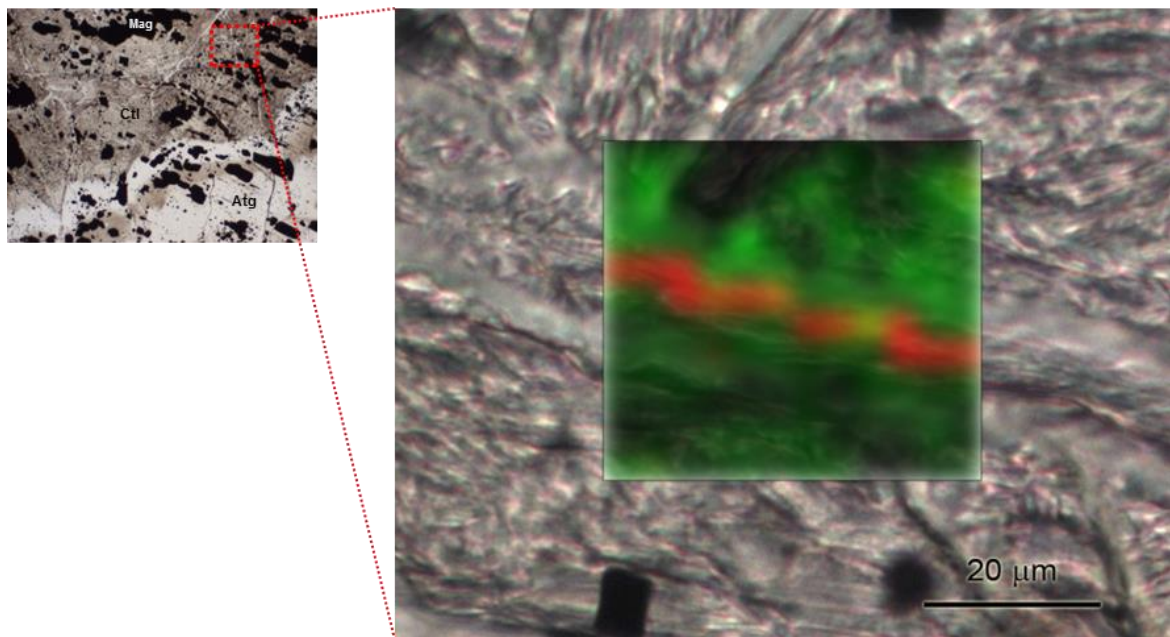
Figure II.21. Raman map obtained in the OH stretching region. Green, chrysotile; red, antigorite (Petriglieri et al. 2015).

acquisition of spot analysis in complex matrices is therefore a restriction in the study of the textural relationships between the different varieties of serpentine and amphibole minerals. This limitation may be overcome by performing two-dimensional maps, linear or rectangular, with Raman spectroscopy. Performing maps in the OH stretching spectral range allows observing variations of the vibrational peaks of OH groups, point by point, in order to recognize minerals in complex areas. A typical example is shown in figure II.21, where a micrometric antigorite vein occurs inside a chrysotile one, not visible by the conventional optical microscopy techniques. This suggests a first crystallization of chrysotile and then, after opening of the vein, a new crystallization of antigorite or partial re-transformation of chrysotile into antigorite. The crystallization of the higher temperature phase antigorite implies that this occurred in an episode of reheating. In this case Raman mapping has shown an unusual situation because the chrysotile is generally formed from the transformation of antigorite to low temperature (Berman 1988).

Non-polarized micro-Raman spectra present in this manuscript have been obtained on thin sections in nearly backscattering geometry with a Horiba Jobin-Yvon LabRam apparatus, equipped with an Olympus microscope with 10x, 50x, Ultra-Long Working Distance 50x, and 100x objectives and a motorized x-y stage. The 632.8 nm line of a He–Ne laser and the 473.1 nm line of a doubled Nd:YAG diode pumped laser have been used as excitation; laser power has been controlled by means of a series of density filters, in order to avoid heating effects. The minimum lateral resolution was about 1 μm (with the 100x objective); the depth resolution was set to few micrometres by means of a confocal hole. The spectral resolution is about 2 and 4 cm^{-1} at the 632.8 and 473.1 nm excitation wavelengths, respectively. The system was calibrated using the 520.7 cm^{-1} Raman peak of silicon before each experimental session. In addition, in the high wavenumber range, the spectra were constantly calibrated using spectral lamps. The 632.8-nm line was mostly used to obtain high-resolution spectra in the low wavenumber range (100-1200 cm^{-1}), whereas the 473.1 nm source was utilized to enhance the OH stretching signal of the water molecules in the high wavenumber range (3000-4000 cm^{-1}). The spectra were collected using the 100x objective with repeated acquisition: 5 acquisitions for 30 s and 15 for 10 s in the low and high wavenumber spectral range, respectively. The background subtraction on each spectrum was performed with LabSpec® software.

II.2.3.2. Portable Raman equipment

In recent years, the advancements in optics and electronics have led to the development of compact Raman spectrometers that allow *in situ* measurements. *In situ* Raman spectroscopy is a developing area with numerous examples already reported in the literature (Vandenabeele et al. 2014). It has been more involved in forensic science for the identification of explosive materials (Hayward et al. 1995; Moore and Scharff 2009);

in the art for the analysis of large artefacts or paintings (Bersani et al. 2006; Barone et al. 2014, 2015; Lauwers et al. 2014), in environmental sciences for the analysis of hazardous materials (Bard et al. 2004), and in geological sciences (Jehlička et al. 2009a, 2009b).

Despite all recent developments, a methodology able to distinguish the asbestos minerals directly on the sample, at the outcrop, in the mining context, without removing the fibres from the rock matrix, has not yet been performed. Portable Raman equipment may be a user-friendly technique, able to provide reliable results in real-time identification. To obtain high-quality spectra, the laser must be accurately focused on the area of interest. The detection limit will depend on the material type and homogeneity and also on the type and size distribution of asbestos fibres. Fluorescence emission phenomena and the difficulty to point and/or focus laser beam on a non-cohesive bundles of fibres are the major disadvantages generally occurring during the time of measurement. Bard *et al.,* (2004) demonstrated that it is possible to detect asbestos in building materials using a simple Raman spectrometer equipped with a fibre-optic probe. At present, as far we are aware, no further studies involving more compact (e.g. handheld Raman) and performant Portable Raman equipment are reported. Additionally, there is no evidence of testing of Portable Raman in mining context.

Raman *in situ* measurements were carried out with an handheld Enspectr RaPort® Raman instrument, weights 2.1 kg, equipped with a 532 nm laser at maximum output power of 30 mW. Raman spectra have been obtained over the wavenumber range 100-4000 cm^{-1} with a spectral resolution of 8 cm^{-1}. The instrument is controlled remotely via a USB 2.0 cable connected laptop. It allows the operator to select a wider range of settings for measurements including more detailed power output selection, number of accumulations, and long accumulation times. The spectra were collected in a single acquisition up to 60 s. The instrument self-calibrate automatically before each set of measurements. Taking into account the large laser spot (about 1 mm) and the lack of rigid mounts for positioning, a real spatial resolution in the range of few cubic millimeter is expected. This could be a disadvantage when analysing very small features or heterogeneous materials. On the other hand, as we had a large volume of scattering, it was easy to focus the laser beam on the bundles of fibres. Working off-line, the long battery life permits an autonomous operation up to 6 hours. A temperature range of 0-40 °C is recommended during operation on field.

II.3. Sampling method

Correct sampling is a delicate operation which requires the utmost care. Concerning asbestos, an inaccurate procedure of sampling can affect not only the goodness of the analytical result, but it can also compromise the safety of people exposed (workers, population, analysists, etc.). Moreover, sampling has to be consistent with the objectives of the research. This work aims to improve the actual procedure envisaged by mining geologists for the mineral identification on field, and to evaluate the impact of supergene alteration on the recognition of asbestos and on fibres genesis. Consequently, an exhaustive sampling of the different types (mineralogy and alteration status) of mineral fibres naturally occurring in geological units of New Caledonia is required. In order to estimate the alteration status to which rock fragments have been subjected, samples have to be preliminary classified according to the nomenclature used in mining context. For this reason, in January 2016 sampling was conducted by the geological sector (by Dott. Stéphane Lesimple) of mining companies of New Caledonia (*Comité Interminier Amiante*). 58 samples identified by mining geologist as antigorite, chrysotile and tremolite, plus 2 not-identified asbestiform fibres, were collected (Table II.11). Sampling was carried out in open mine context (outcrops, quarries, tracks, pit), in different
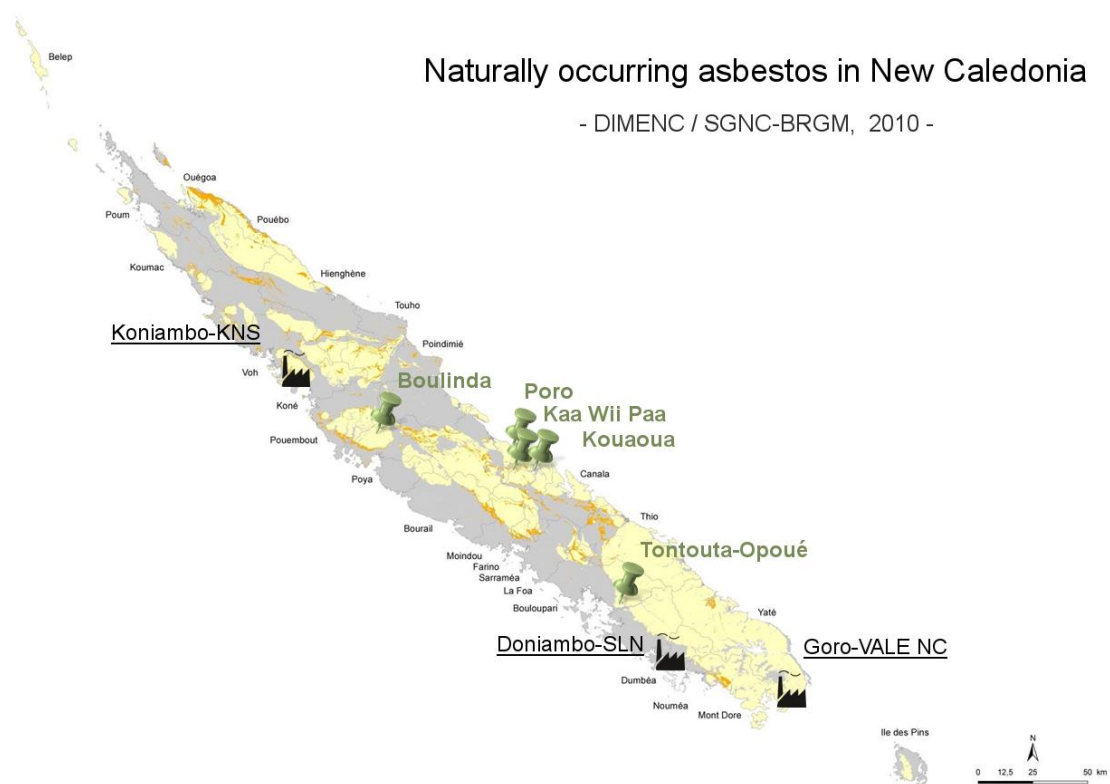
Figure II.22. Geological map of the potential occurrences of asbestos with sampling sites. The three major sites of nickel activity are magnified (modified after DIMENC 2010).

geological units as shown in figure II.22. Moreover, a brief sampling report including the main identification data (mineralogical identification, degree of alteration, weight, sampling area, GPS coordinates) was kindly provided. Samples were collected at both serpentinite sole horizon (chrysotile) and in the lateritic profile (mainly antigorite and tremolite-actinolite). Unfortunately, no photographs of rock fragments embedded in their textural context (e.g. cross-vein, fault planes, dyke, etc.) have been supplied.

In table II.11 all samples have been divided by typology – antigorite, chrysotile and tremolite – and increasing alteration status (from *#1* to *#4*). It is worth noting that no samples of antigorite and tremolite classified as degree of alteration *#3* were present. Conversely, all chrysotile samples were identified with alteration degree *#3*. As shown by figure II.23 (sample 53 as example) all chrysotile samples are in the form of little veins and veinlets (up to 5 mm wide) cross-cutting serpentinized peridotite. Due to the little amount of chrysotile available and to homogeneity morphology, only the sample 57 has been here investigated. In table II.11, samples not included in this manuscript have been highlighted in grey.

A brief description of the main visual features of samples investigated is here reported. Samples classified as antigorite, degree of alteration *#1*, display a compacted, moderately hardened appearance, dominated by a pale-green to green colour (Annexe IA). Platy-shaped lamellae are welded and parallel to each other. Only the samples 11 and 32 show a more fibrous-curvilinear aspect, with poor cleavage into thin laminas. Moreover, a more accurate observation of samples 30 and 34, suggests the presence of minor traces of amphibole. Increasing the alteration degree, antigorite *#2* shows a more friable aspect (Samples 3, 5, 27), coupled with the presence of bundles of laminas. Samples show a massive (Sample 29) to structureless (Sample 4) appearance, from white (Sample 6) to pale-green colour (Sample 14). Moreover, because of less flexible appearance of sample 29, the presence of minor traces of amphiboles is suspected.

Figure II.23. Example of serpentinized peridotite from serpentine sole horizon. Cross-veinlets a few millimetres wide of chrysotile are observed (Sample 53).

Antigorite

LABEL	APPROVAL NUMBER	SAMPLIG AREA		ON FIELD IDENTIFICATION	ALTERATION DEGREE
23-Tontouta-Module1-Antg1	23	Tontouta	Module 1	Antigorite	#1
28-Tontouta-module1-Antg1	28	Tontouta	Module 1	Antigorite	#1
33-Tontouta-module1-Antg1	33	Tontouta	Module 1	Antigorite	#1
13-Tontouta-module4-Antg1	13	Tontouta	Module 4	Antigorite	#1
19-Tontouta-module4-Antg1	19	Tontouta	Module 4	Antigorite	#1
30-Tontouta-Module4-Antg1	30	Tontouta	Module 4	Antigorite	#1
34-Tontouta-module4-Antg1	34	Tontouta	Module 4	Antigorite	#1
11-Kouaoua-Piste-Antg1	11	Kouaoua	Mining track	Antigorite	#1
32-Kouaoua-piste-Antg1	32	Kouaoua	Mining track	Antigorite	#1
3-Tontouta-module1-Antg2	3	Tontouta	Module 1	Antigorite	#2
4-Tontouta-module1-Antg2	4	Tontouta	Module 1	Antigorite	#2
5-Tontouta-module1-Antg2	5	Tontouta	Module 1	Antigorite	#2
7-Tontouta-module1-Antg2	7	Tontouta	Module 1	Antigorite	#2
9-Tontouta-module1-Antg2	9	Tontouta	Module 1	Antigorite	#2
27-Tontouta-module1-Antg2	27	Tontouta	Module 1	Antigorite	#2
6-Tontouta-module4-Antg2	6	Tontouta	Module 4	Antigorite	#2
16-Tontouta-module4-Antg?2	16	Tontouta	Module 4	Antigorite ?	#2
29-Tontouta-Module4-Antg2	29	Tontouta	Module 4	Antigorite	#2
18-Kouaoua-piste-Antg2	18	Kouaoua	Mining track	Antigorite	#2
14-Kouaoua-piste-Antg2	14	Kouaoua	Mining track	Antigorite	#2
31-Kouaoua-piste-Antg2	31	Kouaoua	Mining track	Antigorite	#2
20-Kouaoua-Fosse-Antg2	20	Kouaoua	Mining pit	Antigorite	#2
10-Tontouta-module1-Antg4	10	Tontouta	Module 1	Antigorite	#4
12-Tontouta-module1-Antg4	12	Tontouta	Module 1	Antigorite	#4
17-Tontouta-module1-Antg4	17	Tontouta	Module 1	Antigorite	#4
24-Tontouta-Module1-Antg4	24	Tontouta	Module 1	Antigorite	#4
25-Tontouta-module1-Antg4	25	Tontouta	Module 1	Antigorite	#4
26-Tontouta-module1-Antg4	26	Tontouta	Module 1	Antigorite	#4
35-Tontouta-module1-Antg4	35	Tontouta	Module 1	Antigorite	#4
8-Tontouta-module4-Antg4	8	Tontouta	Module 4	Antigorite	#4
15-Tontouta-module4-Antg?4	15	Tontouta	Module 4	Antigorite ?	#4
1-Kouaoua-Piste-Antg4	1	Kouaoua	Mining track	Antigorite	#4
2-Kouaoua-Piste-Antg4	2	Kouaoua	Mining track	Antigorite	#4
21-Kouaoua-Piste-Antg4	21	Kouaoua	Mining track	Antigorite	#4
22-Kouaoua-Fosse-Antg4?	22	Kouaoua	Mining pit	Antigorite ?	#4

Table II.11. Extract of sampling report. Samples not included in this work are highlighted in grey.

... continued

Chrysotile

53-Tontouta-module3-Chr3	53	Tontouta	Module 3	Chrysotile	#3
43-Opoué-Chr3	43	Opoué		Chrysotile	#3
44-Opoué-Chr3	44	Opoué		Chrysotile	#3
50-Opoué-Chr3	50	Opoué		Chrysotile	#3
51-Opoué-Chr3	51	Opoué		Chrysotile	#3
54-Opoué-Chr3	54	Opoué		Chrysotile	#3
57-Poro-Chr3	57	Poro		Chrysotile	#3
58-Poro-Chr3	58	Poro		Chrysotile	#3
52-KaaWiiPaa-Chr3	52	KaaWiiPaa		Chrysotile	#3
56-KaaWiiPaa-Chr3-4	56	KaaWiiPaa		Chrysotile	#3-4

Tremolite

41-Poro-Trem1	41	Poro		Tremolite	#1
49-Poro-Trem1	49	Poro		Tremolite	#1
37-Poro-Trem2	37	Poro		Tremolite	#2
42-Poro-Trem2	42	Poro		Tremolite	#2
45-Poro-Trem2	45	Poro		Tremolite	#2
46-Poro-Trem2	46	Poro		Tremolite	#2
38-Kouaoua-Fosse-Trem2?-Nephrite?	38	Kouaoua		Tremolite ?	#2
48-Kouaoua-Fosse-Trem2?	48	Kouaoua		Tremolite ?	#2
47-Boulinda-Trem2	47	Boulinda		Tremolite	#2
55-Boulinda-Trem2	55	Boulinda		Tremolite	#2
36-Poro-Trem4	36	Poro		Tremolite	#4

Not identified

40-Tontouta-module4-Fibres2?	40	Tontouta	Module 4	Fibres?	#2
39-Tontouta-Module4-Fibres4?	39	Tontouta	Module 4	Fibres?	#4

On the other hand, sample 18 shows an unusual texture, characterized by the overlaying of dried-like yellowish to pale-green lamellae (Fig. II.24a). More in general, specimens classified as antigorite *2* show a great variability in morphologies, compared to antigorite *1*. Finally the most altered samples, classified as antigorite *4,* appear fibrous and characterized by porous low density material (Sample 15). The friable nature of these specimens is evident (Samples 8, 22). Here, fibrous-lamellar blades occur randomly orientated to form aggregates and bundles (Samples 1, 10).

As mentioned above, chrysotile typically occurs in the form of veins and veinlets cross-cutting serpentinized peridotite, as shown in figure II.23. It is important to point out that this is the typical appearance of chrysotile that mining geologists expect in the outcrops for its identification. Chrysotile veins and veinlets commonly show a reddish-colour, alternating sub-millimeter sized pale-brown–black–reddish banding.
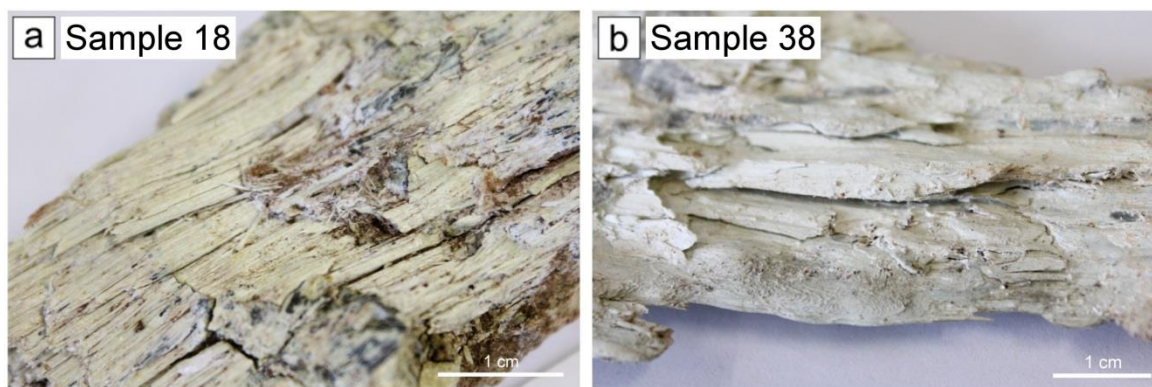
Figure II.24. Antigorite (Sample 18 - #2) and tremolite (Sample 38 - #2) hand samples displaying an unusual texture, characterized by the overlaying of dried-like whitish to pale-green lamellae.

Despite the progressive loss of cohesion reported by mining nomenclature related to increasing alteration status, tremolite samples (Annexe IB) show a little variation in morphology as the degree of alteration increases. Tremolite samples are characterized by compacted, massive (Samples 1, 46) to moderately hardened (Samples 37, 42) appearance, from green to pale-green–whitish colour. Moreover, they exhibit a columnar morphology, characterized by the overlapping of well-formed prismatic crystals. Several individual fibres have also been observed. Only sample 38 shows an unusual texture, characterized by the overlapping of dried-like whitish lamellae, similarly to antigorite sample 18 (degree of alteration *#2*; Fig. II.24b).

Finally, not-identified samples classified as fibres occur in the form of bundles and random aggregates of whitish fibres. The evaluation of the degree of alteration for these two samples is not easy (Samples 39, 40 – Annexe IC).

Additionally, a preliminary study of the potential presence of asbestos in the nickel ores at the mining front was carried out. Two representative samples of soft yellow and red limonite soils have been courtesy provided by mining geologist of *Comité Interminier Amiante*. They consist of a mix of different soils, coming from various mining fronts. Samples were prepared using coning and quartering method. No information are available about specific provenance of soils involved in the preparation of these "standard lateritic soil samples". Moreover, further investigations have been carried out on four more homogeneous samples of yellow and red limonite; the sampling was carried out personally. The aim was to check the presence (or not) of asbestiform fibres in homogenous soils samples, coming from a well-characterized mining front. Due to the confidentiality related to these data, information of provenance and the chemical characterisation will not be reported.

Chapter III.

MINERALOGICAL STUDY OF THE SUPERGENE ALTERATION PRODUCTS OF ASBESTOS, AND TYPOLOGY OF ASSOCIATED FIBRES.

III.1. Mineral identification

Because of the humid tropical to sub-tropical conditions, weathering processes and supergene mineralization had a great deal in the formation and release of mineral fibres into the environment. The samples of New Caledonia show an evident lack of coherence and a very altered appearance at the hand scale. The samples, regardless of their state of alteration (from *#1* to *#4*), are generally more friable and characterized by a structureless aspect (Annexe I) compared to most of the natural worldwide asbestos occurrences (e.g. Western Alps, Haute-Corse; ANSES (2010)). For this reason, a mineralogical approach was performed to characterized these mineral fibres and also to evaluate the impact of supergene alteration in the processes of genesis and dispersion of fibres. Data obtained with the more traditional mineralogical and petrological techniques – such as optical microscopy (PLM), X-ray powder diffraction (XRPD), secondary electron microscopy (SEM-EDS), and transmission electron microscopy (TEM-EDS) – have been completed by the employment of more specialized tools as polarized light microscopy coupled with a dispersion staining method (PLM/DS) and micro-Raman spectroscopy. All data are illustrated in Annexe II. Thus, for each analytical method, an assessment of the advantages and limits in identification of mineral fibres was realized. Moreover analytical performances of a Raman portable equipment, to be used in field observation, were assessed against the other laboratory methods. Portable Raman was preliminary tested in laboratory, under safe conditions (personal protective equipment, extractor hood, etc.), in order to check its reliability even in presence of strong altered samples (*#4*). It is important to remember that a diagnostic analytical strategy able to discriminate and characterize, with certainty, the different varieties of asbestos and their capacity in the emission of fibres is the first requisite in the establishment of an environmental monitoring system (ANSES 2010).

A particular attention has been dedicated to the study of fibrous antigorite, exceptionally recognized as asbestos only by Caledonian legislation. In order to estimate its real fibrous form, a preliminary investigation of size and morphology of antigorite particles was conducted by the Department of Chemistry of University of Turin associated to Centro Scansetti, as part of the CNRT project «*Amiante et Bonnes Pratiques*» (CNRT - ABP project). Measurements were conducted on three samples of antigorite (samples 13, 6, 35 in Annexe IA), presenting different degrees of alteration and coming from the Tontouta mine site. The acquired data were compared to those obtained by a lamellar antigorite from Western Alps, Italy (Italian Antigorite - Fig. III.1). Caledonian samples are all in the form of fibrous-lamellar crystals. After a gentle mechanical stress, they fracture easily releasing elongated fibrous particles, most of which have the dimensional characteristics of breathable fibres (L/D >3, D <3 µm), according to regulated dimensional criteria. Following up on grinding procedure, particles appear still fractured, mainly in the form of acicular or isometric crystals. As clearly shown in figure III.1 the Caledonian

antigorite contains about 40-55% of breathable fibres, compared to 12-15% of the Italian sample. The last one is made up of mostly prismatic fragments. In all Caledonian samples the amount of breathable fibres (D <3 μm) is comparable and it can represent up to 30-40% of the total particles. It is worth noting that the percentage of breathable fibres do not change increasing the alteration status (from *#1* to *#4*).
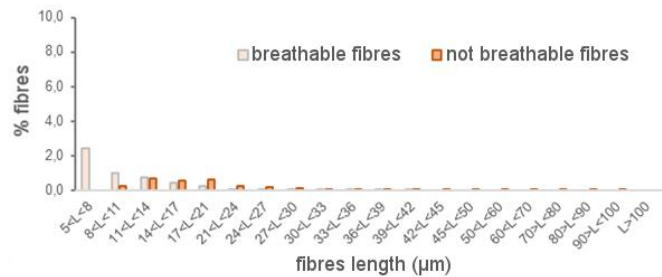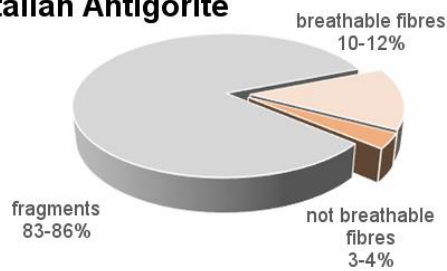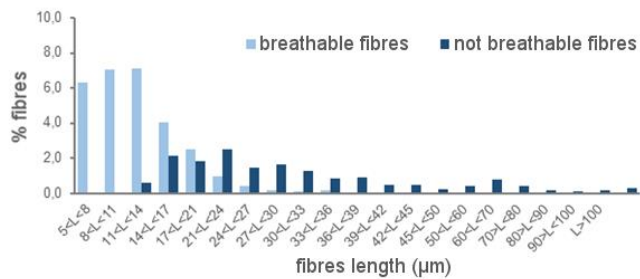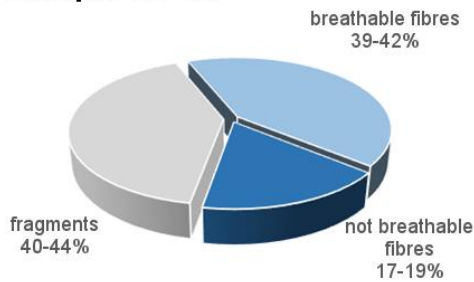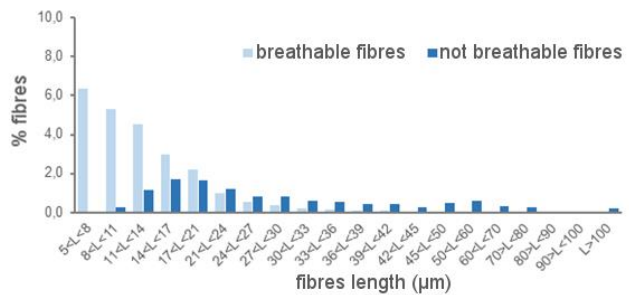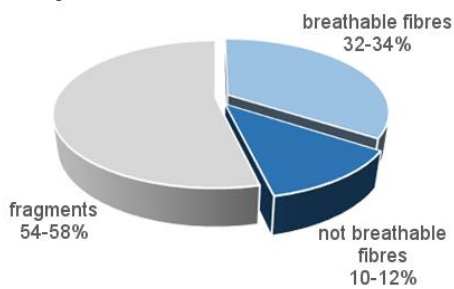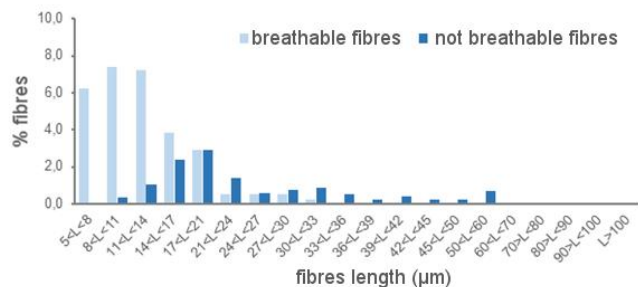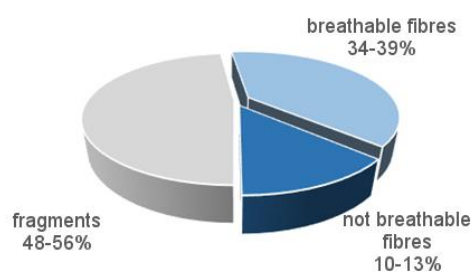

Figure III.1. Antigorite size and morphology. Pie charts: % of particles with L/D >3 (fibres) and fragments with L/D <3 (not fibres). Bar graphs: fibres distribution (% of breathable fibres, D <3 μm, and non-breathable, D >3 μm) as a function of length. The analysis was conducted by an automated image analysis system (FPIA 3000, Malvern; CNRT - ABP project, pers. comm. Dr. Maura Tomatis).
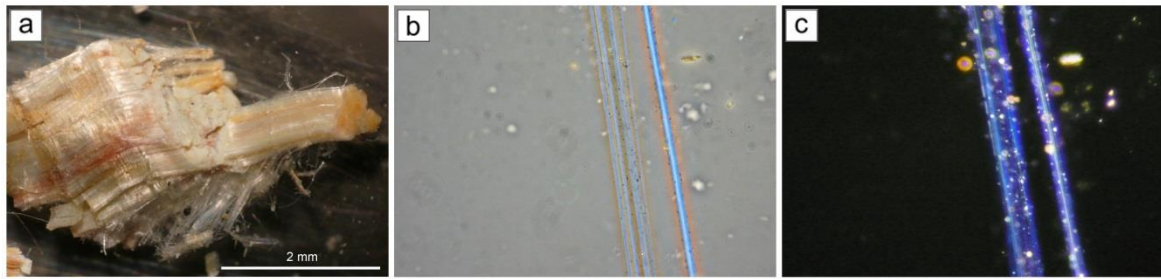
Figure III.2. Identification of chrysotile fibres by PLM/DS, RI 1.550. a) soft fibrous tuft; b) PC: pale-blue with orange halo; b) DF: blue/purple. Sample 57.

III.1.1. MICROSCOPIES

Polarised Light Microscopy associated to Dispersion Staining (PLM/DS) has been applied to 15 fibrous samples, comprising all types of mineralogy in which individual (potential asbestiform) fibres occur at the surface. For each sample, only a few fibres were analysed. In all cases the main mineralogical phase was identified (Annexe II). Applying this methodology to more fibres for each sample, we should therefore assume that also minor fibrous phases will be detected. However, it should be remembered that PLM/DS cannot solve fibres smaller than 1 μm in diameter. A typical example of identification of chrysotile fibres using a standard 1.550 refractive index (RI) oil is shown in figure III.2. The hand specimen shows as a silky, reddish tuft of flexibles fibres (Fig. III.2a). The reddish appearance suggests a great Fe- or Ni-content. Fibres observed in phase contrast (PC) mode exhibit a pale-blue colour with an orange halo (Fig. III.2b), whereas they appear blue to purple in dark field (DF) observation (Fig. III.2c). Tremolite specimens have been analysed with RI 1.580 and RI 1.605 oils. In all cases, tremolite must be better identified with RI 1.605 (Fig. III.3), according to UK Health and Safety Executive (2006). Observed in phase contrast mode, fibres exhibit a pale-blue to dark-grey colour, often coupled with an orange halo (Fig. III.3b). Moreover, they appear yellow to purple in dark
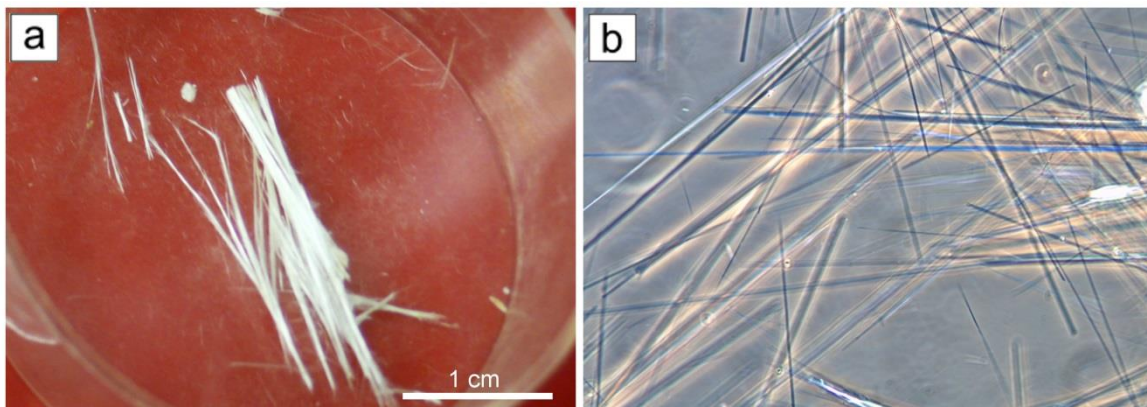
Figure III.3. Identification of asbestos tremolite by PLM/DS, RI 1.605. a) rigid bundles of white fibres; b) PC: pale-blue to dark-grey, with whitish to orange halo. Sample 36.
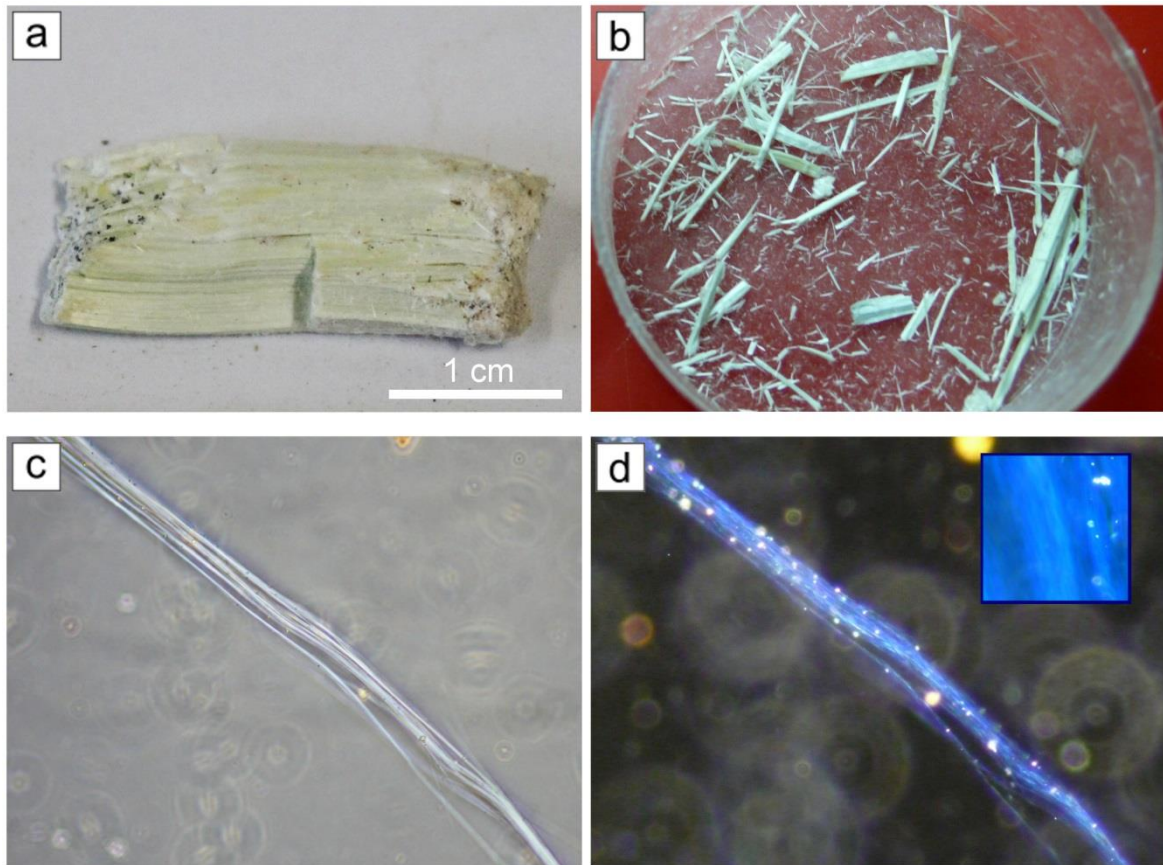
Figure III.4. Identification of fibrous antigorite by PLM/DS, RI 1.5680. a) hand specimen; b) bundles of fibrous-lamellae; c) PC: pale-blue to white, no halo; d) DF: blue/blue indigo. Sample 6.

field observation mode. PLM/DS has proved to be a powerful diagnostic tool also in the identification of natural fibres. Unfortunately, no guidelines are provided by regulations for the discrimination of non-asbestos serpentine minerals, and in particular to fibrous antigorite. As widely reported in literature, lizardite has a mean RI between 1.54 and 1.55, while the slath-shaped lamellae of antigorite generally show an higher RI, on average 1.566 (Deer et al. 1992). Therefore, a specific work aimed to find the RI liquid that match most closely the refractive index value of antigorite has been carried out.
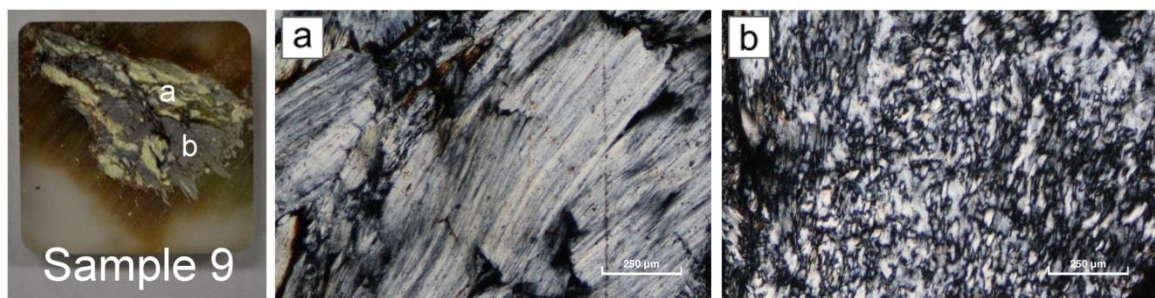
Figure III.5. Textural appearance of antigorite in thin section, with parallel and perpendicular orientation to lamellae elongation, respectively: a) fibrous-lamellar blades; b) interpenetrating texture - (PLM cross-polarizing images).

The RI 1.5680 has provide to be the RI liquid that mostly matches the antigorite phase, showing characteristic dispersive colours which permit to distinguish antigorite from chrysotile. As clearly shown in figure III.4, antigorite fibres show a silky fibrous-lamellar shape, with a pale-green to white colour. In phase contrast observation mode fibres show a pale-blue to white colour, without halo (Fig. III.4c), whereas they are amazing in blue indigo colour in dark field observation (III.4d).

Furthermore, PLM/DS was tested on not-identified 39 and 40 samples (Annexe IC), involving four RI 1.550, 1.5680, 1.580 and 1.605 liquids. While sample 39 has identified as fibrous antigorite (RI 1.5680), sample 40 showed the presence of both antigorite (RI 1.5680) and chrysotile (RI 1.550) fibres. These first results have been confirmed by other analytical techniques (Annexe II).

Several important information about mineralogy, texture and alteration state were obtained by the examination of petrographic thin sections. Generally, the petrographic description of the main textures of serpentine minerals is made according to the classification of Wicks and Whittaker (1977) (e.g. Andreani et al. 2007; Ribeiro Da Costa et al. 2008; Frost et al. 2013; Mothersole et al. 2017). Commonly, the petrographic images are used to show the mineralogy assemblages constituting the rock and to describe the general mineralogical context. It should be noted that, especially for antigorite variety, this classification is strictly related to the preparation of the thin
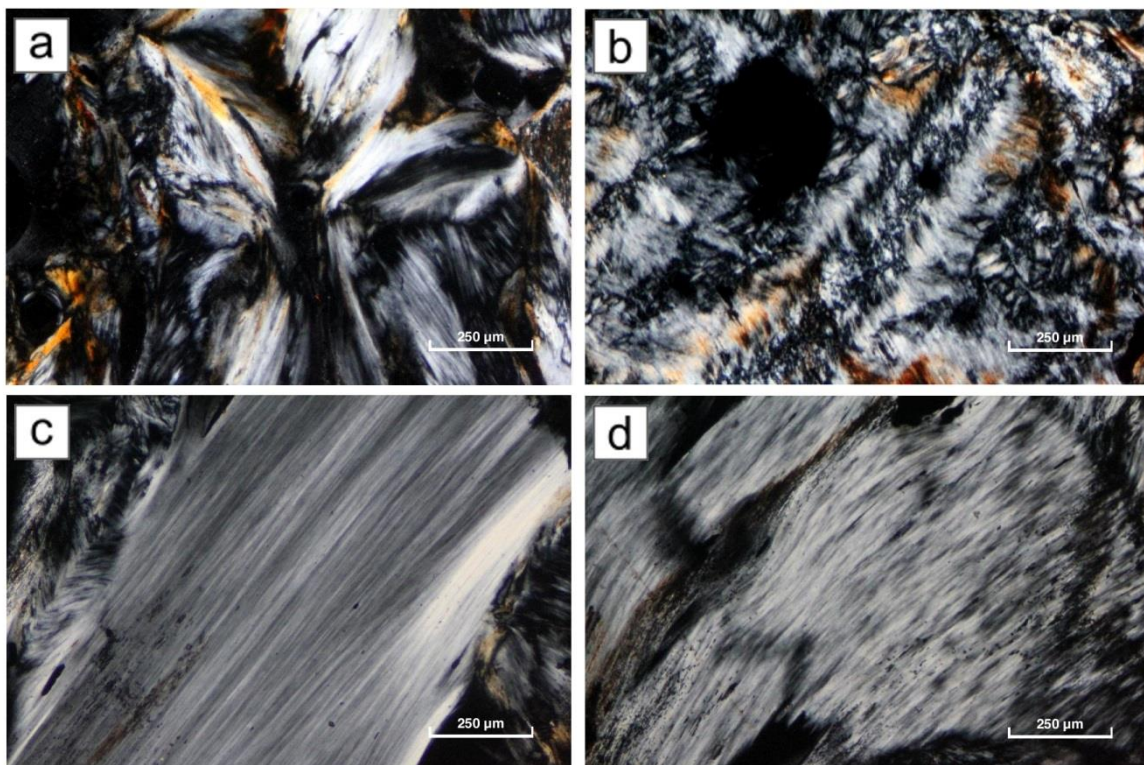
Figure III.6. Textures of fibrous antigorite observed by PLM (cross-polarizing images). a) star and fan formed aggregates; b) interpenetrating texture; c) lath-shaped lamella; d) fibrous-lamellar blade. Sample 35.
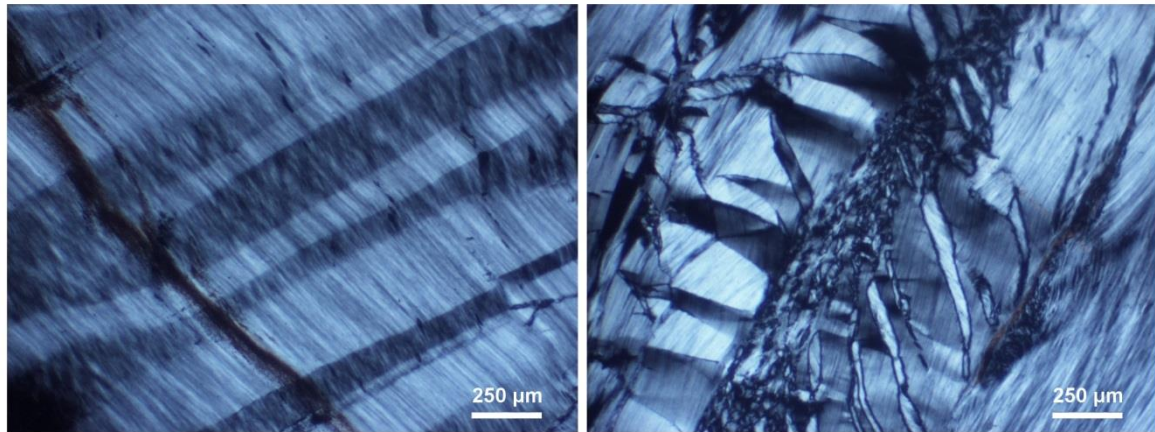
Figure III.7. Kink bands in antigorite (cross-polarizing images). Sample 24.

section itself. As shown in figure III.5, depending on the shear direction of the original sample we can observe antigorite lamellae parallel (Fig. III.5a) or perpendicular to their direction of elongation (Fig. III.5b). Antigorite is typically recognized for its non-pseudomorphic *interpenetrating* or *interlocking* texture; actually these textures should be observed in any direction non-parallel to the elongation of the lath-shaped crystals. Therefore, antigorite samples consisting of randomly orientated aggregates of fibrous-lamellae show more types of shapes and intergrowths, as shown in figure III.6. Only one antigorite specimen has shown a *kink bands* structure (Fig. III.7).
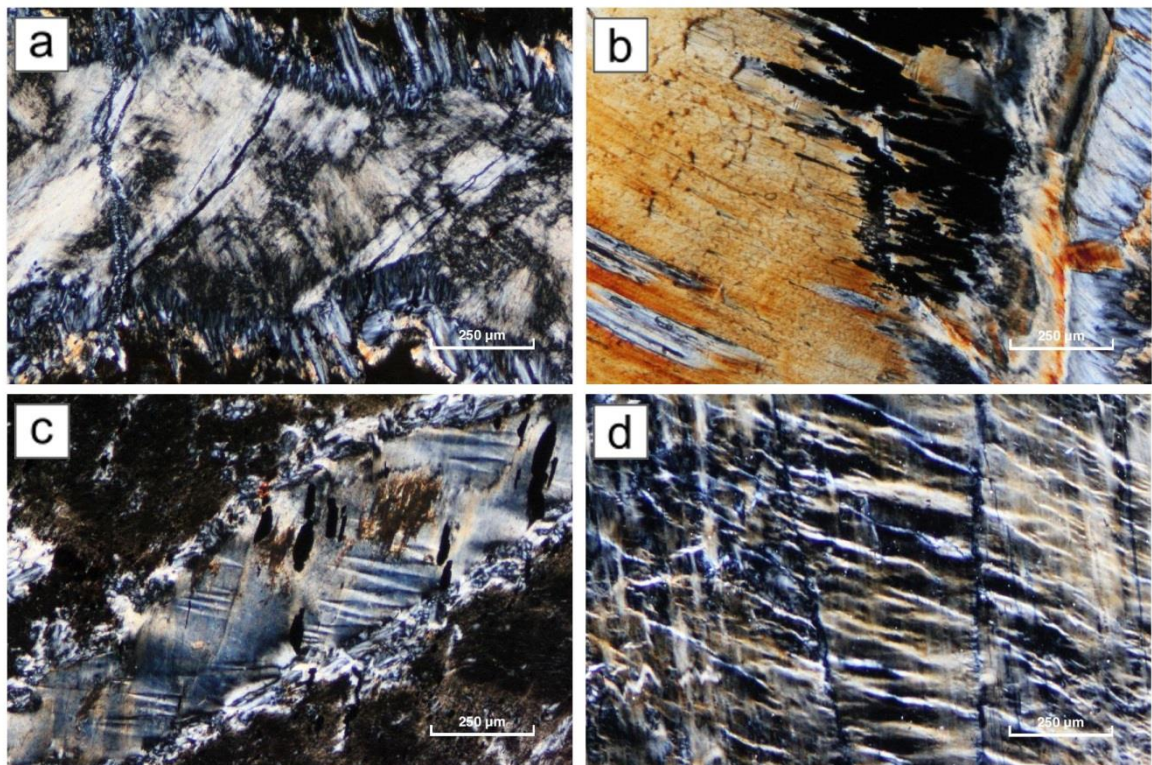
Figure III.8. Chrysotile occurrences observed by PLM (cross-polarizing images). a-c)cross-veins; d) zebra-like appearance, with brown-black and whitish stripes.

Chrysotile samples occur as veins, generally characterized by a banded columnar structure perpendicular to the vein-wall (cross-type; Fig. III.8a-c). This type of vein has a variable birefringence that can reach anomalous 2nd order colours (Fig. III.8b). Even if fibres are often not parallel to each other, they clearly show a preferred orientation perpendicular to the vein-wall. On the other hand, massive samples of chrysotile show the typical zebra-like appearance, with brown-black and whitish stripes (Fig. III.8d). Fibres are not distinguishable optically, but under crossed polars a non-homogeneous extinction across the vein suggests their presence (Fig. III.8d). Furthermore, the extinction position of chrysotile fibres is typically parallel to their long *c*-axis. Crack-seal and isotropic veins of chrysotile have not been observed. Generally, oxides (e.g. magnetite) are concentrated at the vein walls or among antigorite fibrous-lamellae.

Tremolite samples show as prismatic, acicular or needle-like crystals of different sizes. Most of tremolite crystals display a high relief, almost one good cleavage, and interference colours of 1st and 2nd orders (Fig. III.9). There are generally no changes in morphology. Conversely, in a few samples tremolite appears highly fractured, often related to a higher degree of alteration. Secondary serpentine, probably antigorite, was detected in all tremolite thin sections (Fig. III.9b); minor chlorite and talc have been occasionally observed.
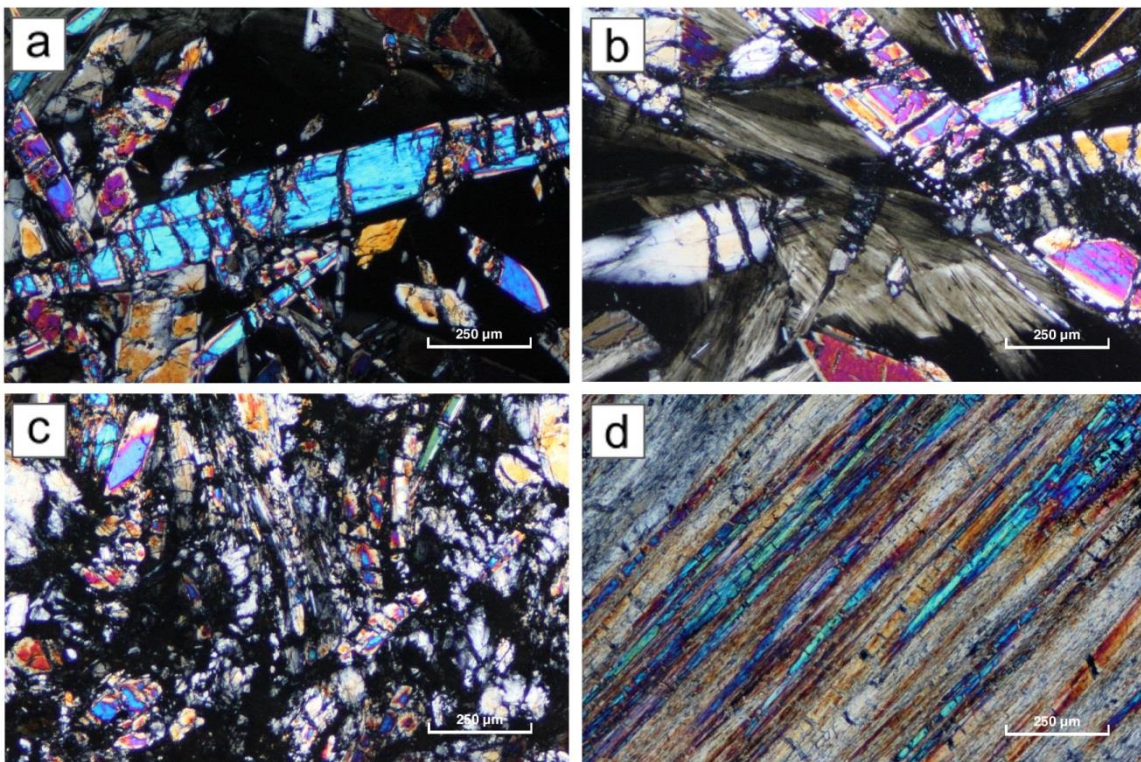
Figure III.9. Tremolite crystals observed by PLM (cross-polarizing images). Bundles and aggregates of acicular crystals more or less fractured occur.
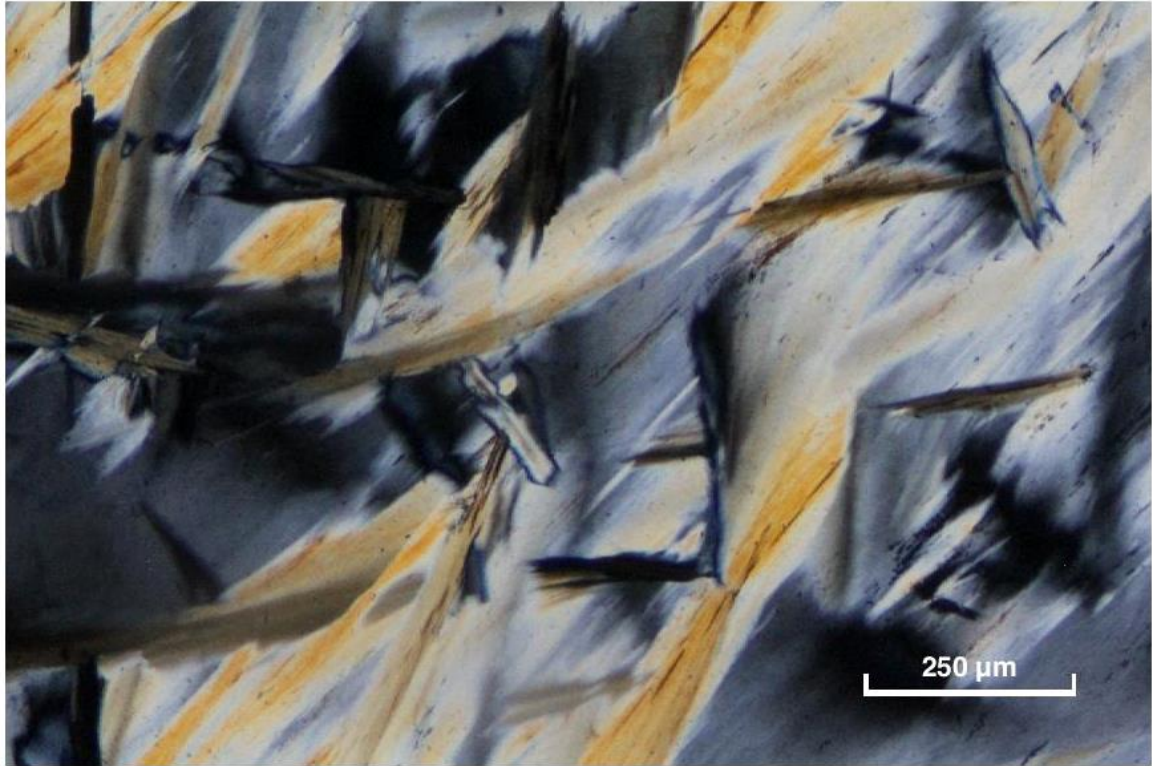
Figure III.10. PLM cross-polarizing image showing an unusual and potential new type of texture, characterized by star and fan formed aggregates. Sample 18.

Although the 2-dimensional nature of thin sections makes difficult to distinguish the crystal habit (e.g. asbestiform, fibrous, acicular and lamellar), PLM observations allow to evaluate the intergrowth of different, fibrous or not, phases in their textural context, revealing also the presence of potential new type of texture (Fig. III.10), as will be discussed in Chapter III.4. Samples that appear massive, lamellar, not altered in the hand sample can display their fibrous shape already at the PLM scale. It should be
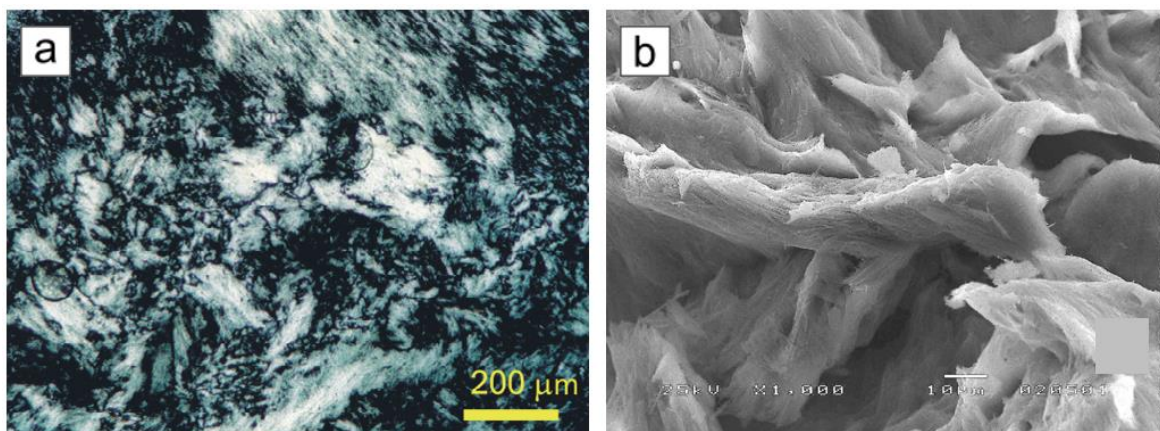
Figure III.11. Blades of antigorite observed by a) PLM - interpenetrating to fibrous serpentine antigorite (cross-polarizing image), and b) SEM - antigorite blade morphology (Ribeiro Da Costa et al. 2008).
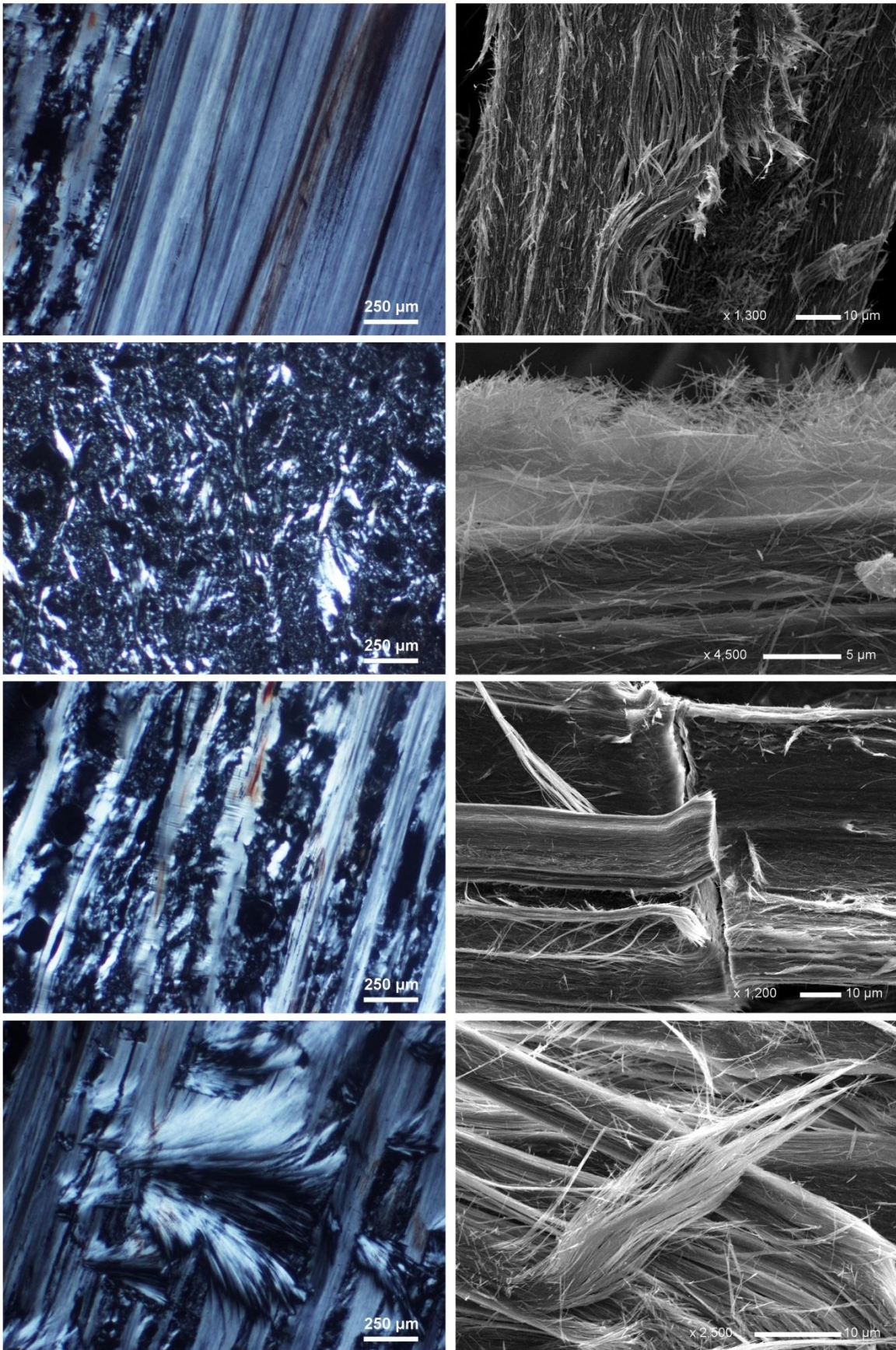
Figure III.12. Intergrowth of antigorite and chrysotile fibres. Texture observation was made with PLM (thin section – cross-polarizing images) and SEM microscopies (SEI images). Sample 30.
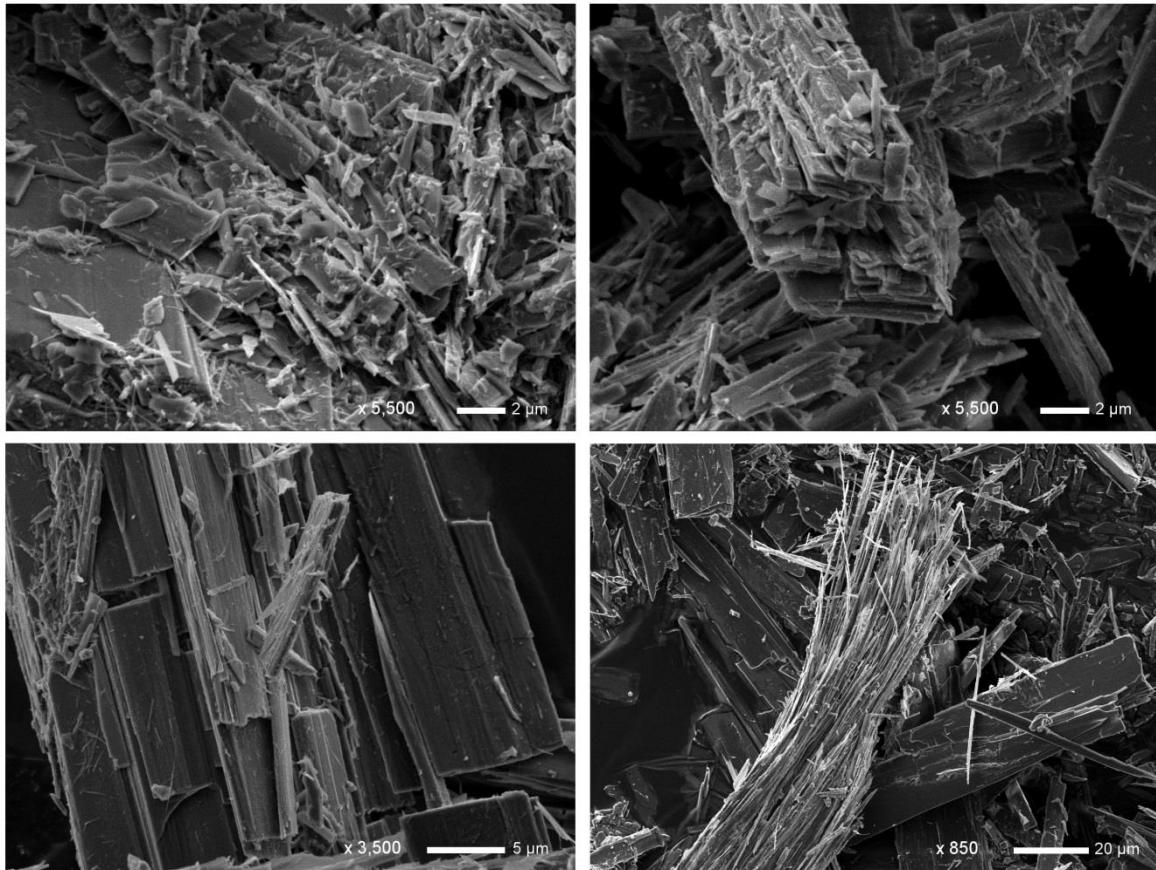
Figure III.13. SEM images of different morphologies of (fibro-)lamellar antigorite. Sample 27.

remembered that only electron microscopy allows to detect the 3D morphology of mineral fibres. An example of fibrous-lamellar blades of antigorite acquired with PLM (thin section, crossed polarizers) and SEM microscopies (Secondary Electron Images SEI) is shown in figure III.11. In this context, a complete atlas comparing the morphologies of asbestos minerals observed with optical and electron microscopies, is still lacking. This information would be of great interest in the identification of these minerals at the different scales of magnification. The example of an antigorite sample identified by mining geologist as massive antigorite, degree of alteration *#1* (Sample 30 – Annexe IA) is in figure III.12. Comparing PLM with SEM images, it is immediately clear that this sample consists of a strictly intergrowth of fibrous-lamellar of antigorite and randomly oriented flexible fibres of chrysotile in spite of the lamellar appearance observed at hand sample. This confirms that despite the intrinsic limits of PLM technique, thin sections retain several kind of morphological information also at low magnification.

SEM images, acquired especially in SEI mode, have provided to be the best way for the description of the huge morphological variability exhibited by mineral fibres of New Caledonia. All the main morphological features observed in this work are reported in Annexe III. Generally, antigorite samples are characterized by the co-existence of both lamellar and fibrous-lamellar shapes (Fig. III.13). Also samples identified by mining

geologist as not altered (*#1*), actually exhibit the appearance of several individual fibres at the surface. As shown in figure III.13, bundles of parallel elongated lath-shaped crystals may present regular or irregular endings. These fragments exhibit the typical habit of phyllosilicate minerals, characterized by the overlapping of platy sheets. Aggregates of randomly oriented not-elongated blades may also occur. However, most of antigorite samples maintain their lamellar habit displaying a gradual fibrous ending. Fibrous-lamellar endings generally appear bent, slinky to curvilinear. It should be noted that antigorite blades are not comparable in size, showing different dimensions depending on sample observed. In addition, antigorite showing a more fibrous aspect can display the appearance of flexible whitish fibres at the surface. Here, a partial conversion into chrysotile is suggested (Annexe IIIA). Chrysotile displays a more complex morphology (Annexe IIIB), although in literature it is usually described as bundles of flexible and sinuous whitish fibres. Several samples, showing a massive compact appearance, have proved to be formed by the close overlapping of thin fibres, as clearly shown in figure III.14. A careful observation of fracturing and cleavage highlights the presence of thin fibrils. Contrary to what expected in published literature (e.g. Andreani et al. 2004), Caledonian samples show a high density of tubes, in which no residual porosity remains between them. Unfortunately, due to the sample geometry, it is not possible to measure the tube dimensions.
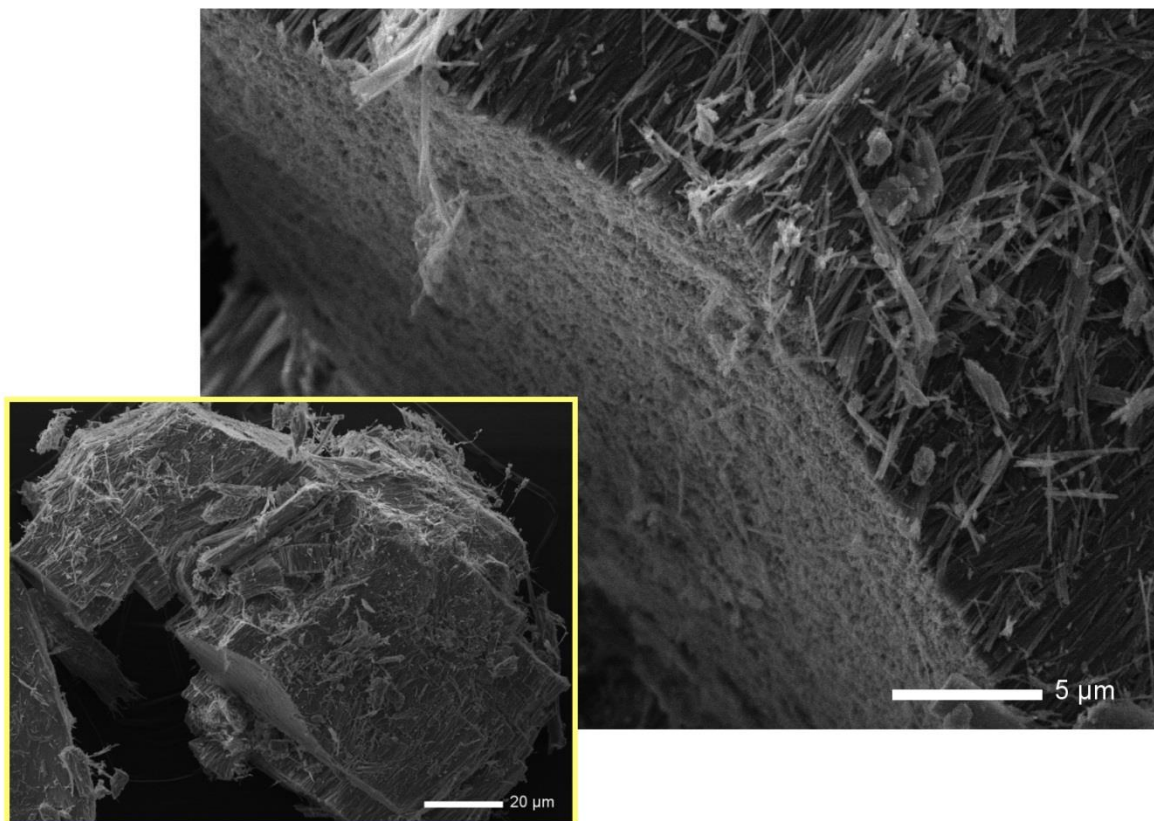

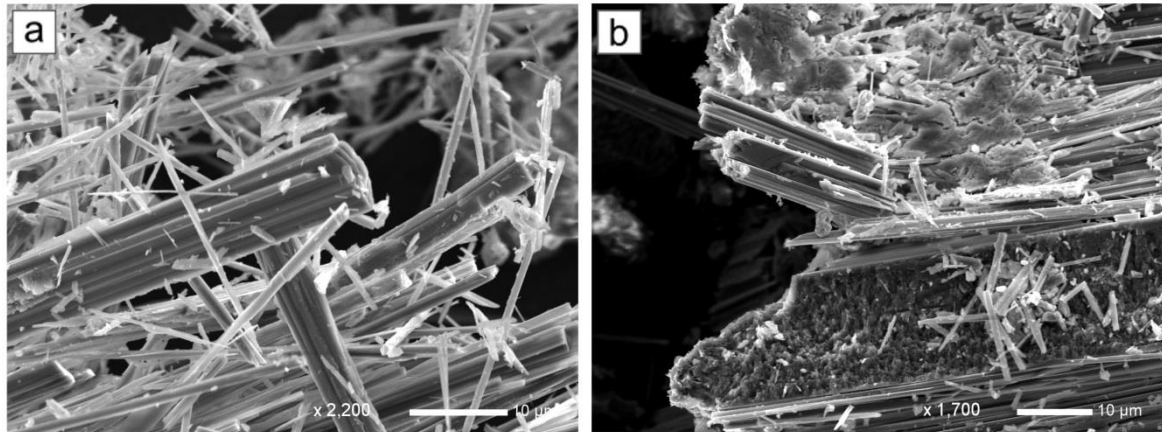Figure III.14. SEM images of compact bundle of parallel fibrils of chrysotile. Sample 23.

Figure III.15. SEM images of fibrous tremolite. a) prismatic and acicular crystals; b) intergrowth of tremolite fibres and serpentine. Sample 41.

SEM images of tremolite samples show the most common prismatic elongated and acicular, needle-like shapes (Fig. III.15a and Annexe IIIC). The tremolite crystals are arranged in parallel aggregates and/or randomly placed around the common *c*-axis. For each sample, the presence of secondary antigorite and/or chrysotile serpentine is observed (Fig. III.15b). Here, the two phases are closely intergrown. According with PLM observation tremolite fibres appear more or less fractured, displaying differences in size as the degree of alteration increases.

TEM microscopy was applied only to three serpentine samples (samples 18, 33 and 57) which have proved to be more difficult in interpretation. No TEM analysis were carried out on tremolite samples. TEM confirms to be the most complete method in the characterisation of mineral fibres, allowing the identification of all particular cases.
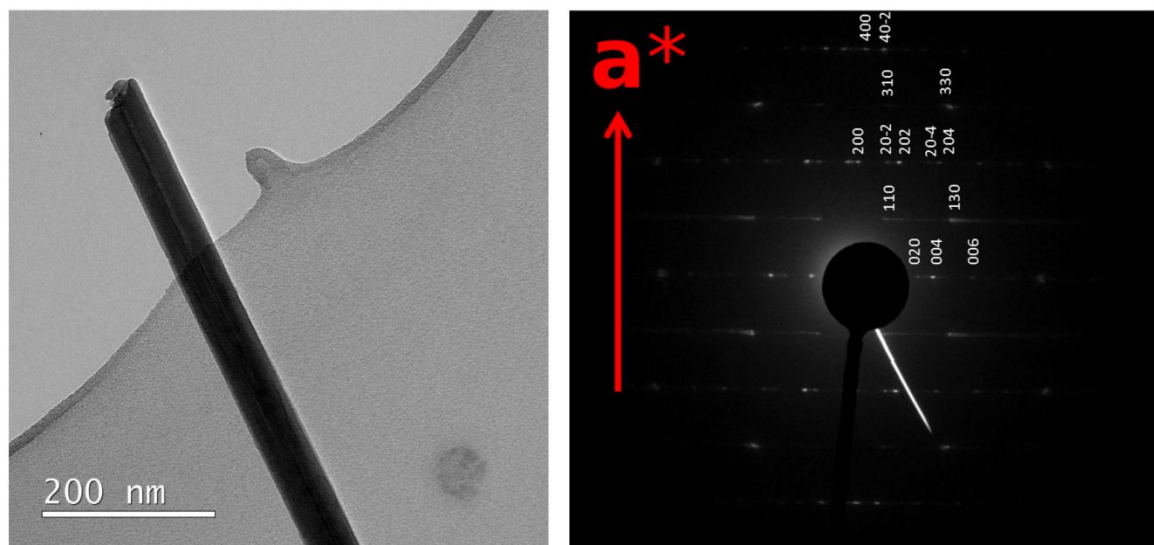
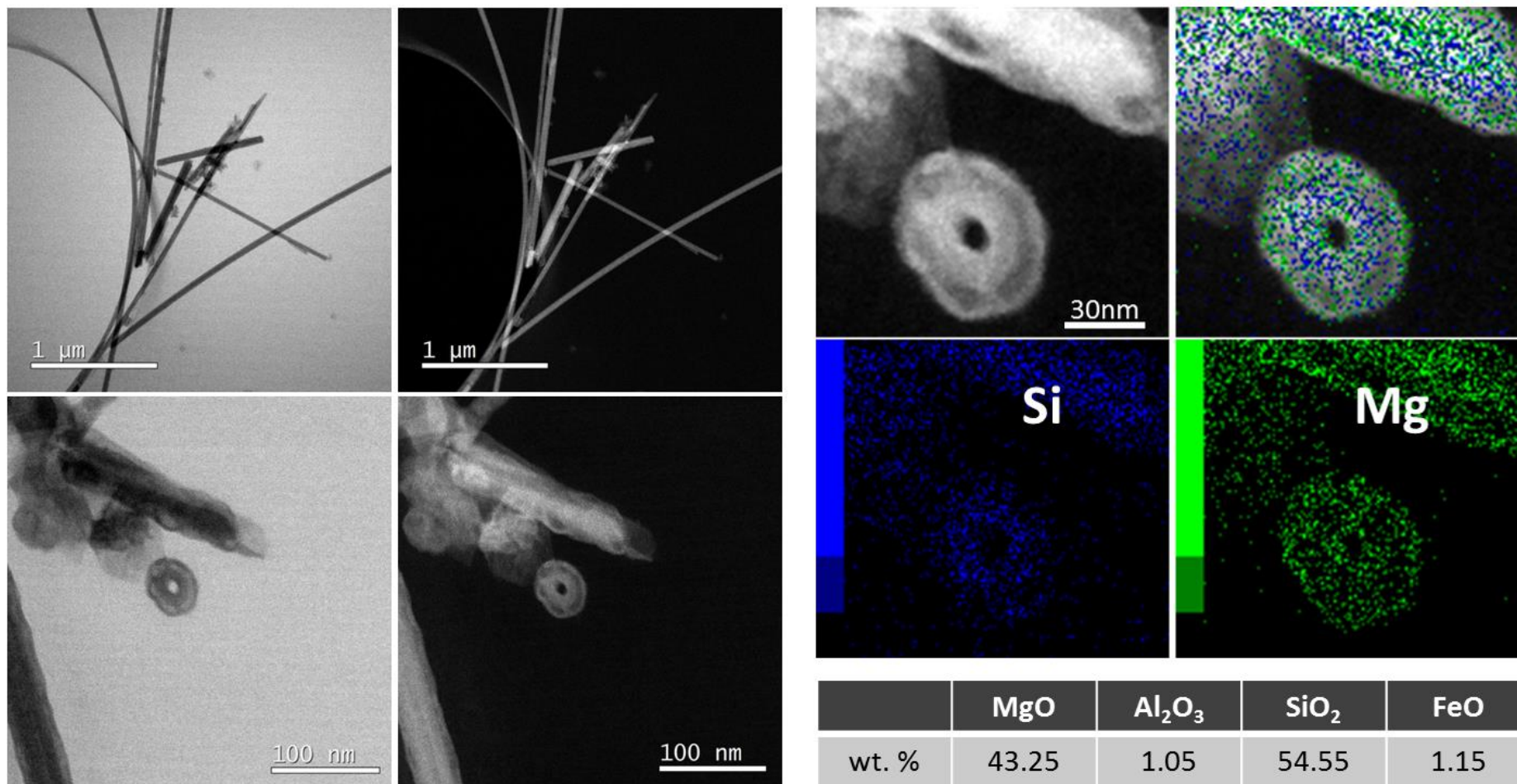*Figure III.16. TEM/SAED of a single clino-chrysotile fibril. Sample 57.*

Figure III.17. Bright Field (BF) and Medium Angle Annular Dark Field (MAADF) STEM coupled with EDS mapping have been applied on chrysotile bundles. The chemical analysis is only semi-quantitative. Sample 57.

	MgO	Al$_2$O$_3$	SiO$_2$	FeO
wt. %	43.25	1.05	54.55	1.15

Only at TEM-scale magnification it is possible to observe certain structural details, such as an unusual enlargement of internal nanotube of chrysotile samples and/or several intimate mineral associations at the microscale. A typical example of identification of a single fibril of clinochrysotile is shown in figure III.16 (sample 57). It is important to remember that from a statistical point of view the acquisition of a few SAED patterns is not representative in the evaluation of clino- and orthopolytypes percentage. Anyway, these measurements confirm chrysotile as major serpentine phase of sample 57. In addition to common TEM identification (Imaging, SAED and EDS), Bright Field (BF) and Medium Angle Annular Dark Field (MAADF) STEM coupled with EDS mapping have been applied on a few bundles of fibres, as shown in figure III.17. While BF and MAADF observation modes allow to better evaluate the morphology, increasing the contrast between fibres and the background, EDS mapping give a qualitative information on chemical composition. Serpentine minerals are not very resistant under the electron beam (Fig. III.17). This constraint has limited the number of analysis conducted; despite this limitation, no chemical differences between serpentine types have been observed. Furthermore, the observation of fibrils perpendicular to the fibre axis has allowed to detect the individual hollow-cored of chrysotile fibrils (Fig. III.17). All measures carried out on sample 57 detect the only presence of chrysotile.

III.1.2. X-Ray POWDER DIFFRACTION

X-ray powder diffraction (XRPD) was performed on all samples for the qualitative determination of the main crystalline components. According to our proposals, all procedures involved have to be compatible with their implementation in the mining professional sector. For this reason no quantification methods (i.e. Rietveld oriented methods, profile fitting techniques) have been carried out. Comparing the overall XPRD
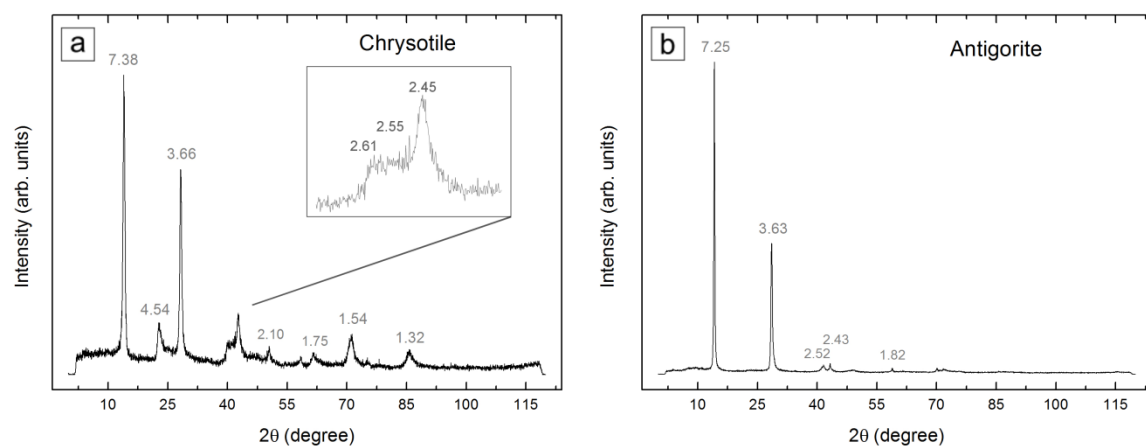

Figure III.18. XRPD patterns of a) chrysotile - sample 33; and b) antigorite - sample 19. Peak positions are reported as d-spacing (Å).
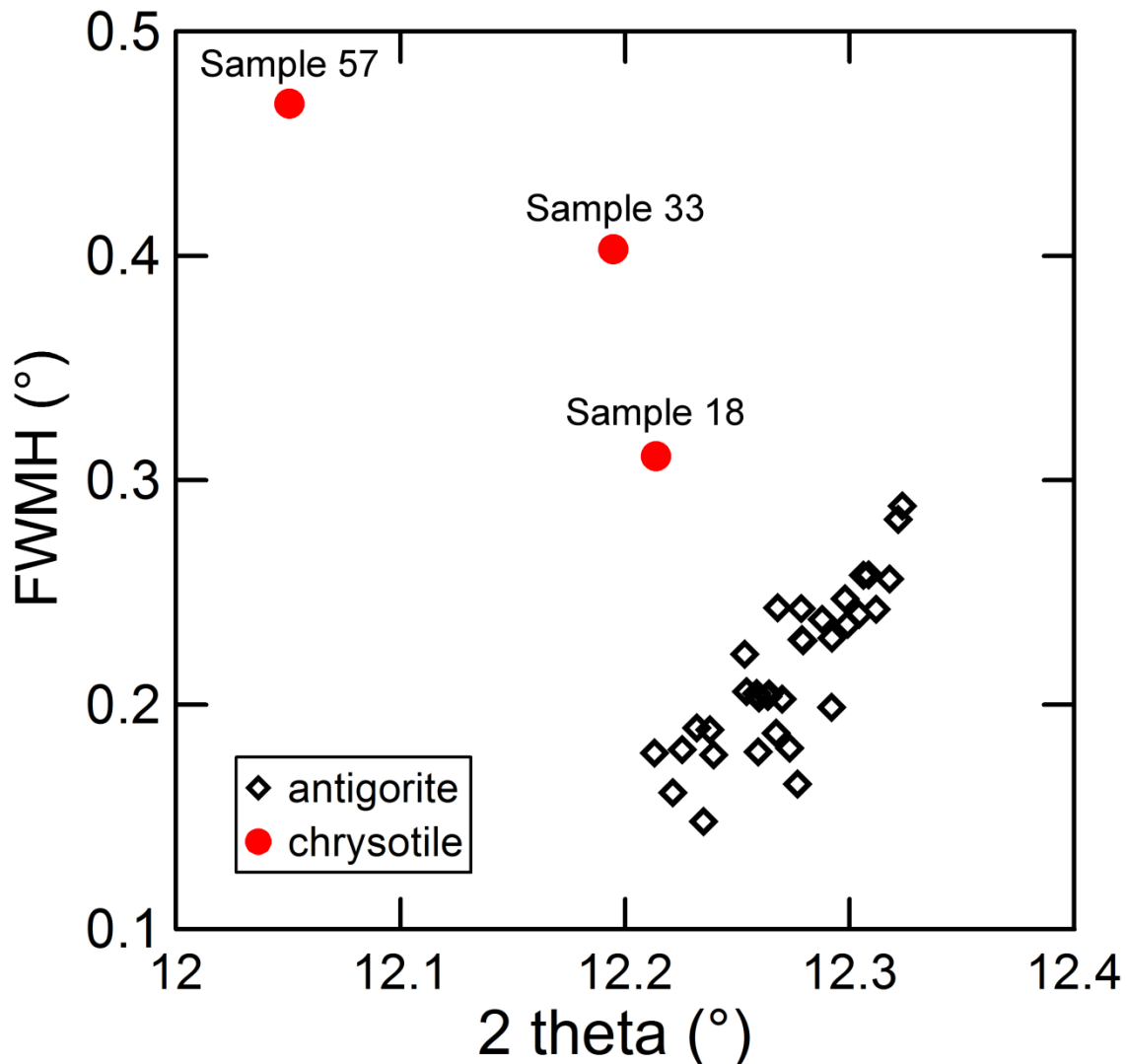
Figure III.19. Discrimination between chrysotile and antigorite by FWHM value of ~12.2 °2ϑ main peak (CuKα radiation; CNRT - ABP project, pers. comm. Pr. Mario Tribaudino).

patterns it was easy to distinguish a serpentine mineral from an amphibole mineral group. However, the right identification of the serpentine or amphibole variety is possible only with pure, less contaminated phases. Comparing XPRD patterns of chrysotile and antigorite serpentines, chrysotile diffraction pattern is more complex, because of anisotropic peak broadening due to anisotropic crystal size, cylindrical structure, disorder, and texture effects (Fig. III.18a). On the contrary, antigorite shows a more resolved pattern, characterized by sharper narrow peaks (Fig. III.18b). In addition, the appearance of three minor peaks with increasing intensity in the range 40-43 °2θ (CoKα radiation) is considered a typical signature of the presence of chrysotile (Fig. III.18a; PDF 25-0645). Basal reflections at *d*-spacing ~7.30Å (001) and 3.65Å (002) are characteristic of serpentine minerals; a little shift at higher *d*-spacing is expected for chrysotile (7.3326Å and 3.6643 Å) rather than for antigorite (7.2500 Å and 3.6253 Å). Reflections occurring at *d*-spacing 7.3826Å (002), 4.5478Å (110), 3.6643Å (004) and

1.5351Å (0.29) confirm the presence of chrysotile as the main mineral phase of the sample, whereas reflections at *d*-spacing 2.5189Å (201), 2.4261Å (211) and 1.8194Å (004) were used to positively identify antigorite, compared to chrysotile (Keeling et al. 2006, 2010). Differences in relative intensity of the peaks are related to preferred orientation of lath-shaped and fibrous particles. Especially for chrysotile, preferred orientation of fibres was certainly present.

A preliminary attempt to discriminate chrysotile from antigorite by the full width at half-maximum (FWHM) of the more intense peak at about 12.2 °2θ (CuKα radiation) is illustrated in figure III.19. FWHM values were determined after deconvolution with a Gaussian curve approximation. Two main groups of points can be observed. Chrysotile samples (sample 33 and 57) could be discriminate from antigorite on the basis of a small differences in the peak position (lower °2θ value) and by a little variation in FWHM value (higher FWHM value). Moreover, the intermediate position of sample 18 is coherent with its mixed mineralogical composition, made up of a fine intergrowth of antigorite and chrysotile (Annexe II). From a statistical point of view further analysis are necessary to confirm (or not) these first results.
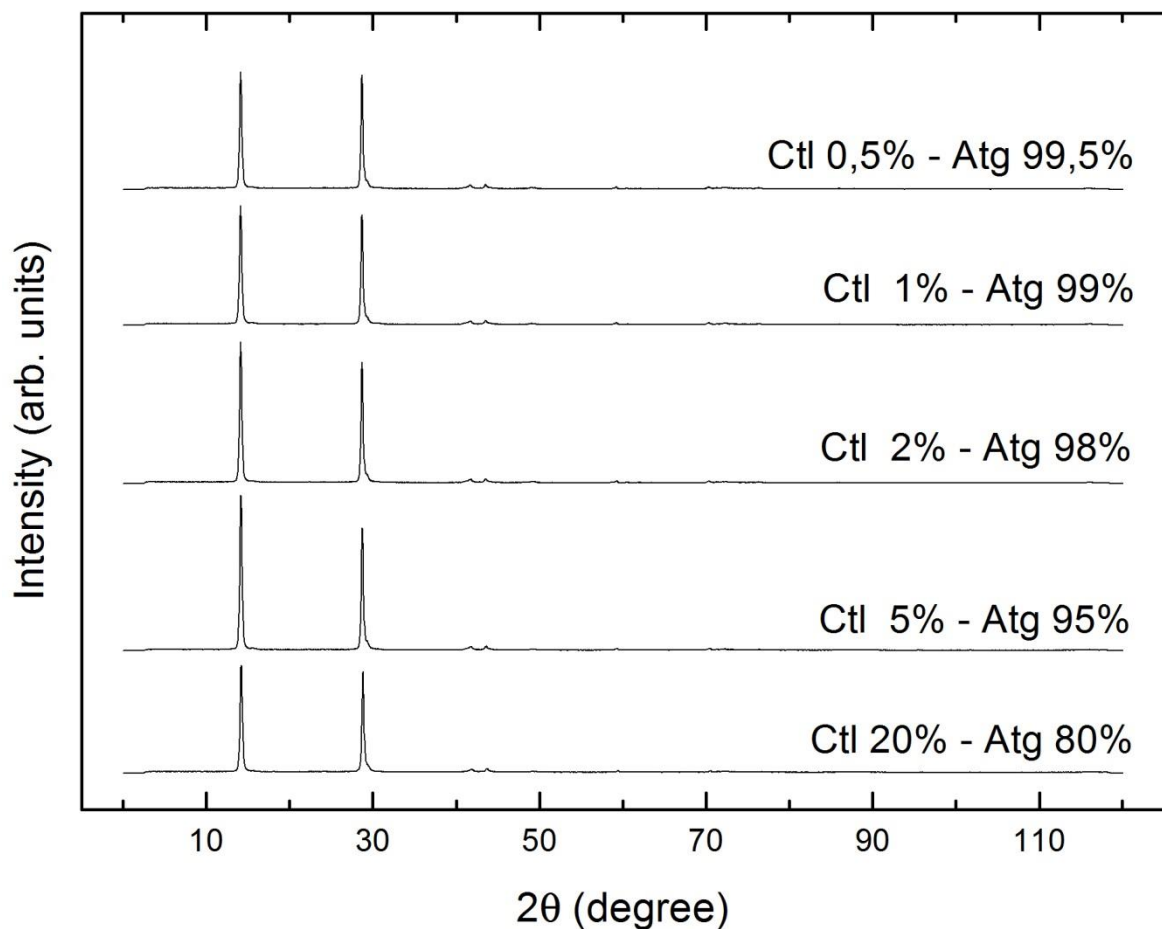

Figure III.20. Limit of detection of chrysotile into antigorite. Ctl = chrysotile; Atg = antigorite
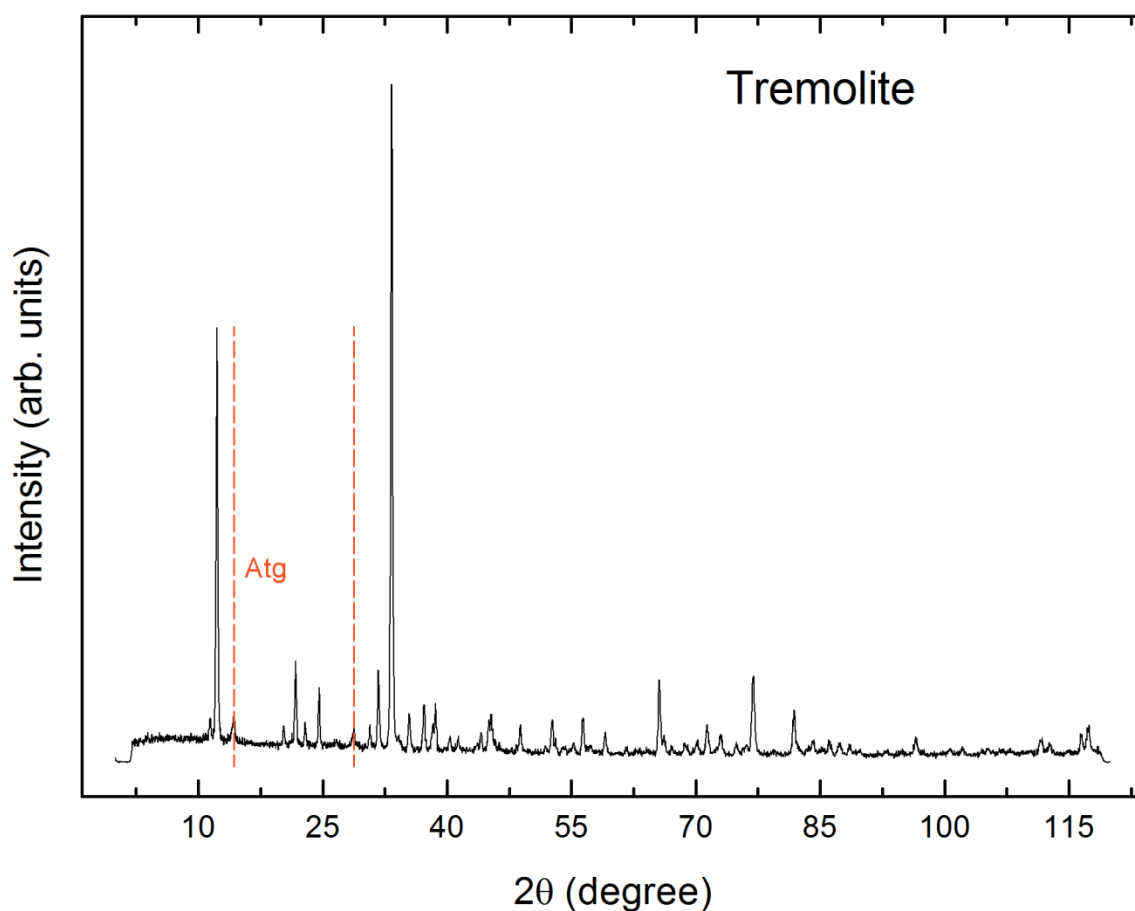
Figure III.21. XRPD pattern of tremolite. Secondary serpentine, probably antigorite (Atg), occur. Sample 42.

As expected, XRPD has proved not efficient in the discrimination of serpentine minerals co-existing in samples constituted by a mix of two or more phases, as in the case of sample 30 (Fig. III.12, Annexe IA). In all these cases, XRPD has displaced the diffraction pattern of the predominant phase, antigorite for the mentioned example, hiding information about any secondary serpentine varieties present. To verify the detection limit of chrysotile into a more complex sample, a preliminary set of tests was performed on controlled mélange with a known percentale, using the same analytical approach. As shown in figure III.20 a suitable amount (0.5, 1 , 2, 5, 20 wt.%) of "pure" chrysotile was added to starting antigorite and the mixture was homogeneously mixed. Even with 20 wt.% of chrysotile into antigorite, XRPD has been not able to detect the presence of chrysotile. It is worth noting that by definition, XRPD may easily detects minerals present in quantities of about 1 wt.% or less. Althought it is well-known that XRPD is less sensitive with serpentine minerals, this result appears remarkable. On the other hand, the preparation method (sample preparation and mouting, counting statistics, etc.) of mélange samples play a key role in the evaluation of low levels of fibres in complex samples. According to Foresti *et al.*, (2003) a more accurate analytical method is required to determine the low levels of fibres in complex samples.

XRPD patterns of tremolite samples have confirmed the presence of secondary serpentine, probably antigorite, as shown in figure III.21. As mentioned above, XRPD is not the reference technique to discerne tremolite from other members of tremolite–Fe-actinolite serie. Finally, talc, chlorite, magnetite, goethite and quartz have been recorded as accessory phases in some samples.

III.1.3. RAMAN SPECTROSCOPY

Micro-Raman spectroscopy was applied to those few samples which are characterized by an unusual (Fig. III.22) and/or a more complex texture (Fig. III.23). It was also used in the most doubtful cases to confirm (or not) XRPD and PLM identifications (Annexe II). All measurements were performed on petrographic thin sections. The example of a micro-Raman investigation of a fibrous sample of antigorite, previously described in this chapter (sample 35 – Annexe IA, Fig. II.6) and characterized by an unconventional non-pseudomorphous texture made up of star- and fan-shape blades, is reported in figure III.22. Raman peaks in high-wavenumber region (3550-3850 cm^{-1}), associated to vibrational peaks of OH groups, confirm the antigorite identification, as illustrated by the typical doublet at 3665 and 3695 cm^{-1} (Petriglieri et al. 2015). Moreover, micro-Raman has proved decisive in the study of the intimate intergrowth of fibrous antigorite and chrysotile fibres observed for sample 30 (Annexe IA, Fig. III.12). As clearly shown in figure III.23, alternate fibrous-lamellae of antigorite (Fig. III.23a) and compact bundle fibres of chrysotile (Fig. III.23b) are observed. Raman peaks at high-wavenumber region confirm the identification of flexible tufts as chrysotile (Fig. III.23c). The appearance of a OH stretching peak of antigorite at about 3665 cm^{-1}, indicating by a red arrow, is strictly linked to the thickness of fibres compared to thin section preparation. Although tufts of chrysotile fibres overlap the antigorite lamellae, the laser beam directed on chrysotile surface penetrates sufficiently to be affected by the underlying antigorite. No micro-Raman analysis were conducted on tremolite samples.
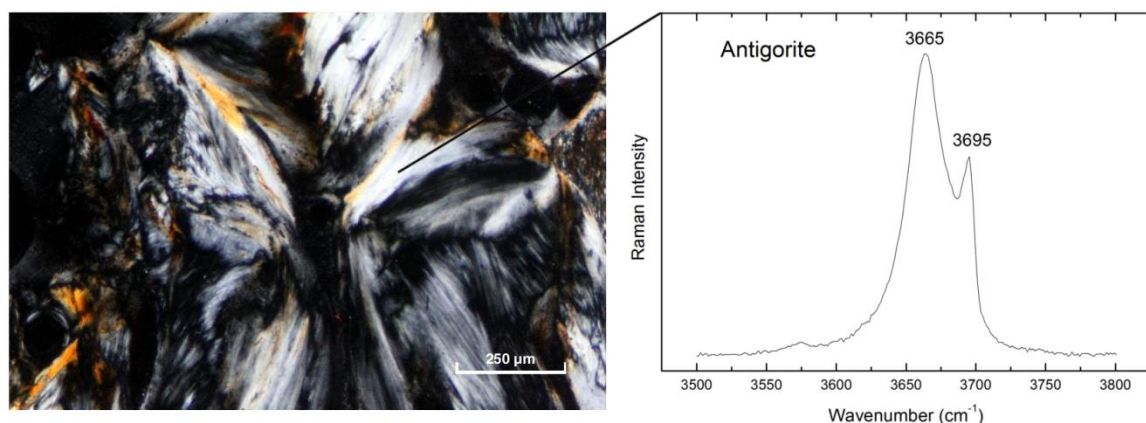

Figure III.22. Identification of fibrous-lamellar blades of antigorite (PLM, cross-polarizing image) by micro-Raman spectroscopy. Raman spectrum was obtained at 473.1 nm in the high-wavenumber region. Sample 35.
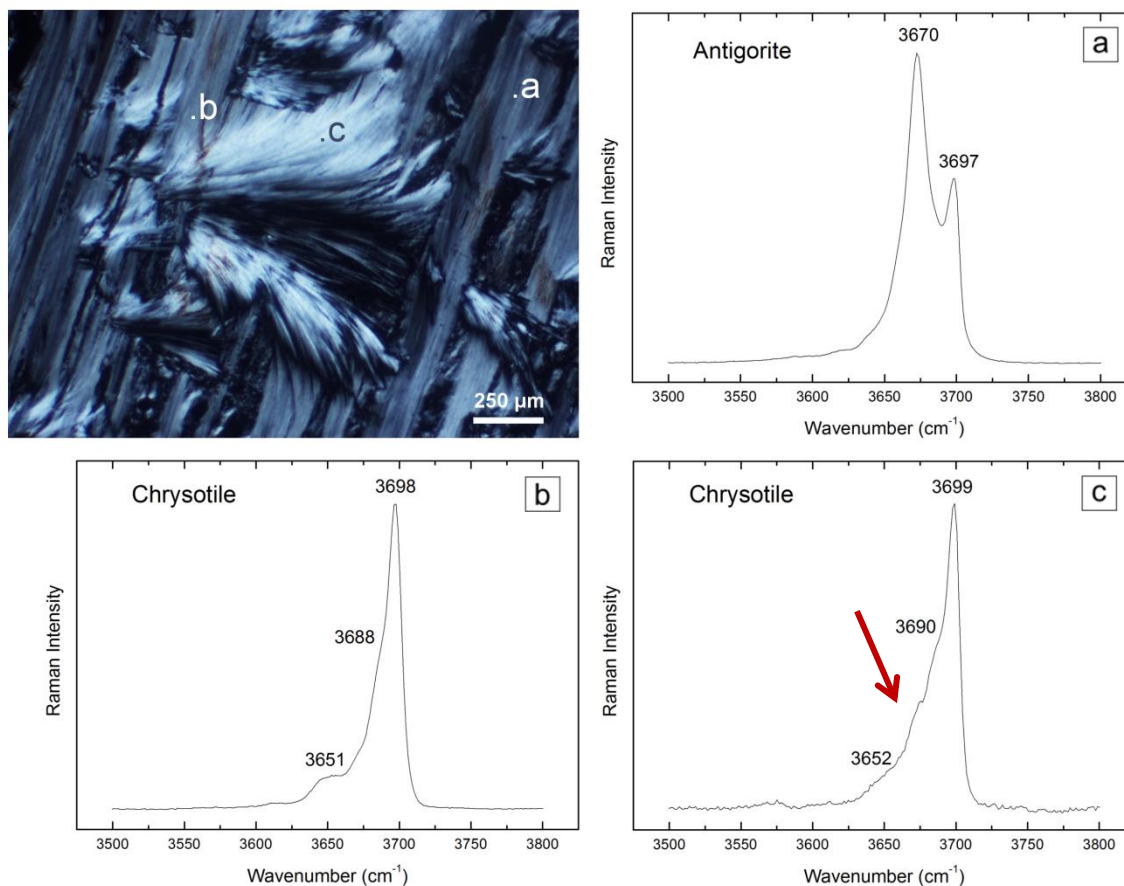
Figure III.23. Investigation of intimately intergrowth (PLM, cross-polarizing image) of fibrous-lamellar antigorite (a) and chrysotile fibres (b,c) by means of micro-Raman spectroscopy. The appearance of OH stretching peak of antigorite (about 3665 cm^{-1}) in spectra C is marked by a red arrow. Raman spectra were obtained at 473.1 nm in the high-wavenumber region. Sample 30.

A set of preliminary measurements, devoted to testing the performances of the portable Raman equipment, was performed in laboratory. A test for each sample was performed (one or two spot analysis at most). On 47 analysed samples, 41 were successfully identified, allowing the discrimination of the main serpentine or amphibole phase (Annexe II). A comparison of spectra obtained with micro-Raman spectrometer (laboratory device) and portable Raman (handheld equipment) on a chrysotile sample (sample 33 as example) is shown in figure III.24. The micro-Raman spectrum was recorded on petrographic thin section, on a polished surface, choosing the optimal conditions of measurement (e.g. spot analysis, objective, time and number of acquisitions, filter, etc.). On the contrary, the portable Raman does not allow the choice of all these instrumental parameters. In this latter case, the acquisition was performed directly on fibre bundles, selecting only the time of acquisition. Moreover, differences in spatial (1-2 µm and 1 mm, respectively) and spectral (4 cm^{-1} and 8 cm^{-1}, respectively)
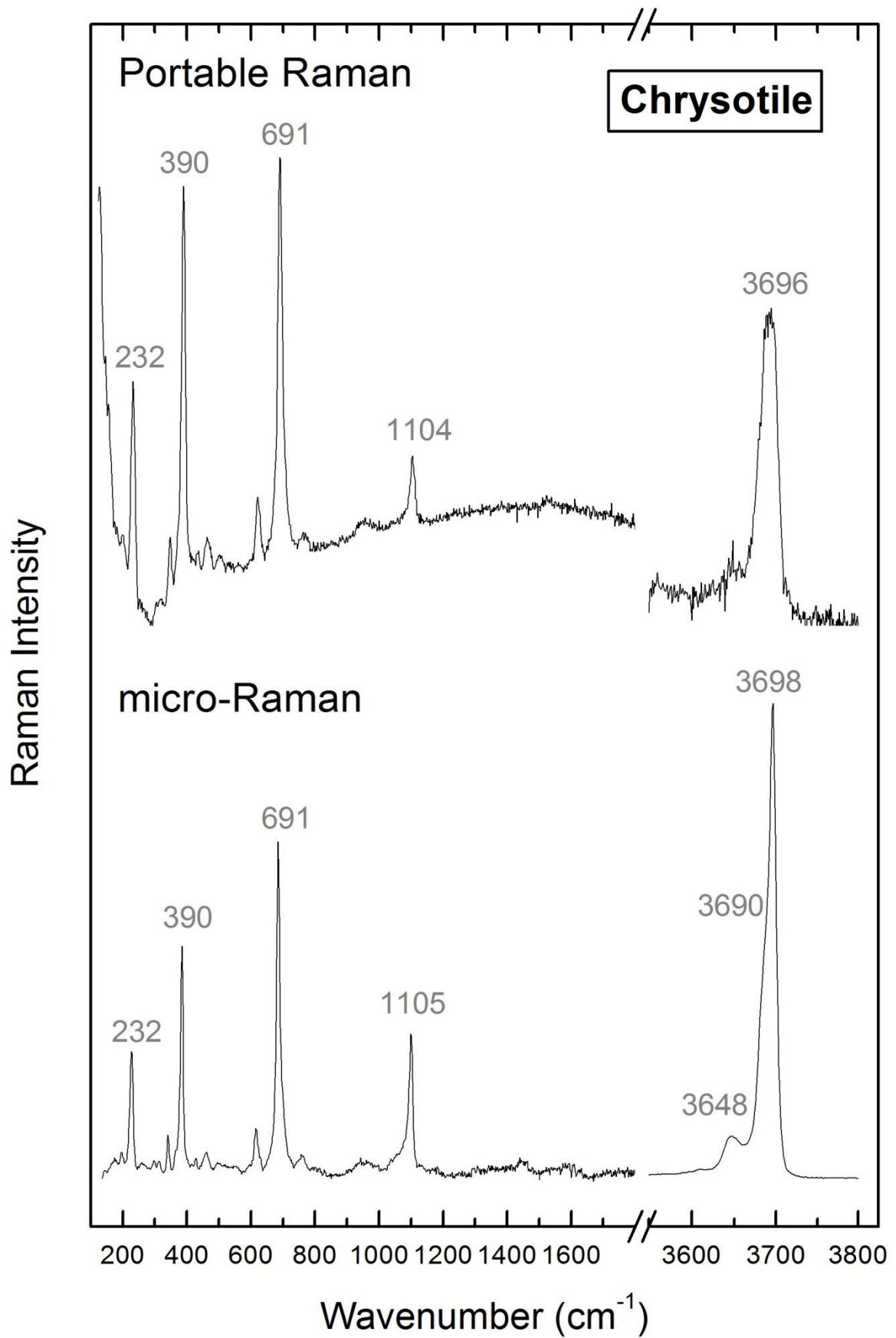
Figure III.24. Comparison of spectra recorded with a micro-Raman spectrometer (473.1 nm laser) and a portable Raman device (532 nm laser). Sample 33.

resolution shall be taken into account. In addition, the quality of the signal-to-noise ratio, and consequently the quality of the spectra, may be affected by the fluorescence interference. Despite all these intrinsic differences, spectra appear perfectly comparable at both low- and high-wavenumber regions, allowing the identification of the mineral phase.

Finally, the spectra obtained for tremolite samples, show the worst signal-to-noise ratio, compared to those of antigorite, due to increased fluorescence interference. Anyway, the identification of the predominant phase was not compromised. On the other hand, it was not possible to discriminate any secondary phase (e.g. antigorite, chrysotile; Annexe II). OH stretching peaks in high-wavenumber region are often partially covered by fluorescence interference.

III.1.4. PERFORMANCES AND LIMITS OF MINERALOGICAL MONITORING

In the context of mining professional sector, the development of a user-friendly efficient analytical strategy, able to discriminate the potential asbestiform fibres from not-harmful fragments, is the first requisite in the implementation of the actual monitoring prevention plan. Data achieved describe a complex situation. Each instrumental device implies advantages and limits. This means that a multidisciplinary routinely approach is the only strategy possible to answer to worker and population requirements. At present, there is not a technique capable to instantly characterize an asbestos fibre on field, providing information about size and distribution, morphology, chemical composition and alteration grade. The acquisition of all these parameters is necessary for determining the real risk associated to fibres exposition. It is worth noting that all these considerations may applied to all type of unconfined sites of exposition, including environmental and domestic expositions.

Polarized Light Microscopy is a preliminary essential technique in the study of textures and mineralogical associations. It has proved to be a valuable tool in the investigation of morphologies but, unfortunately, it cannot be suitable for monitoring operations. Timing of preparation of thin sections is too longer (4-5 days) compared to professional timelines. On the other hand, this approach allows to describe the huge variability in morphology displayed by Caledonian samples. Regardless of the mineralogical nature of sample observed (e.g. chrysotile), no modifications have been observed in texture, at the micro-scale, on the basis of different geological context (mainly serpentine sole and lateritic profile). Also in sample which looks like lamellar and not altered at the hand-scale, optical proprierties have shown a perfect correspondance with their real mineralogical nature (sample 30 as example). In fact, optical properties are comparable for all chrysotile (or antigorite) samples. No changes are observed, for example, by increasing the state of alteration. Conversely, the incongruity recorded in texture at the

macro- (hand-scale specimens) and microscale (thin sections) can probably depends on the type of geological process responsible for the mineral cristallisation. In serpentinite sole, chrysotile veins and veinlets form after a process of later crystallization of lizardite, associated to the presence of fluid circulation in fractures, at determined T-P conditions. In the laterite profile, instead, the presence of massive dykes, made up of the intimate intergrowth of chrysotile and fibrous antigorite (sample 30, degree of alteration *#1* as example) shows a lamellar, moderately hardned appearance. This is probably related to a variation of the equilibrium condition, that has resulted in the conservation of skeleton structure of antigorite, while mineralogically antigorite is transformed into chrysotile (retro-metamorphism). In fact, in lateritic profile antigorite is generally found in discontinuities (fault and/or fractured zones) parallel to the direction of movement (slickenside). As a general rule, antigorite is not common in retrograde serpentines from slow-spreading ocean ridges and fractures zones, where lizardite + chrysotile pseudomorphs and chrysotile veins are predominant (Ribeiro Da Costa et al. 2008). Although antigorite nucleation is often considered an improbable event under low-grade conditions (Wicks and Whittaker 1977), there are indications for the chrysotile → antigorite transition at temperature below 300 °C (Evans et al. 1976), and for antigorite stability relative to talc + chrysotile at temperatures down to 25 °C (Evans 2004). The chrysotile → antigorite reaction requires considerable structural rearrangement (Evans et al. 1976; Mellini et al. 1987) and has a very small driving force ($\Delta G < 5$ kJ; Evans 2004), so that is slow at low temperatures. This transition can, however, be greatly accelerated by deformation processes and/or by the presence of abundant fluids (Viti and Mellini 1996; Wunder et al. 2001). Therefore, plastic deformation, and shearing in particular, can promote the development of non pseudomorphic, foliated antigorite textures (Ribeiro Da Costa et al. 2008), and slip-fibre antigorite veins. It is not surprising that antigorite is found in retrograde serpentinites associated with shear zones and shear surfaces on the ocean floor (Prichard 1979; Ribeiro Da Costa et al. 2008). These processes are consistent with the New Caledonia's obduction.

Moreover, the observation of kinking in serpentine minerals is generally considered unusual. This type of occurrence is generally observed in high-T experimentally-deformed serpentinites, in which mineralogical and micro/nanostructural modification have been induced in lizardite (e.g. Viti and Hirose 2009), and in suprasubduction-zone mantle wedge peridotites as fingerprints of strong tectonic shear (e.g. antigorite schist in a kimberlite from Moses Rock, Colorado Plateau, Boudier et al. 2010). In Caledonian specimens *kink bands* texture was observed only in an altered sample of fibrous antigorite (Sample 24).

PLM/DS observations on mount particles have allowed to successfully identify all fibrous samples analysed, confirming as a diagnostic method also in investigation of natural samples. PLM/DS provides information about mineralogical identification and morphology of fibres and/or lamellae. The implementation of RI 1.5680 in regulated

protocols would allow to discriminate antigorite from chrysotile fibres (RI 1.550). Repeating in routine this simply and rapid technique on more particles for each sample, PLM/DS may be an efficient tool in characterisation of asbestos in rock samples. By contrast, its main limit is essentially related to detection of thin smaller particles. While PLM/DS allow to investigate different population of particles in the range of micrometer scale (10-300 μm), electron microscopies give information until nanometric scale (TEM resolution, 0.01-10 μm; Cavariani et al. 2010).

SEM is a powerful technique that enables the quantity (size and distribution), morphology, and semi-quantitative composition (EDS system) of asbestos fibres. Compared to literature where most of morphological images have been acquired at 10-20 kV, with the intent to better evaluate the general morphology of fibres, we have chosen to work on lower voltage (5-10 kV), in order to focus attention on the study of surface features. This strategy results effective in the evaluation of intermediate and fibro-lamellar morphologies. TEM is the most complete method in the characterisation of small particles, combining morphological information to chemical data and crystallographic characterisation. However, it allows to analyse very small subsamples volumes, so the homogenisation of the sample is crucial if the results are applied to the sample as a whole. Concernig semi-quantitative chimical analyses, EDS allows to distinguish tremolite from serpentine on the basis of the presence of Ca. Moreover, chemical differences between serpentine phases were confirmed to be generally insignificant (Cavallo and Rimoldi 2013) compared to natural variability within individual serpentine phases (Schreier 1989; Wagner 2015). Furthermore, lower concentrations of minor elements in chrysotile may have been due to lower X-ray counts for the thinner chrysotile fibrils.

XRPD may be used as quick, user-friendly technique in the qualitative recognition between amphibole and serpentine minerals only. According to our proposals, a simple conventional preparation of powder samples was performed. In this context, due to the low sensitivity in the distinction of the different varieties of serpentine group, XRPD cannot be involved in a routinely monitoring systems. The information conveyed by simple X-Ray qualitative analysis is not sufficient to handle the complexity of these mineral structures and assemblages (Foresti et al. 2003; Leoni and Scardi 2004; Gualtieri et al. 2014). A good data collected with a proper quantitative analysis (e.g. Rietveld oriented method, profile fitting techniques) may be of help to separate the contribution of the serpentine varieties (chrysotile content in antigorite specimen for example). However, XRPD is the most reliable technique in the identification of crystalline components in complex rock samples, allowing the identification of secondary mineral phases such as talc, chlorite, quartz and oxides.

The acquisition of Raman spectra in low-wavenumber region and OH-stretching region (high-wavenumbers) has been confirmed as the decisive approach for the identification

of the main varieties of the serpentine and amphibole families. OH is a very sensitive probe for the micro-structure investigation of asbestos minerals. In addition, Raman portable has proved to be a user-friendly tool on rock fragments, able to provide reliable results only with a few measurements.

Laboratory results have suggested PLM/DS and portable Raman spectroscopy as the potentially decisive tools in the detection and characterization of asbestos fibres on field, for both serpentine and amphibole. The employment of these specialized tools may provide extremely effective in the improvement of the performance and in the rapidity of data acquisition and interpretation. Moreover, a further development on analytical identification of the alteration effects will be discussed in the following paragraphs (Chapter III.3).

Finally, it is worth noting that the implementation of other analytical techniques such as Infrared Spectroscopy (IR) and thermal analyses (TGA, DTA , DSC) will allow to complete these data in order to obtain an exhaustive overview on behaviour of altered asbestiform fibres of New Caledonia.

III.2. Analytical versus in situ visual identification of asbestos

Data obtained with analytical mineralogical techniques have been compared with the identification realized on field, by mining geologist, employing visual morphological criteria, as illustrated in table III.1. The prevention plan followed by the geological sector of mining companies is not sufficient for discriminating asbestos fibres from not-asbestos fragments. The main reason lies in the great variability in texture and morphologies of these samples, as a consequence of the huge impact of supergene alteration in the genesis of asbestiform minerals.

Crucial is the case of the sample 33. This sample, coming from the mine site of Tontouta, was identified by the mining geologist as antigorite, degree of alteration number *1*; it was manipulated and stored as a not altered, non-pathogenic and non-dangerous rock fragment. At the hand-sample scale it appears pale-green to white, formed by the overlay of parallel and welded well-grown lamellae (Fig. III.25a - Annexe I). Contrary to expectation all analytical techniques confirm that it is chrysotile (Annexe II).
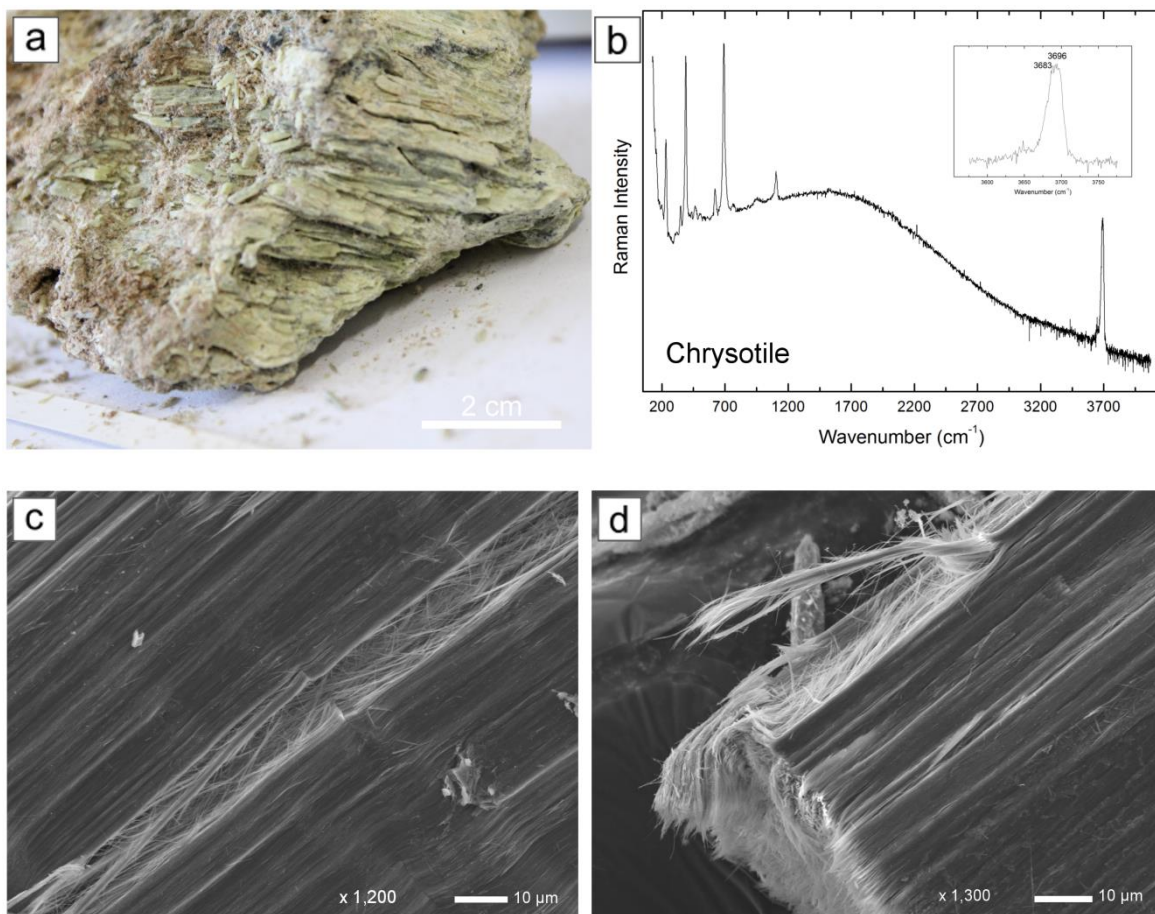
Figure III.25. Sample 33. a) hand specimen; b) Raman spectrum of chrysotile (handheld device, 532 nm laser); c-d) SEM images showing a compact bundle of parallel chrysotile fibrils.
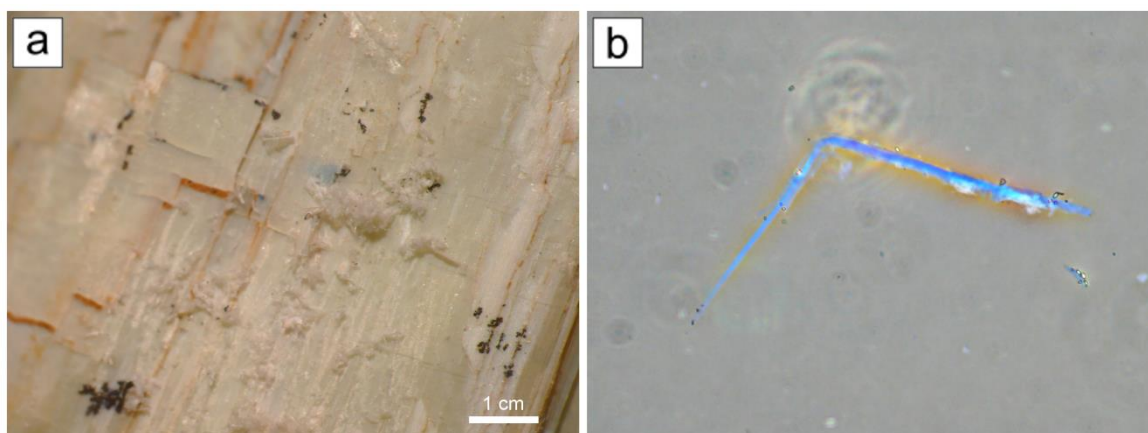
Figure III.26. PLM/DS identification of sample 33, RI 1.550. a); parallel welded lamellae; b) PC: pale-blue with orange halo.

Despite its macroscopic lamellar massive aspect, PLM observations on thin section show the typical zebra-like appearance of chrysotile samples (Fig. III.8d). Meanwhile, PLM/DS observations on mount particles confirm the identification of chrysotile fibre using the standard RI 1.550 oil. Fibres observed in phase contrast mode exhibit the typical pale-blue colour with the orange halo (Fig. III.26b) and appear blue to purple in dark field observation. Increasing the magnification, SEM images display a compact bundle of parallel fibrils of chrysotile (Fig. III.25c,d). Similarly to what observed for sample 23 (Fig. III.14), fibrils are tightly welded and no residual porosity remains between them. Also TEM/SAED analysis confirm the identification of chrysotile (Fig. III.27). Furthermore, both micro-Raman spectroscopy and portable Raman equipment were applied on this sample, allowing the identification of the chrysotile variety. As shown in figure III.24, the acquired
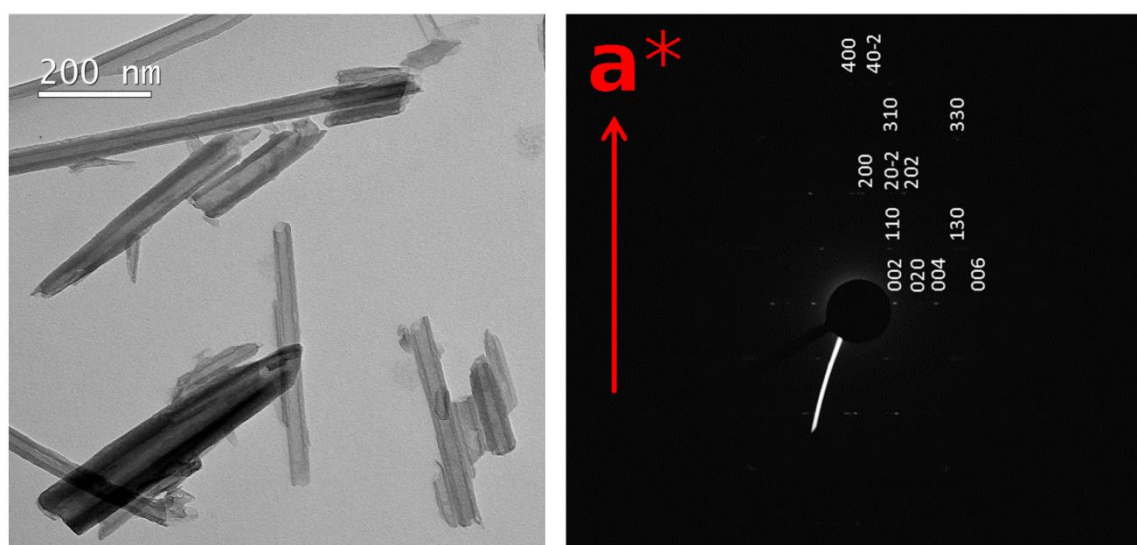
Figure III.27. TEM/SAED of a single fibril of clino-chrysotile. Sample 33.

Antigorite

LABEL	APPROVAL NUMBER	ON FIELD IDENTIFICATION	ALTERATION DEGREE	ANALYTICAL IDENTIFICATION
23-Tontouta-Module1-Antg1	23	Antigorite	#1	Chrysotile
33-Tontouta-module1-Antg1	33	Antigorite	#1	Chrysotile
13-Tontouta-module4-Antg1	13	Antigorite	#1	Antigorite
19-Tontouta-module4-Antg1	19	Antigorite	#1	Antigorite
30-Tontouta-Module4-Antg1	30	Antigorite	#1	Antigorite & Chrysotile
34-Tontouta-module4-Antg1	34	Antigorite	#1	Antigorite & Chrysotile
11-Kouaoua-Piste-Antg1	11	Antigorite	#1	Antigorite & Chrysotile
32-Kouaoua-piste-Antg1	32	Antigorite	#1	Antigorite & Chrysotile
3-Tontouta-module1-Antg2	3	Antigorite	#2	Antigorite
4-Tontouta-module1-Antg2	4	Antigorite	#2	Antigorite & Chrysotile
5-Tontouta-module1-Antg2	5	Antigorite	#2	Antigorite
7-Tontouta-module1-Antg2	7	Antigorite	#2	Antigorite + ?
9-Tontouta-module1-Antg2	9	Antigorite	#2	Antigorite & Chrysotile
27-Tontouta-module1-Antg2	27	Antigorite	#2	Antigorite
6-Tontouta-module4-Antg2	6	Antigorite	#2	Antigorite
16-Tontouta-module4-Antg?2	16	Antigorite ?	#2	Antigorite & Chrysotile
29-Tontouta-Module4-Antg2	29	Antigorite	#2	Antigorite & Chrysotile
18-Kouaoua-piste-Antg2	18	Antigorite	#2	Antigorite & Chrysotile
14-Kouaoua-piste-Antg2	14	Antigorite	#2	Antigorite
31-Kouaoua-piste-Antg2	31	Antigorite	#2	Antigorite & (Chrysotile?)
20-Kouaoua-Fosse-Antg2	20	Antigorite	#2	Antigorite
10-Tontouta-module1-Antg4	10	Antigorite	#4	Antigorite & (Chrysotile?)
12-Tontouta-module1-Antg4	12	Antigorite	#4	Antigorite & Talc
17-Tontouta-module1-Antg4	17	Antigorite	#4	Antigorite & Chrysotile
24-Tontouta-Module1-Antg4	24	Antigorite	#4	Antigorite
25-Tontouta-module1-Antg4	25	Antigorite	#4	Antigorite
26-Tontouta-module1-Antg4	26	Antigorite	#4	Antigorite & (Chrysotile?)
35-Tontouta-module1-Antg4	35	Antigorite	#4	Antigorite
8-Tontouta-module4-Antg4	8	Antigorite	#4	Antigorite
15-Tontouta-module4-Antg?4	15	Antigorite ?	#4	Antigorite
1-Kouaoua-Piste-Antg4	1	Antigorite	#4	Antigorite
21-Kouaoua-Piste-Antg4	21	Antigorite	#4	Antigorite & Chrysotile
22-Kouaoua-Fosse-Antg4?	22	Antigorite ?	#4	Antigorite

Table III.1. Comparison between in situ visual and analytical identification. Misinterpretations are highlighted in pink.

Chrysotile

57-Poro-Chr3	57	Chrysotile	#3	Chrysotile

Tremolite

41-Poro-Trem1	41	Tremolite	#1	Tremolite & Serpentine
37-Poro-Trem2	37	Tremolite	#2	Tremolite & Serpentine
42-Poro-Trem2	42	Tremolite	#2	Tremolite & Serpentine
45-Poro-Trem2	45	Tremolite	#2	Tremolite & Serpentine (Antigorite?)
46-Poro-Trem2	46	Tremolite	#2	Tremolite & Serpentine
38-Kouaoua-Fosse-Trem2?-Nephrite?	38	Tremolite ?	#2	Antigorite & (Chrysotile?)
48-Kouaoua-Fosse-Trem2?	48	Tremolite ?	#2	Antigorite
47-Boulinda-Trem2	47	Tremolite	#2	Tremolite & Serpentine (Antigorite?)
55-Boulinda-Trem2	55	Tremolite	#2	Tremolite & Serpentine & Chlorite
36-Poro-Trem4	36	Tremolite	#4	Tremolite & Serpentine

Not identified

40-Tontouta-module4-Fibres2?	40	Fibres?	#2	Antigorite & Chrysotile
39-Tontouta-Module4-Fibres4?	39	Fibres?	#4	Antigorite

spectra appear perfectly comparable. Spectrum obtained with handheld device (Fig. III.25b) shows a slightly fluorescence interference, which do not compromise the quality of data.

These new results could involve a reviewing of prevention procedures. The adoption of completely different actions in the manipulation and storage of rock fragments at the outcrop is now imperative. In order to improve the current prevention plan, the employment of routinely techniques, which consider the possibility to introduce a benchtop and/or a portable device, might be the answer to requirements of mining sector. Portable devices may provide a non-subjective and reliable answer without delay. Both PLM/DS and Raman portable apparatus satisfy these requirements.

III.3. The impact of alteration on analytical identification

A more detailed study of the impact of alteration status on the formation and consequent release of fibres into the environement was carried out. Further tests were performed on more altered samples in order to estimate the reliability of all instrumental equipment in different working conditions. If microscopies and X-Ray diffraction methods need free asbestos fibres for sample preparation (e.g. free fibres, powder, etc.), the portable Raman device requires more attention during the time of measurement. To obtain high-quality spectra the laser beam must be in fact accurately focused on the area of interest. Especially in the cases of most altered antigorite, the laser beam should be focused on non-cohesive aggregates of randomly orientated fibrous-lamellae. Thus, a set of measurements on the most altered samples (*#4*) was performed *ad hoc*. As shown in figure III.28 despite the complete loss of cohesion of the sample, the goodness of data was not affected, allowing the identification of the antigorite phase. On 15 very altered samples only 4 were not identified with portable Raman (Annexe II).

Conforming to the nomenclature adopted by mining geologist, no samples display the visual features generally attributed to a degree of alteration *#1*. All samples identified as no altered, and therefore no hazardous, actually exhibit the appearance of individual thin fibres at the surface. The example of two specimens of antigorite *#1* (samples 13 and 19, respectively - Annexe IA) is illustrated in figure III.29; they present flexible potentially breathable fibres at the surface. According to WHO dimensional criteria (L >5 μm, D <3 μm, L/D ≥ 3:1), these fibres can be counted as asbestos (IARC 2012).

Despite the great variability of morphologies displayed by Caledonian samples, morphologies and the increasing degree of alteration are not necessarily correlated. Samples identified as not-altered, degree of alteration *#1*, have bundles of fibrous-lamellae with splaying ends (Fig. III.30a), as well as very altered samples show a
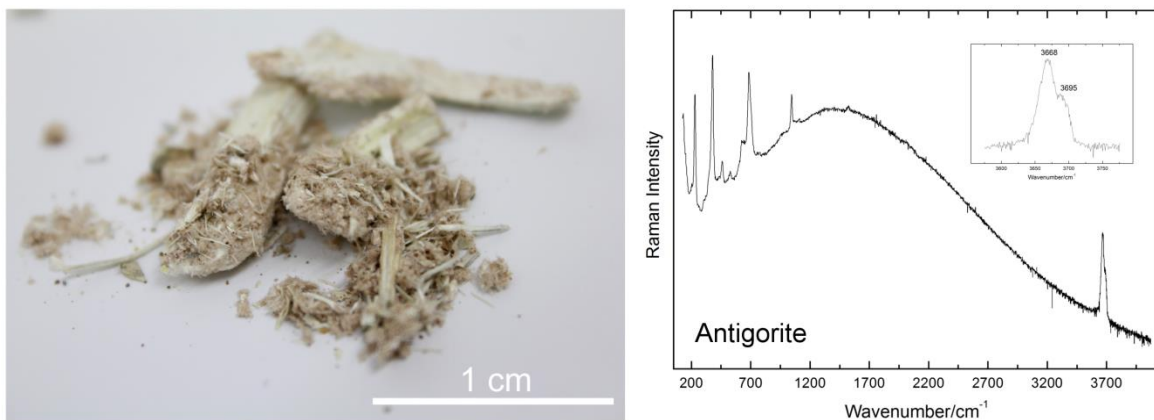

Figure III.28. Identification of very altered antigorite sample by means of portable Raman equipment (532 nm laser). Sample 15.
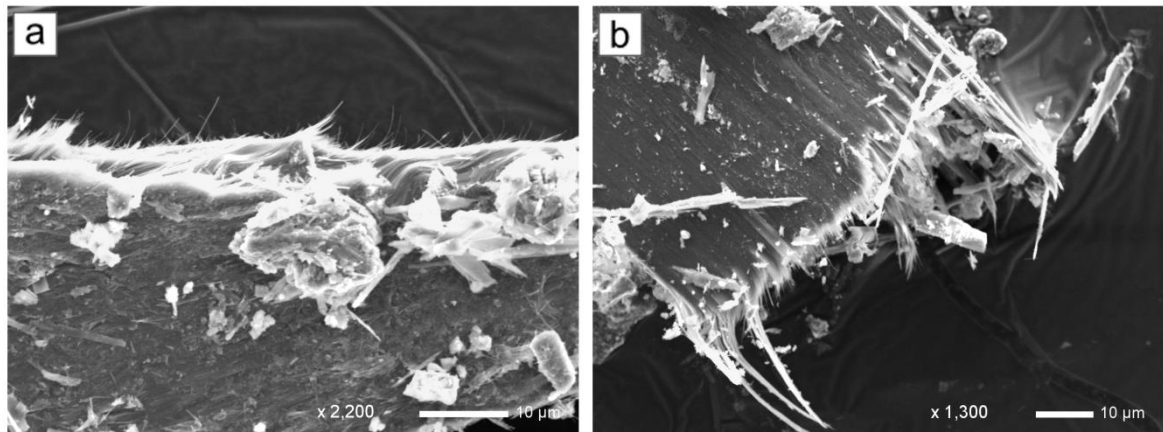
Figure III.29. SEM images of two samples of antigorite #1. Several breathable fibrous-lamellae occur at the surface. Samples 13 and 19.

lamellar shape morphology (Fig. III.30b). We can also state that most of samples identified as degree of alteration *#4* show a more pronounced flexible, curvilinear aspect. At this point, in order to evaluate the presence of any changes in crystalline structure of antigorite and tremolite by increasing alteration, the powder diffraction patterns were compared (Fig. III.31). In both antigorite and tremolite varieties, no changes are observed. XRPD patterns appear perfectly comparable, no differences occur in peak positions (no shift), or even in peak broadening. FWMH and peak area values were determined after deconvolution with a Gaussian curve approximation. Thus, XPRD analyses suggest that, at this scale of observation, weathering do not cause modification in the crystallographic structure of the asbestos varieties. Additionally, no neo-formed mineral phases associated to supergene alteration have been recorded.
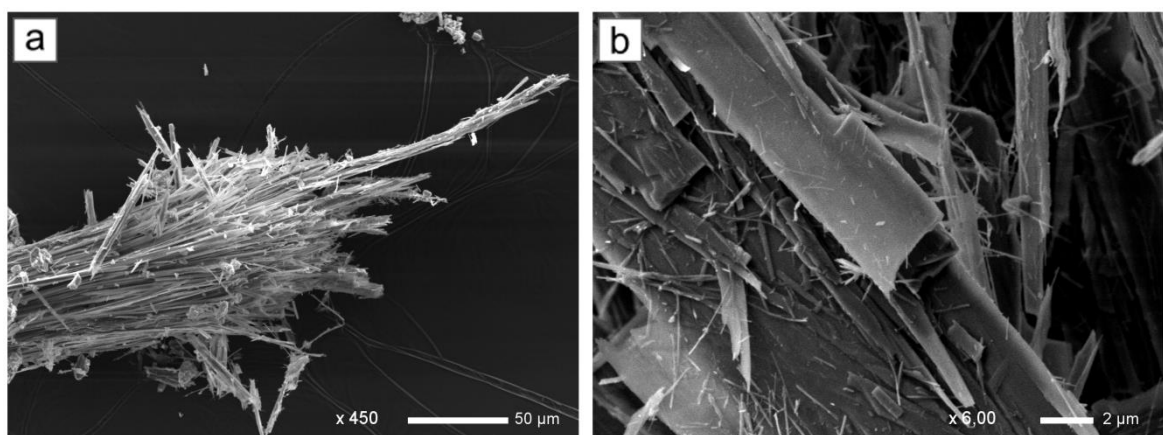
Figure III.30. SEM images of antigorite. a) bundles of fibrous lamellae with splaying ends (#1 - sample 13); b) lamellar-bladed elongated particles (#4 - sample 15).
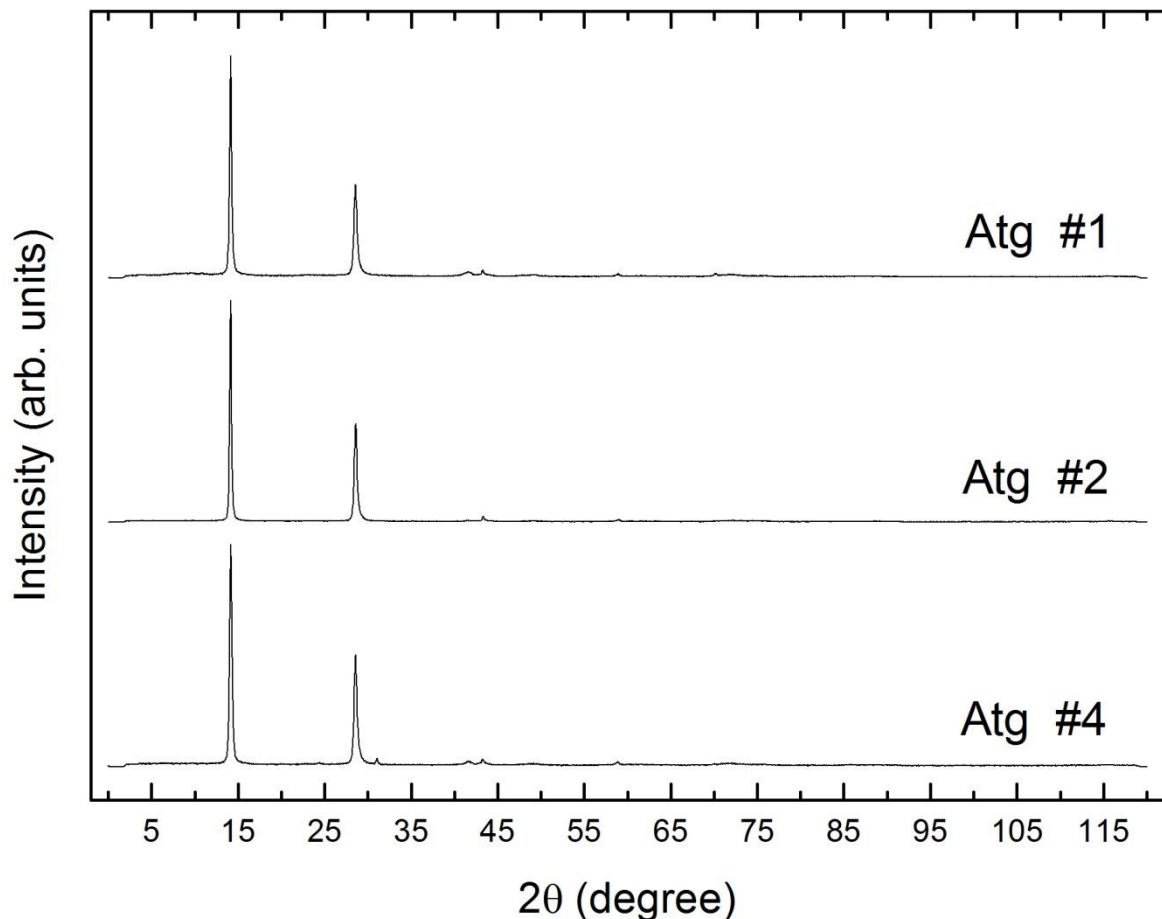
Figure III.31. Diffraction patterns (CoKα radiation) of antigorite samples acquired from increasing alteration. No changes are observed. Samples 19 (#1), 6 (#2), and 39 (#4).

A physico-mechanical stress is probably the main reason for alteration status associated to mineral fibres dissociation. Using the example of serpentine minerals, SEM images show that for both "pure" (e.g. only antigorite) and mixed (e.g. antigorite + chrysotile) samples, we can observe an increase of porosity as the degree of alteration increases. A gradual increase of distance between closely overlapped fibres and/or lamellae is observed (Fig. III.32). This is probably related to the circulation of water, flowing preferentially into cracks, fractures and weakness areas. In mixed samples, a higher density of fibres is observed when samples are altered. It indicates that the dissociation of fibres is more important, and it is related to the intergrowth of antigorite and chrysotile fibres that promote the water circulation. Thus, the penetration of fluids within fibrils is favoured and causes a stronger mechanical stress, until the completely loss of cohesion of the original structure (e.g. sample 40, in Annexe IC). Although the crystalline structure of fibres is not influenced by supergene alteration, there is a natural chemical exchange at the interface fibre/water, resulting in the release of elements. This lead to a modification of the surface chemical composition of fibres. Moreover, antigorite variety, where not in equilibrium conditions, exhibits a strong kinetic of
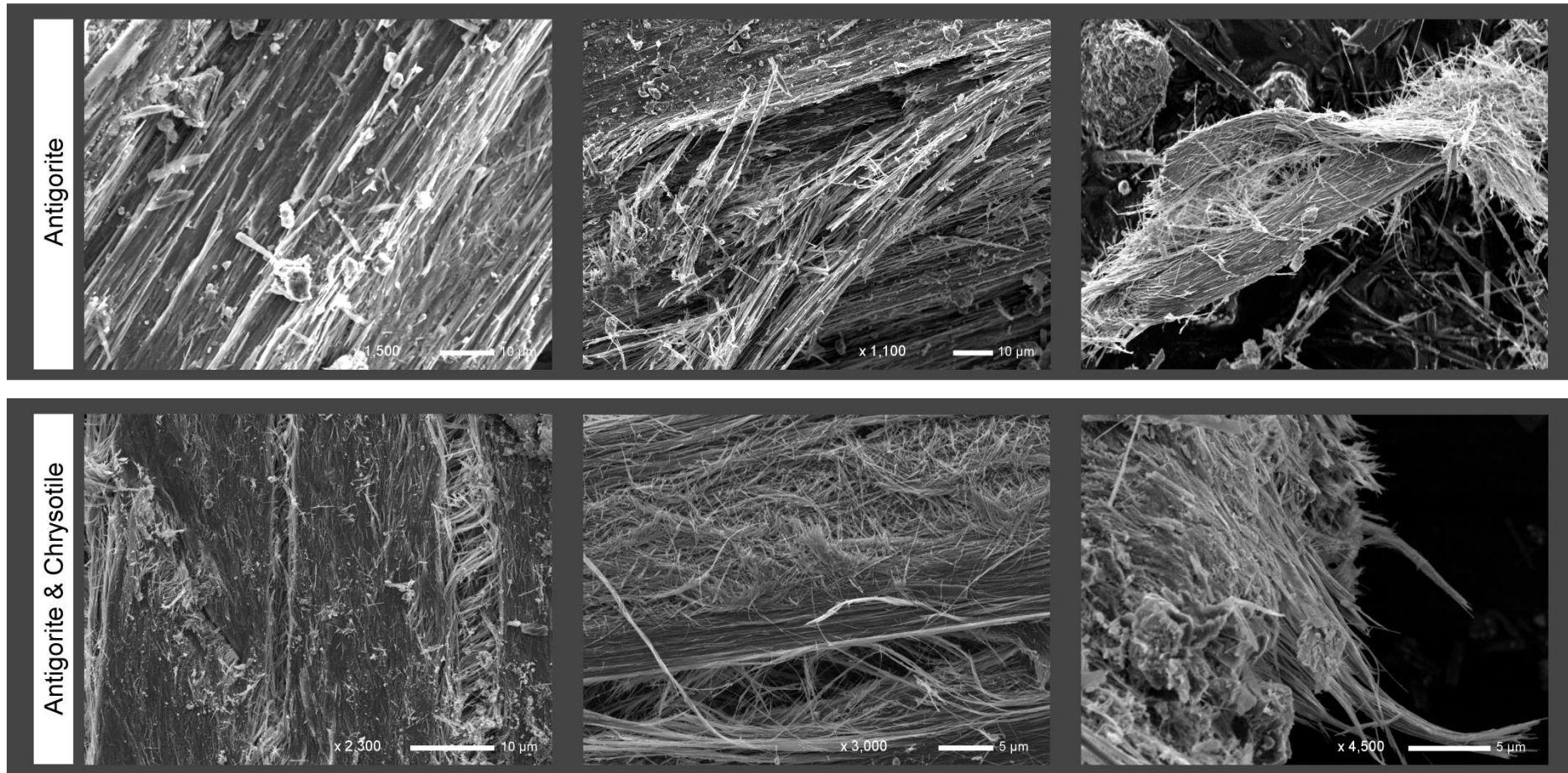
Figure III.32. Evaluation of the impact of alteration status on morphology of antigorite samples. A comparison between pure (only antigorite) and mixed antigorite-chrysotile samples was realised. Increasing the degree of alteration a gradual increase in porosity was observed.

dissolution relative to chrysotile (Lin and Clemency 1981). It is worth noting that the dissolution process is incongruent, because Mg from the octahedral sheets is generally released more rapidly than Si from the tetrahedral sheets (Lin and Clemency 1981). The amount of the mineral dissolved is also a function of the total surface area exposed to contact with the water. The more surface area is exposed, the more mineral dissolves in a given time. Dissolution kinetics have a more pronounced influence on antigorite than on chrysotile, allowing the mechanical modification of fibrous-lamellae, which fragmented and cleaves in progressively thinner fibres. This might explain the surface modifications observed for Caledonian samples.

III.4. A new specific texture: the case of sample 18

Easily recognisable for its peculiar morphological aspect, the sample 18 was collected at the Kouaoua mine site, on the road track. Identified by mining geologist as antigorite, degree of alteration *#2*, at hand-sample scale it exhibits an unusual lamellar aspect, consisting of overlapping of dried-like yellowish to pale-green lamellae (Fig. III.33, Annexe IA). The unusual aspect was confirmed by optical observations of petrographic thin section (PLM). It shows an uncommon texture, characterized by star and fan formed needle-like aggregates. Although it was immediately identified as a serpentine mineral, the cross-polarizing images do not show the typical blue-grey-to-dark interference colours of 1st order (Fig. III.10). Firstly, a rock fragment specimen was investigated with the portable Raman equipment. A Raman spectrum of an unusual antigorite was recorded (Fig. III.33). The appearance of the characteristic peak at about 1044 cm^{-1} suggests the presence of the antigorite phase. On the other hand, in the OH region, the typical doublet attributed to antigorite present in fact a little shift in peaks position (Fig. III.33), suggesting the presence of another mineral phase in addition to antigorite.

To confirm these preliminary results, some fibre bundles have been analysed with PLM/DS method, using RI 1.550 and 1.5680 oils. As clearly shown in figure III.34, fibres exhibit an intermediate behaviour. From a morphological point of view, they display a more rigid lamellar shape, characterized by the occasional presence of smaller thin fibres with splayed ends. Colours staining observations confirm the attribution to a serpentine mineral, but they are not sufficient to discriminate the variety. Fibres immersed in RI 1.550 oil show pale-blue with a soft orange halo in phase contrast mode and a violet to yellow colour in the dark field mode. Using the RI 1.5680 fibres show a whitish to pale-blue colour with a soft orange halo. In dark field observation they appear blue to blue indigo. Fibres show the staining colours of both antigorite and chrysotile varieties.
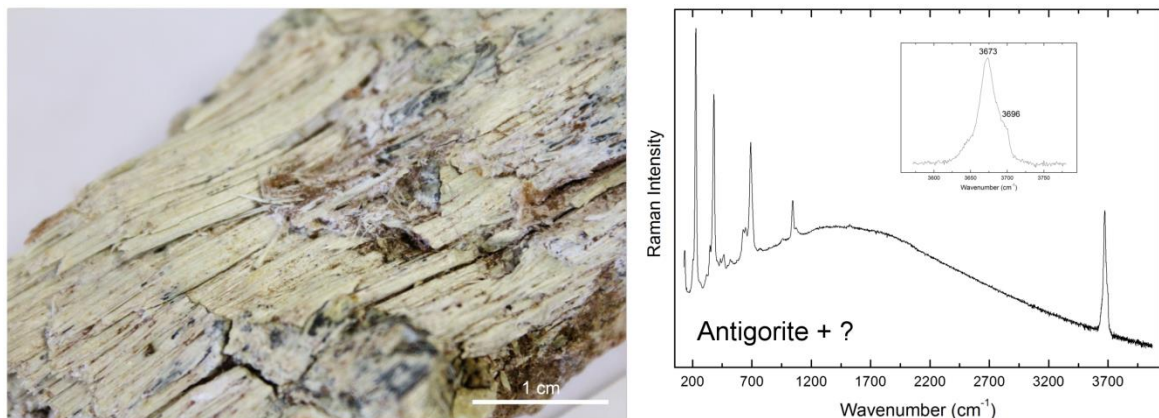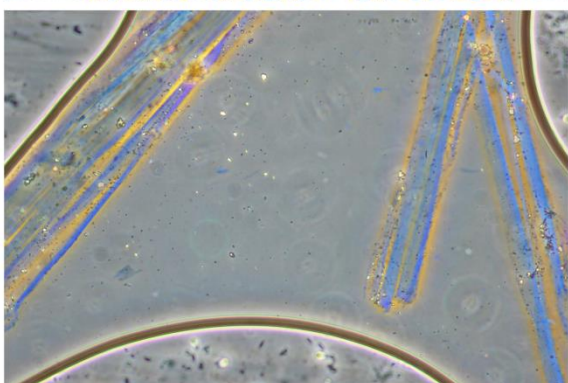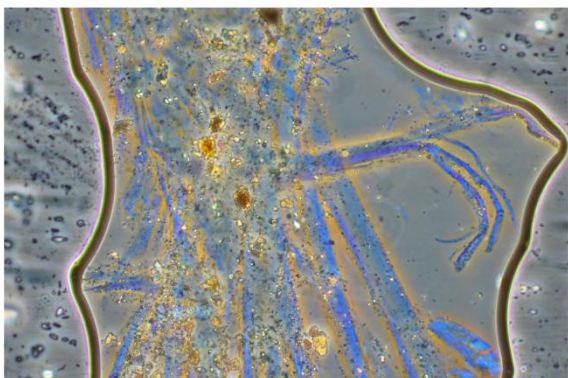

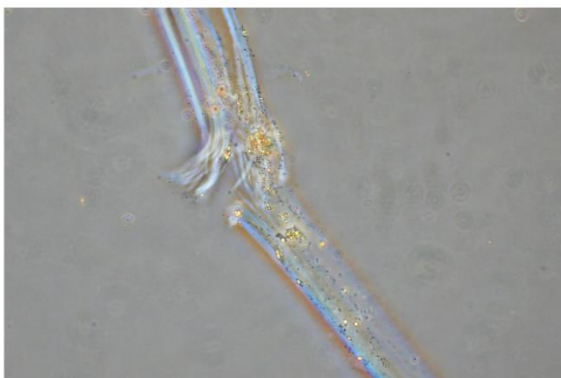*Figure III.33. Investigation of sample 18 by means of portable Raman equipment (532 nm laser).*

Figure III.34. PLM/DS-PC study of fibrous-lamellae of serpentine. left) RI 1.550 – pale-blue with orange halo ; right) RI 1.5680 – white to pale-blue with soft halo. Fibres exhibit the characteristic staining colours of both antigorite and chrysotile varieties.

If portable Raman and PLM/DS analysis suggest the presence of antigorite as the major component of sample 18, the XRPD pattern demonstrates the opposite. The typical diffraction pattern of a chrysotile specimen is shown in figure III.35. On the other hand, the presence of a slightly shift to lower *d*-spacing of the main basal reflections suggests the presence of another serpentine mineral, probably antigorite. This result is supported by the observation of a smaller FWHM value of the more intense peak at d-spacing 7.34, as previously discussed (Fig. III.19).

A systematic micro-Raman study was conducted on petrographic thin section, in order to evaluate the presence of differences in Raman spectra moving across the textural context. 59 spot analyses have been acquired, pointing the laser beam on various lamellar blades, acicular particles and into contact areas between them. No changes in peak position, peak broadening and relative intensity are observed in all 59 spectra, which appear perfectly comparable. The Raman spectrum in the low-wavenumber region (100-1200 cm^{-1}) shows the typical peaks of the antigorite serpentine (Fig. III.36), including the diagnostic peak at 1043 cm^{-1} (Rinaudo et al. 2003; Petriglieri et al. 2015). In the high-wavenumber region of the spectrum (3550-3850 cm^{-1}), it is not possible accurately attribute the OH stretching bands to the serpentine minerals. All OH stretching peaks generally attributed to lizardite, antigorite and chrysotile (Auzende et al.

2004; Petriglieri et al. 2015) co-exist together in a complex "doublet", as shown in figure III.35. We can therefore assume that at the scale of micro-Raman spectroscopy (spatial resolution 1-2 μm) the sample is homogenous! Micro-Raman spectra are not able to identify with certainty the complex nature of this sample. However, Raman spectra suggest the presence of antigorite as one of the main components constituting the specimen. A higher magnification approach is therefore necessary to discover the peculiar nature of this sample.

SEM images show a curvilinear flexible bundle of parallel fibrils, tightly welded together (Fig. III.37). The general appearance of these elongated particles is lamellar confirming what we observed with PLM/DS. Only in the fractures the real fibrous nature of this sample can be detected. TEM/SAED investigation has finally confirmed the double nature of this sample, which is constituted by the intimately intergrowth of fibrous antigorite and chrysotile fibres at the micro-scales, as illustrated in figure III.37.
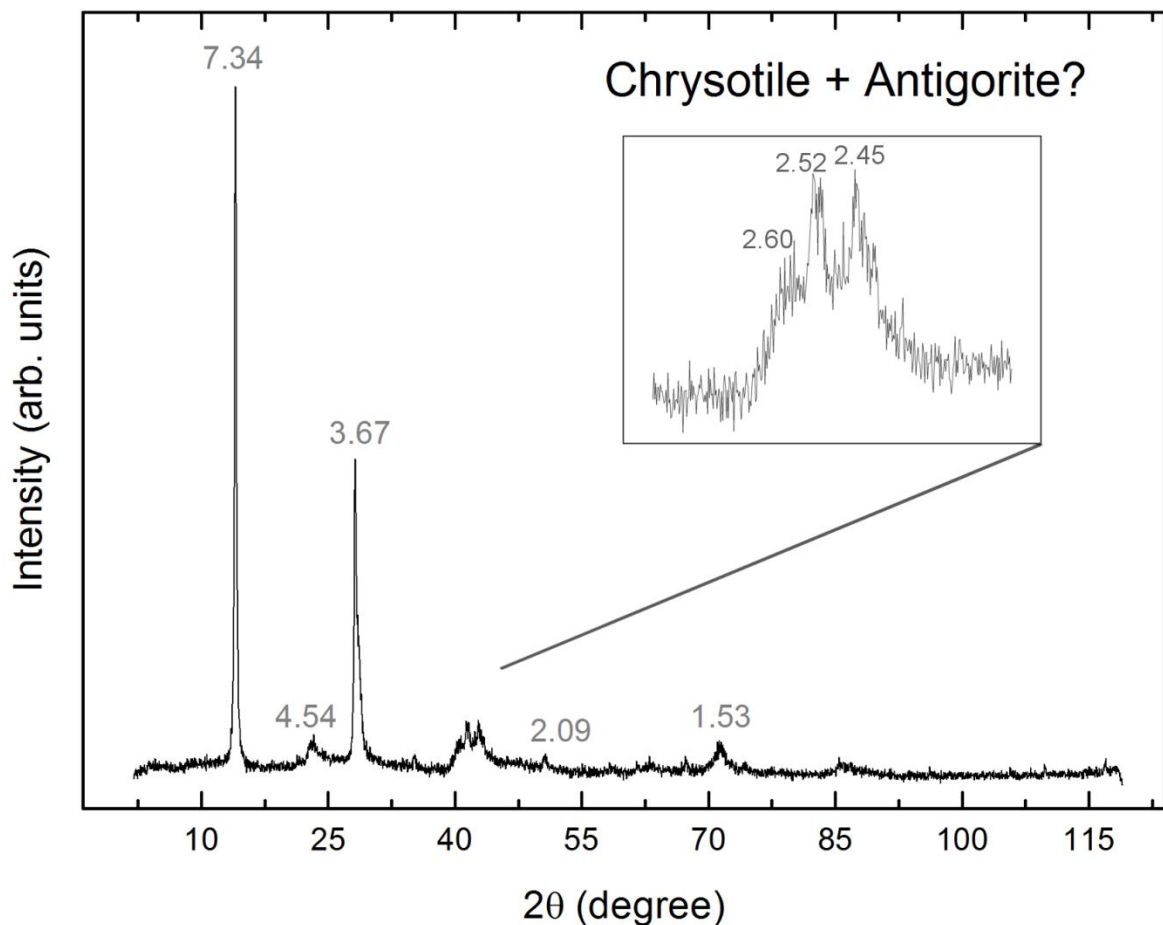

Figure III.35. XRPD pattern of chrysotile (CoKα radiation). A little shift in the position of the main peaks may suggests the presence of another serpentine variety.
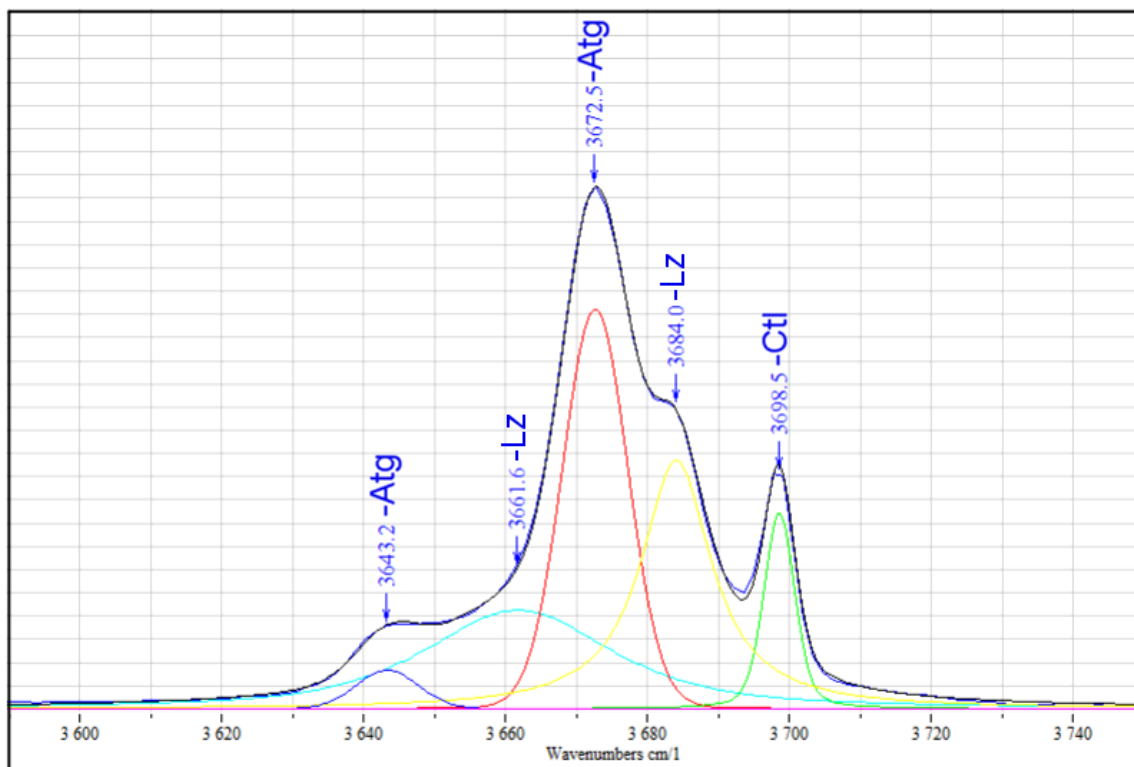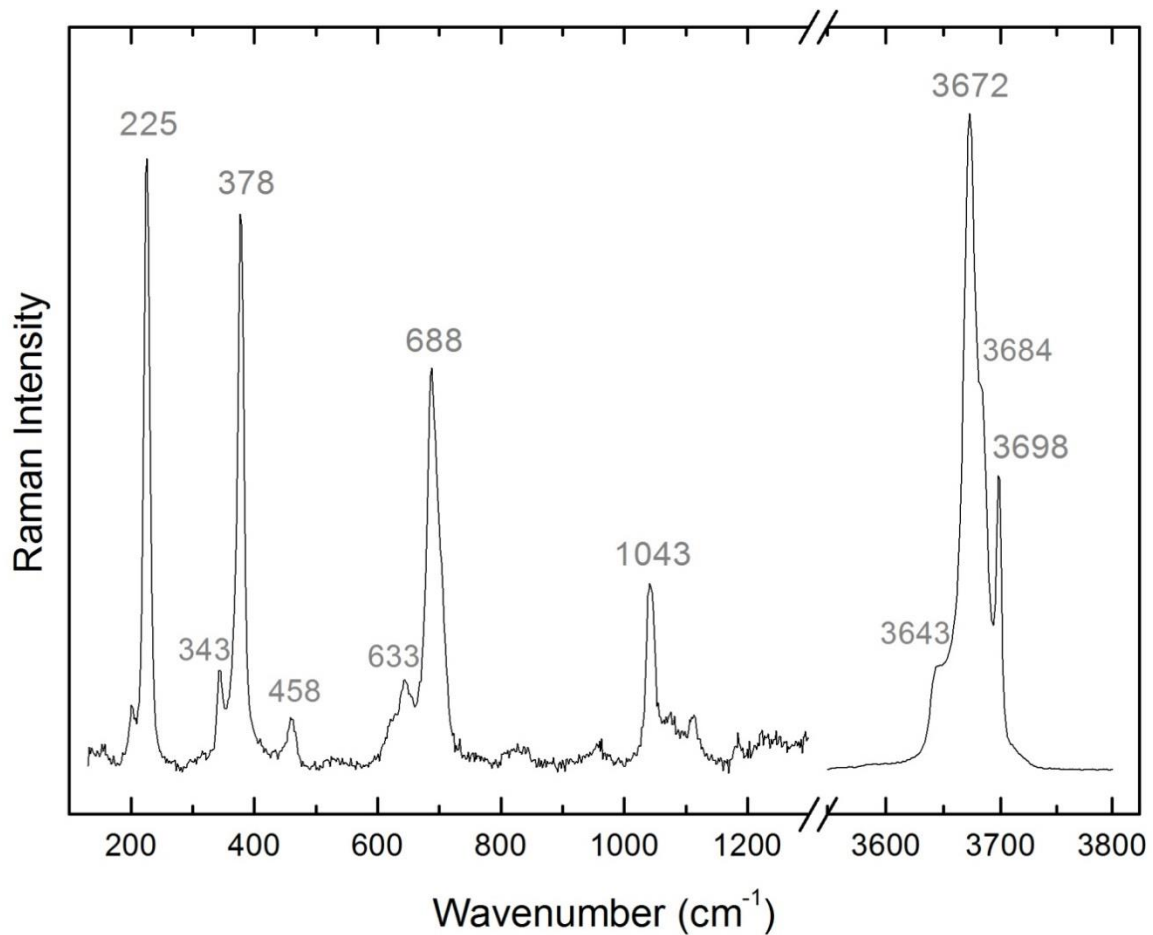
Figure III.36. micro-Raman investigation of sample 18 (473 nm laser). Up) Unidentified Raman spectrum of serpentine. The typical peak of antigorite at about 1043 cm⁻¹ occurs in low-wavenumber region; Down) Deconvolution of OH stretching band (high-wavenumber region). OH stretching peaks of lizardite (-Lz), antigorite (-Atg) and chrysotile (-Ctl) are observed.
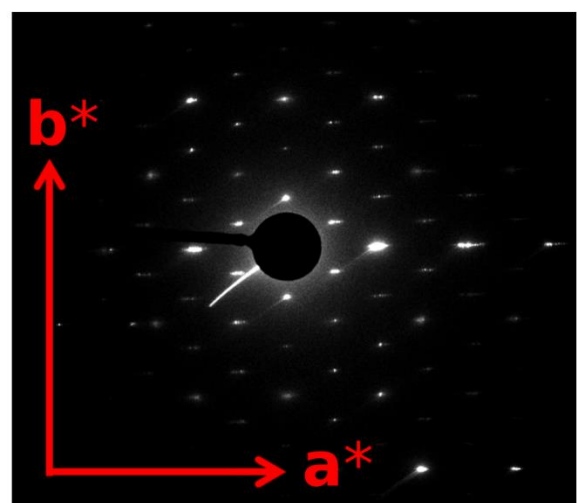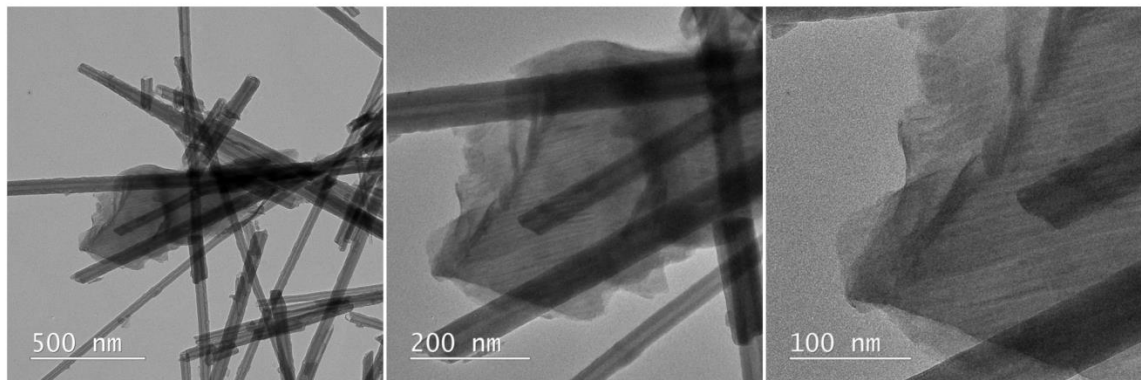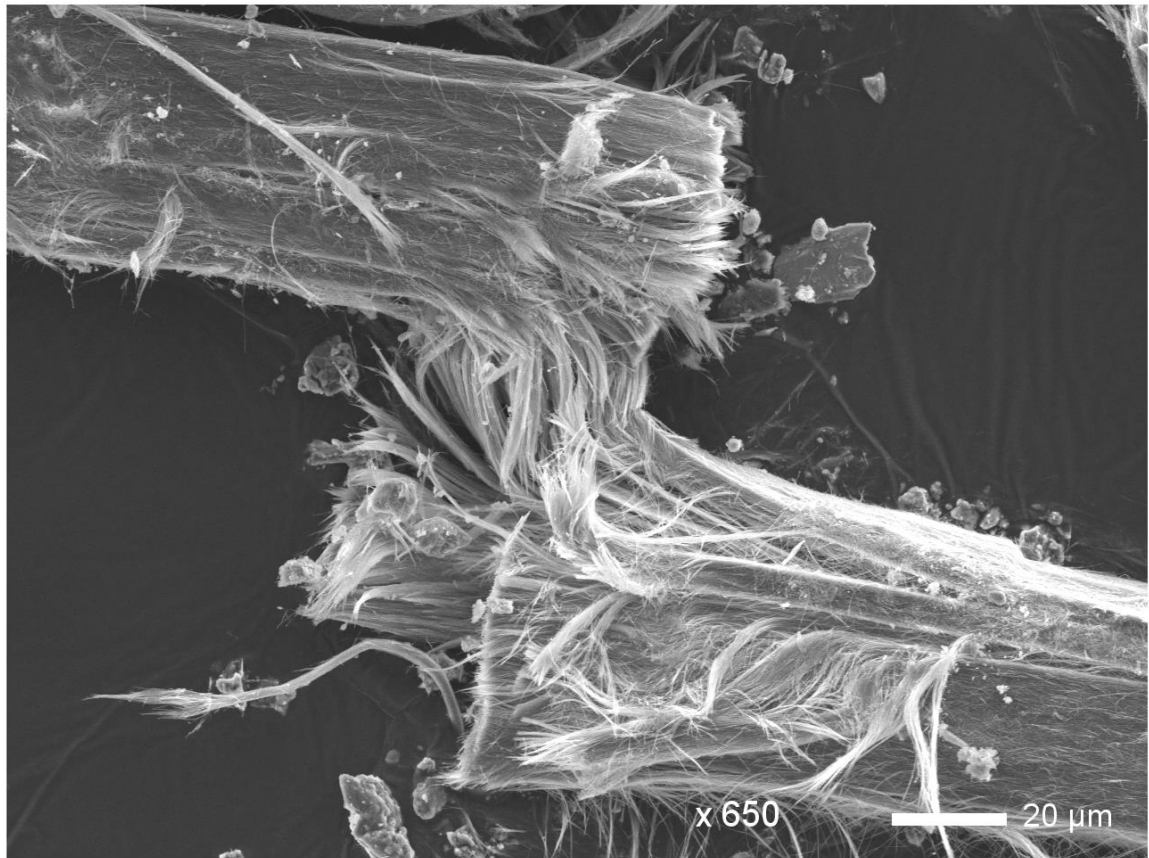
Figure III.37. Electron microscopy investigation of sample 18. TEM/SAED shows a mixed phase constituted by the intimately intergrowth of chrysotile fibres (left) and antigorite blades (right).

Chapter IV.

ALTERATION OF ASBESTOS, ELEMENT RELEASE AND FIBRE EMISSION.

IV.1. Leaching methodologies and samples selection

Because of humid tropical to sub-tropical conditions, chemical processes at the rock/fluid interface play an important role in the supergene alteration processes. The circulation of water is one of the main strong agent in chemical weathering. Surface water trickles down and penetrates rocks, permeating fractures and shear zones. In this context, the main chemical reactions involved at the interface mineral/water are dissolution, redox reactions, hydration, decarbonation, and the most common hydrolysis. Thus, the most soluble elements may be leached by water, leading to the dissociation of fibrous minerals and consequently favouring the emission of fibres. The variation of element solubility is strictly related to the type of element and silicate mineral involved in the mineral/water reactions. The study of major and trace element concentrations may therefor represent a tracer of the impact of weathering on altered rocks. This work aims to evaluate and compare the variation in chemical compositions of Caledonian fibrous minerals at increasing degree of alteration. Chemical signatures of chrysotile, (fibrous) antigorite and tremolite subjected to different degrees of alteration have been compared.

It should be remembered that supergene alteration is a multi-factors process. Laboratory experiments, aimed to simulate the weathering processes under a controlled environment, are recommended to evaluate the influence of physico-chemical parameters (e.g. pH, temperature, etc.) on chemical alteration of rock fragments. To mimic the chemical alteration of mineral fibres, two batch experiments have been launched over time. Primary mineral-fragments have been immersed in the extracting solution for a well-known time, and element concentrations are measured overtime in the supernatant. Afterwards, the supernatant was filtered to evaluate its fibre content.

A prior geochemical survey on serpentine and tremolite-amphibole of New Caledonia, focused to quantify the chemical exchange occurring at the interface minerals/water, was carried out by Bras (2013). Preliminary test bench experiments, able to reproduce the weathering alteration of asbestiform minerals, have been performed over time. The comparison of chemical concentrations of primary mineral-fragments and solid-residues could be a powerful diagnostic method for the investigation of chemical alteration processes. One of the goal of this work is to assess the capacity of fibre emission of mineral fibres after leaching experiments. Finally, the role of leaching processes in the physical-mechanical dissociation of rock fragments into fibres was evaluated.

IV.1.1. ANALYSIS OF MAJOR AND TRACE ELEMENT CONTENT

The content of major and trace elements has been measured in both rock samples and supernatant after batch leaching experiments. Chemical analyses were carried out at the AETE-ISO platform, OSU-OREME at the University of Montpellier (France).

Major element concentration (MgO, FeO_{tot}, Al_2O_3, Na_2O, CaO, P_2O_5, K_2O, and MnO, in wt.%) was investigated with a Thermo Scientific iCAP™ 7400 ICP-OES Analyzer coupled with a Katanax X-600 automatic fusion machine. Sample preparation of rock-fragments requires the acid dissolution of specimens previously crushed into powder. A protocol of successive attacks with $HClO_4$ and HF, followed by HNO_3, was performed to a mass of 100 mg of powdered sample. Several duplicates of random analysis have been realized. Furthermore, measurements of acid blank and international standards were carried out for the data correction and to evaluate the analytical error.

Concentrations in trace elements (Cr, Mn, Co, V, Sc, Cu, Ni, Li, As, Zn) were realized with a Agilent 7700x ICP-MS. SLRS-6, UBN and Ben international standards have also been analysed to ensure the accuracy of acquisitions.

IV.1.2. BATCH LEACHING EXPERIMENTS

Three samples of apparently not-altered antigorite (Sample 13), tremolite (Sample 41) and chrysotile (Sample 57) were selected for these experiments and fragments were cut. Primary mineral-fragments of about 10 g were visually selected in order to get, in so far as possible, homogeneous samples in term of mineralogy, weight, volume and morphology. The objective is to ensure that for each time of leaching, the departure conditions of experiment are similar. Since fragment shapes are not completely comparable, the area of each fragment was measured for further corrections. Fragments including veinlets were excluded.

Before leaching experiments, each fragment was rinsed with ultra-pure water to remove mobile fibres deposited onto the surface. Mineral fragments were then immersed into the extracting solution. The volume of the extracting solution was 50mL, with a liquid/solid ratio of 5:1 v/w. Leaching experiments consisting of several simply steps,

Figure IV.1.Batch leaching experiments: leaching on a shaking table, filtration, solution analysis and filter weighting.

such as leaching on a shaking table, filtration, analysis of solution and filter weighting, as clearly shown in figure IV.1, were carried out over time. Extraction times t were 2, 4, 8, 24, 96, 576 and 1440 hours.

Mineral fragments are thus softly shacked on a shaking table. A strong mechanical shaking was not recommended in order to avoid fibre release related to mechanical impacts. Two extracting solutions were used, a MES buffered solution (2-morpholin-4-ylethanesulfonic acid), 0.01 M, pH = 5.6, and a DTPA buffered solution (diethylenetriaminepentaacetic acid), 0.005M, pH = 7.3. As the pH of rain water ranges from 5.5 to 8.0, with the MES solution we wanted to simulate an acidic rain water, involving the best conditions to solubilize elements. No chelating properties have been included, since MES is a buffer known to have no chelating properties. On the contrary, DTPA is a strong chelating agent, with best chelating properties at slightly basic pH. For this reason, DTPA was used to emphasize element solubilisation and then to emphasize fibre release, if fibre genesis and emission is related to element solubilisation. Batch leaching experiments have been conducted for each time. Each entire extracting solution was filtered with a Cellulose nitrate filter, Sartorius Stedim, pore size 0.45µm. The suspended particulate matter collected on the filter was rinsed, dried and weighed. Twelve chemical blanks have also been realized.

IV.2. Chemical composition of asbestiform minerals

Analysis of major and trace elements were realized with ICP-OES and ICP-MS spectrometry, in order to evaluate the chemical signature of serpentine and tremolite-amphibole samples subjected to supergene alteration (Annexe IV). Moreover, two batch-leaching experiments, aimed to simulate the weathering processes under a controlled environment, have been launched. The experiments will allow to evaluate the capability of the fibrous minerals to release or capture (absorption) heavy metals (e.g. Ni, Cr, Co). Finally, an assessment of the role of leaching processes in the physical-mechanical dissociation of rock fragments into fibres was carried out.

IV.2.1. ANTIGORITE AND ANTIGORITE SERPENTINITES

As mentioned above, over all Caledonian samples identified by mining geologist as antigorite, only 10 display a "pure" - less contaminated - antigorite analytical mineralogy. Actually, the other serpentine-antigorite specimens consist of a strictly intergrowth of fibrous-lamellar antigorite and chrysotile bundles, with sometimes secondary minerals such as magnetite or quartz (Chapter III – Annexe II). It should be remembered that our analytical mineralogical approach was only qualitative, not allowing the quantification of the mineral proportions.

All rock-fragments visually identified as antigorite show the expected high concentration in MgO (from 27,73 to 30,71 wt.%) and FeO_{tot} (from 1,7 to 15,6 wt.%) of iron-magnesium phyllosilicates. Among all the other major element concentrations, aluminium gives the highest values, between 0,03 to 0,5 Al_2O_3 wt.%. At last, Caledonian samples show MnO concentrations from 0,04 to 0,2 wt.%, and less than 0,07 and 0,03 wt.% of CaO and Na_2O, respectively. No correlation between concentration trends and the degree of alteration was observed in the analysis of major elements for all antigorites (pure and mixed with chrysotile). Furthermore, comparing the MgO and FeO_{tot} contents displayed by worldwide serpentine-antigorite (from 35 to 45, and 2 to 5 wt.% respectively; Deschamps et al. 2013; Critelli et al. 2015; Cannaò et al. 2016), the Caledonian samples show a systematically lower MgO and higher FeO_{tot} values, as reported in figure IV.2.

These features can be observed whatever the degree of alteration of our samples. In the other hand, our antigorite type serpentines show a wider range of concentrations of magnesium and iron oxides. Magnesium is known to be a solvable element during spring water circulation on serpentinite rocks. Thus, increasing the alteration of antigorite, an overall decrease of MgO concentration of serpentines should be expected. On the contrary, iron is poorly released by spring water due to its poor solubility.
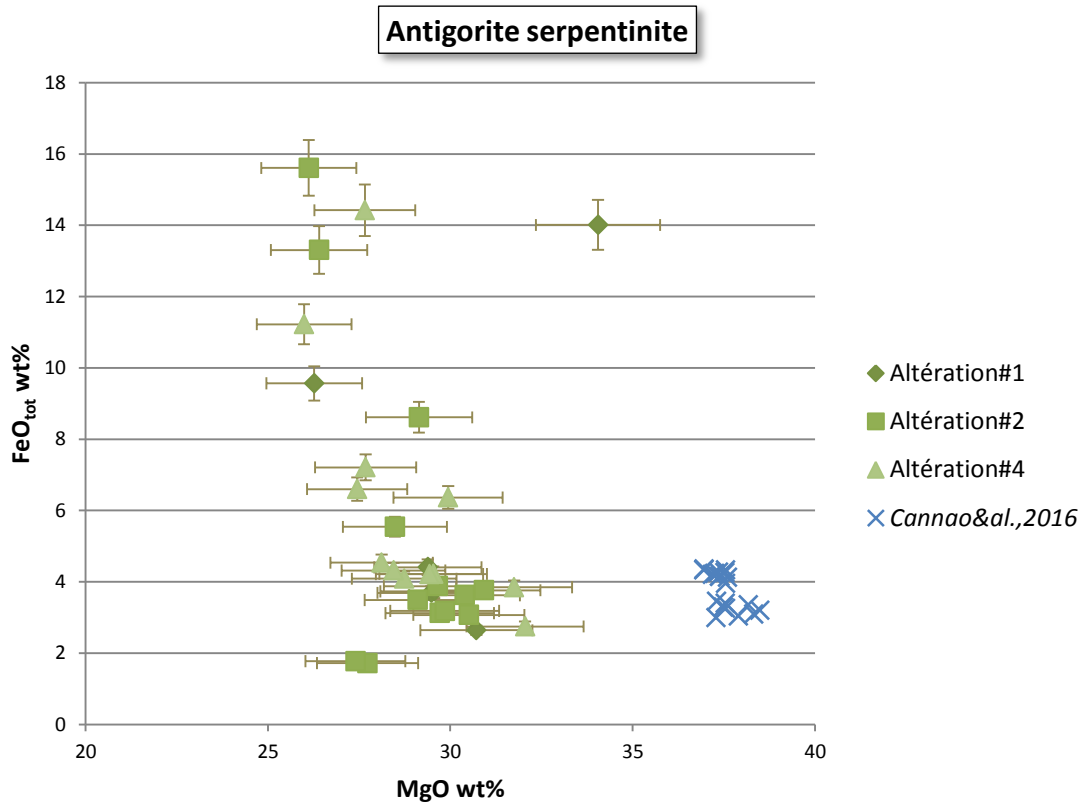
Figure IV.2. FeO$_{tot}$ wt.% versus MgO wt.% for all the samples identified by mining geologist as antigorite. Concentrations of antigorite of the Voltri Massif (Alps, Italy) are reported for comparison (Cannaò et al. 2016).

Critelli *et al.,* (2015) simulate the time evolution of soluble concentrations of Mg and Fe from serpentine under different conditions (Fig. IV.3). In tropical climate, recurrent weathering on serpentine assemblages should result in the increase of FeO$_{tot}$ content in the residual altered antigorite. Thus, the lower MgO and higher FeO$_{tot}$ concentrations of Caledonian pure and mixed antigorite samples, compared with the expected concentrations in no-altered worldwide antigorite, can result from supergene alteration under humid sub-tropical climate, as in the case of New Caledonia. It is worth nothing that even samples classified as no altered (minimum degree of alteration *#1*), consist of significantly altered serpentine, and no alteration-free fragments have been observed. These results are consistent with SEM observations, exhibiting the appearance of individual breathable thin fibres at the surface (Chapter III.3; Fig. III.29).

However, no evidence of correlation between the decrease of MgO and the increase of FeO$_{tot}$, increasing the alteration status, can be observed in figure IV.2. Even if chrysotile and antigorite belong to the same iron-magnesian phyllosilicate group, their mineralogy is distinct. For example, magnesium is not exactly located in the same crystallographic
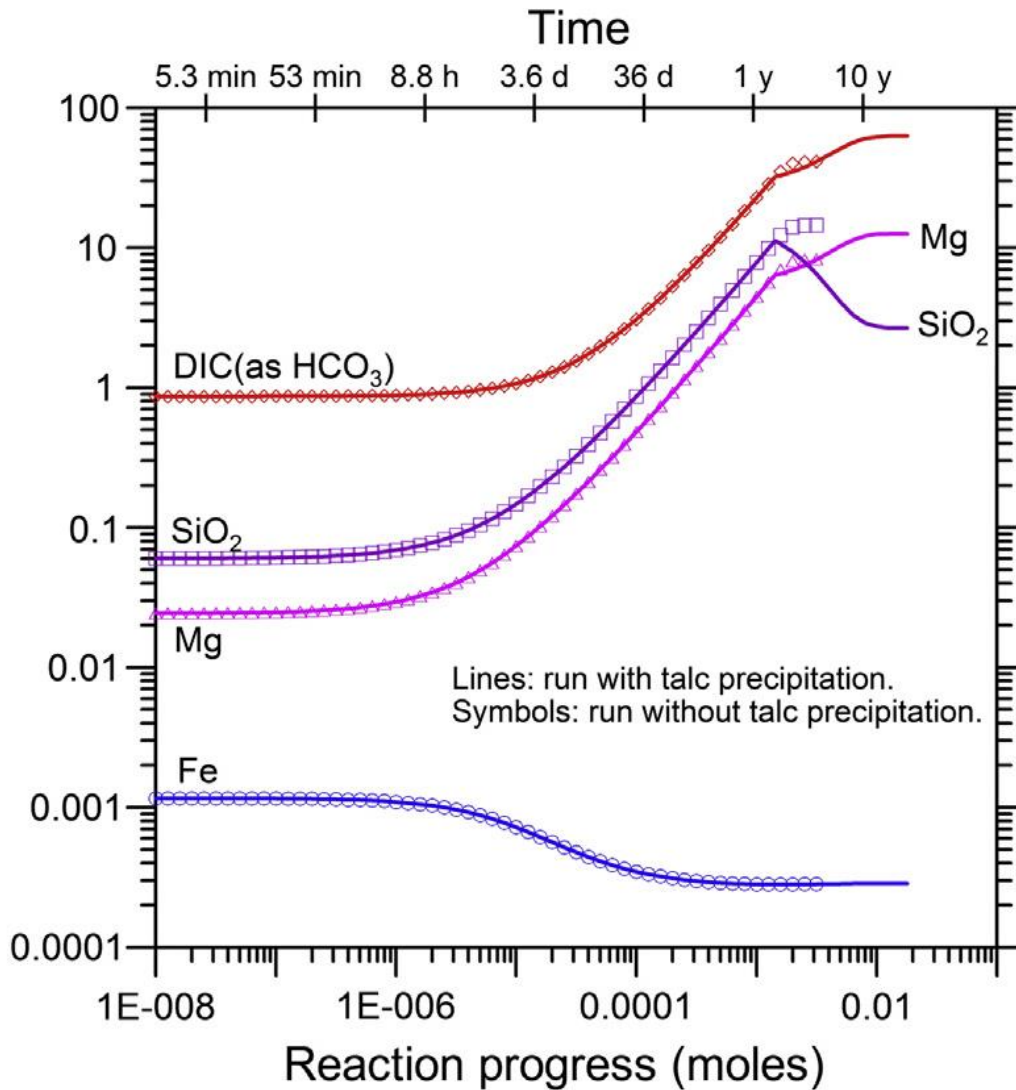
Figure IV.3. Results of two *simulation of serpentine dissolution at 25 °C performed using the EQ3/6 (version 8.0 software package), allowing the talc precipitation in one simulation and inhibiting talc precipitation in the other* (Critelli et al. 2015).

sites in the two serpentine varieties, and this can affect its solubility (Caillaud et al. 2009; Critelli et al. 2015; Peters et al. 2017). Most of the samples identified by mining geologist as antigorite are a mixing of both antigorite and chrysotile, probably in various proportions. This can explain the important variability of their MgO and FeO$_{tot}$ concentrations, together with the lack of correlation with the alteration status. Furthermore, considering only so-called "pure" - less contaminated - antigorite, the highest concentrations in FeO$_{tot}$ occur in the samples associated to the high degree of alteration (i.e. *#4*; Fig. IV.4). This result is crucial in the study of the asbestiform nature of Caledonian samples. The toxicology of asbestos is strictly related to fibres morphology, but also to iron release in lung tissue (Fubini and Fenoglio 2007). Therefore, the increase of iron content in antigorite, due to the increasing alteration, could also involve a
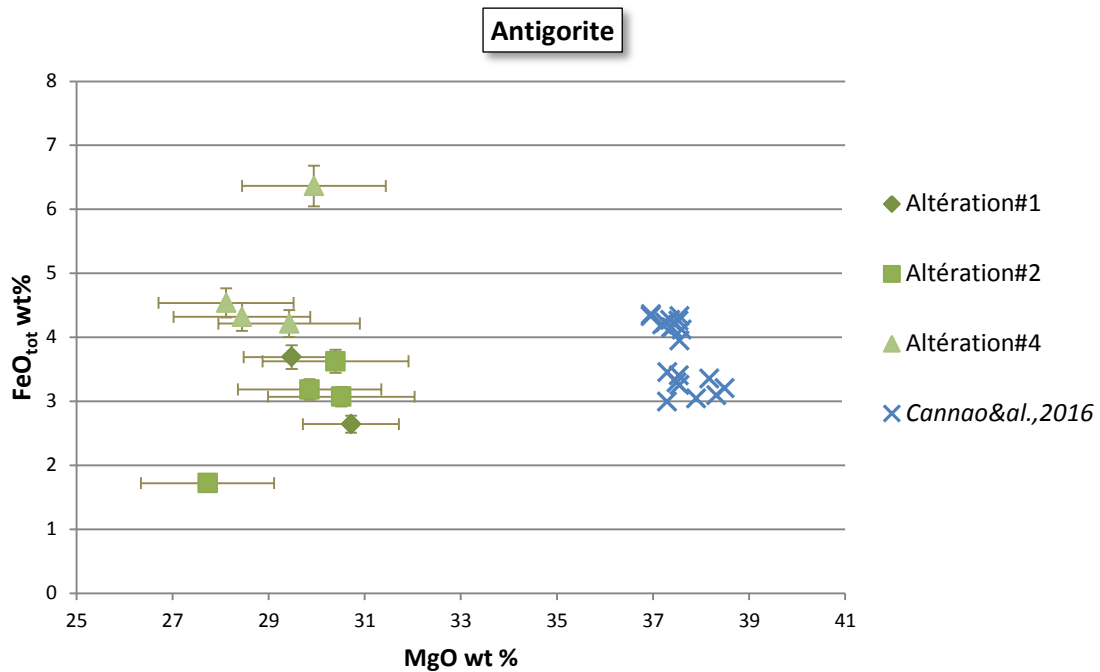
Figure IV.4. FeO$_{tot}$ wt.% versus MgO wt.% for all samples identified by analytical monitoring as antigorite. Elements concentration of antigorite of the Voltri Massif (Alps, Italy) are reported for comparison (Cannaò et al. 2016).

non-negligible toxicity. The correlation between decreasing MgO concentrations and increasing degree of alteration is not so clear, even if the most altered antigorite has particularly low MgO concentrations.

IV.2.2. CHRYSOTILE

Samples macroscopically identified by mining geologist as chrysotile show as vein and veinlets cross-cutting the peridotite assemblages, with a degree of alteration type *#3*. Moreover, results obtained with the implementation of analytical monitoring highlighted the real mineralogical nature of other two specimens - sample 23 and 33 (in Annexe I) - firstly identified as antigorite *#1*, and then reclassified as chrysotile (Chapter III.2, Annexe II). Unfortunately, sampling is not complete enough to allow a reliable discussion of the influence of supergene alteration on chemical compositions of chrysotile serpentine. Anyway, the chemical signature of these three chrysotile samples show a content in major elements similar to those of the antigorite ones (Fig. IV.5).

Moreover, samples 23 and 33 have low MgO (from 27 to 29 wt.%), and high FeO$_{tot}$ (from 2 to 7 wt.%) contents. These values are distinguished from chemical data previously obtained with X-Ray Fluorescence analysis by Ulrich *et al.*, (2012) on chrysotile veins from the serpentine sole.
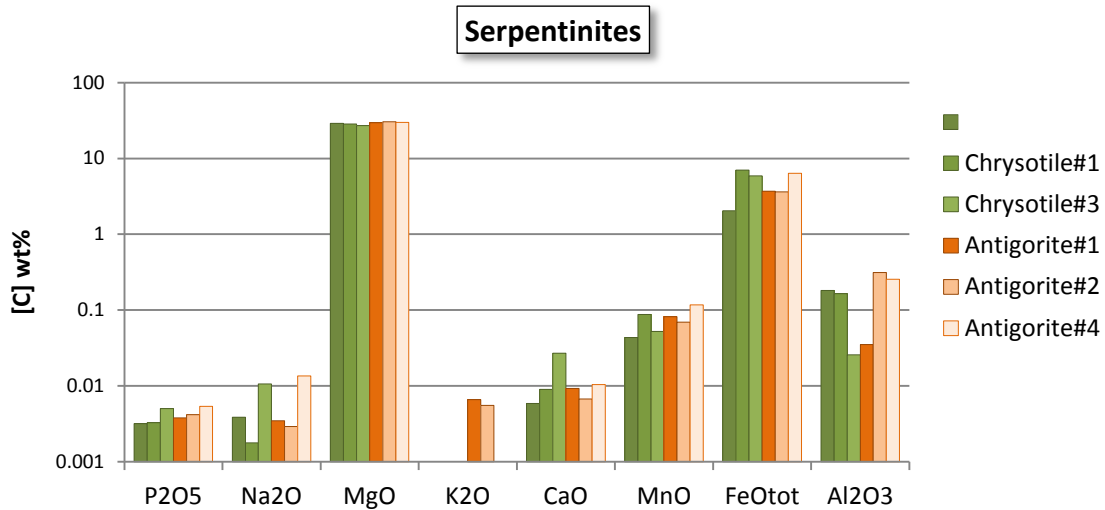
Figure IV.5. Major elements data for samples identified by analytical monitoring as chrysotile and antigorite.

IV.2.3. TREMOLITE

Ten samples identified by the geological sector of mining societies as tremolite have been analysed for major elements. Unfortunately, no one of these samples is formed only by tremolite. The mineralogical monitoring revealed the identification of a complex
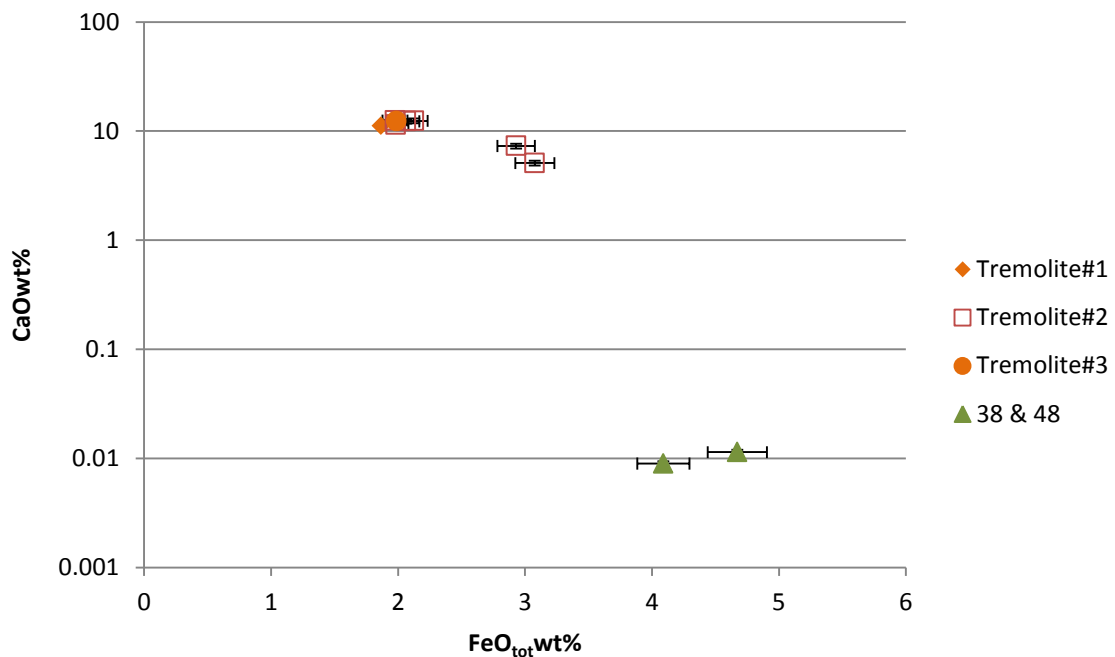

Figure IV.6. CaO wt.% versus FeO_{tot} wt.% for all the samples identified by mining geologists as tremolite. Sample 38 and 48 has been identified by analytical mineralogy as antigorite/chrysotile and antigorite, respectively.

mixture of tremolite and different serpentine phases, mainly antigorite and chrysotile. Moreover, only one sample for each degree of alteration *#1* (Sample 41) and *#4* (Sample 36) is available. Finally, on the basis of the analytical survey, two specimens (Samples 38 and 48) are not tremolite but a mixing of (fibrous) antigorite-chrysotile and antigorite, respectively. These conclusions are strengthened by their chemical compositions. They do not display the usual high CaO and Na_2O content expected for tremolite and observed for the other amphibole samples. On the contrary, samples 38 and 48 have a higher concentration of MgO and FeO_{tot}, comparable with serpentine minerals (Fig. IV.6).

About transition metals, all Caledonian samples display a high concentration in Cr, Mn, Co, V, Sc, Cu and Ni (Annexe IV), together with the Fluid-Mobile Elements (FME) Li and As. This feature is consistent with the contents generally found in published literature for the ultrabasic complexes (Deschamps et al. 2012, 2013). Moreover, also Zn is relatively concentrated in samples. Unfortunately, no variation of trace element concentrations can be clearly linked to the increasing alteration status.

IV.3. Batch alteration of asbestos

Batch leaching experiments on the less altered antigorite and tremolite samples (minimum degree of alteration) have allowed to handle and better understand some of the parameters which influenced the chemical alteration processes (pH, extraction time, ratio solid/liquid). The main objective is to evaluate the influence of extraction of chemical elements in the release of fibres into the environment.

IV.3.1. METAL CONCENTRATIONS IN THE SUPERNATANT

Mg, Ca, Fe, Mn, Ni, Co, and Cr concentrations increase with time in the surpernatant (Table IV.1). It means that these elements are solubilized from mineral fragments since specimens were rinsed before experiments. The comparison between experiments conducted with MES and experiments conducted with DTPA, shows that concentrations are higher when the leaching is realized with a chelating agent, as depicted in figure IV.7.

For antigorite, the ratio "element content extracted with DTPA to element content extracted with MES" ranges from 2 to 797. DTPA is therefore an efficient method to emphasize metal solubilization.

Metal concentrations in the solution increase with time until a maximum value and, then, they decrease (Fig. IV.7). For antigorite and tremolite samples, metal contents decrease after 576 hours in DTPA and for tremolite, after 24 hours, in MES. During leaching experiments, the pH increases in the solution (Fig. IV.8), even though the solution was buffered. The increase of pH could lead to metal precipitation if the solution is saturated.
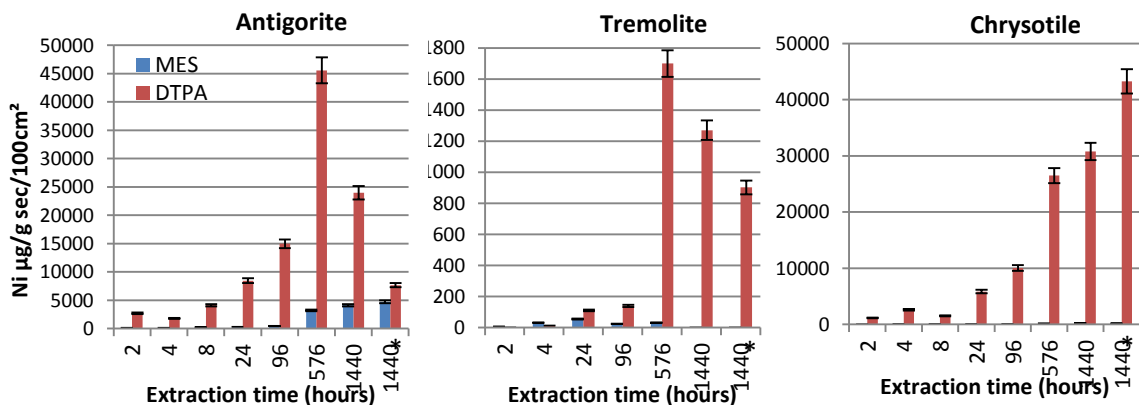

Figure IV.7. Ni concentration in the supernatant as a function of time for leaching experiments with two solutions MES and DTPA, and for antigorite (Sample 13), tremolite (Sample 41) and chrysotile (Sample 57).* for experiments conducted with several pieces of asbestos leading to possible mechanical alteration during shaking.

1	Time hours	Mg	Ca	Fe	Mn	Ni	Co	Cr
		(mg/g/100cm²)		(µg/g/100cm²)				
MES	2	0,013	n.d.	5	0,9	88	2	0,4
	4	0,014	n.d.	3	0,2	95	2	0,6
	8	0,025	n.d.	14	0,1	207	4	1,7
	24	0,030	n.d.	7	1,6	278	4	1,3
	96	0,042	n.d.	13	1,4	444	7	1,8
	576	0,000	n.d.	6	9,2	3203	42	12,4
	1440	0,002	n.d.	35	13,2	4111	47	15,9
	1440	0,001	4,0837E-05	0	10,2	4718	62	10,4
DTPA	2	0,001	9,5451E-05	105	128,3	2680	221	14,6
	4	0,105	0,03103833	73	86,9	1780	157	15,2
	8	0,210	0,02773067	178	196,8	4117	352	15,8
	24	0,323	0,02641428	1247	456,4	8429	739	33,4
	96	0,281	0,02552405	1200	2333,3	14965	5500	41,0
	576	0,455	0,0030524	4100	6933,3	45586	8473	91,7
	1440	0,281	0,00186812	2394	3641,7	23971	4190	43,8
	1440	0,085	0,00081221	881	903,5	7660	1093	17,0
41	hours	Mg	Ca	Fe	Mn	Ni	Co	Cr
MES	2	0,06	nd	0,0	0,0	5,9	0,0	0,2
	4	0,07	0,0065	0,0	0,0	32,0	0,0	2,0
	24	0,13	nd	3,9	0,0	55,9	0,0	3,2
	96	0,45	nd	0,0	5,6	24,1	0,2	1,9
	576	0,11	0,0030	0,0	0,4	31,7	0,0	2,5
	1440	0,13	0,0035	0,0	0,4	0,7	0,0	1,2
	1440	0,15	0,0032	0,0	0,0	1,2	0,0	2,0
DTPA	2	0,01	0,0003	26,8	3,6	1,6	0,1	0,7
	4	0,01	0,0023	20,8	2,7	13,3	0,7	0,5
	24	0,07	0,0051	179,6	39,5	110,9	5,4	3,9
	96	0,13	0,0018	393,6	53,4	140,3	4,8	6,9
	576	4,97	0,0745	15401,5	1939,8	1699,6	90,5	419,2
	1440	4,01	0,0881	8229,1	2306,0	1270,6	57,9	198,8
	1440	3,26	0,0557	10471,7	2082,2	902,2	53,8	237,7
57	hours	Mg	Ca	Fe	Mn	Ni	Co	Cr
MES	2	0,03	0,007	0,0	0,0	23,1	2,0	4,0
	4	0,11	0,020	0,0	0,0	71,3	4,4	28,5
	8	0,07	0,011	0,0	0,0	47,5	2,8	18,9
	24	0,07	0,000	0,8	0,5	94,8	5,0	21,7
	96	0,15	0,034	0,0	3,5	73,5	6,5	6,8
	576	0,28	0,033	0,0	1,3	171,5	12,2	116,0
	1440	0,35	0,043	3,5	2,5	206,4	15,3	43,4
	1440	0,29	0,026	0,0	0,0	159,1	9,0	137,8
DTPA	2	0,26	0,038	143,7	367,1	1168,8	213,7	29,6
	4	0,47	0,134	996,9	273,6	2622,7	608,4	47,3
	8	0,41	0,057	888,9	176,7	1542,7	404,9	130,8
	24	0,50	0,051	2164,5	393,0	5850,4	812,4	90,1
	96	0,87	0,134	4626,2	4730,5	10054,4	2689,7	179,3
	576	0,88	0,099	6387,3	11032,0	26498,2	8973,0	153,3
	1440	1,06	0,133	13010,6	3880,6	30815,1	4329,6	429,1
	1440	0,93	0,084	13500,8	12496,0	43274,7	13134,7	447,5

Table IV.1. Elements concentration of Mg, Ca, Fe, Mn, Ni, Co and Cr in the extraction solution, MES or DTPA for various extracting times. n.d. for not detected
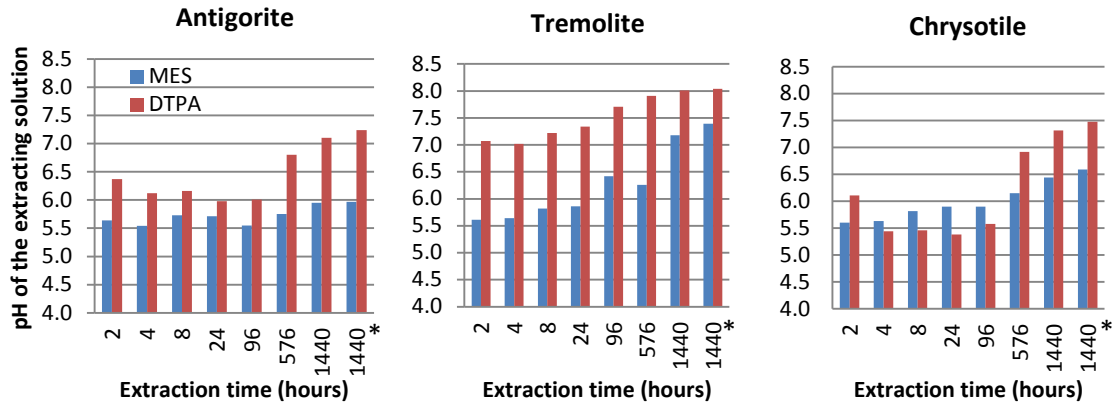
Figure IV.8 pH increase with time in the extracting solution for leaching experiments with two solutions, MES solution and DTPA solution, and for 3 samples: antigorite (Sample 13), tremolite (Sample 41) and chrysotile (Sample 57).* for experiments conducted with several pieces of asbestos leading to possible mechanical alteration during shaking.

The leaching experiments with MES, for antigorite and chrysotile, show an increase of Mg contents in the supernatant solution, with time (Fig. IV.9). These results are consistent with the decrease of MgO concentrations as a consequence of alteration increase, observed in natural samples of antigorite.

For the transition element, only Cr shows an increasing content with time in MES solution, in the serpentine samples (Fig. IV.10). The other transition elements such as Co, Mn, Ni are not solubilized. It is also the case for Fe. The solutions resulting from leaching experiments in MES and including tremolite samples have very low concentrations, even for the longest times.
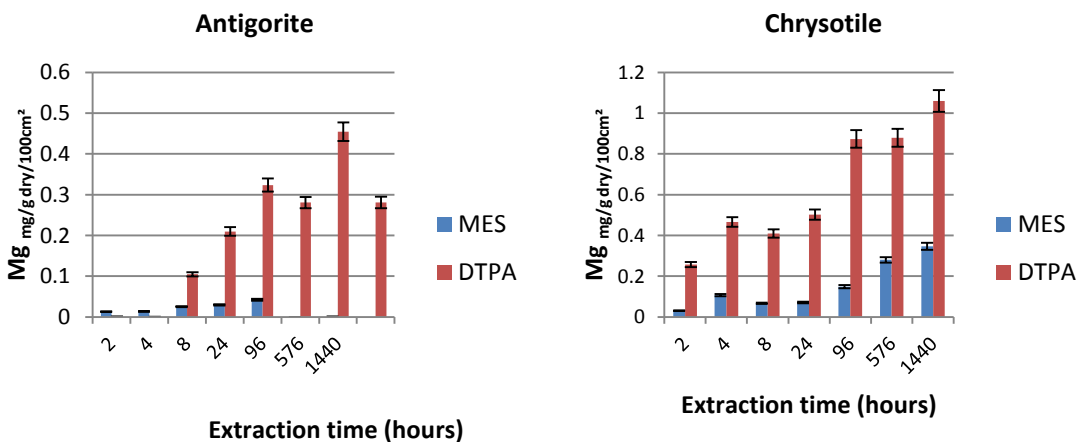

Figure IV.9. Mg concentration in the supernatant as a function of time for leaching experiments with two solutions MES and DTPA, and for antigorite (Sample 13) and chrysotile serpentinite (Sample 57).
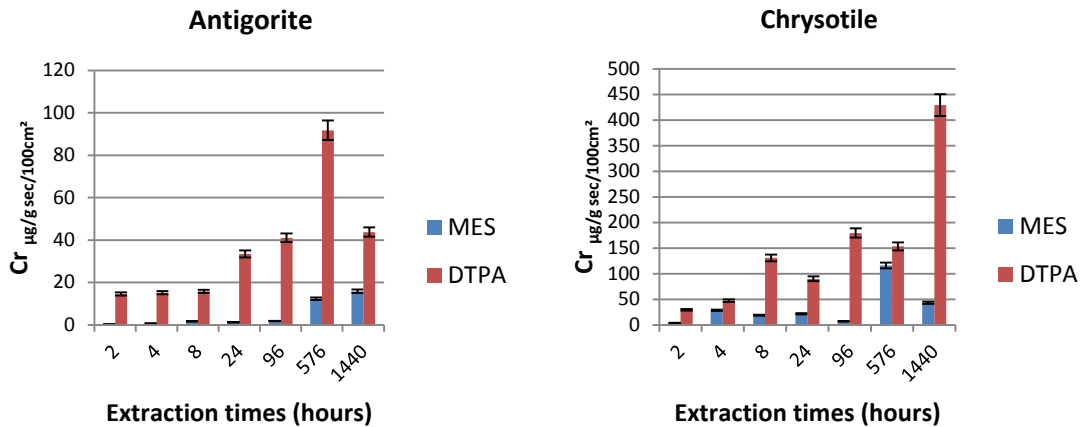
Figure IV.10 Cr concentration in the supernatant as a function of time for leaching experiments with two solutions MES and DTPA, and for antigorite (Sample 13) and chrysotile (Sample 57).

IV.3.2. SUSPENDED PARTICULATE MATTER COLLECTED ON THE FILTER

After filtration, the filter is dried before weighing. The weight of suspended particulate matter released during leaching experiment is then studied. Suspended particulate matter is a mixture of fibres and non-fibrous particles, but they are mainly in the form of fibres, as shown in figure IV.11. Even though a meticulous analysis of filters is required, we assumed that the suspended particulate matter content on the filter can give us a good estimation of the amount of fibres released during leaching experiments.

The amount of suspended particulate matter is different for the three samples with very small amount for tremolite (Fig. IV.12). Regarding the maximum of suspended particulate matter obtained with DTPA (0.0028 g, 0.0000242 g and 0.0056 g for respectively antigorite, tremolite and chrysotile), tremolite releases suspended particulate matter 120 time less than antigorite, and 230 less than chrysotile. About the maximum of
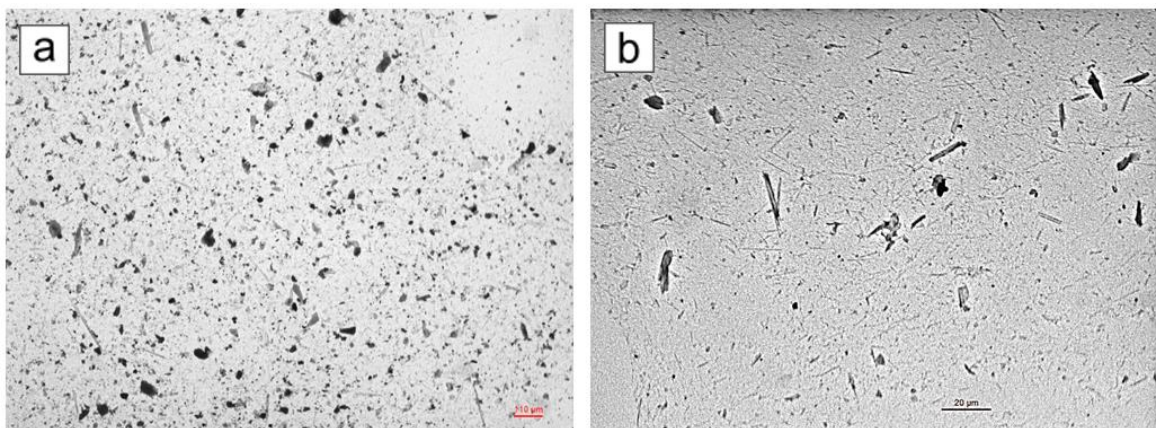

Figure IV.11. Pictures of two filters after leaching of a) antigorite-sample 13 (extraction in DTPA) and of b) tremolite-sample 41 (extraction in MES).
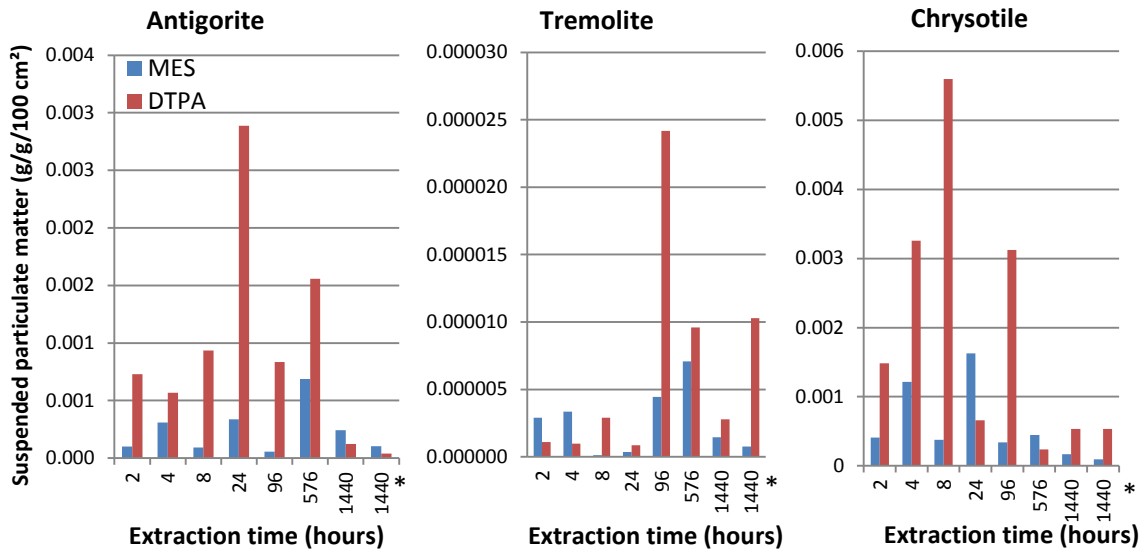
Figure IV.12. Suspended particulate matter increase with time for leaching experiments with two solutions, MES solution and DTPA solution and for 3 samples: antigorite (Sample 13), tremolite (Sample 41) and chrysotile (Sample 57).* for experiments conducted with several pieces of asbestos leading to possible mechanical alteration during shaking.

suspended particulate matter obtained with MES (0.000156 g, 0.0000 96 g and 0.0016 g for respectively antigorite, tremolite and chrysotile), tremolite releases suspended particulate matter 162 times less than antigorite, and 1666 times less than chrysotile. The low amount of suspended particulate matter for tremolite could result from its less porous properties.

The results demonstrate that the weight of suspended particulate matter increases with time (Fig. IV.12). Values increase until a maximum before decreasing. In DTPA, the maximum amount of suspended particulate matter is obtained at 24 hours for antigorite, at 96 hours for tremolite and at 8 hours for chrysotile. In MES, it is obtained at 576 hours for antigorite and tremolite samples, and at 24 hours for chrysotile. After the maximum value, the amount of suspended particulate matter collected on the filter decreases. This observation is surprising and probably related to the physico-chemical properties evolution of the extracting solution. For high extraction times, the decrease of element concentrations in solution is probably related to element precipitation in the solution due to their solubility controlled by pH (Fig. IV.8 and Fig.IV.11). It is then possible that small precipitates slip through the filter. More investigations are anyway needed to better understand the low content of suspended particulate matter collected on the filter for high extraction times. In order to avoid the solution saturation and to better control the pH of the solution, extractions should be performed with higher volumes (i.e. a liquid/solid ratio equal or below 1/10 instead of 1/5).

It is also important to underline that the amount of suspended particulate matter is usually higher when the extracting solution is DTPA (Fig. IV.12). After 24 hours, the ratio of the amount of suspended matter collected after extraction with DTPA on the amount collected after extraction with MES is around 9 for antigorite, around 5 for tremolite after 96 hours, and around 15 for chrysotile after 8 hours. It is then obvious that the amount of suspended particulate matter collected after extraction of elements with DTPA is much more important than in MES. Fibres emission is then undoubtedly due to the element solubilizations.

ENVIRONMENTAL RISK OF FIBROUS MINERALS IN NEW CALEDONIA:

A MONITORING STRATEGY.

V.1. In situ identification of mineral fibres with portable Raman equipment

Two field trips at the open mines of Balangero (Italy) and Tontouta (New Caledonia) have been organized to test portable Raman equipment on field, directly at the mining front, under normal environmental conditions (sun, strong wind, high temperature, etc.), in both temperate and sub-tropical climates.

The first test was performed at Balangero, in Northern Italy (Fig. V.1). Balangero is a village located in the province of Turin which hosts one of the ancient largest and most productive asbestos mine in Italy (1918-1979). During the 1960s, chrysotile production was between 100000 and 150000 metric tons per year. In the 1980s chrysotile production declined until the mine closed in February of 1990 (Ross and Nolan 2003). The Balangero serpentinite body (about 7 km^2) formed from a spinel-plagioclase lherzolite and is interpreted as a satellite body of the Lanzo massif. The asbestos ore contains massive, schistose, and highly fractured serpentinite rocks. Long- and short-fibre chrysotile is present in the open mine but only the short-fibre chrysotile was of commercial use. The short-fibre asbestos occurs as a stockwork of slip-fibre veins >2 mm thick. Furthermore, there is an estimated 10 volume% of tremolite in the tailings (Ross and Nolan 2003). At present a great work of environmental rehabilitation and restoration (e.g. increasing of the stability of the slopes, re-vegetation of the area) is in progress.

On 37 spot analysis, 33 have provided a positive response to test, allowing the identification of the typical mineralogical association, consisting of antigorite, chrysotile, (fibrous) diopside, chlorite, lizardite and balangeroite.

Figure V.1. Portable Raman test at the ex-open mine of Balangero (Torino, Italy). All measurements were carried out in safety conditions (PPE).

Figure V.2. Portable Raman test at the open mine of Tontouta (New Caledonia).

Raman portable device was successfully tested at the open pit of Tontouta, in New Caledonia (Fig. V.2). To verify the user-friendliness of the device, this set of measurements was not carried out by specialized technicians, who are generally more familiar with this kind of devices. So, on 30 spot analyses, 20 were positively identified. Samples of antigorite, chrysotile and altered serpentine, probably saponite, were identified. An example of a raw Raman spectrum of antigorite, recorded with portable equipment, is illustrated in figure V.3. Peaks observed at both low- and high-wavenumber regions allow to identify the antigorite phase. A slightly fluorescence interference occur.
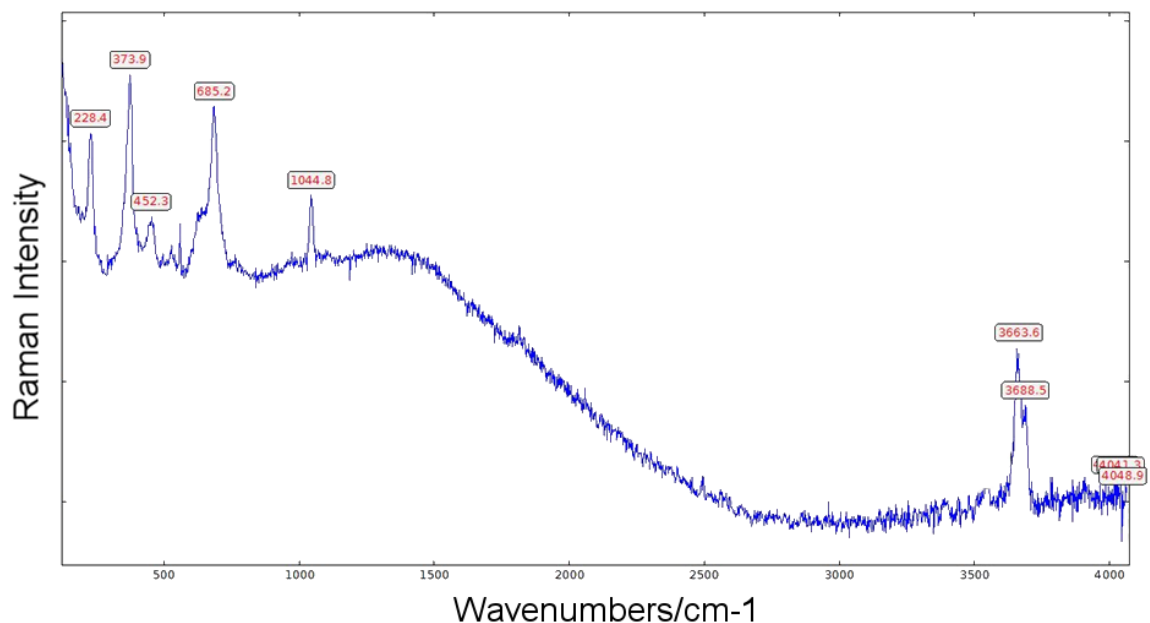
Figure V.3. Example of raw Raman spectrum obtained with portable device (532 nm laser). Raman spectrum of antigorite.

Overall 67 spot were analysed: 80% were successfully identified with the handheld Raman device. Portable Raman has proved to be a reliable user-friendly techniques in the identification of mineral fibres on mining front, under temperate and sub-tropical climate conditions. Moreover, only a little training formation is required to operators for its employment. On the other hand, the implementation of another complementary analytical methodology, as for example PLM/DS, could be the answer for the discrimination of not-identified spot samples (the remaining 20%).

V.2. Evaluation of the presence of fibrous minerals in the ore deposit soils

To better evaluate the real risk for mining workers due to exposition to mineral dusts, a preliminary study on the potential presence of free fibres in contaminated nickel ore deposit soils was carried out. Soils derived from rocks containing asbestiform minerals also contain fibres that may potentially become airborne (Nichols et al. 2002). On the other hand, the impact of chemical and physical weathering processes reduces the amount of asbestos in soils over time. We know very little about the rates of weathering and leaching of asbestos in soil environments, but the available information suggests that a substantial reduction in the amount of chrysotile may take hundreds or thousands of years, depending on the soil environment (Nichols et al. 2002). Acid leaching removes magnesium from chrysotile fibres relatively rapidly, leading to their disintegration. Chrysotile is in fact more soluble in the presence of H_2O and at low pH (Nichols et al. 2002). A longer time is expected for amphibole asbestos dissolution. Amphibole asbestos are typically more resistant to attack by acids, and are more frequently found in soils (Trescases 1997; Gunnar Hillerdal 2003). Likewise, soils can become enriched in amphiboles with time. Asbestos fibres, at least chrysotile fibres, are therefore expected to be less abundant in moderately acid soils with reddish hues (Nichols et al. 2002).

The investigation on the presence of mineral fibres in soils started after the identification of asbestos related pathologies in human populations not-occupationally exposed to asbestos. Contaminated soils may expose local populations, because they contain hazardous fibres easily dispersed in air because of the dry climate (e.g. alternation of hot and rainy/cool seasons). Soils containing less than 1 wt.% of asbestos fibres can release a large quantities of fibres into the air and may constitute an health risks (Gunter et al. 2007). The fibres contained in soils become airborne when the soils are disturbed either by natural processes (mainly wind) or by human activities (such as agriculture, planting trees, bushes, mining extraction) or a combination of the two. Similar situations have been observed in areas of Cyprus, Greece, Turkey, and also in New Caledonia where tremolite is present in the soils (Gunter et al. 2007; Lahondère 2007). In these particular cases the exposure was high because the local rocks were widely used as whitewash, stucco, or plaster for houses (Browne and Wagner 2001). Tremolite-asbestos fibres were also detected in the soils of an area in Basilicata (Southern Italy), and they derive from the natural weathering and erosion of serpentinite (Burragato et al. 2006).

There are only a few detailed studies on the chemical and mineralogical composition of soils containing asbestos fibres, the most of them concerning investigations of asbestos amphiboles (e.g. Thompson et al. 2011). Investigations on tremolite and actinolite amphibole asbestos in soils show that their habits are not substantially different from their counterparts in parental rocks. In fact, fibres eroded from the rocks, transported

and finally deposited in the soil, generally display little or no change in shape. On the contrary, they undergo a sharp reduction in size.

Individual asbestiform fibres, or small bundles of fibres, are typically not detectable in soil hand samples. For this reason, analytical laboratory analyses are necessary. However, the detection, identification and quantification of asbestos fibres in soils is very difficult and should be carried out by a qualified laboratory. Foresti *et al.,* (2003) describe an analytical method for the determination of low-levels (0.0-1 wt.%) of free fibres of chrysotile in contaminated clayey, sandy and sandy-organic soils. The chrysotile quantitative determination is performed combining Fourier-Transform Infrared Absorption spectroscopy and XPRD, using internal standard and Reference Intensity Ratio (RIR). This methodology may be applied to all type of soils.

In order to evaluate the presence and the nature of fibrous minerals in New Caledonian ore deposits, a preliminary characterization of "standard lateritic soil samples" was carried out. Two representative samples of soft red and yellow limonite were investigated by XRPD and SEM-EDS.
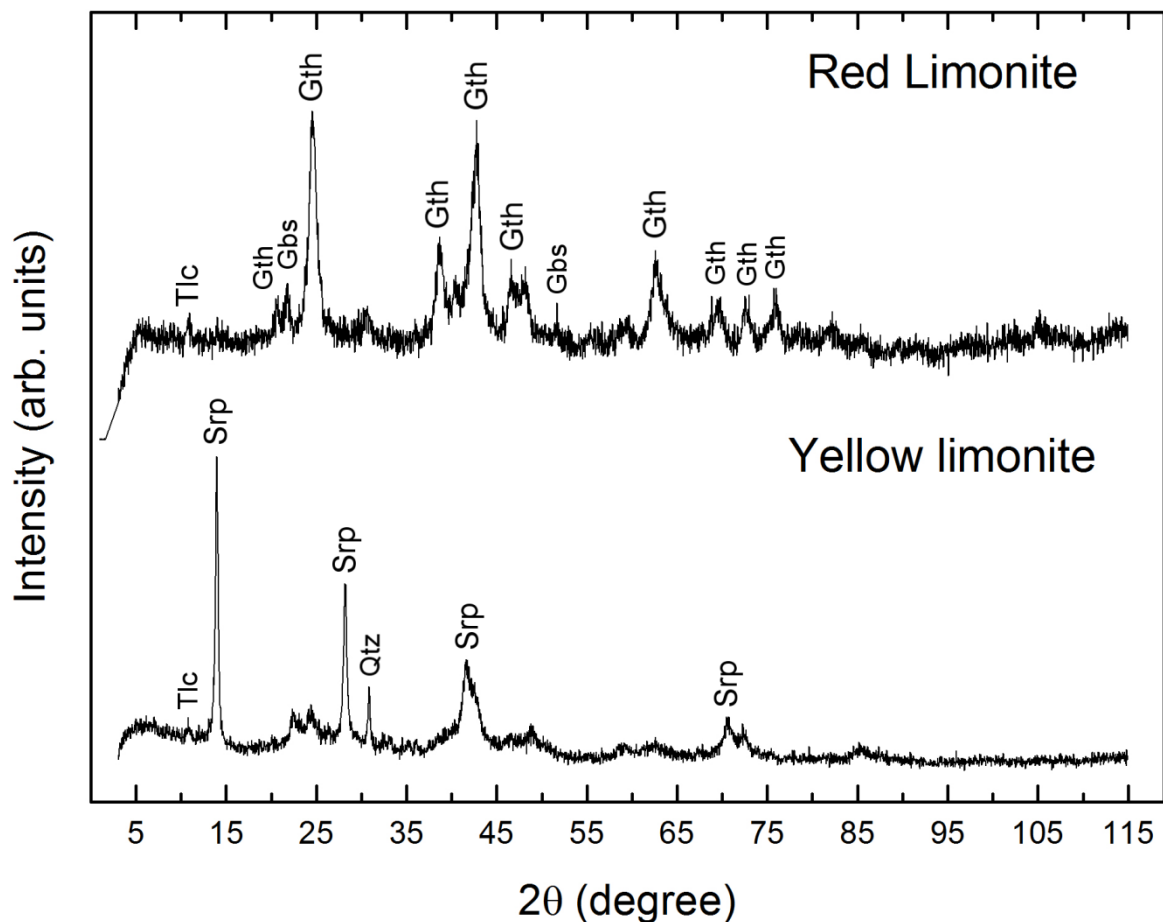

Figure V.4. XRPD patterns of "standard" soft red and yellow limonite ore deposit soils. Intensities are normalized with respect to the major reflection. Fluorescence effects occurs (CoKα radiation).
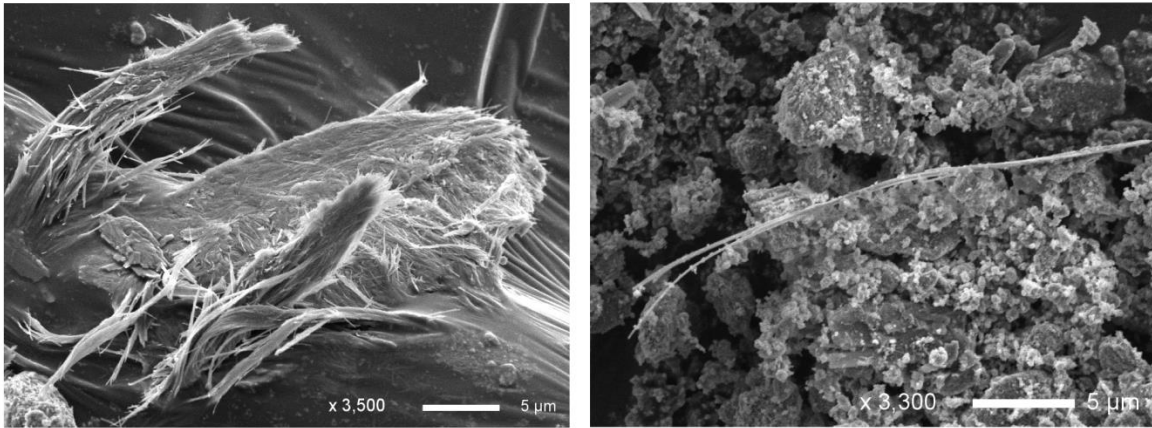
Figure V.5. SEM images of fibrous, potentially breathable, particles occurring in red limonite standard sample.

The red limonite sample shows a homogeneous mineral composition, consisting of Fe-oxyhydroxides, mainly goethite, with subordinated gibbsite and talc (Fig. V.4). On the contrary, SEM/EDS analyses have shown the presence of serpentine fibrous elongated particles, as reported in figure V.5. Moreover, yellow limonite sample shows a more complex mineral association dominated by serpentine, mainly antigorite, with subordinated quartz, talc and goethite (Fig. V.4). By contrast, no fibrous particles were observed with SEM investigation. Serpentine antigorite is in the form of well-formed lamellae.
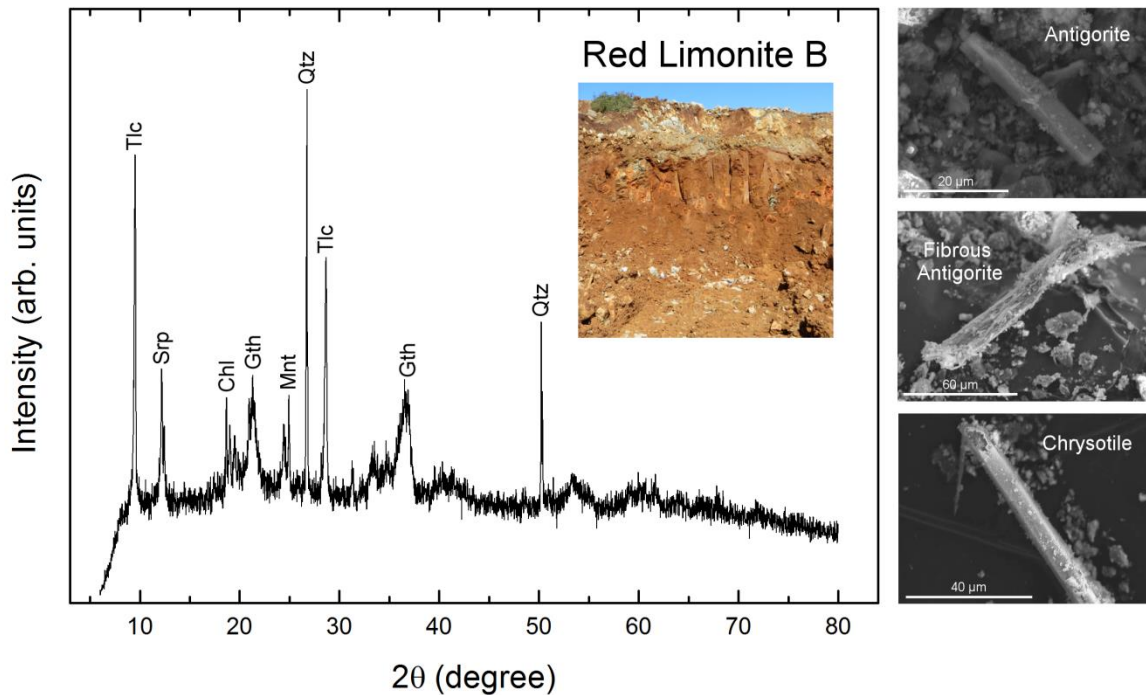
Figure V.6. XRPD and SEM investigation of red limonite soil. Serpentine varieties appear in the form of fibres. Fluorescence effects related to Fe-rich contents are observed in the XRPD pattern (CuKα radiation).
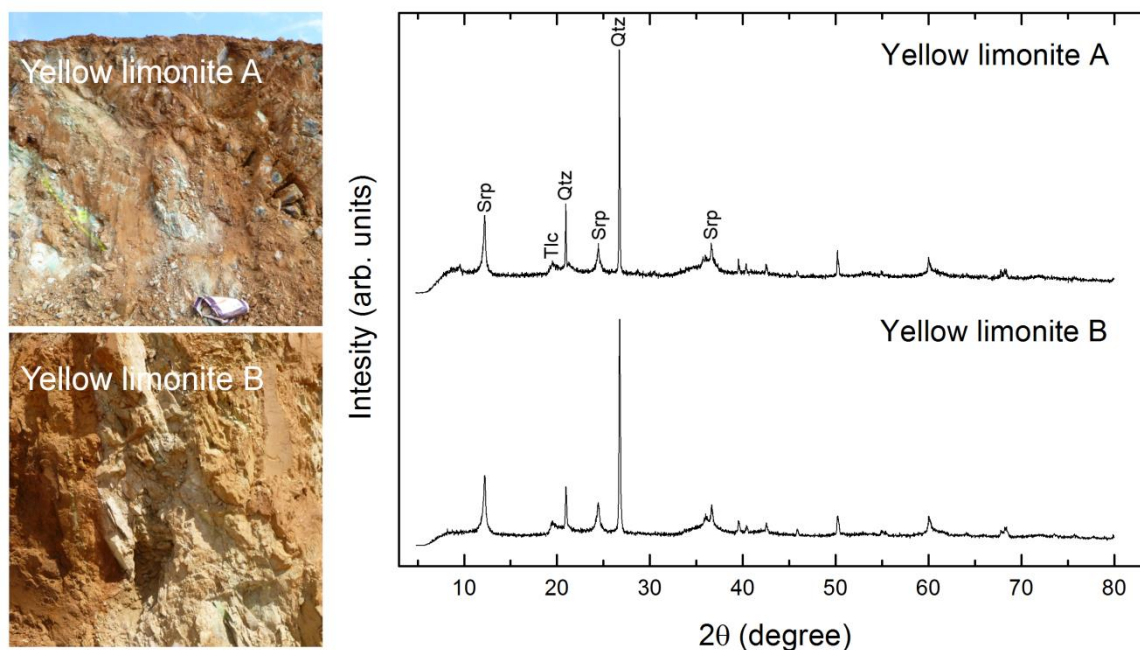
Figure V.7. XRPD investigation of soft yellow limonite soils. Intensities are normalized with respect to the major reflection. Fluorescence effects related to Fe-rich contents are observed in the XRPD pattern (CuKα radiation).

A further investigation was carried out on four more homogeneous soil samples, personally collected from a specific and well-characterized mining front. Compared to standard red limonite references, these samples shows a complex mineralogical association dominated by Fe-oxyhydroxides, mainly goethite, with subordinated gibbsite, or by a wide variety of Ni-rich hydrous Mg-silicate, such as serpentine, talc, chlorite and smectites, as shown in figure V.6. However, the yellow limonite portion displays a homogeneous mineral composition, consisting in quartz, talc and serpentine minerals (Fig. V.7). On four samples analysed, three of them contain antigorite and/or lizardite varieties. Only in one sample of red limonite, serpentine varieties appear in the form of fibres (Fig. V.6).

SEM-EDS analysis confirm the presence of the asbestiform varieties of the serpentine family into the ore deposit soils. Further analyses are required to better understand the real risk related to manipulation of these contaminated lateritic soils.

Conclusion

In the geological context of New Caledonia, in which weathering processes and supergene mineralizations are one of the main responsible for fibre release of asbestos minerals, the development of a user-friendly efficient analytical strategy, able to discriminate an asbestiform fibre from a not-harmful particle, is the first requisite. At present, there is not a technique capable to instantly characterize an asbestos fibre *in situ*, providing information about size and distribution, morphology, chemical composition and alteration grade. However, the acquisition of all these parameters is necessary for determining the real risk associated to fibres exposition. A multidisciplinary routinely approach, based on the use of complementary simply-to-use but reliable analytical methods is the only strategy possible. In addition, the instrumental apparatus has to be easily transportable on the field, directly on the mining site. The employment of specialized tools such as Polarized Light Microscopy associated to Dispersion Staining (PLM/DS) and portable Raman spectroscopy, in the more traditional laboratory strategy, for identification of environmental asbestos are proved extremely effective in the improvement of the performance and rapidity of data acquisition and interpretation. Both PLM/DS and handheld Raman devices confirmed to be discriminant in the detection and characterisation of asbestos fibres for both serpentine and amphibole. Furthermore, they provide extremely effective even in the presence of strongly fibrous and altered samples. PLM/DS observations have allowed to successfully identify all fibrous samples analysed, providing information about the mineralogical identification and the morphology of fibres and/or lamellae. Using the Refractive Index 1.5680 oil it is also possible to discriminate (fibrous) antigorite from chrysotile fibres (RI 1.550 oil). Repeating analysis on more particles, PLM/DS may be an efficient tool in characterisation of natural asbestos. Raman spectroscopy confirms to be a power diagnostic tool in the identification of the main varieties of the serpentine and amphibole families. Tests realized in mining context, at the open pits of Balangero (Italy) and Tontouta (New Caledonia), have confirmed its high diagnostic power. In order to guarantee the optimal employment of both these devices, a training formation of the operators is required. An analytical routinely protocol based on the use of complementary methods allows to ensure the successfully identification of samples observed. On the other hand XRPD cannot be involved in a routinely *in situ* monitoring systems. Despite the possibility to employ a benchtop XRPD instrument, the low sensitivity in the detection of the different varieties of serpentine and amphibole groups prevents the implementation of this methodology. Tests conducted on ore deposit soils confirm the impossibility to detect with certainty asbestiform phases by means of XRPD method.

It is worth noting that this simply monitoring strategy may be applied to all types of unconfined sites of asbestos exposition, including environmental and domestic expositions.

The plan prevention followed by the geological sector of mining companies is not adequate in the discrimination of asbestos fibres. The comparison of data obtained by analytical techniques with field identification confirms that the visual morphological criteria are not sufficient to discriminate asbestos fibres from not-asbestos. The great impact of supergene alteration in the formation of fibres is closely correlated to the large variability in textures and morphologies displayed by Caledonian samples. Geochemical analysis suggests that there is a correlation between the loss of elements after leaching processes and the formation, and consequent dispersion, of fibres. Chemical exchanges at the rock/water interface contribute at the dissociation process of fibres.

Analysis on major elements show a lower Mg-content in all Caledonian antigorite samples, compared to literature data. Moreover, increasing the degree of alteration, antigorite shows a progressively loss of Mg. We can therefore assume that, regardless of the alteration status, all antigorite samples exhibit an initial degree of alteration. No fresh samples have been observed. These results are consistent with the morphological observations: SEM images show the appearance of individual thin, potentially breathable, fibres at the surface of antigorite samples, macroscopically identified as not-altered (minimum degree of alteration). Moreover, increasing the degree of alteration fibrous-lamellar antigorite does not exhibit any modification in morphology. By contrast, they appear progressively more porous. The physical-mechanical effect of fluid circulation within fibres and lamellae, associated to chemical elemental exchange at rock/waters interface favoured the dissociation of fibres and their release into the environment. The same approach will be applied to the investigation of chrysotile and tremolite. For this purpose, a more complete sampling is necessary.

Finally, a textural-morphological survey of both the solid residue and the suspended particulates after leaching experiments, could allow to better understand the physical-mechanical and chemical effects of water circulation on fibres genesis and release. The kinetic of each processes can also be evaluated.

References

Aitchison, J.C., Clarke, G.L., Meffre, S., and Cluzel, D. (1995) Eocene arc-continent collision in New Caledonia and implications for regional Eocene arc-continent collision in New Caledonia and implications for regional southwest Pacific tectonic evolution. Geology, 23, 161–164.

Alleman, J.E., and Mossman, B.T. (1997) Asbestos Revisited. Scientific American, 277, 70–75.

Andreani, M., Baronnet, A., Boullier, A.M., and Gratier, J.P. (2004) A microstructural study of a "crack-seal" type serpentine vein using SEM and TEM techniques. European Journal of Mineralogy, 16, 585–595.

Andreani, M., Mével, C., Boullier, A.M., and Escartín, J. (2007) Dynamic control on serpentine crystallization in veins: constraints on hydration processes in oceanic peridotites. Geochemistry, Geophysics, Geosystems, 8, 1–57.

ANSES (2010) Affleurements naturels d'amiante. État des connaissances sur les expositions, les risques sanitaires et pratiques de gestion en France et à l'étranger., 1-248 p. Maisons-Alfort, France.

ANSES (2014) Évaluation de la toxicité de l'antigorite., 1-116 p. Maisons-Alfort, France.

Aruja, E. (1945) An X-ray study of the crystal structure of antigorite. Mineralogical Magazine, 27, 65–74.

Audet, M.-A. (2008) Le massif du Koniambo, Nouvelle-Calédonie Formation et obduction d'un complexe ophiolitique du type SSZ. Enrichissement en nickel, cobalt et scandium dans les profils résiduels. Universite de la Nouvelle Caledonie et Universite du Quebec a Montreal.

Auzende, A.L. (2003) Evolution des microstructures des serpentinites en contexte convergent: effet du degré de métamorphisme et de la déformation. Universite Blaise Pascal.

Auzende, A.L., Daniel, I., Reynard, B., Lemaire, C., and Guyot, F. (2004) High-pressure behaviour of serpentine minerals: A Raman spectroscopic study. Physics and Chemistry of Minerals, 31, 269–277.

Avias, J. (1967) Overthrust structure of the main ultrabasic New Caledonia massives. Tectonophysics, 4, 531–541.

Bailey, S.W. (1988a) Polytypism of 1:1 Layer Silicates. Reviews in Mineralogy and Geochemistry, 19, 9–27.

Bailey, S.W. (1988b) Structures and Compositions of other Trioctahedral 1:1 Phyllosilicates., 19, 169–188.

Balan, E., Saitta, A.M., Mauri, F., Lemaire, C., and Guyot, F. (2002) First-principles calculation of the infrared spectrum of lizardite. American Mineralogist, 87, 1286–1290.

Ballirano, P., Bloise, A., Gualtieri, A.F., Lezzerini, M., Pacella, A., Perchiazzi, N., Dogan, M., and Dogan, A.U. (2017) The crystal structure of mineral fibres. In A.F. Gualtieri, Ed., Mineral fibres: Crystal chemistry, chemical physical properties, biological interaction and toxicity Vol. 18, pp. 17–64. European Mineralogical Union and the Mineralogical Society of Great Britain & Ireland, UK.

Bard, D., Yarwood, J., and Tylee, B. (1997) Asbestos Fibre Identification by Raman Microspectroscopy. Journal of Raman Spectroscopy, 28, 803–809.

Bard, D., Tylee, B., Williams, K., and Yarwood, J. (2004) Use of a fibre-optic probe for the identification of asbestos fibres in bulk materials by Raman spectroscopy. Journal of Raman Spectroscopy, 35, 541–548.

Barnes, I., O'neil, J.R., and Trescases, J.-J. (1978) Present day serpentinization in New Caledonia, Oman and Yugoslavia. Geochimica et Cosmochimica Acta, 42, 144–145.

Barone, G., Bersani, D., Crupi, V., Longo, F., Longobardo, U., Lottici, P.P., Aliatis, I., Majolino, D., Mazzoleni, P., Raneri, S., and others (2014) A portable versus micro-Raman equipment comparison for gemmological purposes: The case of sapphires and their imitations. Journal of Raman Spectroscopy, 45, 1309–1317.

Barone, G., Bersani, D., Jehlička, J., Lottici, P.P., Mazzoleni, P., Raneri, S., Vandenabeele, P., Di Giacomo, C., and Larinà, G. (2015) Nondestructive investigation on the 17-18th centuries Sicilian jewelry collection at the Messina regional museum using mobile Raman equipment. Journal of Raman Spectroscopy, 46, 989–995.

Baronnet, A., and Belluso, E. (2002) Microstructures of the silicates: key information about mineral reactions and a link with the Earth and materials sciences. Mineralogical Magazine, 66, 709–732.

Baronnet, A., and Devouard, B. (1996) Topology and crystal growth of natural chrysotile and polygonal serpentine. Journal of Crystal Growth, 166, 952–960.

Baronnet (2005) Microstructures of common polygonal serpentines from axial HRTEM imaging, electron diffraction, and lattice-simulation data. Canadian Mineralogist, 43, 513–542.

Baronnet, A., Mellini, M., and Devouard, B. (1994) Sectors in polygonal serpentine. A model based on dislocations. Physical Chemistry Chemical Physics, 21, 330–343.

Baronnet, A., Andréani, M., Grauby, O., Devouard, B., Nitsche, S., and Chaudanson, D. (2007) Onion morphology and microstructure of polyhedral serpentine. American Mineralogist, 92, 687–690.

Bates, T.F. (1959) Morphology and crystal chemistry of 1: 1 layer lattice silicates. American Mineralogist, 44, 78–114.

Baumann, F., Rougier, Y., Ambrosi, J.P., and Robineau, B.P. (2007) Pleural mesothelioma in New Caledonia: An acute environmental concern. Cancer Detection and Prevention, 31, 70–76.

Baumann, F., Maurizot, P., Mangeas, M., Ambrosi, J.-P., Douwes, J., and Robineau, B.P. (2011) Pleural mesothelioma in New Caledonia: associations with environmental risk factors. Environmental health perspectives, 119, 695–700.

Belluso, E., Cavallo, A., and Halterman, D. (2017) Crystal habit of mineral fibres. In A.F. Gualtieri, Ed., Mineral fibres: Crystal chemistry, chemical physical properties, biological interaction and toxicity. Vol. 18, pp. 65–109. European Mineralogical Union and the Mineralogical Society of Great Britain & Ireland, UK.

Berger, V.I., Singer, D.A., Bliss, J.D., and Moring, B.C. (2011) Ni-Co laterite deposits of the world - Database and grade and tonnage models., 1-26 p. Reston, Virginia.

Berman, D.W., and Crump, K.S. (2003) Final draft: technical support document for a protocol to assess asbestosrelated risk. Prepared for office of solid waste and emergency response. Washington DC.

Berman, R.G. (1988) Internally-Consistent Thermodynamic Data for Minerals in the System Na2O-K2O-CaO-MgO-FeO-Fe2O3-Al2O3-SiO2-TiO2-H2O-CO2. Journal of Petrology, 29, 445–522.

Bernstein, D., Castranova, V., Donaldson, K., Fubini, B., Hadley, J., Hesterberg, T., Kane, A., Lai, D., McConnell, E.E., Muhle, H., and others (2005) Testing of fibrous particles: Short-term assays and strategies - Report of an ILSI Risk Science Institute Working Group. Inhalation Toxicology, 17, 497–537.

Bersani, D., Lottici, P.P., Vignali, F., and Zanichelli, G. (2006) A study of medieval illuminated manuscripts by means of portable Raman equipments. Journal of Raman Spectroscopy, 37, 1012–1018.

Bersani, D., Andò, S., Scrocco, L., Gentile, P., Salvioli-Mariani, E., and Lottici, P.P. (2014) Study of the composition of Amphiboles in the Tremolite-ferro-Actinolite serie by micro-Raman and SEM-EDXS. In 11th International GeoRaman Conference p. 5063. St. Louis, Missouri, USA.

Blaha, J.J., and Rosasco, G.J. (1978) Raman Microprobe Spectra of Individual Microcrystals and Fibers of Talc, Tremolite, and Related Silicate Minerals. Analytical Chemistry, 50, 892–896.

Bloise, A., Barrese, E., and Apollaro, C. (2009a) Hydrothermal alteration of Ti-doped forsterite to chrysotile and characterization of the resulting chrysotile fibers. Neues Jahrbuch für Mineralogie-Abhandlungen: Journal of Mineralogy and Geochemistry, 185, 297–304.

Bloise, A., Belluso, E., Barrese, E., Miriello, D., and Apollaro, C. (2009b) Synthesis of Fe-doped chrysotile and characterization of the resulting chrysotile fibers. Crystal Research and Technology, 44, 590–596.

Bloise, A., Belluso, E., Fornero, E., Rinaudo, C., Barrese, E., and Capella, S. (2010) Influence of synthesis conditions on growth of Ni-doped chrysotile. Microporous and Mesoporous Materials, 132, 239–245.

Bloise, A., Belluso, E., Catalano, M., Barrese, E., Miriello, D., and Apollaro, C. (2012) Hydrothermal alteration of glass to chrysotile. Journal of the American Ceramic Society, 95, 3050–3055.

Bloise, A., Critelli, T., Catalano, M., Apollaro, C., Miriello, D., Croce, A., Barrese, E., Liberi, F., Piluso, E., Rinaudo, C., and others (2014) Asbestos and other fibrous minerals contained in the serpentinites of the Gimigliano-Mount Reventino Unit (Calabria, S-Italy). Environmental Earth Sciences, 71, 3773–3786.

Bloise, A., Barca, D., Gualtieri, A.F., Pollastri, S., and Belluso, E. (2016) Trace elements in hazardous mineral fibres. Environmental Pollution, 216, 314–323.

Boffetta, P. (1998) Health effects of asbestos exposure in humans: a quantitative assessment. La Medicina del lavoro, 89, 471–480.

Boudier, F., Baronnet, A., and Mainprice, D. (2010) Serpentine mineral replacements of natural olivine and their seismic implications: Oceanic lizardite versus subduction-related antigorite. Journal of Petrology, 51, 495–512.

Boulanger, G., Andujar, P., Pairon, J.-C., Billon-Galland, M.-A., Dion, C., Dumortier, P., Brochard, P., Sobaszek, A., Bartsch, P., Paris, C., and others (2014) Quantification of short and long

asbestos fibers to assess asbestos exposure: a review of fiber size toxicity. Environmental Health: A Global Access Science Source, 13, 59–76.

Brand, W.N., Butt, C.R.M., and Elias, M. (1998) Nickel laterites : Classification and features. Journal of Australian Geology & Geophysics, 17, 81–88.

Bras, I. (2013) L'amiante du massif minier du Koniambo en Nouvelle-Calédonie Etude des cinétiques d'altération et des propriétés physico-chimiques. Nouméa, Nouvelle Calédonie.

Brindley, G.W., and Hang, P.T. (1973) The nature of garnierites - I structures, chemical compositions and color characteristics. Clays and Clay Minerals, 21, 27–40.

Brindley, G.W., and Maksimovic, Z. (1974) The nature and nomenclature of hydrous nickel-containing silicates. Clay Minerals, 10, 271–277.

Brown, R.C., Hoskins, J.A., and Johnson, N. (2012) Mechanisms in fibre carcinogenesis. Vol. 223. Springer Science & Business Media.

Browne, K., and Wagner, J.C. (2001) Environmental exposure to amphibole-asbestos and mesothelioma. Canadian Mineralogist, 5, 21–28.

Burragato, F., Crispino, M., Monti, A., Monti, F., Montagano, G., Papacchini, L., Rossigni, F., Schettino, B., and Sperduto, B. (2006) Environmental pollution from airborne asbestiform fibres: development of fibre propagation maps. In European conference on asbestos risk and management, Rome, Italy pp. 85–90. Rome, Italy.

Burzo, E. (2009) Phyllosilicates, 4, 1-45 p. (H.P.J. Wijn, Ed.) Vol. 27I5b. Springer Berlin Heidelberg, Berlin, Heidelberg.

Butt, C.R.M., and Cluzel, D. (2013) Nickel Laterite Ore Deposits: Weathered Serpentinites. Elements, 9, 123–128.

Caillaud, J., Proust, D., Philippe, S., Fontaine, C., and Fialin, M. (2009) Trace metals distribution from a serpentinite weathering at the scales of the weathering profile and its related weathering microsystems and clay minerals. Geoderma, 149, 199–208.

Cannaò, E., Scambelluri, M., Agostini, S., Tonarini, S., and Godard, M. (2016) Linking serpentinite geochemistry with tectonic evolution at the subduction plate-interface: The Voltri Massif case study (Ligurian Western Alps, Italy). Geochimica et Cosmochimica Acta, 190, 115–133.

Capitani, G.C., and Mellini, M. (2004) The modulated crystal structure of antigorite: The m = 17 polysome. American Mineralogist, 89, 147–158.

Capitani, G.C., and Mellini, M. (2005) HRTEM evidence for 8-reversals in the m=17 antigorite polysome. American Mineralogist, 90, 991–999.

Capitani, G.C., and Mellini, M. (2006) The crystal structure of a second antigorite polysome (m = 16), by single-crystal synchrotron diffraction. American Mineralogist, 91, 394–399.

Capitani, G.C., and Mellini, M. (2007) High-resolution transmission electron microscopy (HRTEM) investigation of antigorite polysomes (m = 15 to 18). American Mineralogist, 92, 64–71.

Cardile, V., Lombardo, L., Belluso, E., Panico, A., Capella, S., and Balazy, M. (2007) Toxicity and carcinogenicity mechanisms of fibrous antigorite. International Journal of Environmental Research and Public Health, 4, 1–9.

Carson, C.J., Clarke, G.L., and Powell, R. (2000) Hydration of eclogite, Pam Peninsula, New Caledonia. Journal of Metamorphic Geology, 18, 79–90.

Case, B.W., Abraham, J.L., Meeker, G., Pooley, F.D., and Pinkerton, K.E. (2011) Applying definitions of "asbestos" to environmental and "low-dose" exposure levels and health effects, particularly malignant mesothelioma. Journal of Toxicology and Environmental Health - Part B: Critical Reviews, 14, 3–39.

Cattaneo, A., Somigliana, A., Gemmi, M., Bernabeo, F., Savoca, D., Cavallo, D.M., and Bertazzi, P.A. (2012) Airborne concentrations of chrysotile asbestos in serpentine quarries and stone processing facilities in Valmalenco, Italy. Annals of Occupational Hygiene, 56, 671–683.

Cavallo, A., and Rimoldi, B. (2013) Chrysotile asbestos in serpentinite quarries: a case study in Valmalenco, Central Alps, Northern Italy. Environmental science. Processes & impacts, 15, 1341–50.

Cavariani, F., Marconi, A., and Sala, O. (2010) Asbestos : sampling , analytical techniques and limit values Amianto : analisi di laboratorio , tecniche analitiche e valori limite. Italian Journal of Occupational and Environmental Hygiene, 1, 18–29.

Chapman, J.A., and Zussman, J. (1959) Further electron optical observations on crystals of antigorite. Acta Crystallographica, 12, 550–552.

Chardon, D., and Chevillotte, V. (2006) Morphotectonic evolution of the New Caledonia ridge (Pacific Southwest) from post-obduction tectonosedimentary record. Tectonophysics, 420, 473–491.

Chevillotte, V., Chardon, D., Beauvais, A., Maurizot, P., and Colin, F. (2006) Long-term tropical morphogenesis of New Caledonia (Southwest Pacific): Importance of positive epeirogeny and climate change. Geomorphology, 81, 361–375.

Chisholm, J.E. (1991) Geometrical constraints on the growth of sectors in polygonal serpentine. Journal of Physics D: Applied Physics, 24, 199–202.

Chisholm, J.E. (1992) The number of sections in polygonal serpentine. The Canadian Mineralogist, 30, 355–365.

Cluzel, D., and Pelletier, B. (1994) Compte-rendu préliminaire de la visite géologique du secteur de Montfaoué (Poya). Nouméa, Nouvelle Calédonie.

Cluzel, D., and Vigier, B. (2008) Syntectonic Mobility of Supergene Nickel Ores of New Caledonia (Southwest Pacific). Evidence from Garnierite Veins and Faulted Regolith. Resource Geology, 58, 161–170.

Cluzel, D., Aitchison, J.C., Clarke, G.L., Meffre, S., and Picard, C. (1995) Dénudation tectonique du complexe à noyau métamorphique de haute préssion d'âge tertiaire (Nord de la Nouvelle-Calédonie, Pacifique, France). Données cinématiques. Comptes rendus de l'Académie des sciences. Série 2. Sciences de la terre et des planètes, 321, 57–64.

Cluzel, D., Aitchison, J.C., and Picard, C. (2001) Tectonic accretion and underplating mafic terranes in the late Eocene intraoceanic fore-arc of New Caledonia (Southwest Pacific): Geodynamic implications. Tectonophysics, 340, 23–59.

Cluzel, D., Maurizot, P., Collot, J.Y., and Sevin, B. (2012) An outline of the Geology of New Caledonia; from Permian-Mesozoic Southeast Gondwanaland active margin to Cenozoic

obduction and supergene evolution. Episodes, 35, 72–86.

Collegium Ramazzini (2011) Asbestos is still with us: Repeat call for a universal ban. American Journal of Industrial Medicine, 54, 168–173.

Collot, J.Y., Malahoff, A., Recy, J., Latham, G., and Missègue, F. (1987) Overthrust emplacement of New Caledonia ophiolite: geophysical evidence. Tectonics, 6, 215–232.

Cressey, B.A. (1979) Electron Microscopy of Serpentine Textures. Canadian Mineralogist, 17, 741–756.

Cressey, B.A., and Whittaker, E.J.W. (1993) Five-fold symmetry in chrysotile asbestos revealed by transmission electron microscopy. Mineralogical Magazine, 57, 729–732.

Cressey, B.A., and Zussman, J. (1976) Electron microscopic studies of serpentinites. Canadian Mineralogist, 14, 307–313.

Cressey, B.A., Cressey, G., and Cernik, R.J. (1994) Structural Variations in Chrysotile Asbestos Fibers Revealed by Synchrotron X-Ray Diffraction and High-Resolution Transmission Electron Microscoy. The Canadian Mineralogist, 32, 257–270.

Cressey, G., Cressey, B.A., and Wicks, F.J. (2008) Polyhedral serpentine: a spherical analogue of polygonal serpentine? Mineralogical Magazine, 72, 1229–1242.

Cressey, G., Cressey, B.A., Wicks, F.J., and Yada, K. (2010) A disc with fivefold symmetry: the proposed fundamental seed structure for the formation of chrysotile asbestos fibres, polygonal serpentine fibres and polyhedral lizardite spheres. Mineralogical Magazine, 74, 29–37.

Critelli, T., Marini, L., Schott, J., Mavromatis, V., Apollaro, C., Rinder, T., De Rosa, R., and Oelkers, E.H. (2015) Dissolution rate of antigorite from a whole-rock experimental study of serpentinite dissolution from 2< pH< 9 at 25 C: Implications for carbon mitigation via enhanced serpentinite. weathering. Applied Geochemistry, 61, 259–271.

Davis, J.M.G., Addison, J., McIntosh, C., Miller, B.G., and Niven, K. (1991) Variations in the Carcinogenicity of Tremolite Dust Samples of Differing Morphology. Annals of the New York Academy of Sciences, 63, 473–490.

Deer, W.A., Howie, R.A., and Zussman, J. (1992) An introduction to the rock-forming minerals, 2. Ed. Lon., XVI-696 p. Harlow.

Deschamps, F., Godard, M., Guillot, S., Chauvel, C., Andreani, M., Hattori, K., Wunder, B., and France, L. (2012) Behavior of fluid-mobile elements in serpentines from abyssal to subduction environments: Examples from Cuba and Dominican Republic. Chemical Geology, 312–313, 93–117.

Deschamps, F., Godard, M., Guillot, S., and Hattori, K. (2013) Geochemistry of subduction zone serpentinites: A review. Lithos, 178, 96–127.

Devouard, B., Baronnet, A., Van Tendeloo, G., and Amelinckx, S. (1997) First evidence of synthetic polygonal serpentines. European Journal of Mineralogy, 9, 539–546.

DIMENC-SGNC (2010) Cartographie des terrains potentiellement amiantifères en Nouvelle-Caléconie - Etat des connaissances, mars 2010. DIMENC-SGNC, BRGM, Nouméa, Nouvelle Calédonie.

Dodony, I. (1997) Structure of the 30-sectored polygonal serpentine. A model based on TEM and SAED studies. Physics and Chemistry of Minerals, 24, 39–49.

Dódony, I., Pósfai, M., and Buseck, P.R. (2002) Revised structure models for antigorite: An HRTEM study. American Mineralogist, 87, 1443–1457.

Dogan, M., and Emri, S. (2000) Environmental health problems related to mineral dusts in Ankara and Eskisehir, Turkey. Yerbilimleri, 22, 149–161.

Dorling, M., and Zussman, J. (1987) Characteristics of asbestiform and non-asbestiform calcic amphiboles. Lithos, 20, 469–489.

Dublet, G., Juillot, F., Morin, G., Fritsch, E., Fandeur, D., and Brown, G.E. (2015) Goethite aging explains Ni depletion in upper units of ultramafic lateritic ores from New Caledonia. Geochimica et Cosmochimica Acta, 160, 1–15.

Eggleton, R.A. (2001) The regolith glossary: surficial geology, soils and landscapes., 1-144 p. Cooperative Research Centre for Landscape Evolution and Mineral Exploration., Camberra.

Elias, M. (2002) Nickel laterite deposits - geological overview, resources and exploitation. Giant Ore Depositis: Characteristics, genesis and exploration, 4, 205–220.

Elias, M., Donaldson, M.J., and Giorgetta, N. (1981) Geology, Mineralogy, and Chemistry of Lateritie Nickel-Cobalt Deposits near Kalgoorlie, Western Australia. Economic Geology, 76, 1775–1783.

Evans, B.W. (2004) The Serpentinite Multisystem Revisited: Chrysotile Is Metastable. International Geology Review, 46, 459–506.

Evans, B.W. (2007) The Synthesis and Stability of Some End-Member Amphiboles. Reviews in Mineralogy and Geochemistry, 67, 261–286.

Evans, B.W., Johannes, W., Oterdoom, H., and Trommsdorff, V. (1976) Stability of chrysotile and antigorite in the serpentinite multisystem. Schweizerische mineralogische und petrographische Mitteilungen, 56, 79–93.

Evans, B.W., Hattori, K., and Baronnet, A. (2013) Serpentinite: What, Why, Where? Elements, 9, 99–106.

Evans, K.A., Powell, R., and Frost, B.R. (2013) Using equilibrium thermodynamics in the study of metasomatic alteration, illustrated by an application to serpentinites. Lithos, 168–169, 67–84.

Falini, G., Foresti, E., Gazzano, M., Gualtieri, A.F., Leoni, M., Lesci, I.G., and Roveri, N. (2004) Tubular-shaped stoichiometric chrysotile nanocrystals. Chemistry (Weinheim an der Bergstrasse, Germany), 10, 3043–9.

Faust, G.T., Fahey, J.J., Mason, B., and Dwornik, E.J. (1969) Pecoraite, $Ni_6Si_4O_{10}(OH)_8$, Nickel Analog of Clinochrysotile, Formed in the Wolf Creek Meteorite. Science, 165, 59–60.

Faust, G.T., Fahey, J.J., Mason, B., and Dwornik, E.J. (1973) The disintegration of the Wolf Creek meteorite and the formation of pecoraite, the nickel analog of clinochrysotile. Professional Paper.

Fitz Gerald, J.D., Eggleton, R.A., and Keeling, J.L. (2010) Antigorite from Rowland Flat, South Australia: asbestiform character. European Journal of Mineralogy, 22, 525–533.

Fitzgerald, S.M., and Harty, E.A. (2014) Antigorite Is It the Forgotten Asbestos? Professional Safety, 59, 43–48.

Foresti, E., Gazzano, M., Gualtieri, A.F., Lesci, I.G., Lunelli, B., Pecchini, G., Renna, E., and Roveri, N. (2003) Determination of low levels of free fibres of chrysotile in contaminated soils by X-ray diffraction and FTIR spectroscopy. Analytical and Bioanalytical Chemistry, 376, 653–658.

Freyssinet, P., Butt, C.R.M., Morris, R.C., and Piantone, P. (2005) Ore-forming processes related to lateritic weathering. In J.W. Hedenquist, J.F.H. Thomson, R.J. Goldfarb, and J.P. Richards, Eds., Economic Geology 100th Anniversary Volume pp. 681–722. Economic Geology Publishing Company, New Haven, Connecticut.

Frost, B.R., Evans, K.A., Swapp, S.M., Beard, J.S., and Mothersole, F.E. (2013) The process of serpentinization in dunite from New Caledonia. Lithos, 178, 24–39.

Fubini, B., and Fenoglio, I. (2007) Toxic Potential of Mineral Dusts. Elements, 3, 407–414.

Fubini, B., and Otero Arean, C. (1999) Chemical aspects of the toxicity of inhaled mineral dusts. Chem. Soc. Rev., 28, 373–381.

Gazzano, E., Riganti, C., Tomatis, M., Turci, F., Bosia, A., Fubini, B., and Ghigo, D. (2005) Potential Toxicity of Nonregulated Asbestiform Minerals: Balangeroite From the Western Alps. Part 3: Depletion of Antioxidant Defenses. Journal of Toxicology and Environmental Health, Part A, 68, 41–49.

Glenn, R.E., Lee, R.J., Jastrem, L.M., Bunker, K.L., Van Orden, D.R., and Strohmeier, B.R. (2008) Asbestos: By any other name is it still., 22-33 p. Chemical Regulation Reporter Vol. 32.

Goldberg, P., Goldberg, M., Marne, M.J., Hirsch, A., and Tredaniel, J. (1991) Incidence of pleural mesothelioma in New Caledonia: a 10-year survey (1978–1987). Archives of Environmental Health, 46, 306–309.

Goldberg, P., Luce, D., Billon-Gailland, M.A., Quénel, P., Salomon-Nekiriai, C., and Nicolau, J. (1995) Identification d'un excès de risque de cancer de la plèvre en Nouvelle-Calédonie lié à l'exposition environnementale et domestique à la trémolite. Rev Epidemiol Santé Publique, 43, 444–450.

Golightly, J.P. (1979) Nickeliferous laterites: a general description. In International Laterite Symposium, New Orleans, Society of Mining Engineers, American Institute of Mining, Metallurgical, and Petroleum Engineers (pp. 38-56). In D.J.I. Evans, R.S. Shoemaker, and H. Veltman, Eds., International Laterite Symposium pp. 3–23. Society of Mining Engineers, New York, USA.

Golightly, J.P. (2010) Progress in understanding the evolution of nickel laterites. In R.J. Goldfarb, E.E. Marsh, and T. Monecke, Eds., The Challenge of Finding New Mineral Resources: Global Metallogeny, Innovative Exploration, and New Discoveries. pp. 451–475. Society of Economic Geologist Special Publication.

Golightly, J.P., and Arancibia, N.O. (1979) The chemical composition and infrared spectrum of nickel-and iron-substituted serpentine from a nickeliferous laterite profile, Soroako, Indonesia. Canadian Mineralogist, 17, 719–728.

Granieri, A. (2015) Community exposure to asbestos in Casale Monferrato: from research on psychological impact to a community needs-centered healthcare organization. Annali dell'Istituto superiore di sanita, 51, 336–341.

Groppo, C., and Compagnoni, R. (2007a) Metamorphic veins from the serpentinites of the Piemonte Zone, western Alps, Italy : a review. Periodico di Mineralogia, 76, 127–153.

Groppo, C., and Compagnoni, R. (2007b) Ubiquitous fibrous antigorite veins from the Lanzo Ultramafic Massif, Internal Western Alps (Italy): characterisation and genetic conditions. Periodico di Mineralogia, 76, 169–181.

Groppo, C., Tomatis, M., Turci, F., Gazzano, E., Ghigo, D., Compagnoni, R., and Fubini, B. (2005) Potential toxicity of nonregulated asbestiform minerals: Balangeroite from the western Alps. Part 1: Identification and characterization. Journal of Toxicology and Environmental Health - Part A, 68, 1–19.

Groppo, C., Rinaudo, C., Cairo, S., Gastaldi, D., and Compagnoni, R. (2006) Micro-Raman spectroscopy for a quick and reliable identification of serpentine minerals from ultramafics. European Journal of Mineralogy, 18, 319–329.

Gualtieri, A.F. (2017) Introduction. In A.F. Gualtieri, Ed., Mineral fibres: Crystal chemistry, chemical physical properties, biological interaction and toxicity. Vol. 18, pp. 1–15. European Mineralogical Union and the Mineralogical Society of Great Britain & Ireland, UK.

Gualtieri, A.F., Pollastri, S., Gandolfi, N.B., Ronchetti, F., Albonico, C., Cavallo, A., Zanetti, G., Marini, P., and Sala, O. (2014) Determination of the concentration of asbestos minerals in highly contaminated mine tailings: An example from abandoned mine waste of Crètaz and Èmarese (Valle d'Aosta, Italy). American Mineralogist, 99, 1233–1247.

Gunnar Hillerdal, M.D. (2003) Health problems related to environmental fibrous minerals. In H.C.. Skinner and A.R. Berger, Eds., Geology and Health: Closing the Gap pp. 113–118. Oxford University Press, New York, New York, USA.

Gunter, M.E., Belluso, E., and Mottana, A. (2007a) Amphiboles: Environmental and Health Concerns. Reviews in Mineralogy and Geochemistry, 67, 453–516.

Gunter, M.E., Sanchez, M.S., and Williams, T.J. (2007b) Characterization of chrysotile samples for the presence of amphiboles: The Carey Canadian deposit, southeastern Quebec, Canada. Canadian Mineralogist, 45, 263–280.

Hawthorne, F.C., and Oberti, R. (2007a) Amphiboles: Crystal Chemistry. Reviews in Mineralogy and Geochemistry, 67, 1–54.

Hawthorne, F.C., and Oberti, R. (2007b) Classification of the Amphiboles. Reviews in Mineralogy and Geochemistry, 67, 55–88.

Hayward, I.P., Kirkbride, T.E., Batchelder, D.N., and Lacey, R.J. (1995) Use of a fiber optic probe for the detection and identification of explosive materials by Raman spectroscopy. Journal of Forensic Science, 40, 883–884.

Health and Safety Executive (2006) Asbestos: The analysts' guide for sampling, analysis and clearance procedures, 1-120 p. (Executive Health and Safety, Ed.)HSE Books Vol. 248.

Hiern, M.N. (1976) Asbestos-South Australia. Economic geology of Australia and Papua New Guinea, 4, 12–14.

Hirth, G., and Guillot, S. (2013) Rheology and tectonic significance of serpentinite. Elements, 9, 107–113.

Hodgson, J.T., and Darnton, A. (2000) The quantitative risks of mesothelioma and lung cancer in relation to asbestos exposure. Annals of occupational hygiene, 44, 565–601.

Houchot, M.-A. (2008) De l'évaluation en santé publique à une démarche de géographie de la santé: Le risque amiante environnemental en Nouvelle-Calédonie. Université de Nouvelle Calédonie.

IARC (1977) Some miscellaneous pharmaceutical substances., 1-255 p. IARC monographs on the evaluation of the carcinogenic risk of chemicals to man. Vol. 13.

IARC (2012) Arsenic, Metals, Fibres, and Dusts. A review of human carcinogens., 1-501 p. IARC Monographs on the Evaluation of Carcinogenic Risks to Humans Vol. 100C. Lyon, France.

INSERM U88 (1997) Aspects épidémiologiques de la relation entre exposition environnementale à la trémolite et cancers respiratoires en Nouvelle-Calédonie., 1-33 p. Saint-Maurice.

Jehlička, J., Vítek, P., Edwards, H.G.M., Heagraves, M., and Čapoun, T. (2009a) Application of portable Raman instruments for fast and non-destructive detection of minerals on outcrops. Spectrochimica Acta - Part A: Molecular and Biomolecular Spectroscopy, 73, 410–419.

Jehlička, J., Vítek, P., Edwards, H.G.M., Hargreaves, M.D., and Čapoun, T. (2009b) Fast detection of sulphate minerals (gypsum, anglesite, baryte) by a portable Raman spectrometer. Journal of Raman Spectroscopy, 40, 1082–1086.

Jones, R.H. (1890) Asbestos, Its Properties, Occurrence & Uses: With Some Account of the Mines of Italy and Canada., 236 p. (C. Lockwood, Ed.).

Kadır, S., Aydoğan, S.M., Elİtok, Ö., and Helvaci, C. (2015) Composition and genesis of the nickel-chrome-bearing nontronite and montmorillonite in lateritized ultramafic rocks in the muratdağ i region (Uşak, western anatolia), Turkey. Clays and Clay Minerals, 63, 163–184.

Kane, A.B., Boffetta, P., Saracci, R., and Wilbourn, J.D. (1996) Mechanisms of fibre carcinogenesis. In IARC Scientific Publications Vol. 140, pp. 11–34. International Agency for Research on Cancer; WHO, Lyon, France.

Keeling, J.L., Raven, M.D., and McClure, S.G. (2006) Identification of fibrous mineral from Rowland Flat area, Barossa Valley, South Australia., 1-27 p. Vol. 2.

Keeling, J.L., Raven, M.D., Self, P.G., and Eggleton, R.A. (2008) Asbestiform antigorite occurrence in South Australia. In 9th International Congress for Applied Mineralogy, ICAM 2008 pp. 329–336.

Keeling, J.L., Raven, M.D., and Self, P.G. (2010) Asbestiform antigorite – implications for the risk assessment of fibrous silicates. In Extended Abstracts – 21st Australian Clay Minerals Conference pp. 87–90. Brisbane.

Krstanovic, I., and Pavlovic, S. (1964) X-ray study of chrysotile. The american mineralogist, 49, 1769–1771.

Kunze, G. (1961) Antigorite. Fortschritte der Mineralogie, 39, 206–324.

Lagabrielle, Y., Chauvet, A., Ulrich, M., and Guillot, S. (2013) Passive obduction and gravity-driven emplacement of large ophiolitic sheets: The New Caledonia ophiolite (SW Pacific) as a case study? Bulletin de la Societe Geologique de France, 184, 545–556.

Lahondère, D. (2007) L'amiante environnemental en Nouvelle Calédonie : Expertise géologique

des zones amiantifères. Evaluation des actions engagées., 1-55 p. Nouméa, Nouvelle Calédonie.

Lahondère, D. (2012) Serpentinisation et fibrogenèse dans les massifs de péridotite de Nouvelle-Calédonie. Atlas des occurrences et des types de fibres d'amiante sur mine., 1-128 p. Nouméa, Nouvelle Calédonie.

Lahondère, D., and Maurizot, P. (2009) Typologie et protocole d'échantillonnage des occurrences naturelles d'amiante en Nouvelle-Calédonie., 1-164 p. Nouméa, Nouvelle Calédonie.

Langer, A.M., Mackler, A.D., and Pooley, F.D. (1974) Electron microscopical investigation of asbestos fibers. Environmental Health Perspectives, 9, 63–80.

Lauwers, D., Hutado, A.G., Tanevska, V., Moens, L., Bersani, D., and Vandenabeele, P. (2014) Characterisation of a portable Raman spectrometer for in situ analysis of art objects. Spectrochimica Acta - Part A: Molecular and Biomolecular Spectroscopy, 118, 294–301.

Lee, R.J., Strohmeier, B.R., Bunker, K.L., and Van Orden, D.R. (2008) Naturally occurring asbestos - A recurring public policy challenge. Journal of Hazardous Materials, 153, 1–21.

Leguere, J. (1976) Des correlations entre la tectonique cassante et l'alteration supergene des peridotites de Nouvelle Caledonie. University of Montpellier, France.

Lemaire, C., Guyot, F., and Reynard, B. (1999) Vibrational spectroscopy (IR and Raman) of OH groups in chrysotile lizardite and antigorite. In European Union of Geosciences Vol. 10, p. 654.

Lemen, R.A. (2004) Asbestos in Brakes: Exposure and Risk of Disease. American Journal of Industrial Medicine, 45, 229–237.

Lentzen, D.E., Brantly, E.P.J., Gold, K.W., and Myerz, L.E. (1982) Test Method. Interim Method for the Determination of Asbestos in Bulk Insulation samples, 2-54 p. EPA-800 Vol. M4-82–20. Washington DC.

Leoni, M., and Scardi, P. (2004) Nanocrystalline domain size distributions from powder diffraction data. Journal of Applied Crystallography, 37, 629–634.

Lewis, I.R., Chaffinl, N.C., Gunter, M.E., and Griffiths, P.R. (1996) Vibrational spectroscopic studies of asbestos and comparison of suitability for remote analysis. Spectrochimica Acta Part A, 52, 315–328.

Lin, F.-C., and Clemency, V.C. (1981) The dissolution kinetics of brucite, antigorite, talc, and phlogopite at room temperature and pressure. American Mineralogist, 66, 801–806.

Luce, D., Brochard, P., Quenel, P., Salomon-Nekiriai, C., Goldberg, P., Billon-Galland, M.-A., and Goldberg, M. (1994) Malignant pleural mesothelioma associated with exposure to tremolite. The Lancet, 344, 1777.

Luce, D., Bugel, I., Goldberg, P., Goldberg, M., Salomon, C., Billon-Galland, M.-A., Nicolau, J., Quénel, P., Fevotte, J., and Brochard, P. (2000) Environmental exposure to tremolite and respiratory cancer in New Caledonia: a case-control study. American journal of epidemiology, 151, 259–265.

Luce, D., Billon-Galland, M.-A., Bugel, I., Goldberg, P., Salomon, C., Févotte, J., and Goldberg, M. (2004) Assessment of environmental and domestic exposure to tremolite in New Caledonia.

Archives of environmental health, 59, 91–100.

Manceau, A., and Calas, G. (1985) Heterogeneous distribution of nickel in hydrous silicates from New Caledonia ore deposits. American Mineralogist, 70, 549–558.

Marmo, B.A., Clarke, G.L., and Powell, R. (2002) Fractionation of bulk rock composition due to porphyroblast growth: Effects on eclogite facies mineral equilibria, Pam Peninsula, New Caledonia. Journal of Metamorphic Geology, 20, 151–165.

Mellini, M. (1986) Chrysotile and polygonal serpentine from the Balangero serpentinite. Mineralogical Magazine, 50, 301–305.

Mellini, M., and Zanazzi, P.F. (1987) Crystal structures of lizardite-1T and lizardite-2H1 from Coli, Italy. American Mineralogist, 72, 943–948.

Mellini, M., Trommsdorff, V., and Compagnoni, R. (1987) Antigorite polysomatism: behaviour during progressive metamorphism. Contributions to Mineralogy and Petrology, 97, 147–155.

Middleton, A.P., and Whittaker, E.J.W. (1976) The structure of Povlen-type chrysotile. Canadian Mineralogist, 14, 301–306.

Mitchell, R.H., and Putnis, A. (1988) Polygonal Serpentine in Segregation-Textured Kimberllite. Canadian Mineralogist, 26, 991–997.

Monti, R., and Fazakerley, V.W. (1996) The Murrin Murrin nickel cobalt project., 191-195 p. Grimsey, EJ, Neuss, & I.(eds). Nickel Vol. 96.

Moore, D.S., and Scharff, R.J. (2009) Portable Raman explosives detection. Analytical and Bioanalytical Chemistry, 393, 1571–1578.

Mossman, B.T., Light, W., and Wei, E. (1983) Asbestos: mechanisms of toxicity and carcinogenicity in the respiratory tract. Annu Rev Pharmacol Toxicol, 23, 595–615.

Mothersole, F.E., Evans, K., and Frost, B.R. (2017) Abyssal and hydrated mantle wedge serpentinised peridotites: a comparison of the 15°20'N fracture zone and New Caledonia serpentinites. Contributions to Mineralogy and Petrology, 172, 1–25.

Mugnaioli, E., Logar, M., Mellini, M., and Viti, C. (2007) Complexity in 15- and 30-sectors polygonal serpentine: Longitudinal sections, intrasector stacking faults and XRPD satellites. American Mineralogist, 92, 603–616.

Nichols, M.D., Young, D., and Gray, D. (2002) Guidelines for geologic investigations of Naturally Occurring Asbestos in California., 1-85 p. Vol. Special Pu.

NIOSH (1990) Comments of the National Institute for Occupational Safety and Health on the Occupational Safety and Health Administration's Notice of Proposed Rulemaking on Occupational Exposure to Asbestos, Tremolite, Anthophyllite, and Actinolite. OSHA Docket Vol. No H-033d. Washington DC.

NIOSH (2011) Asbestos Fibers and Other Elongate Mineral Particles: State of the Science and Roadmap for Research., 1-159 p. Current Intelligence Bulletin 62 Vol. 159.

NIOSH-OSHA (1980) Workplace Exposure to Asbestos. Review and Recommendations., 1-47 p. DHHA (NIOSH) Publication Vol. 81–103. Washington DC.

O'Hanley, D.S. (1996) Serpentinites. (O.U.P. on Demand, Ed.).

Oberdörster, G. (2000) Determinants of the pathogenicity of man-made vitreous fibers (MMVF). International archives of occupational and environmental health, 73 Suppl, S60–S68.

Orloff, O., and Gonord, H. (1968) Note préliminaire sur un nouveau complexe sédimentaire continental situé sur les massifs du Goa N'Doro et de Kadjitra (région côtière à l'Est de la Nouvelle-Calédonie), définition de la formation et conséquences de cette découverte sur l'âge des fractures. CR Acad. Sci. Paris, 267, 5–8.

Papp, G. (1990) A review of the multi-layer lizardite polytypes. Annales historico-naturales Musei nationalis hungarici, 82, 9–17.

Pelletier, B. (1996) Serpentine in nickel silicate ore from New Caledonia. Nickel '96 : Mineral to market, 197–205.

Peters, D., Bretscher, A., John, T., Scambelluri, M., and Pettke, T. (2017) Fluid-mobile elements in serpentinites: Constraints on serpentinisation environments and element cycling in subduction zones. Chemical Geology, 466, 654–666.

Petriglieri, J.R. (2014) I polimorfi del serpentino: identificazione mediante spettroscopia Raman. Università di Parma.

Petriglieri, J.R., Salvioli-Mariani, E., Mantovani, L., Tribaudino, M., Lottici, P.P., Laporte-Magoni, C., and Bersani, D. (2015) Micro-Raman mapping of the polymorphs of serpentine. Journal of Raman Spectroscopy, 46, 953–958.

Petry, R., Mastalerz, R., Zahn, S., Mayerhöfer, T.G., Völksch, G., Viereck-Götte, L., Kreher-Hartmann, B., Holz, L., Lankers, M., and Popp, J. (2006) Asbestos mineral analysis by UV raman and energy-dispersive X-ray spectroscopy. ChemPhysChem, 7, 414–420.

Pollastri, S., D'Acapito, F., Trapananti, A., Colantoni, I., Andreozzi, G.B., and Gualtieri, A.F. (2015) The chemical environment of iron in mineral fibres. A combined X-ray absorption and Mössbauer spectroscopic study. Journal of hazardous materials, 28, 282–293.

Pollastri, S., Perchiazzi, N., Lezzerini, M., Plaisier, J.R., Cavallo, A., Dalconi, M.C., Gandolfi, N.B., and Gualtieri, A.F. (2016) The crystal structure of mineral fibres. 1. Chrysotile. Periodico di Mineralogia, 85, 249–259.

Prichard, H.M. (1979) A petrographie study of the process of serpentinisation in ophiolites and the ocean crust. Contributions to Mineralogy and Petrology, 68, 231–241.

Prinzhofer, A. (1981) Structure et pétrologie d'un cortège ophiolitique: Le massif du sud (Nouvelle Calédonie). ENSM - Paris.

Pugnaloni, A., Giantomassi, F., Lucarini, G., Capella, S., Mattioli Belmonte, M., Orciani, M., and Belluso, E. (2010) Effects of asbestiform antigorite on human alveolar epithelial A549 cells : A morphological and immunohistochemical study. Acta histochemica, 112, 133–146.

Quénel, P., and Cochet, C. (2001) Trémolite (Pö) et cancers respiratoires en Nouvelle Calédonie., 1-35 p. Nouméa, Nouvelle Calédonie.

Quesnel, B. (2015) Alteration supergene, circulation des fluides et deformation interne du massif de Koniambo, Nouvelle-Caledonie: implication sur les gisements nickeliferes lateritiques. Universite Rennes 1.

Quesnel, B., Gautier, P., Cathelineau, M., Boulvais, P., Couteau, C., and Drouillet, M. (2016) The internal deformation of the Peridotite Nappe of New Caledonia: A structural study of serpentine-bearing faults and shear zones in the Koniambo Massif. Journal of Structural Geology, 85, 51–67.

Rawling, T.J., and Lister, G.S. (1999) Oscillating modes of orogeny in the Southwest Pacific and the tectonic evolution of New Caledonia. Geological Society, London, Special Publications, 154, 109–127.

Ribeiro Da Costa, I., Barriga, F.J.A.S., Viti, C., Mellini, M., and Wicks, F.J. (2008) Antigorite in deformed serpentinites from the Mid-Atlantic Ridge. European Journal of Mineralogy, 20, 563–572.

Rinaudo, C., Gastaldi, D., and Belluso, E. (2003) Characterization of Chrysotile, Antigorite, and Lizardite by FT-Raman Spectroscopy. The Canadian Mineralogist, 41, 883–890.

Rinaudo, C., Belluso, E., and Gastaldi, D. (2004) Assessment of the use of Raman spectroscopy for the determination of amphibole asbestos. Mineralogical Magazine, 68, 455–465.

Rinaudo, C., Gastaldi, D., Belluso, E., and Capella, S. (2005) Application of Raman spectroscopy on asbestos fibre identification. Neues Jahrbuch Fur Mineralogie-Abhandlungen, 182, 31–36.

Robinson, K., and Shaw, E.R.S. (1952) Summarized proceedings of a conference on structures of silicate minerals-London November 1951. British Journal of Applied Physics, 3, 277–282.

Ross, M., and Nolan, R.P. (2003) History of asbestos discovery and use and asbestos-related disease in context with the occurrence of asbestos within ophiolite complexes. Geology Society of America, 447–470.

Ross, M., Kuntze, R.A., and Clifton, R.A. (1984) A definition for asbestos. Special Technical Publication, 834, 139–147.

Ross, M., Langer, A.M., Nord, G.L., Nolan, R.P., Lee, R.J., Van Orden, D.R., and Addison, J. (2008) The mineral nature of asbestos. Regulatory Toxicology and Pharmacology, 52, S26–S30.

Roveri, N., Falini, G., Foresti, E., Fracasso, G., Lesci, I.G., and Sabatino, P. (2006) Geoinspired synthetic chrysotile nanotubes. Journal of Materials Research, 21, 2711–2725.

Sanchez, M.S., and Gunter, M.E. (2006) Quantification of amphibole content in expanded vermiculite products from Libby, Montana U.S.A. using powder X-ray diffraction. American Mineralogist, 91, 1448–1451.

Schreier, H. (1989) Asbestos in the natural environment Vol. 37. Elsevier.

Seaton, A., Tran, L., Aitken, R., and Donaldson, K. (2010) Nanoparticles, human health hazard and regulation. Journal of The Royal Society Interface, 7, S119–S129.

Sevin, B. (2014) Cartographie du régolithe sur massifs ultrabasiques de Nouvelle-Calédonie: distribution dans l'espace et le temps des gisements nickelifères. Université de Nouvelle Calédonie.

Smolikov, A., Vezentsev, A., Beresnev, V., Kolesnikov, D., and Solokha, A. (2013) Morphology of Synthetic Chrysotile Nanofibers (Mg-Hydro Silicate). Journal of Materials Science and Engineering, A, 523–530.

Song, Y., Moon, H.S., and Chon, H.T. (1995) New Occurrence and Characterization of Ni-

Serpentines in the Kwangcheon Area, Korea. Clay Minerals, 30, 211–224.

Spinnler, G.E. (1985) HRTEM study of antigorite, pyroxene-serpentine reactions, and chlorite. Arizona State University.

Sporn, T.A. (2014) The Mineralogy of Asbestos. In T.D. Oury, T.A. Sporn, and V.L. Roggli, Eds., Pathology of Asbestos-Associated Diseases pp. 1–10. Springer Berlin Heidelberg, Berlin, Heidelberg.

Stemple, I.S., and Brindley, G.W. (1960) A Structural Study of Talc and Talc-Tremolite Relations. Journal of the American Ceramic Society, 43, 34–42.

Suzuki, Y., Yuen, S.R., and Ashley, R. (2005) Short, thin asbestos fibers contribute to the development of human malignant mesothelioma: Pathological evidence. International Journal of Hygiene and Environmental Health, 208, 201–210.

Thompson, B.D., Gunter, M.E., and Wilson, M.A. (2011) Amphibole asbestos soil contamination in the U.S.A.: A matter of definition. American Mineralogist, 96, 690–693.

Trescases, J.-J. (1975) Supergenic Geochemical Evolution of the Ultrabasic Rocks in the Tropical Zone—Formation of the Nickeliferous Deposits in New Caledonia., Memoires., 1-259 p. (ORSTOM, Ed.). Paris, France.

Trescases, J.-J. (1997) The lateritic nickel-ore deposits. In Soils and sediments pp. 125–138. Springer.

Troly, G., Esterle, M., Pelletier, B., and Reibell, W. (1979) Nickel deposits in New Caledonia, some factors influencing their formation. In International Laterite Symposium pp. 85–119. American Institute of Mining Metallurgy and Petroleum Engineering Society, New Orleans.

Trotet, F. (2012) Fibrous serpentinites in oxyded nickel ores from New Caledonia: risk management in a modern mining company - societal implications. In Serpentine Days p. 87.

Turci, F., Tomatis, M., Gazzano, E., Riganti, C., Martra, G., Bosia, A., Ghigo, D., and Fubini, B. (2005) Potential Toxicity of Nonregulated Asbestiform Minerals: Balangeroite From the Western Alps. Part 2: Oxidant Activity of the Fibres. Journal of Toxicology and Environmental Health, Part A, 68, 21–39.

Uehara, S., and Shirozu, H. (1985) Variations in chemical composition and structural properties of antigorites. Mineralogical Journal, 12, 299–318.

Ulmer, P., and Trommsdorff, V. (1995) Serpentine Stability to Mantle Depths and Subduction-Related Magmatism. Science, 268, 858–861.

Ulrich, M. (2010) Péridotites et serpentinites du complexe ophiolitique de la Nouvelle-Calédonie. Études pétrologiques, géochimiques et minéralogiques sur l'évolution d'une ophiolite de sa formation à son altération. Université de la Nouvelle-Caledonie / Université Joseph Fourier de Grenoble.

Ulrich, M., Picard, C., Guillot, S., Chauvel, C., Cluzel, D., and Meffre, S. (2010) Multiple melting stages and refertilization as indicators for ridge to subduction formation: The New Caledonia ophiolite. Lithos, 115, 223–236.

Ulrich, M., Guillot, S., Muñoz, M., and Picard, C. (2011) Origin of multiple serpentinization events in New Caledonia. In AGU Fall Meeting Abstracts.

Ulrich, M., Bureau, S., Chauvel, C., and Picard, C. (2012) Accurate Measurement of Rare Earth Elements by ICP-MS after Ion-Exchange Separation: Application to Ultra-Depleted Samples. Geostandards and Geoanalytical Research, 36, 7–20.

United States Department of Labor (1975) Occupational exposure to asbestos. Federal Register., 47650-47665 p. Vol. 40. Washington DC.

Utembe, W., Potgieter, K., Stefaniak, A.B., and Gulumian, M. (2015) Dissolution and biodurability: Important parameters needed for risk assessment of nanomaterials. Particle and Fibre Toxicology, 12, 1–12.

Van Gosen, B.S. (2007) The geology of asbestos in the United States and its practical applications. Environmental and Engineering Geoscience, 13, 55–68.

Van Gosen, B.S., Lowers, H.A., Sutley, S.J., and Gent, C.A. (2004) Using the geologic setting of talc deposits as an indicator of amphibole asbestos content. Environmental Geology, 45, 920–939.

Vandenabeele, P., Edwards, H.G.M., and Jehlička, J. (2014) The role of mobile instrumentation in novel applications of Raman spectroscopy: archaeometry, geosciences, and forensics. Chemical Society Reviews, 43, 2628.

Veblen, D.R. (1980) Anthophyllite asbestos : microstructures , intergrown sheet silicates , and mechanisms of fiber formation. American Mineralogist, 65, 1075–86.

Veblen, D.R. (1991) Polysomatism and polysomatic series: A review and applications. American Mineralogist, 76, 801–826.

Veblen, D.R., and Wylie, A.G. (1993) Mineralogy of amphiboles and 1: 1 layer silicates. In G.D. Guthrie and B.T. Mossman, Eds., Health effects of mineral dust. Reviews in Mineralogy Vol. 28, pp. 61–137. Mineralogical Society of America, Washington, DC (United States), Washington DC.

Vigliaturo, R. (2015) Microstructures of potentially harmful fibrous minerals. University of Torino, Italy.

Vignaroli, G., Ballirano, P., Belardi, G., and Rossetti, F. (2014) Asbestos fibre identification vs. evaluation of asbestos hazard in ophiolitic rock mélanges, a case study from the Ligurian Alps (Italy). Environmental Earth Sciences, 72, 3679–3698.

Virta, R.L. (1985) The phase relationship of talc and amphiboles in a fibrous talc sample., 1-16 p. Vol. 8923.

Virta, R.L. (2002) Asbestos: Geology, Mineralogy, Mining, and Uses. (Open-File Report 02-149), 1-28 p. U.S . Department of the Interior - U.S . Geological Survey. Reston, Virginia.

Viti, C., and Hirose, T. (2009) Dehydration reactions and micro/nanostructures in experimentally-deformed serpentinites. Contributions to Mineralogy and Petrology, 157, 327–338.

Viti, C., and Mellini, M. (1996) Vein antigorites from Elba Island, Italy. European Journal of Mineralogy, 8, 423–434.

Wagner, J. (2015) Analysis of serpentine polymorphs in investigations of natural occurrences of asbestos. Environmental science. Processes & impacts, 17, 985–96.

Wang, A., Dhamelincourt, P., and Turrell, G. (1988) Raman microspectroscopic study of the cation

distribution in amphiboles. Applied Spectroscopy, 42, 1441–1450.

Ward, L.K. (1937) Asbestos deposit northeast of Lyndoch on the North Para River. Min. Rev. Adelaide, 66, 58–59.

Wells, M.A., Ramanaidou, E.R., Verrall, M., and Tessarolo, C. (2009) Mineralogy and crystal chemistry of "garnierites" in the Goro lateritic nickel deposit, New Caledonia. European Journal of Mineralogy, 21, 467–483.

Whitney, D.L., and Evans, B.W. (2010) Abbreviations for names of rock-forming minerals. American Mineralogist, 95, 185–187.

Whittaker, E.J.W. (1957) The structure of chrysotile. V. Diffuse reflexions and fibre texture. Acta Crystallographica, 10, 149–156.

Whittaker, E.J.W., and Zussman, J. (1956) The characterization of serpentine minerals by X-Ray diffraction. Mineralogical Magazine and Journal of the Mineralogical Society, 31, 107–126.

WHO (1997) Determination of airborne fibre number concentrations. A recommended method, by phase-contrast optical microscopy (membrane filter method). Geneva.

Wicks, F.J. (2000) Status of the reference X-ray powder-diffraction patterns for the serpentine minerals in the PDF database—1997. Powder Diffraction, 15, 42–50.

Wicks, F.J., and O'Hanley, D.S. (1988) Serpentine minerals; structures and petrology. Reviews in Mineralogy and Geochemistry, 19, 91–167.

Wicks, F.J., and Plant, A.G. (1979) Electron-Microprobe and X-Ray-Microbeam studies of serpentine textures. Canadian Mineralogist, 17, 785–830.

Wicks, F.J., and Whittaker, E.J.W. (1975) A Reappraisal of the Structures of the Serpentine Minerals. Canadian Mineralogist, 13, 227–243.

Wicks, F.J., and Whittaker, E.J.W. (1977) Serpentine Texture and Serpentinization. Canadian Mineralogist, 15, 459–488.

Williams, C., Dell, L., Adams, R., Rose, T., and Van Orden, D.R. (2013) State-of-the-science assessment of non-asbestos amphibole exposure: Is there a cancer risk? Environmental Geochemistry and Health, 35, 357–377.

Wozniak, H., Wiecek, E., and Stetkiewicz, J. (1988) Fibrogenic and carcinogenic effects of antigorite. Polish journal of occupational medicine, 1, 192–202.

Wozniak, H., Wiecek, E., Stetkiewicz, J., and Wyszynska, K. (1993) Experimental carcinogenicity and mutagenicity of non-asbestos natural fibres - preliminary report. Polish journal of occupational medicineJ Occup Med Environ Health, 6, 55–60.

Wunder, B., and Schreyer, W. (1997) Antigorite : High-pressure stability in the system MgO-SiO2-H2O (MSH). Lithos, 41, 213–227.

Wunder, B., Wirth, R., and Gottschalk, M. (2001) Antigorite: Pressure and temperature dependence of polysomatism and water content. European Journal of Mineralogy, 13, 485–495.

Yada, K. (1967) Study of Chrysotile Asbestos by a High Resolution Electron Microscope. Acta Crystallographica, 23, 704–707.

Yada, K. (1971) Study of microstructure of chrysotile asbestos by High-Resolution Electron Microscopy. Acta Crystallographica Section A, 27, 659–664.

Yada, K., and Iishi, K. (1977) Growth and microstructure of synthetic chrysotile. American Mineralogist, 62, 958–965.

Zussman, J., Brindley, G.W., and Comer, J.J. (1957) Electron diffraction studies of serpentine minerals. American Mineralogist, 42, 133–153.

Asbestos Regulation

Arrêté n° 2010-4553/GNC du 16 novembre 2010 - Pris pour l'application de la délibération relative à la protection des travailleurs contre les poussières issues de terrains amiantifères dans les activités extractives, de bâtiment et de travaux publics. JONC du 25 Novembre 2010.

Décret n° 2015-789 du 29 juin 2015 - Relatif aux risques d'exposition à l'amiante. JORF n°0150 du 1 Juillet 2015.

Délibération n° 82 du 25 août 2010 - Relative à la protection des travailleurs contre les poussières issues de terrains amiantifères dans les activités extractives, de bâtiment et de travaux publics. JONC du 9 Septembre 2010.

D.Lgs.n257 del 25/07/2006 - Attuazione della direttiva 2003/18/CE relativa alla protezione dei lavoratori dai rischi derivanti dall'esposizione all'amianto durante il lavoro. Pubblicato nella Gazzetta Ufficiale n. 211 del 11 settembre 2006. Italia.

D.M. 06/09/1994 - Normative e metodologie tecniche di applicazione dell'art. 6, comma 3, e dell'art. 12, comma 2, della legge 27 marzo 1992, n. 257, relativa alla cessazione dell'impiego dell'amianto. Pubblicato nella Gazzetta Ufficiale n. 220 del 20 Settembre 1994.

EU (2003) - Directive 2003/18/EC of the European Parliament and of the Council of 27 March 2003 amending Council Directive 83/477/EEC on the protection of workers from the risks related to exposure to asbestos at work. Official Journal L 097, 15/04/2003 P.0048-0052.

ISO 22262-2:2014 - Air quality - Bulk materials - Part 2: Quantitative determination of asbestos by gravimetric and microscopical methods.

NF X 43-050 (Janvier 1996) - Qualité de l'air - Détermination de la concentration en fibres d'amiante par microscopie électronique à transmission - Méthode indirecte.

XP X 43-269 (Mars 2002) - Qualité de l'air - Air des lieux de travail - Détermination de la concentration en nombre de fibres par microscopie optique en contraste de phase - Méthode du filtre à membrane. AFNOR (Indice de classement: X43-269).

XP X 43-269 (Avril 2012) - Qualité de l'air - Air des lieux de travail - Prélèvement sur filtre à membrane pour la détermination de la concentration en nombre de fibres par les techniques de microscopie: MOCP, MEBA et META - Comptage par MOCP. AFNOR (Indice de classement: X43-269)

SUPPLEMENTARY MATERIALS

ANNEXE I

Samples classification according to mining criteria (on field survey): ANTIGORITE *#1*

- Samples subjected to misinterpretations are marked with a pink rhombus -
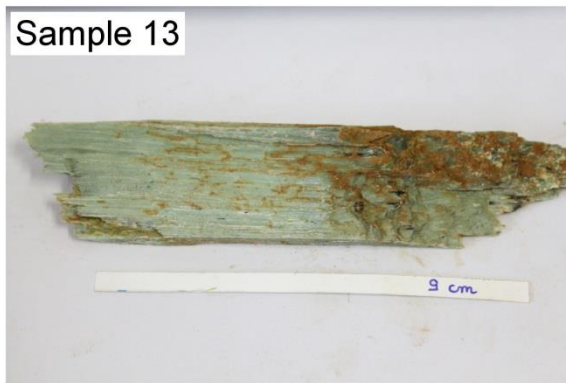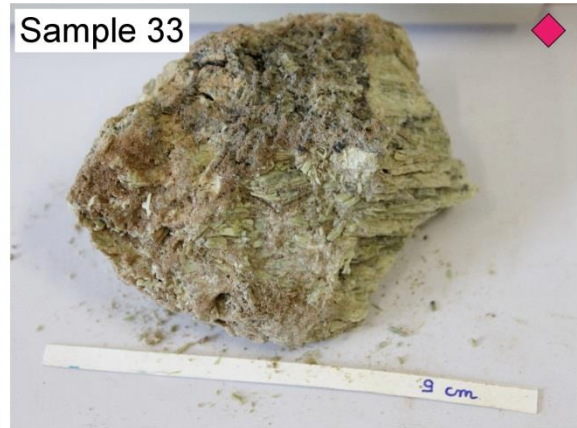
Samples classification according to mining criteria (on field survey): ANTIGORITE *2*

Sample 3

Sample 4

Sample 5

Sample 7

Sample 9

Sample 27

Sample 6

Sample 16

Sample 29

Sample 18

Sample 14
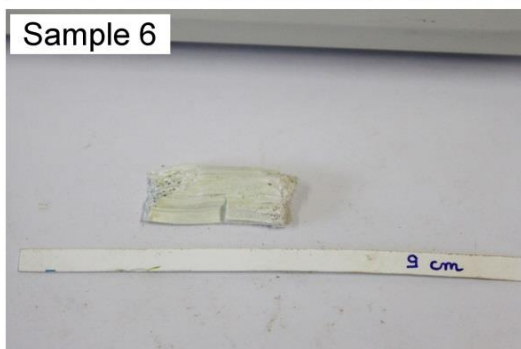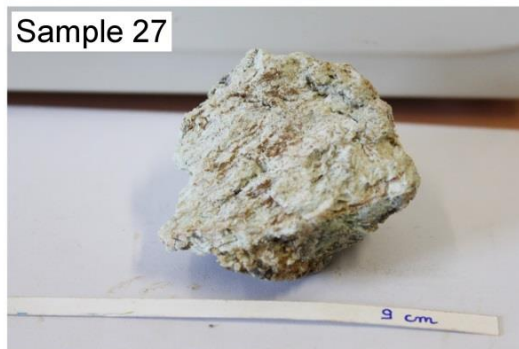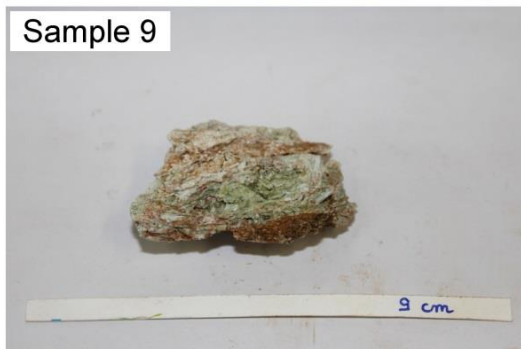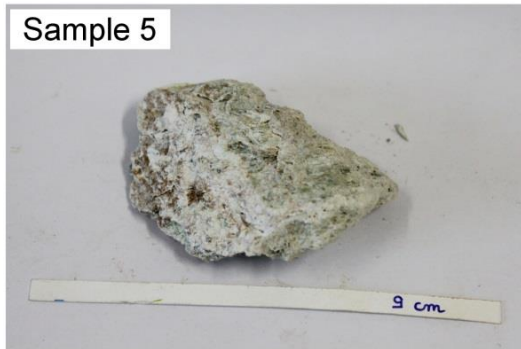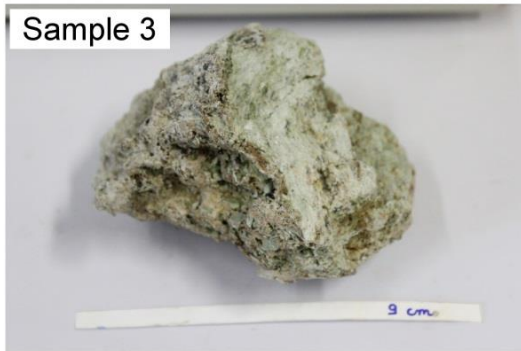
Sample 31

Sample 20

Samples classification according to mining criteria (on field survey): ANTIGORITE *#4*

Sample 10

Sample 12

Sample 17

Sample 24

Sample 25

Sample 26

Sample 35

Sample 8

Sample 15
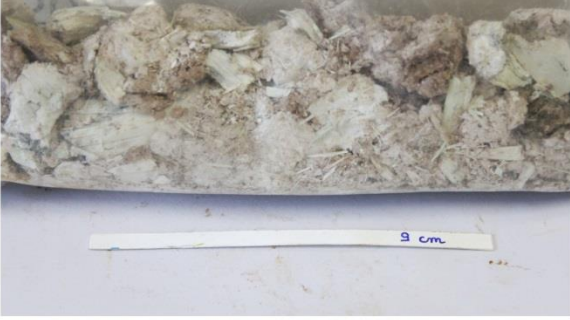
Sample 1

Sample 21
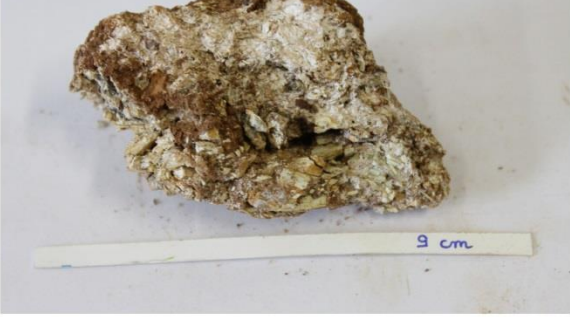
Sample 22

ANNEXE I

Samples classification according to mining criteria (on field survey): TREMOLITE

Sample 41 #1

Sample 37 #2

Sample 42 #2

Sample 45 #2

Sample 46 #2

Sample 38 #2

Sample 48 #2

Sample 47 #2

Sample 55 #2

Sample 36 #4
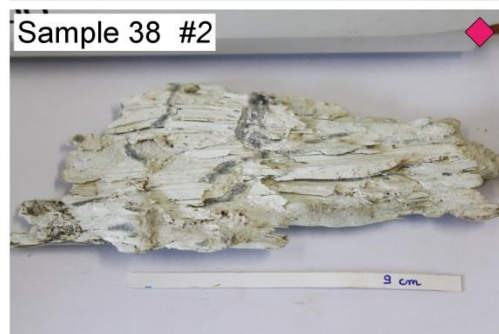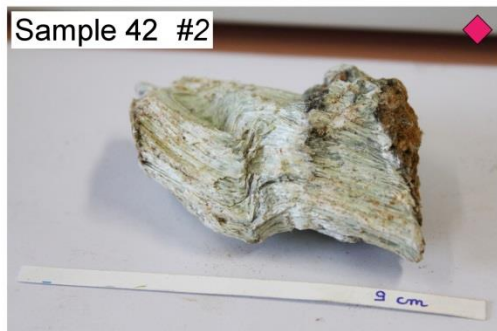
ANNEXE I

Samples classification according mining criteria (on field survey): NOT IDENTIFIED FIBRES

Sample 40 #2

Sample 39 #4

ANNEXE II

Mineral identification of samples

- Minerals abbreviations follow the convention described by Whitney and Evans (2010)*: Srp = serpentine; Atg = antigorite; Lz = lizardite; Ctl = chrysotile; Tr = tremolite; Chl = chlorite; Tlc = talc; Px = pyroxene; Qz = quartz; Ox = oxides; Mag = magnetite; Gth = goethite -*

SAMPLES

	1	3	4	5	6	7	8	9	10	11	12
Mining Nomenclature	Antigorite #4	Antigorite #2	Antigorite #2	Antigorite #2	Antigorite #2	Antigorite #2	Antigorite #4	Antigorite #2	Antigorite #4	Antigorite #1	Antigorite #4
PLM	Atg + Ox	Srp + Ox	Srp + Qz + Ox	Srp + Ox	Srp + Ox	Srp + Ox	Srp + Ox + Qtz + Px	Srp (Atg)	Srp (Atg) + Qz	Srp (Atg)	Srp + Tlc + Ox
PLM/DS *Arpae Lab.*	—	—	RI 1.5680 & 1.550 Srp group	—	RI 1.5680 Atg	—	—	—	—	—	—
XRPD *UNC-ISEA Lab.*	Atg	Atg + Mag	Atg + Mag	Atg + Mag	Atg	Atg + Mag	Atg + Gth	Atg	Atg + Qz	Atg	Atg + Tlc + Qz
XRPD* *UNC-ISEA Lab.*	Atg	Atg	Atg + Ctl ?	Atg	Atg	Atg	Atg + Gth + Mag + Qz	Atg	Atg + Qz	Atg	Atg + Qz + Gth
XRPD* *UniPR - SCVSA Dep.*	Atg	Atg + Lz?	Atg + Qz	Atg	Atg	Atg + Lz	Atg (Lz?) + Gth + Mag + Qz	Atg +?	Atg + Qz	Atg	Atg + Qz
SEM/EDS	Atg	Atg	Atg + Ctl ?	Atg	Atg	Atg + ?	Atg	Atg + Ctl ?	Atg + Ctl?	Atg + Ctl	Atg (+Ctl?) + Tlc
TEM/SAED/STEM	—	—	—	—	—	—	—	—	—	—	—
micro-Raman	—	—	—	—	—	—	—	Atg + Ctl	—	Atg + Ctl	—
Raman portatile	Atg	Atg	Atg + Ctl	Atg	Atg + ?	Atg + ?	n.a.	Atg	Atg + Ctl	Atg	n.a.

n.a. = not available; * performed on the same sample powder

|	13	14	15	16	17	18	19	20	21	22	23
Mining Nomenclature	Antigorite #1	Antigorite #2	Antigorite? #4	Antigorite? #2	Antigorite #4	Antigorite #2	Antigorite #1	Antigorite #2	Antigorite #4	Antigorite? #4	Antigorite #1
PLM	Atg	Atg	—	Atg + Ctl + Qz	Atg + Ctl + Ox	Srp (?) + Ox	Atg + Ox	Srp (Atg)	Atg+ Ctl ?	Srp	—
PLM/DS Arpae Lab.	—	—	RI 1.5680 Atg	RI 1.5680 Srp group	—	RI 1.5680 Srp group (?)	—	—	—	RI 1.5680 Atg	—
XRPD UNC-ISEA Lab.	Atg + Mag	Atg	Atg + Qz	Atg + Qz	Atg	Atg + Ctl + Mag	Atg	Atg	Atg	Atg	Ctl
XRPD* UNC-ISEA Lab.	Atg + Mag	Atg	Atg	Atg + Qz	Atg	Atg + Ctl + Mag	Atg	Atg + ?	Atg + Mag	Atg	—
XRPD* UniPR - SCVSA Dep.	Atg	Atg	Atg	Atg + Qz	Atg	Atg + Ctl + Mag	Atg	Atg + Lz?	Atg	Atg!	—
SEM/EDS	Atg	Atg	Atg	Atg + Ctl	Atg	Ctl + Atg	Atg	Atg	Atg	Atg	Ctl
TEM/SAED/STEM	—	—	—	—	—	Atg + Ctl	—	—	—	—	—
micro-Raman	Atg	—	—	—	—	Atg (?)	Atg	—	—	—	—
Raman portatile	Atg	Atg	Atg	Atg + ?	Atg + Ctl	Atg + ?	Atg	Atg	n.a.	n.a.	—

n.a. = not available; * performed on the same sample powder

|	24	25	26	27	29	30	31	32	33	34	35	36
Mining Nomenclature	Antigorite #4	Antigorite #4	Antigorite #4	Antigorite #2	Antigorite #2	Antigorite #1	Antigorite #2	Antigorite #1	Antigorite #1	Antigorite #1	Antigorite #4	Tremolite #4
PLM	Srp (Atg) + Ox	Srp (Atg) + Ox	Atg + Ox	Srp (Atg)	n.a.	Atg + Ctl?	Srp	Atg + Ctg	Ctl	Atg + Ctl?	Srp (Atg)	Tr + Srp (Atg)
PLM/DS *Arpae Lab.*	—	—	—	—	—	—	—	—	RI 1.550 Ctl	—	—	RI 1.605 Tr
XRPD *UNC-ISEA Lab.*	Atg + Mag	Atg + Mag	Atg	Atg + Mag	Atg	Atg + Mag	Atg	Atg	Ctl + Mag	Ctl + Mag	Atg	Tr + Atg (Lz?)
XRPD* *UNC-ISEA Lab.*	Atg	Atg	Atg + Lz?	Atg	Atg	Atg	Atg	Atg + Lz?	Ctl	Atg	Atg + Lz?	Tr + Srp (Lz?)
XRPD* *UniPR - SCVSA Dep.*	Atg	Atg + Lz?	Atg	Atg? Lz?	Atg? Lz?	Atg? Lz?	Atg	Atg + Gth	Ctl	Atg	Atg + ?	Tr + Atg
SEM/EDS	Atg	Atg	Atg	Atg	Atg + Ctl	Atg + Ctl	Atg + Ctl?	Atg + Ctl	Ctl	Atg + Ctl	Atg	Tr + Atg
TEM/SAED/STEM	—	—	—	—	—	—	—	—	Ctl	—	—	—
micro-Raman	—	—	—	—	—	Atg + Ctl	—	—	Ctl	—	Atg	—
Raman portatile	Atg	Atg	Atg	Atg	Atg + ?	Atg + ?	Atg	Atg	Ctl	Atg + ?	Atg	Tr

n.a. = not available; * performed on the same sample powder

	37	38	39	40	41	42	45	46	47	48	55	57
Mining Nomenclature	Tremolite #2	Tremolite? #2	Fibre? #4	Fibre? #2	Tremolite #1	Tremolite #2	Tremolite #2	Tremolite #2	Tremolite #2	Tremolite? #2	Tremolite #2	Chrysotile #3
PLM	n.a.	Srp (Atg) + Ox	Atg + Qz	Atg + Ctl + Qz	Tr + Srp (Atg)	Tr + Srp	Tr + Srp	Tr	Tr + Srp (Atg)	Srp (Atg)	Tr + Srp + Chl	Srp (Ctl) + Ox
PLM/DS *Arpae Lab.*	RI 1.605 Tr	RI 1.5680 Srp group	RI 1.5680 & 1.550 Atg	RI 1.5680 & 1.550 Srp group	—	—	—	—	—	RI 1.605 No Tr	RI 1.605 Tr	RI 1.550 Ctl
XRPD *UNC-ISEA Lab.*	Tr + Atg (Lz?)	Atg + Gth	Atg + Qz	Atg + Qz	Tr + Atg	Tr + Atg	Tr + Atg	Tr + Atg	Tr + Atg + Gth	Atg	Tr + Atg	Ctl + Mag
XRPD* *UNC-ISEA Lab.*	Tr + Srp (Lz?)	Atg	Atg + Lz? + Qz	Atg	Tr + Srp (Lz?)	Tr + Srp (Lz?)	Tr + Srp (Lz?)	Tr + Srp (Lz?)	Tr + Atg + Gth	Atg	Tr + Srp (Atg) + Chl	Ctl
XRPD* *UniPR - SCVSA Dep.*	Tr + Atg	Atg	Atg + Lz? + Qz	Atg	Tr + Atg	Tr + Atg	Tr + Atg	Tr + Atg	Tr + Atg + Ox?	Atg	Tr + Atg	Ctl
SEM/EDS	Tr	Atg + Ctl?	Atg	Atg + Ctl ?	Tr + Atg	Tr	Tr + Srp	Tr + Srp (Atg)	Tr + Srp	Atg	Tr + ?	Ctl
TEM/SAED/STEM	—	—	—	—	—	—	—	—	—	—	—	Ctl
micro-Raman	—	Atg + Ctl?	—	—	—	—	—	—	—	—	—	—
Raman portatile	Tr	Atg	Atg	Atg	Tr	Tr	Tr	Tr	Tr	Atg	Tr	Ctl

n.a. = not available; * performed on the same sample powder

ANNEXE III

SEM images acquired with Secondary Electron (SEI) of ANTIGORITE blades. Various morphological features, from lath-shaped to fibrous-lamellar crystals, are depicted.
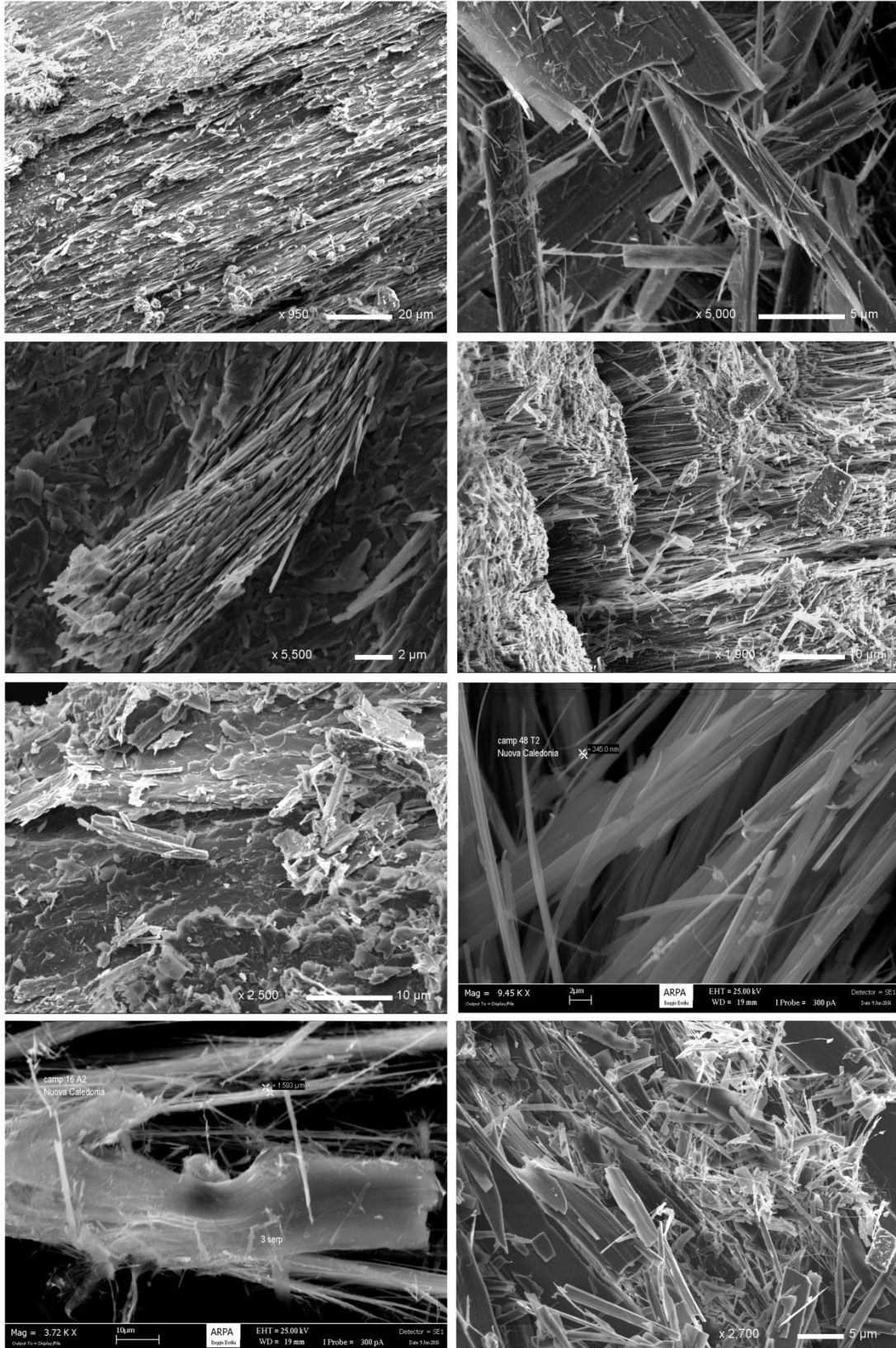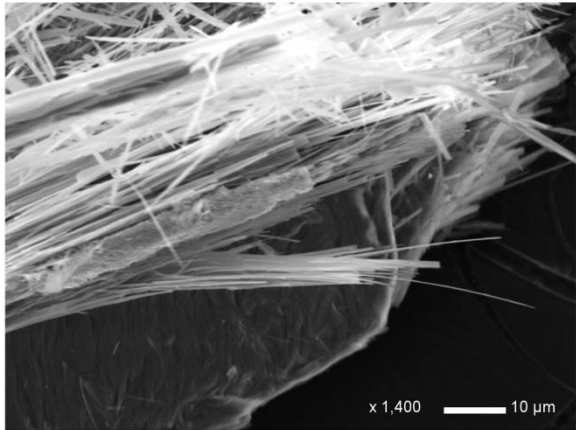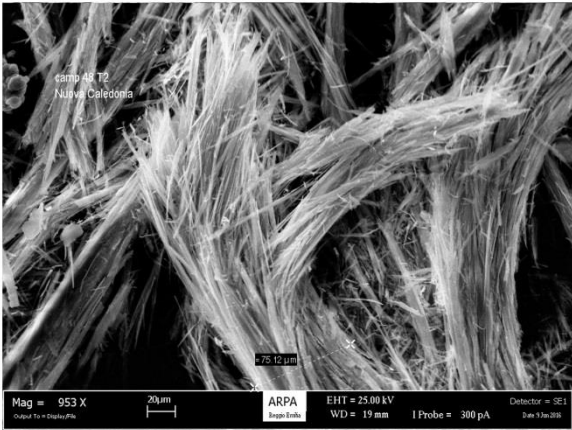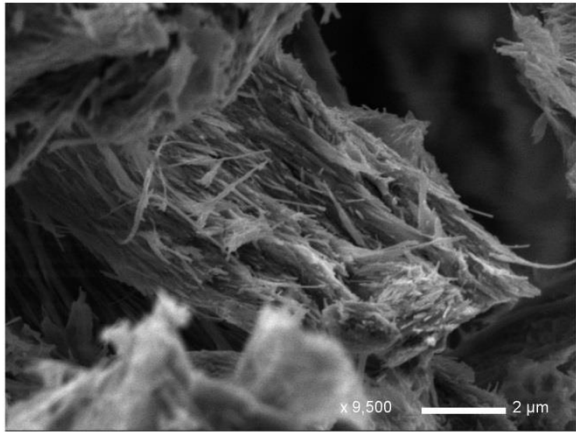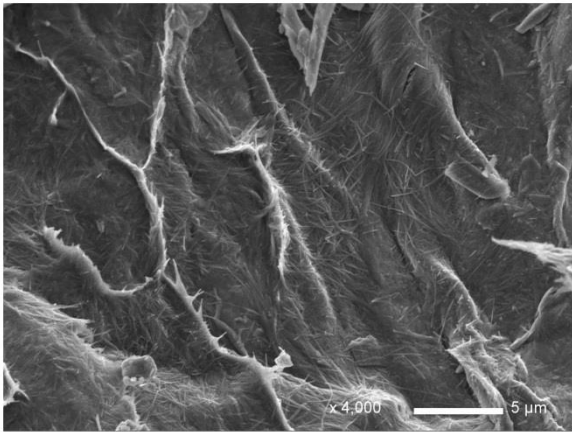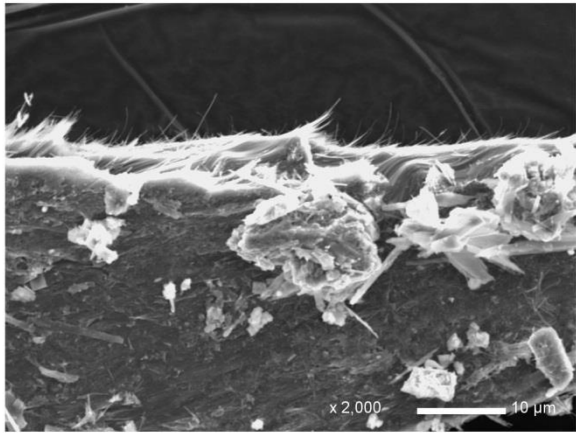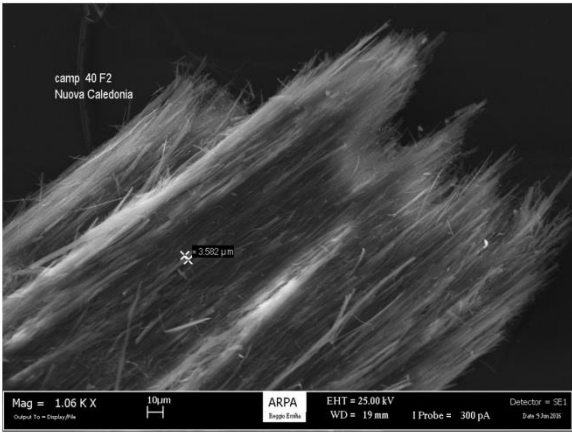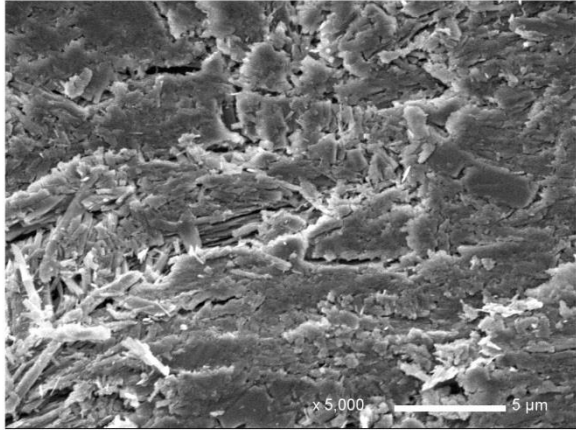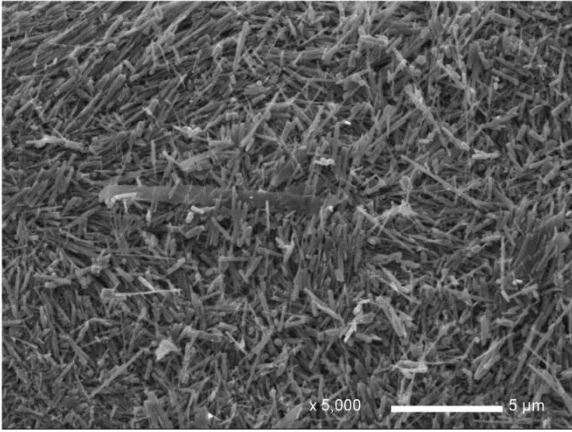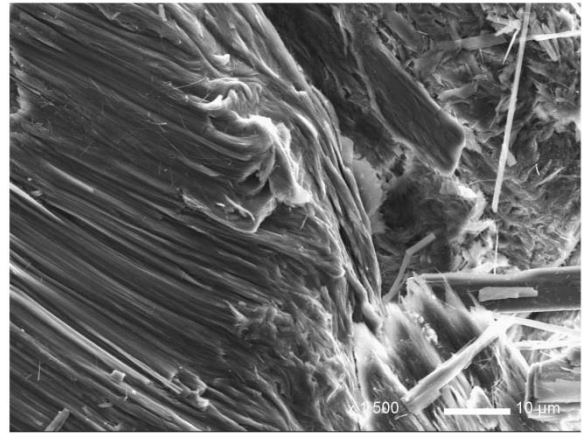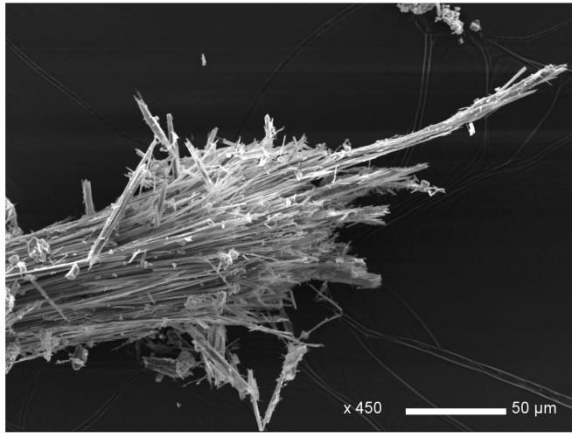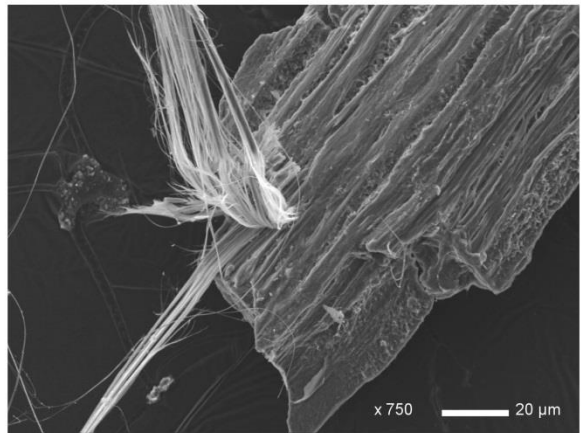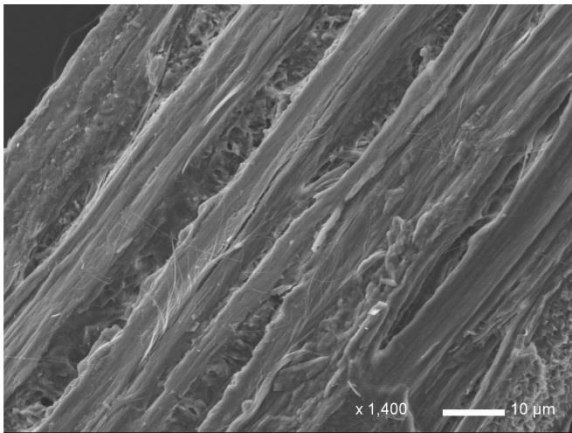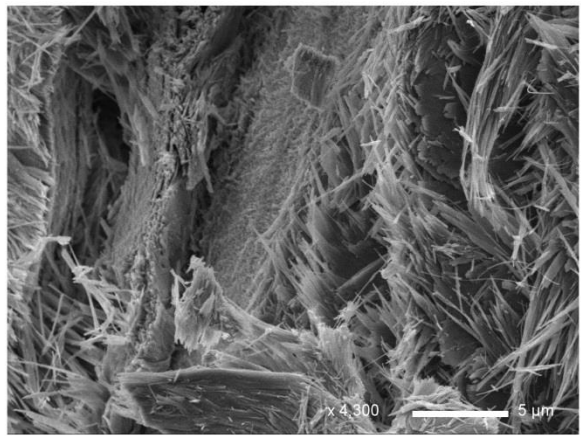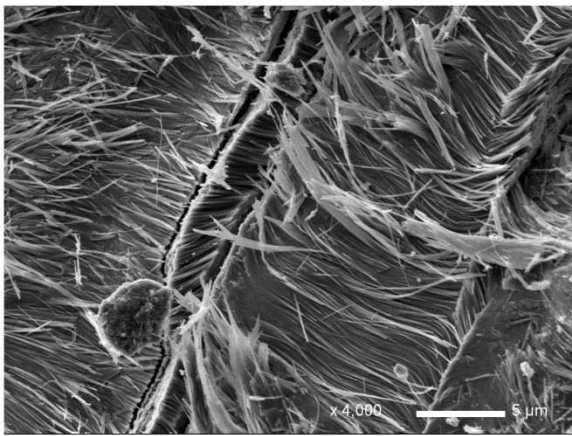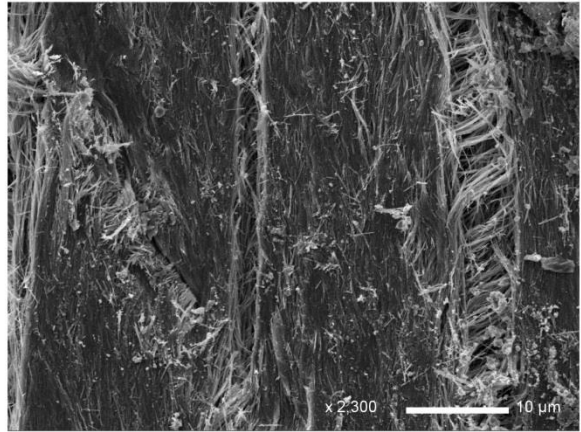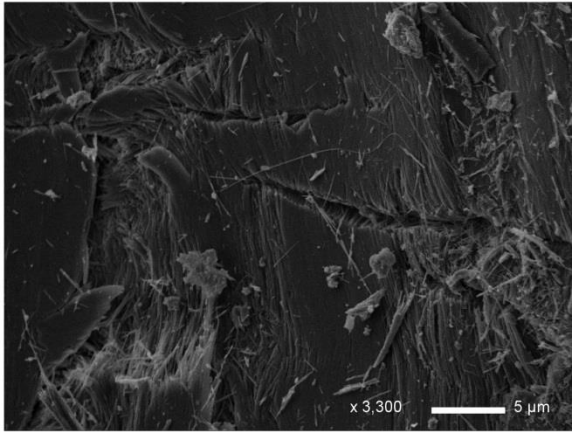
ANNEXE III

SEM images (SEI) of CHRYSOTILE fibres. Various morphological features are observed.
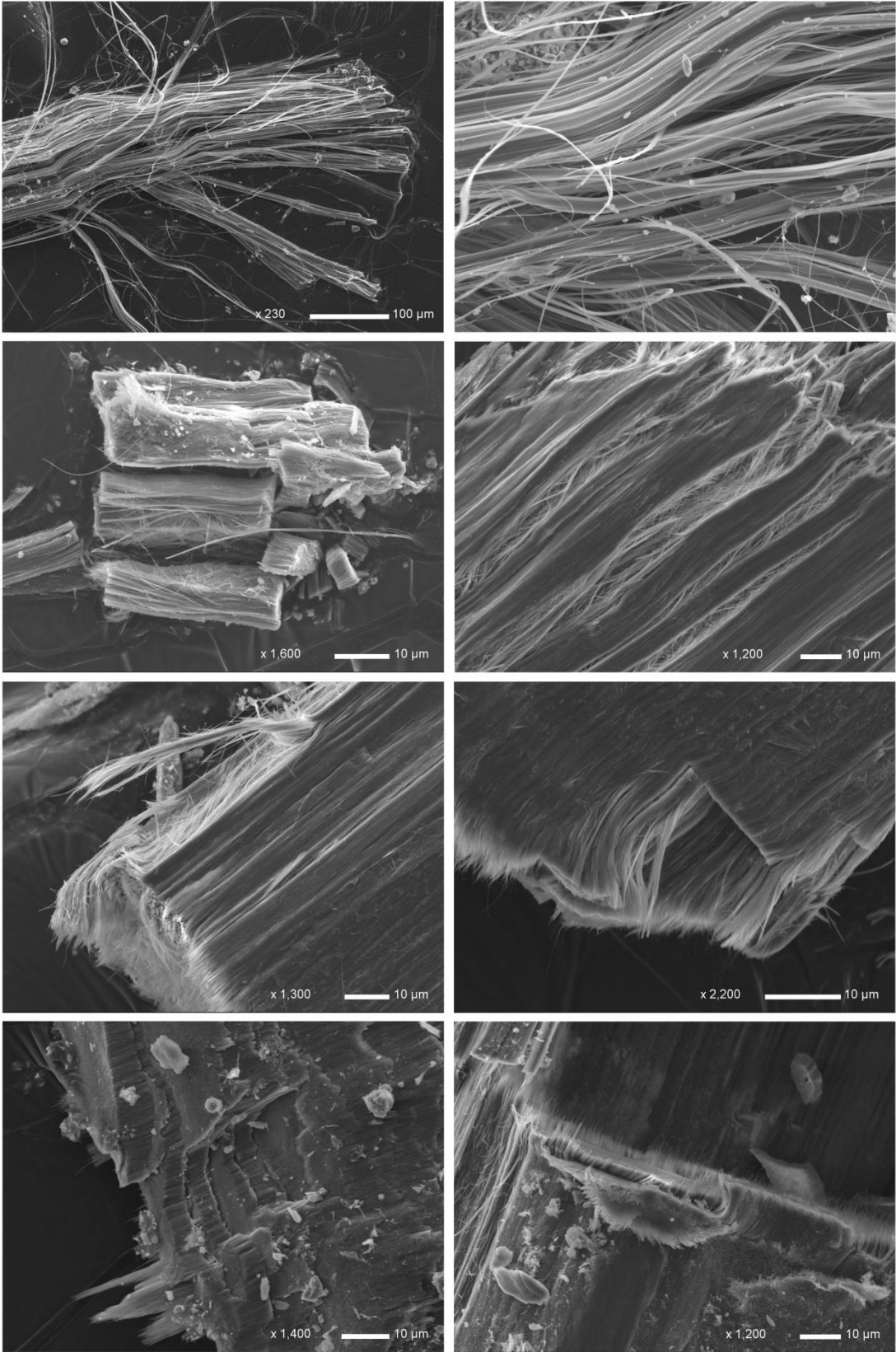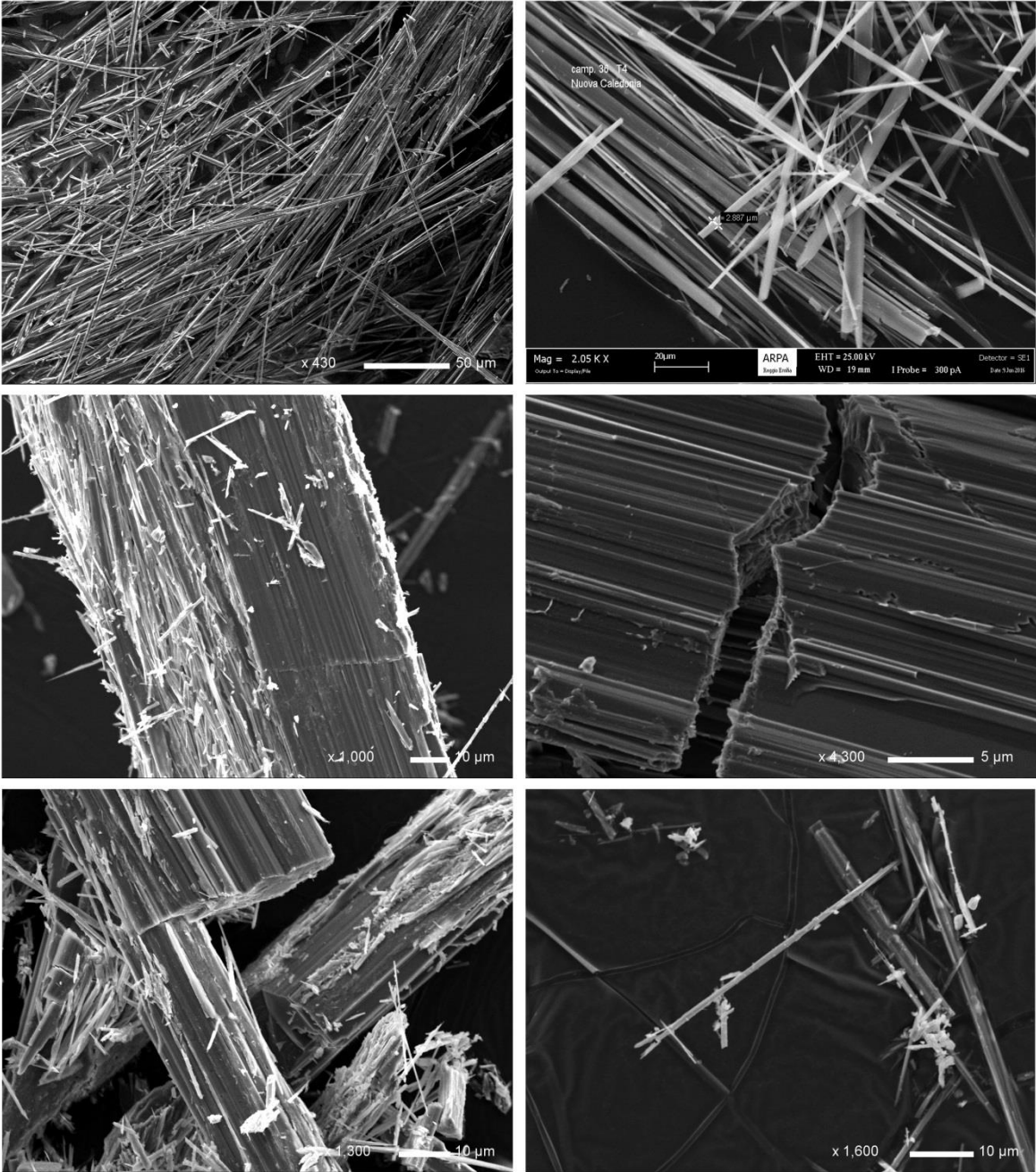
ANNEXE III

SEM images (SEI) of TREMOLITE, depicting its characteristic acicular, needle-like shape.

ANNEXE IV
Chemical composition of New Caledonian samples.

- MAJOR ELEMENT CONCENTRATIONS -

SAMPLE	P (ppm)	P$_2$O$_5$ (wt.%)	Na (ppm)	Na$_2$O (wt.%)	Mg (ppm)	MgO (wt.%)	K (ppm)	K$_2$O (wt.%)	Ca (ppm)	CaO (wt.%)	Mn (ppm)	MnO (wt.%)	Fe (ppm)	FeO$_{tot}$ (wt.%)	Al (ppm)	Al$_2$O$_3$ (wt.%)
1	17.38	0.00	63.27	0.01	169558.44	28.12	32.92	0.00	64.17	0.01	673.84	0.09	35274.59	4.54	1394.68	0.264
3	17.00	0.00	28.09	0.00	157516.15	26.12			64.83	0.01	865.50	0.11	121313.08	15.61	1525.59	0.288
4	14.17	0.00	62.72	0.01	175733.21	29.14			302.70	0.04	616.36	0.08	66952.89	8.61	1037.61	0.196
5	16.89	0.00	53.52	0.01	171770.20	28.48			526.69	0.07	819.74	0.11	43089.10	5.54	1757.16	0.332
6	20.49	0.00	34.12	0.00	167222.62	27.73	68.96	0.01	117.35	0.02	415.52	0.05	13370.45	1.72	691.15	0.131
7	27.41	0.01	41.81	0.01	178879.42	29.66	12.07	0.00	81.10	0.01	630.62	0.08	30134.95	3.88	600.94	0.114
8	17.58	0.00	112.18	0.02	166911.21	27.68			55.79	0.01	723.07	0.09	56045.90	7.21	1615.74	0.305
9	17.03	0.00	18.75	0.00	179162.85	29.71			60.71	0.01	671.58	0.09	24270.89	3.12	1542.96	0.292
10	19.50	0.00	32.64	0.00	173307.88	28.74	13.30	0.00	33.05	0.00	655.85	0.08	31777.20	4.09	2852.91	0.539
11	16.52	0.00	25.67	0.00	177773.60	29.48	54.61	0.01	66.22	0.01	634.44	0.08	28691.83	3.69	184.80	0.035
12	31.23	0.01	91.70	0.01	156739.78	25.99			109.54	0.02	1634.93	0.21	87243.72	11.22	2830.89	0.535
13	40.51	0.01	17.34	0.00	205362.31	34.05	15.64	0.00	19.62	0.00	1026.22	0.13	108891.85	14.01	869.12	0.164
14	18.16	0.00	21.66	0.00	183281.20	30.39	45.92	0.01	48.11	0.01	534.33	0.07	28176.61	3.62	1654.86	0.313
15	14.61	0.00	29.78	0.00	193283.59	32.05			68.24	0.01	668.69	0.09	21361.72	2.75	881.57	0.167
16	12.06	0.00	2.47	0.00	165235.43	27.40	38.96	0.00	47.23	0.01	299.74	0.04	13789.71	1.77	582.64	0.110
17	12.01	0.00	67.88	0.01	178100.53	29.53	19.00	0.00	35.72	0.00	660.89	0.09	32804.96	4.22	1233.31	0.233
18	17.81	0.00	13.72	0.00	186493.56	30.92			55.13	0.01	311.15	0.04	29250.05	3.76	393.80	0.074
19	31.49	0.01	17.19	0.00	185228.17	30.71	35.60	0.00	53.93	0.01	706.12	0.09	20541.57	2.64	858.69	0.162
20	10.05	0.00	45.17	0.01	180010.62	29.85			60.06	0.01	630.41	0.08	24745.99	3.18	1353.26	0.256
21	18.99	0.00	186.71	0.03	191476.69	31.75			73.11	0.01	472.57	0.06	29917.47	3.85	2932.82	0.554
22	17.23	0.00	172.59	0.02	177468.31	29.43			139.88	0.02	681.10	0.09	32765.58	4.22	1842.05	0.348
23	13.85	0.00	28.55	0.00	174279.64	28.90			41.94	0.01	336.85	0.04	15806.68	2.03	961.75	0.182
24	13.37	0.00	25.84	0.00	166792.50	27.66			31.96	0.00	996.48	0.13	112101.48	14.42	1070.45	0.202

SAMPLE	P ppm	P$_2$O$_5$ wt.%	Na ppm	Na$_2$O wt.%	Mg ppm	MgO wt.%	K ppm	K$_2$O wt.%	Ca ppm	CaO wt.%	Mn ppm	MnO wt.%	Fe ppm	FeO$_{tot}$ wt.%	Al ppm	Al$_2$O$_3$ wt.%
25	16.76	0.00	73.96	0.01	165521.90	27.45			53.43	0.01	1007.57	0.13	51302.35	6.60	1906.85	0.360
26	15.04	0.00	39.27	0.01	171542.12	28.45			38.64	0.01	743.90	0.10	33564.44	4.32	1584.55	0.299
27	12.73	0.00	24.11	0.00	159226.28	26.40			70.73	0.01	937.71	0.12	103434.59	13.31	1109.78	0.210
29	14.04	0.00	62.33	0.01	175508.74	29.10			84.22	0.01	688.37	0.09	27137.84	3.49	1337.42	0.253
30	18.57	0.00	58.85	0.01	177196.52	29.38			36.61	0.01	686.75	0.09	34256.25	4.41	949.44	0.179
31	16.33	0.00	45.90	0.01	183993.39	30.51			55.23	0.01	309.19	0.04	23873.68	3.07	228.98	0.043
32	17.52	0.00	100.26	0.01	178269.77	29.56	31.44	0.00	64.92	0.01	553.23	0.07	29018.32	3.73	2221.71	0.420
33	14.25	0.00	13.14	0.00	171788.63	28.49			64.25	0.01	675.93	0.09	54439.64	7.00	870.31	0.164
34	31.67	0.01	35.81	0.00	158420.90	26.27			32.61	0.00	391.55	0.05	74356.34	9.57	877.05	0.166
35	23.37	0.01	100.16	0.01	180566.62	29.94			74.19	0.01	908.89	0.12	49472.58	6.36	1353.54	0.256
36	19.93	0.00	4266.21	0.58	125711.69	20.85	57.67	0.01	87952.12	12.31	544.32	0.07	15440.92	1.99	8793.27	1.661
37	27.19	0.01	4591.48	0.62	126992.99	21.06	86.27	0.01	89276.01	12.49	582.26	0.08	15359.72	1.98	8986.51	1.698
38	16.11	0.00	74.70	0.01	174682.94	28.97			64.13	0.01	469.52	0.06	31790.64	4.09	561.06	0.106
39	16.26	0.00	119.06	0.02	175222.11	29.06			59.19	0.01	429.11	0.06	16277.80	2.09	597.73	0.113
40	13.76	0.00	42.52	0.01	170721.55	28.31			45.10	0.01	277.50	0.04	11535.11	1.48	586.30	0.111
41	16.74	0.00	3288.32	0.44	125387.29	20.79	65.33	0.01	79678.08	11.15	611.27	0.08	14499.87	1.87	6790.66	1.283
42	26.14	0.01	3373.74	0.45	130769.17	21.68			81627.18	11.42	620.93	0.08	15413.00	1.98	7381.04	1.395
45	21.54	0.00	4435.06	0.60	124596.41	20.66	156.18	0.02	87830.75	12.29	546.21	0.07	16038.77	2.06	8628.66	1.630
46	29.74	0.01	4482.08	0.60	121870.96	20.21	70.40	0.01	88578.22	12.39	578.14	0.07	16529.28	2.13	8524.73	1.611
47	21.49	0.00	3826.94	0.52	142433.18	23.62	133.80	0.02	52191.47	7.30	1419.31	0.18	22773.65	2.93	11869.89	2.243
48	17.62	0.00	111.46	0.02	174031.61	28.86			81.69	0.01	674.52	0.09	36318.93	4.67	1652.22	0.312
55	20.11	0.00	2423.95	0.33	139486.07	23.13	68.19	0.01	36362.61	5.09	1595.41	0.21	23911.71	3.08	9452.57	1.786
57	21.99	0.01	78.45	0.01	163886.98	27.18			192.68	0.03	404.19	0.05	45772.93	5.89	135.66	0.026

- TRACE ELEMENT CONCENTRATIONS -

SAMPLE	Dilution	7 Li Conc. [ppb]	45 Sc Conc. [ppb]	51 V Conc. [ppb]	52 Cr Conc. [ppb]	55 Mn Conc. [ppb]	59 Co Conc. [ppb]	60 Ni Conc. [ppb]	65 Cu Conc. [ppb]	66 Zn Conc. [ppb]	75 As Conc. [ppb]
SLRS 6	1.01	0.51994	0.36674	0.36546	0.24613	2.16107	0.05641	0.59995	25.72210	2.08991	0.63715
SLRS 6-2	1.01	0.53883	0.42459	0.36482	0.24900	2.19889	0.05086	0.53032	25.22223	2.10498	0.58455
UBN1	1840.1	19200.70579	10750.07559	60035.35561	2150015.55951	861808.76987	94030.19985	1739902.01613	21812.28053	79393.11224	10306.46618
UBN2	1865.2	18745.85949	11194.39474	58995.81842	2013708.48696	865586.65872	93337.07730	1742319.61218	21614.29142	70832.65190	10438.41992
Ben1	7573.6	9093.37131	19471.00706	195791.41955	329882.02705	1413882.05106	55668.24268	244981.90866	63829.27063	116179.63528	2823.17012
Ben2	7573.6	8117.62018	19288.10936	197983.14049	307025.73501	1323999.19889	51468.75451	222753.06589	57729.58346	104265.02687	2575.04524
1	1954.4	639.86724	6734.22040	9033.55478	712373.50424	692445.37927	87743.54247	4092000.51589	735.79363	34086.27028	782.54675
3	1838.9	384.40385	417.97599	21644.66637	16523.23390	865195.61878	74229.73791	2430267.63217	540.45797	32647.90810	190.80015
4	1948.4	629.06660	212.60693	10940.17699	12763.77024	607462.43516	38032.00220	1150710.44687	1933.23249	28637.29682	1135.93935
5	1980.2	333.47250	2772.33635	9333.21405	57468.07461	810632.53009	51636.24731	3295576.78914	567.69306	32038.60099	402.49124
6	1814.7	181.81769	1041.10394	4816.92885	44236.93893	421003.34502	109490.32990	1970025.10147	5099.22894	22760.19173	223.36712
7	1868.9	597.75815	253.63690	4783.47684	76242.59109	637404.12466	69415.12746	12716673.87525	10816.22535	24952.34354	200.22314
8	1935.4	5943.61797	3458.82668	15558.30652	951993.09754	701660.94610	70863.92775	3930101.11481	3996.71245	43670.40141	1413.79380
9	1864.5	460.07692	360.95419	4750.52875	13770.25625	661800.72666	49708.15719	3109001.64705	562.91707	32671.01139	273.79725
10	1852.2	846.28297	1768.57343	10730.44106	332786.93077	640881.26511	60137.01471	4029968.97515	868.38418	33516.95473	407.79971
11	1873.1	313.40122	276.39449	1378.29665	51098.82753	625191.73230	96416.62388	2184617.92824	257.99541	19486.30894	181.89767
12	1944.6	877.07419	7653.83815	30795.02825	1938742.49899	1530128.45615	183274.75426	5372403.77787	10090.16968	201752.03658	2068.57321
13	1883.1	352.81879	164.80278	10560.97217	18561.30606	779587.66485	245007.29662	12643460.30910	316.60450	34686.92103	171.69812
14	1966.2	3319.52224	1092.85734	11832.40819	38045.31914	503812.05722	71181.17237	4354041.76370	352.16815	48889.21206	5153.65447
15	1981.7	289.31906	1493.38417	6893.22384	231784.33225	632573.42116	174066.25682	2374714.35097	5417.14252	35576.36555	157.54977
16	1863.4	328.81160	1594.87660	6281.99712	157202.92696	293845.65109	27362.34412	1288760.12595	34183.74889	16212.54635	1325.56049
17	1950.1	430.29138	789.92113	7973.71525	52654.54156	650550.67150	56786.99799	1380521.28163	612.06941	26861.73770	428.99294
18	1964	56.44623	2277.64670	2259.97359	55982.09688	298271.83003	62271.21158	3941887.20802	368.42338	14003.87813	941.32642
19	1966.4	408.27130	468.55446	5118.26345	42437.47851	679867.25000	315063.30000	16797500.50825	565.76899	54471.00046	142.21107
20	1961.5	51.45343	1755.32227	5196.62074	11128.27150	636898.80017	79034.62989	1579272.94731	338.64730	25934.47217	83.62452

SAMPLE	Dilution	7 Li Conc. [ppb]	45 Sc Conc. [ppb]	51 V Conc. [ppb]	52 Cr Conc. [ppb]	55 Mn Conc. [ppb]	59 Co Conc. [ppb]	60 Ni Conc. [ppb]	65 Cu Conc. [ppb]	66 Zn Conc. [ppb]	75 As Conc. [ppb]
21	1863.2	6211.78984	2301.20002	11939.08040	243110.05252	425863.27911	75825.18089	3719682.10598	505.15377	169523.20739	12160.14048
22	1996.9	86.48398	1791.36727	6572.83177	214594.41626	643642.46192	102425.74102	1790459.41887	761.31821	28029.59868	1418.23131
23	1869.1	79.61531	1388.88718	5829.33454	13347.62105	324355.80943	54430.96049	1783675.40607	249.83943	18745.85468	161.14079
24	1975.6	1370.96342	554.77139	20220.12679	36675.76609	930220.76170	96883.66178	922083.97864	1972.47163	30910.38963	149.06366
25	1770.1	494.69377	2318.54255	9687.81625	138290.68612	978169.10096	77668.58167	4788554.55221	1009.57203	37024.39832	433.43870
26	1891.3	427.91667	1143.62811	6725.71750	9460.70876	753371.76594	43398.23369	2392399.46273	312.08508	29090.27675	251.71129
27	1923.7	202.92284	334.60007	11367.39823	23598.74847	952036.01308	70234.74858	950321.82137	462.79772	27416.58549	255.28328
29	1960.6	227.82612	2430.12148	11361.87253	290164.34211	690838.48119	431438.79839	3899547.63748	6081.20671	181516.71451	219.07394
30	1855.7	211.26704	1402.75005	5986.10813	356783.22673	685892.45352	462852.94014	4504328.67261	25296.47328	181442.95067	142.32468
31	1958.6	162.11324	1549.83885	2001.29600	334109.32859	300450.64509	55549.08532	2490701.75623	502.94557	13623.60747	446.63267
32	1848.4	10669.20831	2661.90682	12185.76230	72137.56290	544842.98681	79369.71725	5557243.62986	386.07075	75391.32117	24458.54593
33	1788.6	142.74745	649.15111	11890.51136	20202.80609	666854.86219	97959.00410	1498910.02074	295.92711	19778.41665	221.22417
34	1761.2	69.69099	1338.53944	7791.19336	402623.45002	383323.17235	819050.60592	12566854.20484	4304.85699	219045.75780	216.57870
35	1914.9	624.64213	2537.58610	10308.52587	822333.83685	854217.89149	451499.99017	6733206.07156	1365.42430	97962.73978	165.02597
36	1868.4	871.28204	11598.25732	204199.45002	2856006.08732	500831.46820	22348.52499	1748004.24377	880.59549	6833.98450	43.20374
37	1835.9	830.69644	11606.16818	217998.56791	2920673.61498	526441.90186	21172.00924	2030312.19537	246.25975	5709.72037	70.72253
38	1981.3	111.82601	2449.22178	6556.63687	23029.19036	440923.88026	69468.54048	1730802.46962	401.81625	12883.34466	538.83988
39	1944.1	229.43748	1488.69050	7545.94095	102932.90860	415382.57272	31155.02466	2489110.82174	8510.27246	14868.97106	412.02096
40	1867.4	151.18622	925.44043	3606.69937	3597.36507	273289.34881	12722.11116	1575806.34264	1658.00300	10424.25956	187.80361
41	1812.4	1271.21441	6738.11255	172201.86433	1969292.11758	555553.41203	30128.07718	839605.12526	318.12539	8244.96006	60.56058
42	2000.6	1170.40313	9960.52988	159503.81885	2137340.72777	546892.20796	35216.07651	4840098.86725	179.92313	7602.37750	92.07322
45	1929.6	2197.75124	10094.84681	192269.07644	2180986.20466	504337.24994	176367.72124	3327027.68129	345.70890	48701.80701	115.92312
46	1769.2	2158.24858	9353.11298	193370.60040	2016053.06799	519333.18854	172545.66413	3338410.99910	332.62307	49511.14779	120.68294
47	1844.4	590.37016	15811.01357	68984.47848	1609714.04975	1249114.65370	483826.35381	3105669.13766	979.83675	63536.18929	211.98014
48	1911.2	4855.01866	523.45546	7592.46507	293170.62164	614699.05692	93561.18537	3727422.02365	1137.17606	227201.53963	14958.36129
55	1908.5	626.01255	15016.86351	46183.77396	1023503.54337	1434843.94489	640196.92466	3970394.97028	1203.20602	63660.12162	248.03195
57	1938.4	170.16023	1382.95530	3041.30638	330166.69792	369647.71436	1203046.04878	7524708.94203	3115.36135	42255.21011	512.71418

Acknowledgments